Proceedings of the Integrated Ocean Drilling Program, Volume 320/321
Pälike, H., Lyle, M., Nishi, H., Raffi, I., Gamage, K., Klaus, A., and the Expedition 320/321 Scientists

Site U1332[1]

Expedition 320/321 Scientists[2]

Chapter contents

[1]Expedition 320/321 Scientists, 2010. Site U1332. *In* Pälike, H., Lyle, M., Nishi, H., Raffi, I., Gamage, K., Klaus, A., and the Expedition 320/321 Scientists, *Proc. IODP,* 320/321: Tokyo (Integrated Ocean Drilling Program Management International, Inc.).
doi:10.2204/iodp.proc.320321.104.2010
[2]Expedition 320/321 Scientists' addresses.

Background and objectives

Integrated Ocean Drilling Program (IODP) Site U1332 (11°54.722′N, 141°02.743′W; 4924 meters below sea level [mbsl]) (Fig. F1; Table T1) is located ~120 km east and slightly south of IODP Site U1331, near the northwesternmost area drilled during the Pacific Equatorial Age Transect (PEAT) program (IODP Expedition 320/321). This site is situated on 50 Ma crust ~750 km north of the Clipperton Fracture Zone, ~380 km south of the Clarion Fracture Zone, and ~270 km northeast of the nearest previously drilled Ocean Drilling Program (ODP) Site 1220 (56 Ma crust).

The Eocene was a time of extremely warm climates that reached a global temperature maximum (the Early Eocene Climatic Optimum [EECO]) near 52 Ma (Zachos et al., 2001; Shipboard Scientific Party, 2004). During that time, atmospheric pCO_2 concentrations were elevated (Lowenstein and Demicco, 2007) and the early Eocene calcium carbonate compensation depth (CCD) was very shallow, estimated between 3200 and 3300 mbsl (Lyle, Wilson, Janecek, et al., 2002; Lyle et al., 2005; Rea and Lyle, 2005). From this temperature maximum there was a gradual climatic cooling through the Eocene to the Eocene/Oligocene boundary. Throughout the Eocene, the CCD lay near 3.2–3.3 km depth, albeit with potentially significant short-term fluctuations (Lyle et al., 2005). Thus, although recovering carbonate sediments from the equatorial region is a substantial challenge, it is not impossible if the depth of the East Pacific Rise lay near the global average of 2.7 km.

During the early Eocene, a very shallow CCD and typical rapid tectonic plate subsidence of young crust near the shallow ridge crest conspired to make the time window during which carbonate is preserved very short (~2 Ma) before each site sinks below the CCD (Rea and Lyle, 2005). Thus, although good records of pelagic carbonates during and just after the Paleocene/Eocene Thermal Maximum (PETM) were recovered at ODP Leg 199 sites (Lyle, Wilson, Janecek, et al., 2002; Raffi et al., 2005; Nuñes and Norris, 2006), the time period of the EECO (Zachos et al., 2001) and the shallowest CCD is not well sampled. In combination with Site U1331, which is located on crust with an age of 53 Ma, Site U1332 is located on crust with an expected age of ~50 Ma to intercept the interval between 50 and 48 Ma in biogenic sediments above the CCD. Thus, Site U1332 forms the second oldest time slice component of Expedition 320/321.

One of the common objectives of the PEAT program for all sites is to provide a limited depth transect for several Cenozoic key horizons, such as the Eocene–Oligocene transition (Coxall et al., 2005). For this objective, Site U1332 will form the second deepest paleodepth constraint, with an estimated crustal paleodepth of ~4 km during the Eocene–Oligocene transition.

All Expedition 320/321 drill sites have in common the objective to improve and extend the extensive intercalibrated bio-, magneto-, chemo-, and astronomical stratigraphies for the Cenozoic (e.g., Shackleton et al., 2000; Pälike et al., 2006).

Site U1332 is located in abyssal hill topography with a general slope in topography to the north. The topography is dominated by small ridges that trend north–south and troughs of ~5 km width (Fig. **F1B**). Bathymetric relief across the abyssal hills is 50–200 m, and sediment cover is around 200 ms two-way traveltime (TWT), or ~155 m using the velocity model developed by Busch et al. (2006).

The 48-channel stacked and migrated data (e.g., seismic Lines PEAT-2C-sl-1 and PEAT-2C-sl-6 in Pälike et al., 2008) (Lyle et al., 2006) reveal a region at the flanks of tilted ridges where older horizons are exposed nearer the surface. The site survey piston coring suggested that the surface sediments were formed at ~20 Ma. Site survey seismic Line 6 (Fig. **F2**), on which Site U1332 is located, suggests ~160 m of sediment above basement. An interpretation of the site survey seismic data (Fig. **F2**) indicated that Site U1332 would penetrate seismic Reflectors P2 and P3 of Lyle, Wilson, Janecek, et al. (2002).

We positioned Site U1332 and the other PEAT sites to the south of the estimated paleoequatorial position at the target age in order to maximize the time that drill sites remain within the equatorial zone (i.e., ±2° of the Equator), to allow for some southward bias of the equatorial sediment mound relative to the hotspot frame of reference (Knappenberger, 2000), and to place the interval of maximum interest above the basal hydrothermal sediments. We located the site using the digital grid of seafloor age from Müller et al. (1997), heavily modified and improved with additional magnetic anomaly picks from Petronotis (1991), Petronotis et al. (1994), and Deep Sea Drilling Project (DSDP)/ODP basement ages, as well as the magnetostratigraphic data compiled by Cande et al. (1989) and Cande and Kent (1995). From the digital age grid, each point is backrotated in time to zero age, using the fixed-hotspot stagepoles from Koppers et al. (2001) and Engebretson et al. (1985) and the paleopole data from Sager and Pringle (1988). From the backtracked latitudes for each grid point we then obtained the paleoequator at the crustal age by contouring the paleolatitude on the original grid.

Science summary

Three holes were cored at Site U1332 (11°54.722′N, 141°02.743′W; 4924 mbsl) (Fig. **F1;** Table **T1**), which is the second northwesternmost site drilled during the PEAT program. At Site U1332, seafloor basalt is overlain by ~150 m of pelagic sediment, containing radiolarian and nannofossil ooze with varying amounts of clay and zeolitic clay. The oldest sediment is of earliest middle Eocene age. Hole U1332A provided high-quality and high-recovery advanced piston corer (APC)-cored sediments from the mudline to 125.9 m core depth below seafloor (CSF) (Core 320-U1332A-14H), where we encountered porcellanite and chert and switched to the extended core barrel (XCB) cutting shoe. XCB coring advanced to 152.4 m drilling depth below seafloor (DSF) through a ~10 m thick porcellanite-rich interval with reduced recovery. In the basal section, we recovered a short, ~3.8 m long interval of barren very dense and stiff clay above basalt, ~10 m shallower than predicted from the seismic profile, in Core 320-U1332A-18X. Basement was reached at 152.4 m CSF. For detailed coring activities, see **"Operations."**

The uppermost 17.7 m consists of upper Miocene to Pleistocene–Pliocene clay, with varying amounts of radiolarians and zeolite minerals, overlying ~130 m of Oligocene to middle Eocene nannofossil and radiolarian ooze with porcellanite deep in the section. A thin ~3 m thick unit of middle Eocene zeolite clay bearing small porcellanite and chert nodules was recovered at the base of the sedimentary sequence, above basaltic basement. The sedimentary sequence at Site U1332 was divided into five major lithologies (Fig. **F3**).

The upper stratigraphy at Site U1332 has a strong resemblance to that of Site U1331 but without the sharp erosive contacts described at Site U1331. Several meters of white to beige-colored Pleistocene–Pliocene clay (lithologic Unit I) overlie lower Miocene to lowermost Oligocene nannofossil ooze (Units II and III). There is a sharp lithologic change at the Eocene–Oligocene transition to alternating radiolarian ooze with nannofossils and nannofossil ooze (Subunit IVa). The lithology gradationally changes downhole into a dominance of radiolarian nannofossil ooze and nannofossil radiolarian ooze (Subunit IVb) and then into an interval of alternating radiolarian ooze, radiolarian nannofossil ooze, and nannofossil radiolarian ooze with porcellanite layers (Subunit IVc). Lithologic Unit V is composed of very dark grayish brown to black clay, very dark grayish brown to black zeolite clay, and chert. The sediments directly above basaltic basement are partially lithified. Basalt is designated as lithologic Unit VI, at ~150 m CSF.

Carbonate content approaches 85 wt% in Unit III within the Oligocene nannofossil oozes and cycles between 0 and 40–60 wt% in the middle Eocene section (Unit IV) (Fig. **F4**). All major microfossil groups were found in sediments from Site U1332 and provide a consistent, coherent, and high-resolution biostratigraphic succession from basement to the top of Unit II. Calcareous nannofossils are abundant and moderately well preserved in the Oligocene and poor to moderately well preserved in the Miocene and Eocene. Most middle Eocene sediments commonly contain nannofossils; however, there are several barren intervals. Radiolarians are common to abundant throughout most of the section, apart from the lowermost sediment section above basalt. Radiolarians are well preserved in the Eocene and moderately well preserved in the Oligocene to lower Miocene section above. Radiolarian and nannofossil datums and zonal determinations agree, ranging from nannofossil Zones NP13/NP14 in the basal dark clay section (~48.4–50.7 Ma) to Zone NN1 and radiolarian Zones RP13 above basement through RN1 (lowermost Miocene, ~22.3 Ma) below the upper Pliocene–Pleistocene clay cover in Core 320-U1332A-3H (Fig. **F4**). Planktonic foraminifers are generally rare throughout the Oligocene but are absent in the Miocene and Eocene. Benthic foraminifers are present through most of the section but are rare in Miocene and Eocene sediments. They indicate lower bathyal to abyssal paleodepths. Sedimentation rates, as implied by biostratigraphic age determinations, vary throughout the section and are ~5 m/m.y. in the Eocene section and ~2.5 m/m.y. in the Oligocene, with two prominent hiatuses in the Miocene and between the Miocene and younger sediments. The presence of all major fossil groups as well as a detailed and well-resolved magnetostratigraphy will allow us to achieve one of the main PEAT objectives, to arrive at an integrated Cenozoic stratigraphy and age calibration (e.g., Pälike et al., 2006) for major parts of the Oligocene and Eocene.

Magnetostratigraphic studies as well as high-resolution biostratigraphy and stratigraphic correlation determined that a 4 m interval from the base of Core 320-U1332A-8H was repeated in the top of Core 9H, which comprises Chron C13n and the lowermost Oligocene. This repetition also occurs in Cores 320-U1332B-8H and 9H and within Core 320-U1332C-9H. The lithologic succession from the lower occurrence of Chron C13n downhole as well as from the upper occurrence of Chron C13n uphole both appear complete and continuous; hence Site U1332 achieved the fortuitous feat of recovering the complete Eocene–Oligocene transition four times and the upper part of Chron C13n five times at a triple-cored site. A likely explanation for this is the widespread occurrence of a slumped interval.

A full physical property program was run on cores from all three holes, including Whole-Round Multisensor Logger (WRMSL) measurements of magnetic susceptibility, bulk density, *P*-wave velocity, and noncontact resistivity, along with natural gamma radiation (NGR), followed by discrete measurements of color reflectance, index moisture and density properties, sound velocities, and thermal conductivity. Bulk density measurements show a marked increase in the carbonate-rich Oligocene section, as well as in carbonate-bearing horizons in the Eocene (carbonate accumulation event [CAE] cycles; Lyle et al., 2005). Magnetic susceptibility is variable throughout the section, allowing a detailed correlation among holes. NGR measurements are elevated by an order of magnitude in the surficial clay layer. Porosity values are generally high in the radiolarian-rich sediments (85%) and decrease in the Oligocene and Eocene carbonate section, which also shows higher thermal conductivity values of ~0.9 to 1.2 W/(m·K), compared with ~0.8 W/(m·K) in the radiolarian oozes and surficial clay.

Stratigraphic correlation allowed us to obtain a complete section to ~125.5 m CSF near the top of the porcellanite interval in Hole U1332A, equivalent to a composite depth of ~140 m core composite depth below seafloor (CCSF-A) (see **"Core composite depth scale"** in the "Methods" chapter). The overall core expansion (growth factor), which is calculated by the ratio between the CCSF-A and CSF (formerly meters composite depth [mcd] and meters below seafloor [mbsf]) depth scales, is ~10%. The tops of APC cores were often affected by ~3 m heave that occurred during operations at Site U1332. Stratigraphic correlation supports the biostratigraphic, paleomagnetic, and sedimentologic description of a repeated sequence, possibly due to slumping, spanning the Eocene–Oligocene transition.

A full range of paleomagnetic analyses was conducted on cores and samples from Site U1332 and resulted in a well-resolved magnetostratigraphy. Shipboard analyses suggest that a useful magnetic signal is preserved in all APC-cored intervals and that it was possible to remove the drilling-induced steep inclination overprint by alternating-field demagnetization. Comparison of biostratigraphic data and changes in magnetic paleodeclinations suggests the recovery of magnetic reversals Chrons C1n/C1r.1r to C2An.3n/C2Ar above a hiatus and then a continuous sequence of magnetic reversals from Chrons C5En/C5Er (18.52 Ma) in the Miocene at ~12.95 m CSF (interval 320-U1332C-2H-4, 95 cm) to C19r/C20n (42.54 Ma) at interval 320-U1332A-14H-5, 80 cm. Magnetostratigraphic interpretation supports the presence of a slump through multiple recovery (five times) of parts of Chron C13n in a triple-cored sequence. Paleomagnetic directions from discrete samples agree well with those from split-core results.

A standard shipboard suite of geochemical analyses of pore water and organic and inorganic sediment properties was conducted on samples from Site U1332. Alkalinity values increase from ~2.2 to 3.4 mM downsection, and Sr^{2+} increases from ~80 to ~110 µM. H_4SiO_4 remains relatively stable between 400 and 600 µM above 90 m depth in the Oligocene nannofossil oozes but increases to 800–1000 µM in the Eocene silica-rich radiolarian oozes. Carbonate coulometry yielded carbonate contents of ~85 wt% in the Oligocene nannofossil ooze and horizons with up to 60 wt% $CaCO_3$ in the middle Eocene radiolarian-rich oozes. Total organic carbon (TOC) contents were measured both by difference between total carbon (TC) and total inorganic carbon (IC) as well as by using an acidification method. Using the acidification method, TOC values were <0.3 wt% for all measured samples. The top ~5 m shows values of 0.18–0.17 wt% TOC. Between ~40 and 70 m CSF the measurements indicate TOC below the detection limit of 0.03 wt%, and downhole from this, values are generally low. We conducted a high-resolution Rhizon pore water experiment across an alkalinity trough around 40 m CSF, which highlighted comparisons between squeezed and Rhizon-sampled pore waters. Additional ephemeral samples were taken for shore-based microbiology and permeability studies.

Wireline logging provided valuable information to constrain the interval of porcellanite and chert formation within the borehole. Downhole NGR, density, and magnetic susceptibility logs provide important constraints on the poorly recovered lithologies below and between porcellanite-bearing horizons. The logging data document the presence of two thin porcellanite horizons at ~126 and 130 m wireline log depth below seafloor (WSF) and an ~14 m thick interval of increased magnetic susceptibility, reduced conductivity, and enhanced density and photoelectric factor that appears to be the dark and dense clays and zeolitic clays above basement, rather than carbonate. Integration with the seismic data will allow further improvements with the regional seismic interpretations. Data from Site U1332 indicate that the top of seismic Horizon P2 (Lyle et al., 2002) correlates with the top of the porcellanite section, just as it did for Site U1331. No Formation MicroScanner (FMS) data were collected, as it was not possible to retrieve the "paleo-" triple-combination (triple combo) tool string back into the bottom-hole assembly (BHA). Eight downhole temperature measurements were conducted in Holes U1332B and U1332C with the advanced piston corer temperature (APCT-3) tool. Three of these yielded good data; the other measurements were impaired by strong, sometimes >3 m heave during operations in Hole U1332B.

Downhole temperature measurements, when combined with the thermal conductivity values obtained from the cores, indicate that Site U1332 has a heat flow of 70.7 mW/m^2 and a thermal gradient of 75.0°C/km. This is significantly higher than the values obtained for Site U1331 but comparable to values obtained for Sites 1218 and 1219.

Highlights

Shallow early Eocene CCD

Coring at Site U1332 was designed to capture a very short period of time (~2 m.y.) at ~50 Ma during which this site was thought to be located above the very shallow Eocene CCD (~3.3 km) (Lyle, Wilson, Janecek, et al., 2002; Rea and Lyle, 2005) just after the EECO (Zachos et al., 2001). Unlike Site U1331, at Site U1332 we cored a ~10 m thick section of dense and dark brown clays, zeolite clays, and chert above basement, although relatively common nannofossils were present in the lowermost samples from Hole U1332B. This finding will provide important new constraints on the depth of the CCD at ~48–50 Ma at the paleoequator, indicating that the CCD was shallower than previously thought.

Stratigraphic integration

One of the primary objectives of the PEAT science program is the integration of different stratigraphic methodologies and tools. Site U1332 contains all major fossil groups (nannofossils, radiolarians, foraminifers, and diatoms), as well as an excellent magnetostratigraphy and composite depth correlation, which can be tied to nearby Leg 199 sites (e.g., Site 1220) by way of physical property variations. The possibility of a cycle-by-cycle match between Sites U1332 and 1220 has been demonstrated using magnetic susceptibility and bulk density data, providing additional stratigraphic tie points and a verification of the completeness of the stratigraphic section on a regional scale. Thus, Site U1332 will help us to achieve an integrated stratigraphy for the Cenozoic Pacific Ocean, ranging from the Miocene to the middle Eocene.

Eocene–Oligocene and Oligocene–Miocene transitions and depth transects

Site U1332 forms the second oldest and deepest component of the PEAT depth transect, which will allow the study of critical intervals (such as the Eocene–Oligocene transition; see Coxall et al., 2005) and variations of the equatorial CCD. Site U1332 is estimated to have been ~4 km deep during the Eocene–Oligocene transition, ~1 km shallower than today and 200 m shallower at that time than Site U1331. Sediments rapidly change from radiolarian ooze below the transition into nannofossil oozes above, and unlike Site U1331, Site U1332 also contains carbonate-bearing sediments across the Oligocene–Miocene transition. For the Eocene–Oligocene transition, Site U1332 will provide a tie point for calcium carbonate burial at ~4° to 5° paleolatitude.

Variations in the CCD

Site U1332 has provided important constraints for variations and depth of the CCD from the early Eocene to the late Miocene. This site shows increased carbonate content and much increased mass accumulation rates approaching 200 mg $CaCO_3/cm^2/k.y.$ around the middle of Chron C18r to the base of Chron C19r during the middle Eocene, which can be correlated to an interval of enhanced carbonate burial that was previously documented by Lyle et al. (2005) in Leg 199 cores. The early Oligocene high $CaCO_3$ concentrations decrease significantly in sediments younger than ~27 Ma. By ~22 Ma, in the early Miocene, carbonate was no longer preserved. This is presumably related to Site U1332 sinking below the prevalent CCD and coincides with a CCD shoaling event between ~20 and 15.5 Ma described by Lyle (2003).

Formation of porcellanite and chert

Together with Site U1331, Site U1332 provides important new information on the formation of porcellanite and chert. Coring has shown that the top of the porcellanite-rich interval is mapped by seismic Horizon P2 (Lyle et al., 2002). In lithologic Subunit IVc, layers and pebbles of very dark brown partially to well-lithified mudstones, often layered or even laminated, are observed within alternating sequences of nannofossil ooze and radiolarian ooze of late to late middle Eocene age. In hand specimen, the partially lithified mudstones are particularly rich in clay and show evidence of partial secondary silicification. Pieces of porcellanite contain clay minerals, microcrystalline quartz, opaques, and calcite, as well as biogenic shells and fragments from radiolarians and foraminifers. Sediments from Sites U1331 and U1332 appear to document the silicification process in clay-rich horizons near basement, which will likely extend the findings of Moore (2008).

Age transect of seafloor basalt

At Site U1332 we recovered what appear to be fresh fragments of seafloor basalt, aged between 49 and 50 Ma as estimated from biostratigraphic results. This material will, when combined with other PEAT basalt samples, provide important sample material for the study of seawater alteration of basalt.

Operations

Unless otherwise noted, times are local ship time, which was Hawaii Standard Time (UTC – 10 h) for Site U1332.

Transit to Site U1332

Following completion of Site U1331, we started heading east to Site U1332. The vessel made slow progress into a 20 kt wind and against a strong current with moderate pitching and rolling into a 6–8 ft swell with spray occasionally over the bow. This reduced the average speed of the 66.1 nmi voyage to Site U1332 to 7.1 kt.

Site U1332

Hole U1332A

After the 9.25 h transit, we began positioning over the site at 1445 h on 22 March 2009. We assembled the BHA, and spaceout of the colletted delivery system was verified. Because the precision depth recorder (PDR) was still not working, it was necessary for the driller to carefully lower the bit and tag the seafloor to verify the exact depth. As the driller was preparing to spud the hole, the display that indicates coring line position relative to the rig floor failed. Because it is imperative for the core winch operator to know where the coring line is at all times, operations had to be suspended for 3 h while the defective unit was replaced.

Hole U1332A was spudded with the APC at 1050 h on 23 March. The water depth calculated from the recovery of the first core was established as 4935.1 m drilling depth below rig floor (DRF) (4923.9 mbsl) (Table T1). APC Cores 1H through 14H penetrated from 0 to 125.9 m DSF, and we recovered 131.9 m (104%) (Table T1). All piston cores were oriented with the FlexIt tool. Because of the potential presence of chert horizons, no downhole temperature measurements were attempted in Hole U1332A. Core 14H required 70,000 lb of overpull to extract the core barrel from the sediment, after which we switched to XCB coring.

We recovered 13.8 m (51%) in XCB Cores 15X through 18X (125.9 to 152.4 m DSF). Coring was terminated when Core 18X was recovered with a piece of basaltic basement. Hole U1332A was cored to 152.4 m, and we recovered 145.6 m (96%).

After coring was finished, we prepared the hole for logging by flushing it with 65 bbl of attapulgite mud and then dropping a go-devil to open the lockable float valve (LFV). We then displaced the hole with 80 bbl of attapulgite mud and raised the bit to 78 m DSF.

We then deployed a tool string consisting of the magnetic susceptibility, GRA density, and NGR tools. This tool string acquired good downhole logs over the entire open hole interval. Unfortunately, the tool string parted from the logging wireline when attempting to recover the tool and the tool string was lost in the hole.

We spent ~18 h conducting three unsuccessful coring line fishing attempts to recover the logging tool string. After acknowledging that spending more time fishing for the tool string would not be productive, the decision was made to seal Hole U1332A with 15 bbl of cement (from 125 to 90 m DSF) above the lost logging tool. Deploying the cement had to be delayed for 4 h while the cement pumps were repaired.

After the cementing operations were completed, the bit was pulled free of the seafloor at 0800 h on 26 March and the vessel was offset 20 m north of Hole U1332A. Before coring could resume, the drill string was flushed with seawater to remove any cement from the tubulars and bit nozzles.

Hole U1332B

Hole U1332B was spudded at 1230 h on 26 March. We started coring Hole U1332B with the bit offset 5 m deeper than the seafloor depth established for Hole U1332A but only penetrated to 2.1 m CSF below the mudline. We recovered 118.4 m (107%) in APC Cores 1H through 13H (0–110.1 m DSF). In an attempt to maintain an offset with the first hole, there were short advances with Cores 3H (8.0 m) and 11H (5.0 m). The APCT-3 was deployed while taking cores at six different depths: 11.6, 19.6, 38.6, 57.6, 76.6, and 100.6 m DSF (Cores 2H, 3H, 5H, 7H, 9H, and 12H, respectively). Nonmagnetic core barrels were used on all cores except 13H.

We then switched to the XCB and took Cores 14X to 18X from 110.1 to 148.6 m DSF and recovered 23.4 m (61%). Coring was terminated when we recovered ~2.4 m of dark brown sediment above several small pieces of basalt in Core 18X.

In Hole U1332B we cored a total of 148.6 m and recovered 141.8 m (95%). The drill string was pulled out of the hole and the bit cleared the seafloor at 2230 h on 27 March.

Hole U1332C

Hole U1331C was designed to provide stratigraphic overlap and confirm stratigraphic correlations with Holes U1332A and U1332B. After the vessel was offset 30 m north of Hole U1332B, Hole U1332C was spudded at 0105 h on 28 March. The seafloor depth calculated from the recovery of the first core was 4934.0 m DRF (4922.8 mbsl). Piston coring then routinely proceeded to 85.0 m DSF, during which the advances of Cores 6H (4.0 m advance) and 8H (7.0 m advance) were adjusted to maintain overlap with previous holes. At ~1330 h on 28 March, while retrieving Core 10H, an electrical transient attributed to the rotating condenser caused two of the three main generators to trip off the main bus and resulted in a load shedding sequence to various systems on the vessel, which included loss of control voltage to all Thyrig bays for ~10 min. The consequence of the loss of Thyrig control voltage was a short-term loss of power to thrusters, propulsion, and drilling motors. During this short event, the dynamic positioning (DP) 3% watch circle (percentage of water depth or ~150 m off the hole) was not exceeded. The main breakers quickly reset and power was restored to all main systems by 1341 h. We thought the switching circuit for removing the rotating condenser from the main bus was defective.

Because of the power loss, the coring line parted while attempting to recover Core 10H, and we had to make two fishing trips with the coring line to recover the sinker bars and the full core barrel. Unfortunately, this APC core was near the Eocene/Oligocene boundary and was very disturbed. APC coring continued to 113.5 m DSF, where coring was switched to the XCB. All the APC cores were obtained with nonmagnetic core barrels and with the FlexIt core orientation tool except Core 13H, for which we used a standard steel core barrel. APCT-3 formation temperature measurements were made at 36.0 m DSF (Core 4H) and 75.5 m DSF (Core 9H). APC Cores 1H through 13H extended from 0 to 113.5 m DSF, and we recovered 122.04 m (108%). XCB Cores 14X through 18X extended from 113.5 to 155.5 m DSF, where basement was encountered, and we recovered 26.02 m (62%). The total core interval with both coring systems was 155.5 m with 148.1 m recovered (95%).

Once the final core was on deck, we started recovering the drill string. The seafloor beacon was successfully recovered on deck at 1202 h on 29 March. At

1930 h on 29 March, the drilling equipment had been secured and we departed for Site U1333.

Lithostratigraphy

Drilling at Site U1332 recovered a 150.4 m thick section of pelagic sediments overlying seafloor basalt. The uppermost 17.7 m of the section is a late Miocene to Pliocene–Pleistocene clay with varying amounts of radiolarians and zeolite minerals (~6 to 22 Ma based on radiolarians and magnetostratigraphy). These sediments are underlain by ~130 m of Oligocene to middle Eocene nannofossil and radiolarian ooze with porcellanite deep in the section. A thin (~3 m thick) unit of middle Eocene zeolite clay bearing small chert nodules was recovered at the base of the sedimentary sequence above basement basalt.

The sedimentary sequence at Site U1332 is divided into five major lithologic units, with one of these units further divided into three subunits (Fig. F3; Table T2). Unit and subunit boundaries are defined by differences in lithology, measured physical properties, and calcium carbonate ($CaCO_3$) content. Lithologic differences, based on both visual core descriptions and smear slide and thin section analysis, are primarily attributable to varying distributions of biogenic components (e.g., nannofossils and radiolarians) and clay-sized lithogenic material, as well as the presence of porcellanite (Table T2; Figs. F3, F5, F6, F7; see "Site U1332 thin sections" and "Site U1332 smear slides" in "Core descriptions"). Lithologic descriptions are primarily based on sediments recovered in Hole U1332A, supplemented with observations from Holes U1332B and U1332C.

Unit I

Intervals: 320-1332A-1H-1, 0 cm, through 3H-3, 130 cm; 320-U1332B-1H-1, 0 cm, through 3H-4, 150 cm; 320-U1332C-1H-1, 0 cm, through 3H-1, 70 cm

Depths: Hole U1332A = 0–17.7 m CSF; Hole U1332B = 0–17.6 m CSF; Hole U1332C = 0–17.7 m

Age: Miocene–Pliocene–Pleistocene

Lithology: clay and radiolarian clay

The major lithology in Unit I is light yellowish brown (10YR 6/4) to very dark brown (10YR 3/2) to dark gray (10YR 4/1) clay. The light yellowish brown clay with radiolarians occurs in the uppermost ~8 m of the sedimentary section (in Hole U1332A), overlying the darker zeolite clay. The downhole transition from radiolarian clay to zeolite clay is characterized by a change to darker color and shifts to higher magnetic susceptibility but lower gamma ray attenuation (GRA) bulk densities and L* (lightness) (Fig. F3; see "Physical properties" for discussion of additional reflectance parameters a* and b*). $CaCO_3$ contents are near zero throughout Unit I. The contact with underlying Unit II takes place over a ~5 cm thick-interval.

Unit II

Intervals: 320-U1332A-3H-3, 130 cm, through 5H-1, 150 cm; 320-U1332B-3H-4, 150 cm, through 5H-1, 150 cm; 320-U1332C-3H-1, 70 cm, through 4H-7, 30 cm

Depths: Hole U1332A = 17.7–33.9 m CSF; Hole U1332B = 17.6–30.6 m CSF; Hole U1332C = 17.7–35.8 m

Age: early Miocene to late Oligocene

Lithology: alternations of clayey radiolarian ooze and nannofossil ooze

The dominant lithologies in Unit II are dark brown (10YR 3/2) to very dark grayish brown (10YR 3/2) clayey radiolarian ooze, yellowish brown (10YR 5/4) to pale brown (10YR 6/3) nannofossil ooze, and dark brown (10YR 3/3) radiolarian ooze. Bioturbation is generally minor to moderate in these sediments. Within the major lithologies, nannofossil ooze sometimes occurs with radiolarians and sometimes occurs with radiolarians and clay as minor lithologic components, whereas radiolarian ooze occurs with clay as a minor lithologic component. Alternating sequences of nannofossil ooze and radiolarian ooze occur at decimeter to meter scales. The contact with underlying Unit III takes place over a 5 cm interval. Unit II sediments have $CaCO_3$ contents (typically ≤40%) that are lower than those of the underlying Unit III, whereas magnetic susceptibility, GRA bulk densities, and L* all show systematically lower values in Unit II than in Unit I (Fig. F3; see "Geochemistry").

Unit III

Intervals: 320-U1332A-5H-2, 0 cm, through 9H-4, 124 cm; 320-U1332B-5H-2, 0 cm, through 9H-6, 50 cm; 320-U1331B-4H-7, 30 cm, through 10H-1, 41 cm

Depths: Hole U1332A = 33.9–76.14 m CSF; Hole U1332B = 30.6–75.1 m; Hole U1332C 35.8–75.91 m CSF

Age: early Oligocene

Lithology: nannofossil ooze, nannofossil ooze with radiolarians, and radiolarian nannofossil ooze

The dominant lithology in Unit III is white (10YR 8/1) to brown (10YR 5/3) nannofossil ooze, but brown radiolarian nannofossil ooze is also a major lithology in this unit. Within the major lithologies, nannofossil ooze occurs with diatoms as a minor lithologic component. Bioturbation intensity is minor to intense in these sediments. Baseline values of magnetic susceptibility are low with large-amplitude variability in comparison to the overlying units. Data series for GRA bulk density, L*, and $CaCO_3$ all show high baseline values with large-amplitude variability in comparison to the overlying units (see Fig. F3). The contact with underlying Unit IV is marked by a light to dark color change over a 20 cm bioturbated boundary.

Unit IV

Intervals: 320-U1332A-9H-4, 124 cm, through at least 16X-CC, 42 cm; 320-U1332B-9H-6, 50 cm, through at least 17X-CC, 40 cm; 320-U1332C-10H-1, 41 cm, through at least 17X-2, 7 cm

Depths: Hole U1332A = 76.14–138.29 m CSF; Hole U1332B = 75.1–135.08 m CSF; Hole U1332C = 75.91–138.77 m CSF

Age: middle to late Eocene

Lithology: clayey radiolarian ooze, radiolarian ooze, radiolarian nannofossil ooze, nannofossil radiolarian ooze, nannofossil ooze, and porcellanite

Unit IV is distinguished from Unit III by the dominance of radiolarian ooze. The major lithologies in Unit IV are dark brown (10YR 3/3) to brown (10YR 5/3) radiolarian ooze, very dark grayish brown (10YR 3/2) to brown (10YR 4/3) clayey radiolarian ooze, dark yellowish brown (10YR 3/4) to light gray (10YR 7/2) nannofossil radiolarian ooze, brown (10YR 5/3) to light gray (10YR 7/2) radiolarian nannofossil ooze, and brown (10YR 5/3) nannofossil ooze. Downhole lithologic changes within Unit IV allow division into three subunits based on the significance of nannofossil ooze, radiolarian nannofossil ooze, and porcellanite as secondary major lithologies and the downhole profile of $CaCO_3$ (Fig. F3; see "Geochemistry").

Subunit IVa

Intervals: 320-U1332A-9H-4, 124 cm, through 13H-1, 20 cm; 320-U1332B-9H-7, 0 cm, through 13H-5, 120 cm; 320-U1332C-10H-1, 41 cm, through 13H-2, 150 cm

Depths: Hole U1332A = 76.14–108.6 m CSF; Hole U1332B = 75.1–107.8 m CSF; Hole U1332C = 75.91–107.0 m CSF

Age: middle to late Eocene

Lithology: alternations of nannofossil ooze, radiolarian nannofossil ooze, radiolarian ooze, and clayey radiolarian ooze

Subunit IVa is distinguished from Subunits IVb and IVc based on the dominance of radiolarian ooze and absence of porcellanite. The major lithologies in Subunit IVa are dark brown (10YR 3/3) to brown (10YR 5/3) radiolarian ooze, dark brown (10YR 3/3) clayey radiolarian ooze, and brown (10YR 4/3) to pale brown (10YR 6/3) radiolarian nannofossil ooze. Within the major lithologies, radiolarian ooze occurs with either clay or nannofossils. Bioturbation is generally minor to moderate in these sediments. GRA bulk density, L*, and $CaCO_3$ content all decrease downhole across the Unit III/Subunit IVa boundary and maintain relatively low values throughout (Fig. F3). Magnetic susceptibility is generally higher in the upper portion of Subunit IVa than in Unit III and decreases toward the boundary with Subunit IVb. The contact with underlying Subunit IVb takes place over a 5 cm interval.

Subunit IVb

Intervals: 320-U1332A-13H-1, 20 cm, through 14H-1, 150 cm; 320-U1332B-13H-5, 120 cm, through 15H-4, 40 cm; 320-U1332C-13H-3, 0 cm, through 15H-2, 50 cm

Depths: Hole U1332A = 108.6–119.4 m CSF; Hole U1332B = 107.8–121.0 m CSF; Hole U1332C = 107.0–120 m CSF

Age: middle Eocene

Lithology: alternations of nannofossil ooze, radiolarian nannofossil ooze, and nannofossil radiolarian ooze

Subunit IVb is distinguished from Subunits IVa and IVc based on the dominance of radiolarian nannofossil and nannofossil oozes and absence of porcellenite. The major lithologies in Subunit IVb are brown (10YR 5/3) nannofossil ooze, dark yellowish brown (10YR 4/4) radiolarian nannofossil ooze, and dark brown (10YR 3/3) nannofossil radiolarian ooze. Within the major lithologies, nannofossil ooze occurs with radiolarians as a minor component and nannofossil radiolarian ooze occurs with clay as a minor component. Alternations of nannofossil ooze and radiolarian nannofossil ooze in Subunit IVb occur at decimeter to meter scales. Bioturbation is generally minor to moderate in these sediments.

Subunit IVc

Intervals: 320-U1332A-14H-2, 0 cm, through at least 16X-CC, 42 cm (base not recovered); 320-U1332B-15H-4, 40 cm, through at least 17X-CC, 40 cm (base not recovered); 320-U1332C-15H-2, 50 cm, through 17X-2, 7 cm

Depths: Hole U1332A = 119.4 to at least 138.39 m CSF; Hole U1332B = 121.0 to at least 135.08 m CSF; Hole U1332C = 121.0 to least 138.77 m CSF

Age: middle Eocene

Lithology: alternations of radiolarian nannofossil, radiolarian ooze, and nannofossil radiolarian ooze with porcellanite layers or nodules

Subunit IVc is distinguished from Subunits IVa and IVb based on the presence of porcellanite. The major lithologies in Subunit IVc are dark brown (10YR 3/3) to dark yellowish brown (10YR 4/4) radiolarian ooze, brown (10YR 5/3) radiolarian nannofossil ooze, very dark grayish brown (10YR 3/2) clayey radiolarian ooze, and porcellanite. Within the major lithologies, radiolarian ooze occurs with clay as well as with clay and nannofossils as minor components. Nannofossil radiolarian ooze is a minor lithology in Hole U1332A. Alternations of nannofossil radiolarian ooze with radiolarian nannofossil ooze and of radiolarian ooze with clay and radiolarian ooze with clay and nannofossils occur on decimeter to meter scales in Subunit IVc. Bioturbation is generally minor to moderate in these sediments. Magnetic susceptibility, GRA bulk density, and L* are comparatively low in Subunit IVc at Site U1332. In thin section, porcellanite layers and nodules contain flat flakes of clay minerals, radiolarians, nannofossils, and foraminifers. Radiolarian and foraminifer tests are partially replaced with microcrystalline quartz.

Unit V

Intervals: At least 320-U1332A-17X-1, 0 cm (top not recovered), through 17X-CC, 3 cm; 320-U1332B-18X-1, 0 cm, through at least 18X-CC, 16 cm (base not recovered); 320-U1332C-17X-2, 7 cm, through at least 18X-CC, 46 cm (base not recovered)

Depths: Hole U1332A = 144.50 to at least 148.15 m CSF; Hole U1332B = 143.90 to at least 146.09 m CSF; Hole U1332C = 138.77 to at least 147.36 m CSF

Age: middle Eocene

Lithology: clay, zeolite clay, and chert

The major lithologies in Unit V are very dark grayish brown (10YR 3/2) to black (10YR 2/1) clay, very dark grayish brown (10YR 3/2) to black (10YR 2/1) zeolite clay, and chert. Sediments at the very base of the sedimentary section directly overlying basalt are partially lithified with nonvisible bioturbation.

Unit VI

Intervals: 320-U1332A-17X-CC, 3 cm, to at least 18X-CC, 52 cm; 320-U1332B-18X-CC, 16 cm, to at least 18X-CC, 34 cm; 320-U1332C-18X-CC, 46 cm, to at least 18X-CC, 62 cm

Depths: Hole U1332A = 148.15–150.56 m CSF; Hole U1332B = 146.09–146.27 m CSF; Hole U1332C = 147.36–147.52 m

Small broken basalt pieces were recovered at the base of each hole at Site U1332. Thin section analysis indicates a highly altered phyric basalt with sparse plagioclase (Sample 320-U1332A-18X-CC (Piece 3A, 16–19 cm) (see **"Site U1332 thin sections"** in "Core descriptions"). Fragments of glass in the groundmass are highly altered and show spherulitic texture, and ferromagnesian minerals (mainly clinopyroxene) are replaced with chlorite. Sample 320-U1332A-18X-CC (Piece 2A, 12–16 cm) is a partly altered phyric basalt with sparse plagioclase. Glass and clinopyroxene in the groundmass are preserved in a chilled margin. Calcite veins are observed in both pieces and show a distinct radiaxial fabric.

Sediments across the Eocene–Oligocene transition

An Eocene–Oligocene transition was recovered in two of the three holes at Site U1332 (Holes U1332A and U1332B) (Fig. **F8**). The transition was not recovered in Hole U1332C because of core disturbance associated with a shipboard power outage (see **"Operations"**). The Eocene/Oligocene boundary is formally defined by the extinction of the planktonic foraminifer genus *Hantkenina* but cannot be identified at Site U1332 because of poor preservation of planktonic foraminifers (see **"Biostratigraphy"**). Radiolarian and nannofossil bio- and magnetostratigraphy provide excellent age control, indicating that the Eocene/Oligocene boundary falls somewhere between the base of Chron 13n and the Biozone RP20/RP19 boundary (within Cores 320-U1332A-9H, 320-U1332B-9H, and 10H). The lithostratigraphy of the Eocene–Oligocene transition at Site U1332 is well captured in both of these holes and consists of a downhole change from light gray (10YR 7/2) and very pale brown (10YR 7/3) nannofossil ooze with diatoms to very pale brown (10YR 8/2) nannofossil ooze to brown (10YR 4/3) radiolarian nannofossil ooze and dark yellow brown (10YR 3/4) radiolarian ooze with clay (Fig. **F8**). The transition from pale nannofossil ooze to radiolarian ooze is comparatively abrupt (~1 m interval) and defines the Unit III/Unit IV boundary. An associated pronounced downhole increase occurs in magnetic susceptibility, together with pronounced downhole decease in GRA bulk density, L*, and $CaCO_3$ content (Figs. **F3, F8**). These lithostratigraphic results for the Eocene–Oligocene transition at Site U1332 are consistent with those obtained from Site U1331 and multiple sites drilled during ODP Leg 199, in particular Site 1220 (Shipboard Scientific Party, 2002b).

Approximately 8 m above the Eocene–Oligocene transition in Hole U1332C, a prominent sharp contact (interval 320-U1332C-9H-2, 95 cm) occurs between very pale brown (10YR 8/2) radiolarian nannofossil ooze to overlying brown (10YR 5/3) radiolarian nannofossil ooze (Fig. F9). In turn, this radiolarian nannofossil ooze transitions uphole into light gray (10YR 7/2) nannofossil ooze with radiolarians over an ~3.5 m thick interval. Magnetostratigraphy and radiolarian and nannofossil biostratigraphy, together with physical property series from the WRMSL and Section Half Multisensor Logger (SHMSL), demonstrate that this 3.5 m thick sequence is a duplication of latest Eocene through earliest Oligocene age interval cored below (see **"Biostratigraphy," "Paleomagnetism," "Physical properties,"** and **"Stratigraphic correlation and composite section"**). A similar duplicated (or replicated) sequence is also documented in Hole U1332B, but in this hole the sharp contact between pale earliest Oligocene sediments and darker overlying latest Eocene sediments occurs in the core catcher (Sample 320-U1332B-8H-CC, 3 cm) and is consequently disturbed (Fig. F9). This duplicated sequence, with its sharp basal contact, is interpreted to result from a mass movement, probably a slump or slide that reworked older sediments (that happened to be of Eocene–Oligocene transition age) into sediments of early Oligocene (C12r) age (Fig. F9). The lithostratigraphic integrity of the Eocene–Oligocene transition that lies ~8 m deeper in the section in all holes cored at Site U1332 is not affected (Fig. F8) and is very well correlated with that at Site 1220 using WRMSL physical property data (see **"Stratigraphic correlation and composite section"**).

Discussion

Eocene intervals with nannofossil ooze

The dominant lithology of Unit IV at Site U1332 is radiolarian ooze, but this unit also contains four discrete intervals where nannofossil ooze and radiolarian nannofossil ooze is a second major lithology (Fig. F3; see **"Site U1332 smear slides"** in "Core descriptions"). Two of these carbonate-rich intervals are comparatively thin (≤5 m thick each), consist entirely of radiolarian nannofossil ooze, and occur in Subunit IVa. The third carbonate-rich interval is thicker (~25 m), consists of an alternating sequence of nannofossil ooze and radiolarian nannofossil ooze, and spans almost all of Subunit IVb. The fourth interval occurs in the upper half of Subunit IVc (Fig. F3) and consists of alternating radiolarian ooze with clay and radiolarian nannofossil ooze. All four intervals show $CaCO_3$ contents (as measured by coulometry) that are above background for Unit IV with up to 60 wt% obtained in Subunit IVb (Fig. F3) and are separated by intervals dominated by radiolarian ooze. According to shipboard magnetostratigraphic results, the uppermost of these carbonate-rich intervals at Site U1332 occurs in sediments of late Eocene age (C16n.2n to C16r; ~35.5–36.5 Ma) (Fig. F3). The other three carbonate-rich intervals fall in the middle Eocene (estimated ages: Interval 2 = C18n.1n to C18n.1r, ~38.5–39.5 Ma; Interval 3 = within C18r middle RP15 to upper RP14 radiolarian zone, ~40–41.5 Ma; Interval 4 = middle to lower part of RP14, 42.5–43.8 Ma). These lithostratigraphic results are broadly consistent with those of Leg 199, especially ODP Sites 1218 and 1219 (Shipboard Scientific Party, 2002a) and the carbonate accumulation events (CAE [2?], 3, 4, and 6/7) of Lyle et al. (2005) that have been used to refine the Paleogene record of the CCD for the equatorial Pacific (Shipboard Scientific Party, 2002a; Van Andel, 1975).

Porcellanite and chert

In Subunit IVc, layers and pebbles of very dark brown (10YR 2/2) partially to well-lithified claystones, often layered or even laminated, are observed within alternating sequences of radiolarian nannofossil ooze, radiolarian ooze, and nannofossil radiolarian ooze of middle Eocene age in Cores 320-U1332A-15X through 17X. Within this sequence (Core 320-U1332A-16X = ~130 wireline log matched depth below seafloor [WMSF], ~135 CSF) (see **"Downhole measurements"**), a small peak above a stepwise change in NGR is observed in the downhole logging data but no equivalent feature is seen in the core NGR data. In hand specimen, the partially lithified claystones cleave along bedding planes that are particularly rich in clay and the well-lithified specimens exhibit some concoidal fracture indicative of partial secondary silicification. In a single sample (320-U1332-17X-1, 0–4 cm), a black very hard and vitreous pebble with distinct concoidal fracture was recovered. During thin section preparation this single sample proved significantly more resistant to cut by rock saw than the other samples taken from Subunit IVc for this purpose.

In thin section, all of the samples taken from Subunit IVc at Site U1332 show evidence of partial secondary silicification (see **"Site U1332 smear slides"** in "Core descriptions"). All but one of these samples are porcellanites (Fig. F6A, F6B, F6C). The single black very hard and vitreous pebble (Sample 320-U1332-17X-1, 0–4 cm), is termed "chert" (Fig. F6D; see **"Site U1332 smear slides"** in "Core descriptions"). In thin section, major components of the porcellanites are clay minerals, microcrystalline quartz, opaques (Fe oxides), and calcite, as well as biogenic shells and fragments from radiolarians and foraminifers. Foraminifer tests are predominantly filled with microcrystalline quartz. In many cases the original calcite mineralogy of the foraminifer test wall is preserved, but some are partially or entirely replaced by diagenetic silica. All of the porcellanite samples retain a distinct sedimentary fabric, with layers rich in clay, radiolarians and foraminifers, and microcrystalline quartz. Chert is mainly composed of microcrystalline quartz, clay minerals, and opaques. Areas show a breccia-like fabric of angular material with infill of chalcedonic quartz (Fig. F6D). No biogenic components were observed within the chert.

Summary

At Site U1332, Eocene seafloor basalt is overlain by ~150.4 m of pelagic sediments that are divided into five major lithologic units and subunits. Sediments are dominated by radiolarian and nannofossil ooze with varying amounts of clay and can be correlated with Sites 1219 and 1220 using biostratigraphic, magnetostratigraphic, and cyclostratigraphic (magnetic susceptibility and GRA density) results. The early Miocene sedimentary sequence is dominated by clay with radiolarians followed downhole by a late Oligocene alternation of radiolarian ooze with clay, nannofossil ooze with radiolarians, and nannofossil ooze. The early Oligocene is predominantly characterized by white nannofossil ooze with minor intercalations of radiolarian nannofossil ooze in the middle early Oligocene. The early middle Eocene sequence is very low in carbonate followed by a porcellanite interval of ~5 m. The middle through late Eocene section (Hole U1332A; ~95–140 CSF) is dominated by radiolarian ooze with varying amounts of clay, whereas nannofossil ooze is a secondary major lithology and occurs in four distinct intervals that broadly correlate with the lithostratigraphic results of Leg 199 and the CAEs of Lyle et al. (2005). The Eocene/Oliocene boundary is marked by a transition from dark brown radiolarian ooze to pale brown nannofossil ooze with radiolarians. A transition from Eocene siliceous sedimentation to Oligocene carbonate deposition is also observed in sediments from several other sites in the equatorial Pacific Ocean (e.g., Sites 1218 and 1219 and DSDP Sites 161 and 162) and probably reflects a deepening of the CCD associated with Antarctic glaciation (van Andel et al., 1975; Coxall et al., 2005).

Biostratigraphy

At Site U1332, we recovered a 148 m thick sequence of lower Miocene–lower middle Eocene radiolarian ooze, radiolarian clays with nannofossils, nannofossil ooze, and chert/porcellanite. The uppermost 10 m of clay is barren of calcareous microfossils and contains no age-diagnostic radiolarians. Nannofossil ooze is dominant in the Oligocene, and radiolarian ooze and clay are dominant in the Miocene and Eocene. A poorly recovered chert/porcellanite-rich sequence occurs in the lower middle Eocene. Radiolarians are present through most of the section and are well preserved in the Eocene. They provide a coherent high-resolution biochronology. Calcareous nannofossils are abundant and moderately well preserved in the Oligocene and poor to moderately well preserved in the Miocene and Eocene. Nannofossil datums and zonal determinations agree well with the radiolarian biostratigraphy; an integrated calcareous and siliceous microfossil biozonation is shown in Figure F10. A detailed age-depth plot including biostratigraphic and paleomagnetic datums is shown in Figure F11. Planktonic foraminifers are rare through the Oligocene and absent in the Miocene and Eocene. Benthic foraminifers are present through most of the section but are rare in all but the Oligocene lithologies. They indicate lower bathyal to abyssal paleodepths.

Calcareous nannofossils

Calcareous nannofossil biostratigraphy is based on analysis of core catcher samples from all three holes and from additional samples from each core section, predominantly from Hole U1332A. Depth positions and age estimates of biostratigraphic marker events are shown in Table T3. Nannofossils are abundant in the nannofossil oozes of the Oligocene and are consistently present through the Eocene, excepting short barren intervals in Cores 320-U1332A-9H through 12H and 15X through 17X, where radiolarian ooze with clay lithology dominates. When present in radiolarian clays and basal dark brown clays, nannofossils are common to abundant, but typically etched, and characterized by abundant disaggregated and/or fragmented placolith shields. Discoasters are much less affected by etching and are virtually the only nannofossils present in several lower middle Eocene and lower Miocene samples. In the nannofossil ooze lithology, preservation is moderately good.

The clay of Unit I in the uppermost portion of the section (0–17.4 m CSF) is barren of calcareous nannofossils. The interval from Samples 320-U1332A-3H-4, 100 cm, to 4H-CC (18.90–32.95 m CSF) yields low diversity and relatively poorly preserved nannofossil assemblages dominated by *Discoaster deflandrei* and *Triquetrorhabdulus carinatus*. The presence of rare *Sphenolithus delphix* in Sample 320-U1332A-3H-CC (23.51 m CSF) is indicative of a short interval (23.1–23.2 Ma) within Zone NN1, very close to the Oligocene/Miocene boundary.

The upper Oligocene interval yields low diversity nannofossil assemblages, and the most distinct bioevent is the top of *Sphenolithus predistentus* in Sample 320-U1332A-5H-1, 80 cm (33.20 m CSF). The marker species *Sphenolithus ciperoensis* is rare and sporadically distributed through much of the upper Oligocene, so the Zone NP24/NN1 boundary cannot be determined. The crossover from *Triquetrorhabdulus longus* to *T. carinatus* is an intra–Zone NP25 event (24.7 Ma) and occurs between Samples 320-U1332A-4H-2, 60 cm, and 4H-3, 60 cm (25.0 and 26.50 m CSF). Very small specimens (<4 µm) of *S. ciperoensis* occur alongside rare *Sphenolithus distentus* between Samples 320-U1332A-5H-1, 80 cm, and 6H-3, 70 cm, but the two species cannot be reliably distinguished because of small size and the occurrence of intermediate morphologies. As a result, we have not differentiated Zones NP24 and NP23. The base of *S. distentus* is an intra–Zone NP23 datum (30 Ma) and occurs in Sample 320-U1332A-6H-5, 70 cm (48.60 m CSF).

The lower Oligocene Zones NP23 and NP22 are determined by the top of *Reticulofenestra umbilicus* in Sample 320-U1332A-7H-7, 80 cm (61.20 m CSF), and the top of *Coccolithus formosus* in Sample 320-U1332A-8H-5, 50 cm (67.40 m CSF). The Eocene/Oligocene boundary lies between the top of *C. formosus* and the top of *Discoaster saipanensis,* which occurs in Sample 320-U1332A-10H-3, 80 cm (83.70 m CSF). The boundary is apparently complete at the resolution provided by the nannofossil biostratigraphy. This interval is associated with a lithologic change from pale nannofossil ooze to brown radiolarian clay.

The Eocene nannofossil Zones NP18–NP20 through NP14 are recognized using the top of *Chiasmolithus grandis* in Sample 320-U1332A-11H-6, 70 cm (97.60 m CSF); top of *Chiasmolithus solitus* in Sample 320-U1332A-13H-1, 140 cm (109.80 m CSF); the total range of *Nannotetrina fulgens* from Samples 320-U1332A-15X-2, 137 cm (128.77 m CSF), to 16X-2, 39 cm (137.39 m CSF); and the presence of *Discoaster sublodoensis* in Sample 320-U1332B-18X-CC (146.21 m CSF). The base of *Dictyococcites bisectus,* total range of *Discoaster bifax,* top and base of *Nannotetrina,* and top of *Discoaster lodoensis* datums were also useful in supporting these zonal determinations.

The dark brown clays resting on basalt in Hole U1332A are mostly barren of nannofossils, but several samples from Holes U1332B and U1332C contain age-diagnostic taxa indicative of Zone NP14. Samples 320-U1332B-18X-2, 48 cm (145.88 m CSF), and 18X-CC (146.21 m CSF) contain dissolution-affected assemblages that nevertheless contain common *D. lodoensis* and rare *D. sublodoensis*. In Hole U1332C, Sample 320-U1332C-18X-CC (147.25 m CSF) contains an etched assemblage without *D. lodoensis* but with rare *Nannotetrina*. These observations within a succession that was poorly recovered and which is largely barren of nannofossils suggests that the top of *D. lodoensis* and base of *Nannotetrina* datums occur within these lowermost sediments, indicating an age between 48.0 and 48.4 Ma.

Radiolarians

Radiolarian stratigraphy at Site U1332 spans the interval between Zone RN1 (base of the lower Miocene) and the upper part of Zone RP13 (middle Eocene) (Tables T4, T5, T6). At the top of the section the first two cores are barren of radiolarians (Table T7). The third core (Sample 320-U1332A-3H, 93–95 cm) contains a highly mixed assemblage ranging in age from middle Eocene through Miocene. The youngest species found in this mixture (*Theocorythium vetulum*) has a first appearance at ~7 Ma. This sample is probably from the upper Miocene but could be mixed with still younger, nonfossiliferous sediments. Preservation of the lower Miocene and Oligocene assemblages is generally poor to moderate, with the common occurrence of reworked, older microfossils.

Preservation improves somewhat in the lower Oligocene (Zone RP20); however, near the base of the Oligocene the sequence of first and last appearances of species within Zone RP20 seems to be repeated in the lower part of Core 320-U1332A-8H and the upper part of Core 9H. The base of Core 9H (Sample 320-U1332A-9H, 92–98 cm) is within the upper Eocene Zone RP19. There is substantial reworking of older middle Eocene microfossils in the Eocene part of Core 9H extending down into Cores 320-U1332A-10H and 11H. Radiolarians are generally abundant and well preserved throughout the Eocene section.

The oldest radiolarian-bearing sediments are found in Cores 320-U1332C-16X and 17X (Zone RP13). The lowermost cores in all three holes at this site are barren of radiolarians.

Diatoms

Diatoms were examined in core catcher samples from Holes U1332A–U1332C. The examined sequence represents the interval extending from the *Bogorovia veniamini* Zone through the *Coscinodiscus excavatus* Zone of Barron (1985, 2006) and Barron et al. (2004). Diatoms range in abundance from rare to abundant. Diatom preservation is variable but is generally poor to moderate. The intervals from Cores 320-U1332A-1H and 2H, 320-U1332B-1H and 2H, and U1332C-1H are barren of or contain rare diatoms. The interval is unzoned.

The interval from Samples 320-U1332A-3H-CC through 5H-CC is assigned to the *B. veniamini* Zone based on the occurrence of *B. veniamini* in these samples without *Rocella gelida*. Supporting these zonal assignments is the occurrence of *Cavitatus jouseanus* and *Rocella vigilans* in Sample 320-U1332A-5H-2, 115–116 cm; the occurrence of *Rossiella symmetrica* in Sample 320-U1332A-4H-4, 110–111 cm; and the occurrences of *Cestodiscus kugleri, R. vigilans,* and *C. jouseanus* in Samples 320-U1332A-4H-CC and 320-U1332C-5H-CC.

Samples 320-U1332A-6H-CC and 320-U1332C-6H-CC are assigned to the *R. vigilans* Zone based on the occurrence of *R. vigilans* without *B. veniamini*. The occurrence of *Kozloviella minor* and *C. jouseanus* in Sample 320-U1332C-6H-CC suggests placement of this sample into Subzone C of this zone, but such a zonal assignment is tentative given the typical poor state of diatom preservation. The *Cestodiscus trochus* Zone was not recognized because of sample spacing and/or preservation.

The *C. excavatus* Zone is recognized from Samples 320-U1332A-7H-4, 110–111 cm, through 8H-CC based on the occurrence of *C. excavates* in this interval. The occurrence of *C. trochus* and *Cestodiscus robustus* in occasional samples through this interval support this zonal assignment.

Diatoms are typically rare or absent from samples below Core 320-U1332A-8H. The exceptions are Samples 320-U1332A-13H-2, 100–101 cm, and 320-U1332C-13H-CC, which contain few diatoms with poor preservation. The assemblage is representative of the middle Eocene. Sample 320-U1332A-13H-2, 100–101 cm, contains specimens of *Triceratium brachitium* and *Hemiaulus* spp. Sample 320-U1332C-13H-CC contains specimens of *Triceratium inconspicum* and *Hemiaulus* spp.

Planktonic foraminifers

Core catcher samples were analyzed from all three holes, and additional samples were taken in Hole U1332A (two per core) from any light-colored sediment intervals, which we assumed had a higher carbonate content. Planktonic foraminifers are absent from the Miocene and Eocene sediments but are consistently present in the Oligocene (from Zone O6 to the latest Eocene/earliest Oligocene); however, distinction of zones between Zone O2 and the late Eocene was hindered by the absence of age-diagnostic taxa of *Hantkenina* spp., *Turborotalia cerroazuloensis,* and *Pseudohastigerina naguewichensis*. Depth positions and age estimates of biostratigraphic marker events identified are shown in Table T8. Taxon ranges and abundances are shown in Table T9. Planktonic foraminifer assemblages show good to moderate preservation in the upper Oligocene, but both preservation and abundance of planktonic foraminifers decrease downcore. We note that a higher diversity of Oligocene taxa is recorded at Site U1332 than at Site U1331, ~20 versus 12 species, respectively, which is consistent with the better preservation of fauna observed at this site (see Table T9).

The lowermost part of planktonic foraminifer Zone O6 was inferred between Samples 320-U1332A-3H-7, 75–77 cm, and 4H-7, 38–40 cm, and in Sample 320-U1332B-5H-CC based on the presence of a number of different *Dentoglobigerina* spp., which range to the latest Oligocene (Olsson et al., 2006), and the absence of *Paragloborotalia opima, Paragloborotalia kugleri,* and *Paragloborotalia pseudokugleri*. A Zone O6 assignment for these samples is also consistent with nannofossil (Zone NP24) and radiolarian (Zone RP21) determinations. The presence of the biostratigraphic marker species *P. opima* indicates the presence of planktonic foraminifer Zones O2–O5 between Samples 320-U1332A-5H-2, 100–102 cm, and 6H-CC, in Sample 320-U1332B-6H-CC, and in Samples 320-U1332C-4H-CC through 5H-CC. The general absence of age-diagnostic Oligocene taxa, assumed to be dissolution susceptible based on their general absence here and during biostratigraphic investigations during ODP Leg 199 (Shipboard Scientific Party, 2002a), hindered further differentiation of the Oligocene. An exception is in Sample 320-U1332C-5H-CC where *Globigerina angulisuturalis* and *P. opima* were both found, which allowed the identification of planktonic foraminifer Zones O4 and O5. However, the absence of *Chiloguembelina cubensis* prevented further differentiation between Zones O4 and O5. Typical Oligocene taxa identified in samples were *Catapsydrax dissimilis, Catapsydrax unicavus, Dentoglobigerina tripartita, Dentoglobigerina galavisi, Dentoglobigerina pseudovenezuelana, Globoquadrina euapertura, Globoquadrina venezuelana, Paragloborotalia nana, Subbotina angiporoides, Subbotina utilisindex,* and *Turborotalia increbescens*. Below Samples 320-U1332A-6H-CC, 320-U1332B-7H-CC, and 320-U1332C-6H-CC, the low abundance of planktonic foraminifers coupled with the absence of age-diagnostic taxa meant that the assemblage could only be assigned to a broad zonal range (e.g., Zones E13–O2).

Benthic foraminifers

Benthic foraminifers were examined semiquantitatively in three Site U1332 holes. Benthic foraminifers occurred continuously in calcareous nannofossil ooze of the Oligocene, whereas they were generally rare in radiolarian ooze of the Eocene. Occurrence of benthic foraminifers at this site is shown in Table T10.

The upper two samples in Hole U1332A (320-U1332A-1H-CC and 2H-CC; 3.86–13.62 m CSF) did not contain benthic foraminifers. In the interval from Samples 320-U1332A-3H-CC through 7H-CC (23.51–61.49 m CSF), *Nuttallides umbonifer, Oridorsalis umbonatus, Cibicidoides mundulus, Globocassidulina subglobosa,* and *Gyroidinoides* spp. were common and *Cibicidoides havanensis* and *Cibidoides grimsdalei* were subordinate. *O. umbonatus* and *Cibicidoides* spp. were generally common in the lower part of the interval (maximum = 24% and 16%, respectively), whereas *N. umbonifer* was abundant in the upper part of the interval (maximum = 22%). A similar faunal transition was recognized in Hole U1332B (Samples 320-U1332B-4H-CC through 8H-CC; 29.61–67.47 m CSF) and Hole U1332C (Samples 320-U1332C-4H-CC through 9H-CC; 36.52–75.91 m CSF). In addition, tube-shaped agglutinated forms (e.g., *Rhizammina* spp.) and *Reophax* spp. were sometimes abundant (maximum = 47% and 13%, respectively) in the uppermost part of the interval (e.g., Sample 320-U1332B-3H-CC; 19.97 m CSF). Preservation of foraminifer tests is very good to good. These faunal compositions indicate lower bathyal and abyssal paleodepths during the Oligocene, based on van Morkhoven et al. (1986). The Oligocene fauna are characterized by abundant calcareous hyaline forms, such as *N. umbonifer, O. umbonatus, C. mundulus, G. subglobosa,* and *Gyroidinoides* spp., and are similar to those observed in previous studies in the eastern equatorial Pacific (Site 573, Thomas, 1985; Sites 1218 and 1219, Nomura and Takata, 2005). However, assemblages dominated by agglutinated foraminifers occur much earlier (late Oligocene) at this site than at Sites 1218 and 1219. This temporal offset may be represent a preservational bias caused by the greater water depth at this site than those found at Sites 1218 and 1219.

Samples 320-U1332A-10H-CC through 15X-CC (89.89–132.93 m CSF) rarely contain benthic foraminifers. Agglutinated forms, such as *Rhizammina* spp. and *Spiroplectammina spectabilis,* were found with some calcareous hyaline taxa (e.g., *Siphonodosaria antillea*). Preservation of these tests was poor. Similar occurrences were also recognized in Samples 320-U1332A-9H-CC through 17X-CC (77.09–135.06 m CSF) and in Samples 320-U1332A-10H-CC through 17X-CC (85.53–139.91 m CSF). Calcareous hyaline forms, such as *O. umbonatus, Nuttallides truempyi, Cibicidoides eocanus,* and *C. grimsdalei,* were present at least in two horizons, Samples 320-U1332A-11H-CC (98.52 m CSF) and 13H-CC (118.38 m CSF). Similar occurrences were also recognized in Samples 320-U1332B-13H-CC (110.76 m CSF) and 10H-CC through 17X-CC (85.53–139.91 m CSF). However, preservation of calcareous foraminifer tests was poor in the lower part of the study interval. These fauna suggest lower bathyal to abyssal paleodepth at this site in the middle to late Eocene. Faunal associations of these calcareous taxa in the middle to late Eocene are similar to those observed at Site U1331 and previous preliminary studies in the eastern equatorial Pacific (Shipboard Scientific Party, 2002a). Common occurrences of these calcareous foraminifers in Hole U1332A roughly coincide with high-carbonate intervals (see **"Lithostratigraphy"** and **"Geochemistry"**) that may be related to carbonate accumulation events noted by Lyle et al. (2005).

Paleomagnetism

We measured and analyzed the remanent magnetization of archive-half sections from 47 cores (39 APC and 8 XCB cores) collected from three holes at Site U1332, excluding core catcher sections and other sections completely disturbed during coring. The natural remanent magnetization (NRM) of each section was measured before and after alternating-field (AF) demagnetization, with AF demagnetization typically consisting of a single 20 mT step. When time permitted, NRM was also measured after 5, 10, and/or 15 mT steps.

We processed the data extracted from the Laboratory Information Management System (LIMS) database by removing all measurements collected from disturbed intervals, which are listed in Table **T11,** and all measurements that were made within 5 cm of the sections ends, which are biased by sample edge effects. Cleaned data are available for each hole by AF demagnetization level in Tables **T12, T13, T14, T15, T16, T17, T18, T19,** and **T20.** Curation errors occurred for Sections 320-U1332A-10H-4 and 14H-4, in which the halves that should have been treated as the working halves (with double lines along the core liner) were switched with the archive halves (with a single line along the core liner). We measured these two sections as archive halves before the errors were noted. Thus, the working halves were measured in the magnetometer instead of the archive halves and discrete samples were taken from the archive halves instead of the working halves. In Tables **T12, T16, T21,** and **T22,** we corrected the declinations of samples from these sections by flipping them by 180° (note that data in the LIMS database are not corrected). We also noticed that Section 320-U1332C-6H overlaps Section 320-U1332C-7H by ~3 m CSF. This happened because Core 6H was advanced 4 m but recovered >7 m of core. The upper 2.6 m was slurry (soupy mixed sediments). To partially fix the overlap, we subtracted 2.6 m from the Core 6H depths. This brought the top of the good part of Core 6H beneath the base of Core 320-U1332C-5H and reduced the overlap between Cores 6H and 7H to ~50 cm (Tables T19, T20).

For data from the 20 mT demagnetization step, we computed the mean paleomagnetic direction for each core using Bingham statistics (Table T23) with a program developed by Tanaka (1999). Unlike Fisher statistics, Bingham statistics can treat bipolar data sets and compute a principal axis as well as two associated semiaxes of the data set. When a data set consists of a sufficient number of paleomagnetic direction data with normal or reversed polarity, this principal axis corresponds to the orientation of the normal or reversed polarity field. We used all declination and inclination data for the computation and adopted the resultant principal axes as the mean paleomagnetic directions. These mean directions were inverted when they were interpreted to be representative of reversed polarity. By subtracting the mean declination from each observed declination, the azimuth of the core can be approximately reoriented back into geographic coordinates as discussed in "Paleomagnetism" in the "Site U1331" chapter.

In the absence of other evidence, this reorientation method has ambiguity in distinguishing magnetic north and south. By correlating downhole polarity reversal sequences among holes, using distinct reversal patterns, and taking advantage of age constraints provided by biostratigraphy, it is fairly straightforward to determine a continuous polarity stratigraphy downhole and hence to obtain the correct azimuthal orientation of the core. This only breaks down when significant coring gaps occur or when rotation occurs between pieces of core within a single core, which is the case for all cores collected with the XCB. Hence XCB cores are not reoriented, nor can we confidently determine polarity from these cores because the inclination is generally too shallow at paleoequatorial sites, like all of the sites cored during Expedition 320/321. Reoriented declinations are provided for Holes U1332A–U1332C in Tables T16, T18, and T20, respectively, for the data collected after AF demagnetization at 20 mT.

We also measured NRM, mass, and bulk magnetic susceptibility for 91 discrete paleomagnetic samples, with one sample collected about every section from Hole U1332A. Of these, 76 samples were subjected to progressive AF demagnetization up to 60 mT. Remanence measurements and characteristic remanent magnetization (ChRM) directions computed using principal component analysis (PCA) are given in Tables T21 and T22, respectively. Magnetic susceptibilities and masses, along with volumes estimated using moisture and density (MAD) data (see "Physical properties"), are given in Table T24. This table also includes whole-core magnetic susceptibilities for depth intervals corresponding to the discrete samples, which are used for checking the scale factor for converting the whole-core raw susceptibility meter measurements into true volume normalized susceptibility values (0.68×10^{-5}) (see "Paleomagnetism" in the "Methods" chapter).

Results

Downhole variations in paleomagnetic data from split-core and discrete samples and magnetic susceptibility data from whole-core and discrete samples are shown in Figures F12, F13, and F14. As is typical for cores from DSDP, ODP, and IODP (e.g., Shipboard Scientific Party, 2002a), Site U1332 cores suffer a substantial drilling overprint. The overprint is primarily a viscous isothermal remanent magnetization (IRM), which results from the sediments residing inside the relatively magnetic BHA, drill pipe, and steel core barrel (and, to a lesser extent, the nonmagnetic core barrel) for about 15–45 min from the time it is collected until it is removed from the core barrel on the rig floor.

The most obvious evidence of the overprint is the steep inclination (typically ~70°–80°) measured prior to demagnetization. After AF demagnetization at 10 to 20 mT, the inclination becomes very shallow in general, as expected for sediments deposited near the equator. The effect and removal of the drilling overprint are evident from AF demagnetization behavior of the discrete samples (Fig. F15).

Following removal of the drilling overprint, a stable component of magnetization is resolved for AF demagnetization between 10 and 60 mT (Fig. F15). We interpret this ChRM to be the primary depositional remanent magnetization. Discrete samples have ChRM directions, as determined with PCA, that commonly agree within a few degrees with those of the coeval intervals of the split-core samples (Table T22; Fig. F12), for which the 20 mT demagnetization results are used as an estimate of the ChRM. This indicates that any overprint generally is successfully removed with AF demagnetization up to 20 mT. Within some intervals, however, the inclinations remain steep even after demagnetization, indicating the drilling overprint still dominates in these intervals. For example, Core 320-U1332A-2H (4.0–13.4 m CSF) has a mean inclination of –76.09° (Table T23). Inclinations and remanent magnetization intensities from a few discrete samples from this core do not agree with those from the split-core samples (Fig. F12). These are mainly limited to the upper 20 m in

Hole U1332A, and it is considered that in this interval the split-core samples were more strongly overprinted.

It is likely that a small overprint remains in many intervals even after magnetic cleaning because the inclinations are not symmetrically distributed about zero. Instead, they are biased several degrees toward positive values, which could possibly result from a Brunhes field overprint or a drilling overprint. Regardless, any overprint is sufficiently small that variations in inclination can be used to aid in determining polarity even though the mean inclination at the site is very shallow. In such cases, reversed polarity intervals consistently have slightly shallower inclination than normal polarity intervals. The declination is, however, the primary parameter used for polarity determination, as it changes by ~180° across polarity reversals (Figs. **F12, F13, F14**).

Magnetostratigraphy

Interpretation of the magnetostratigraphy is relatively uncomplicated, as summarized in Table **T25** and Figures **F16, F17,** and **F18.** We consider that the bottom of the APC cores extended down through reversal boundaries Chron C19r/C20n (42.536 Ma) for Hole U1332A (124.70 m CSF) and Chron C18n.2n/C18r (40.084 Ma) for Holes U1332B (102.25 m CSF) and U1332C (106.95 m CSF). The chron boundary closest to the Oligocene/Miocene boundary (C6Cn.2n/C6Cn.2r; 23.030 Ma) occurs at 22.40 m CSF in Hole U1332A and at 22.88 m CSF in Hole U1332C. The Eocene/Oligocene boundary occurs just below the Chron C13n/C13r reversal (33.705 Ma), which is at 75.33 m CSF in Hole U1332A and 74.33 m CSF in Hole U1332B. The magnetostratigraphies for the three holes are compared in Figure **F19.**

Complications include (1) the upper few cores of each hole and (2) a slump that occurs just above the Eocene/Oligocene boundary. Paleontological age estimates from core catcher samples are Quaternary age for Core 320-U1332A-1H, 23.29–22.98 Ma for Core 3H, 22.26–22.35 Ma for Core 320-U1332B-3H, and 21.9–22.2 Ma for Core 320-U1332C-2H (see **"Biostratigraphy"**). No age estimates were obtained for Cores 320-U1332A-2H, 320-U1332B-1H and 2H, and 320-U1332C-1H. Age data indicate that hiatuses occur between sediments of Pleistocene–Pliocene and early Miocene age. We tentatively assign geomagnetic chrons from C1n to C2Ar for Cores 320-U1332A-1H and 2H, C1n to C2An.3n for Cores 320-U1332B-1H and 2H, and C1n to C2r.1r for Core 320-U1332C-1H. The hiatuses are considered to occur below these horizons. Below the hiatus, we identify the occurrence of Chron C6An.1r at 14.20 m CSF in Hole U1332A, Chron C6n at 13.60 m CSF in Hole U1332B, and Chron C5En at 12.30 m CSF in Hole U1332C, which agree with paleontological age constraints (Figs. **F16, F17, F18**).

Lithostratigraphic observations, paleomagnetic data, magnetic susceptibility data, and paleontological age estimates from core catcher sections suggest that Cores 320-U1332A-8H and 9H, 320-U1332B-8H and 9H, and 320-U1332C-9H penetrated a slump (see **"Lithostratigraphy," "Biostratigraphy,"** and **"Physical properties"**). The slump occurs just above the Eocene/Oligocene boundary. As a result, the upper part of Chron C13n and the lower part of Chron C12r are repeated in the sedimentary succession as evidenced by the polarity reversal sequence and the distinct and coherent variations in remanent magnetization (Figs. **F20, F21, F22**). The basal surface of the slump (the décollement) is a sharp contact, with sediment above and below having sustained no visible or measurable deformation.

Geochemistry

Sediment gases sampling and analysis

Headspace gas samples were taken at a frequency of one sample per core in Hole U1332A as part of the routine environmental protection and safety monitoring program. All headspace samples had nondetectable levels of methane (C_1; <1 ppmv), with no higher hydrocarbons, consistent with the low organic carbon content of these sediments.

Interstitial water sampling and chemistry

Twenty interstitial water samples were collected using the whole-round squeezing approach (Table **T26**). Additionally, 43 samples were collected using Rhizon samplers from Sections 320-U1332B-4H-1 through 7H-6 with a sampling frequency of two samples per section (Table **T27**). These sections were selected for Rhizon sampling because of a decrease in alkalinity revealed by the whole-round samples (Fig. **F23**). Rhizons were applied as described in **"Geochemistry"** in the "Site U1331" chapter. Chemical constituents were determined according to the procedures outlined in **"Geochemistry"** in the "Methods" chapter. In the following, we first describe the overall site geochemistry, combining the squeezed and Rhizon samples into single profiles with depth, and then present a more detailed comparison of squeezed and Rhizon samples in the depth interval where they overlap.

Chlorinity varies relatively little with depth, with values ranging mainly from 556 to 570 mM (Fig. **F23**). However, chlorinity values reveal a distinct increase from 556 to 565 mM in the uppermost 30 m CSF, potentially reflecting the change from the more saline ocean at the Last Glacial Maximum to the present (Adkins and Schrag, 2003). Alkalinity ranges from 2.3 to 3.4 mM. Alkalinities increase in the uppermost 30 m CSF from 2.3 to 3.1 mM and then drop to a distinct minimum of ~2.3 around 40 m CSF. Below 50 m CSF alkalinities increase steadily toward a value of 3.4 mM in the deepest sample. Sulfate concentrations are relatively constant and near seawater values. Low alkalinities and high sulfate concentrations indicate that organic matter supply is not sufficient to drive redox conditions to sulfate reduction. Dissolved phosphate concentrations are ~2 µM in the shallowest sample, decreasing to below detection limit in the uppermost ~25 m CSF. Dissolved manganese is 8–9 µM from 7 to 11 m CSF, with peak manganese values shallower than the peak dissolved iron value of ~1.0 µM at ~11 m CSF. Because of the high sulfate concentrations, dissolved Ba concentrations are low and relatively homogeneous, with values between 2 and 3 µM.

Concentrations of dissolved silicate increase with depth from ~400 to ~1000 µM. Superimposed on the gradual increase in dissolved silicate with depth is a pronounced minimum at ~80 m CSF. This is slightly deeper than the color change from light to dark that occurs at the lithologic Unit III to Unit IV transition (see **"Lithostratigraphy"**).

Calcium concentrations increase slightly with depth, with values ranging from 10 to 12 mM and a local minimum around 50 m CSF (Fig. **F23**). Magnesium concentrations are relatively constant, ranging from 50 to 53 mM (Figs. **F23**).

Lithium concentrations decrease from ~26 µM at the surface to 20 µM near basement, with the strongest decrease apparent between 40 and 50 m CSF. Strontium shows relatively little variation, with concentrations ranging from 77 to 93 µM. Boron concentrations range between 400 and 490 µM, slightly decreasing between 40 and 50 m CSF.

Interstitial water samples derived from Rhizon samplers (Fig. **F24**) and whole-round squeezing generally show good agreement (Fig. **F25**). Because these two data sets were collected in different holes (Hole U1332B is 20 m north of Hole U1332A), data are plotted in CCSF-A, to facilitate comparison. Elements that show good agreement with respect to absolute concentrations as well as observed trends include Li, K, and Sr. Magnesium and calcium show similar trends in both data sets but with constant offsets of 1.25 and 0.25 mM, respectively. These correspond to 2.5% of the measured values, and they might be related to day to day variability of the inductively coupled plasma–atomic emission spectroscopy (ICP-AES) analyses. However, Mg/Ca ratios show a good agreement between both sampling techniques, irrespective of the applied corrections for Mg and Ca. Boron concentrations are identical in the upper part of the investigated interval, but Rhizon samples are slightly enriched in boron in the lower part. However, it is unclear if this feature is an analytical or sampling artifact. The same holds true for alkalinity values. Between 28 and 30 m CCSF-A and 50 and 65 m CCSF-A both sampling techniques reveal results indistinguishable within typical analytical precision. Rhizon samples did not reproduce the distinct decrease in alkalinity centered at 40 m CCSF-A obtained from the whole-round samples. Several aspects of Rhizon sampling might be responsible for this. First, Rhizon sampling was only conducted after the core sections were processed through the fast track system. Second, Rhizon sampling pulls a vacuum on the sediment to withdraw fluid. Third, because of work flow imposed by the rapidly acquired samples, alkalinities of the Rhizon samples were not measured directly after retrieval. We expect this third factor to have only small effects in these samples with no/limited sulfate reduction and relatively low alkalinities.

Bulk sediment geochemistry: major and minor elements

At Site U1332, bulk sediment samples for minor and major element analyses were distributed over the complete depth range to target all major lithologic units (0–150 m CSF; Hole U1332A). We analyzed concentrations of silicon, aluminum, iron, manganese, magnesium, calcium, sodium, potassium, titanium, phosphorus, barium, copper, chromium, scandium, strontium, vanadium, yttrium, and zirconium in the sediment by ICP-AES (Table **T28**).

Bulk sediment SiO_2 ranges between 12 and 75 wt%, with values around 50 wt% from 0 to 40 m CSF and low values (10–20 wt%) between 40 and 65 m CSF. Below 70 m CSF, SiO_2 concentrations vary between 40 and 75 wt%. Concentrations of Al_2O_3 range from 0.5 to 13 wt%, with values decreasing in the upper 60 m CSF from 13 to 0.5 wt%. Below 60 m CSF, Al_2O_3 concentrations are between 0.5 and 2 wt%, with two peaks at 80 and 145 m CSF with values of 6 and 4 wt%, respectively. A similar pattern is displayed by TiO_2 (0.01–0.6 wt%), K_2O (0.25–2.4 wt%), Zr (20–205 ppm), and Sc (1.4–30 ppm).

Iron decreases from 6 wt% Fe_2O_3 at the surface to 0.4 wt% at 55 m CSF. Between 60 and 130 m CSF, concentrations vary between 1 and 5 wt%. Below 140 m CSF, values increase up to >13 wt% (measured value exceeded the calibrated concentration range). Similar trends are shown by MnO (0.03 to >0.2 wt%), MgO (0.03–21 wt%), copper (53 to >140 ppm) and vanadium (60 to >330 ppm). The peak concentrations of Mn, Cu, and V could not be quantified because they exceeded the calibrated range (see Table T9 in the "Methods" chapter).

Calcium (CaO) ranges from 0.4 to 40 wt%, with high values corresponding to the minimum in SiO_2 and Al_2O_3 between 40 and 70 m CSF and at 80 m CSF. Strontium concentrations range from 60 to >700 ppm, showing a similar pattern to CaO.

Bulk sediment geochemistry: sedimentary inorganic and organic carbon

$CaCO_3$, IC, and TC concentrations were determined on sediment samples from Hole U1332A (Table T29; Fig. F26). $CaCO_3$ concentrations range between <1 and 90 wt%. In the uppermost ~17 m CSF, $CaCO_3$ concentrations are very low (<1 wt%), below which concentrations vary up to 70 wt% at depths from ~17 to 32.6 m CSF. From 32.6 to 75.5 m CSF, $CaCO_3$ concentrations are consistently very high (48–90 wt%), and between 75.5 and 110 m CSF, $CaCO_3$ concentrations are low, except for a high of ~40 wt% at 98 m CSF. Below 98 m CSF, $CaCO_3$ concentrations are variable, ranging from 1.2 to 60 wt%. Variations in $CaCO_3$ concentrations correspond to lithostratigraphic changes (see **"Lithostratigraphy"**).

TOC concentrations were determined separately by a difference method and by an acidification method (see **"Geochemistry"** in the "Methods" chapter) (Table T29; Fig. F26). TOC concentrations determined by the normal difference method range from <0.1 to 1.6 wt% (Table T29). These values are probably overestimates because they are determined as a small difference between two numbers comparable in magnitude. Therefore, TOC analyses were performed only by the acidification method for the remaining PEAT sites. For Site U1332, we analyzed TOC on carbonate-free sediments after treatment by acidification. We calculated a detection limit of 0.03 wt% for the TC measurements using the acidification technique. TOC concentrations by this acidification method are very low throughout the sediment column, with a range from below the detection limit to 0.18 wt% (Fig. F26). In the uppermost ~2.5 m CSF, TOC concentrations are slightly elevated (0.16–0.18 wt%). TOC concentrations are very low (below detection limit) from 32.6 to 75.5 m CSF, corresponding to the depths where $CaCO_3$ concentrations are high. Below 95 m CSF, TOC concentrations are slightly higher (0.04–0.05 wt%).

Physical properties

Physical properties at Site U1332 were measured on whole cores, split cores, and discrete samples. WRMSL (GRA bulk density, magnetic susceptibility, and *P*-wave velocity), thermal conductivity, and NGR measurements comprised the whole-core measurements. Compressional wave velocity measurements on split cores and MAD analyses on discrete core samples were made at a frequency of one per undisturbed section in Cores 320-U1332A-1H through 18X. Compressional wave velocities were measured toward the bottom of sections. MAD analyses were located 10 cm below the carbonate analyses (see **"Geochemistry"**). Lastly, the SHMSL was used to measure spectral reflectance on archive-half sections.

Density and porosity

GRA provided wet bulk density from whole cores (Fig. F27), and MAD samples gave a second, independent measure of wet bulk density, along with providing dry bulk density, grain density, water content, and porosity from discrete samples (Table T30; Fig. F28). MAD and GRA bulk density measurements display the same trends and are also similar in absolute values through the entire section (Fig. F28). Cross-plots of wet and dry bulk density versus GRA density show excellent correlation between MAD and GRA data (Fig. F29).

Generally, wet bulk density corresponds to changes in lithology (Fig. F27). Wet bulk density is ~1.24 g/cm^3 at the seafloor and varies between 1.2 and 1.25 g/cm^3 through Units I and II. A slight step toward lower values (1.2 g/cm^3) at ~12 m CSF shows the change from clay- to radiolarian-dominated lithology. The top of Unit III is marked by an increase in density to 1.5 g/cm^3, with high-amplitude variation in this unit (from 1.4 to 1.6 g/cm^3). A sharp decrease in wet bulk density (to ~1.2 g/cm^3) occurs at the base of Unit III. Wet bulk density is relatively uniform with low-amplitude variations at ~1.2 g/cm^3 in Subunit IVa. An increase in wet bulk density accompanies the lithologic change toward more carbonate in Subunit IVb. Density is lower in Subunit IVc. An increase in GRA bulk density in Unit V is corroborated by a single discrete MAD wet bulk density value (1.45 g/cm^3).

Variation in grain density in Hole U1332A generally matches changes in lithology (Fig. F28). Grain density averages 2.7 g/cm^3 in Unit III. In other units grain density averages 2.5 g/cm^3 with variation from 2.1 to 2.8 g/cm^3 and a high of 2.9 g/cm^3 present near the seafloor. This variation is expected to be related to variations in the radiolarian content (opal = 2.2 g/cm³) and carbonate material (calcite = 2.7 g/cm³).

Porosity averages 85% in Units I and II, decreases to 70% in Unit III (Fig. **F28**), and rises again to ~80% in Subunit IVa. Porosity averages 80% in Subunits IVb and IVc and Unit V.

Magnetic susceptibility

Whole-core magnetic susceptibility measurements correlate well with the major differences in lithology and changes in bulk physical properties (Fig. **F27**). Magnetic susceptibility values increase gradually through Unit I from 20 × 10^{-5} to 40 × 10^{-5} SI, with a major spike occurring at ~12 m CSF (100 × 10^{-5} SI). A decrease in susceptibility marks the top of Unit II, and susceptibility remains low to the top of Unit III, where it gradually rises to ~10 × 10^{-5} SI. The base of Unit III contains a sharp rise in susceptibility to 40 × 10^{-5} SI. Magnetic susceptibility shows small amplitude variations in Unit IV, with a marked decrease in average magnetic susceptibility values from 28 × 10^{-5} to 18 × 10^{-5} SI at ~100–108 m CSF. Susceptibility appears to be higher in Unit V; however, core recovery is incomplete in this interval.

Compressional wave velocity

Shipboard results

Compressional wave velocity was measured by the *P*-wave logger (PWL) on all whole cores from Holes U1332A–U1332C and by the insertion and contact probe systems on undisturbed sections of split cores from Hole U1332A (Table **T31;** Fig. **F30**), allowing determination of velocities in the *x*-, *y*-, and *z*-directions. Initial processing revealed an offset of ~50 m/s between PWL and discrete *x*- and *y*-directions and a difference of ~100 m/s for the *x*-direction. Values returned from the PWL generally varied between 1400 and 1450 m/s—considerably lower than the expected values and the calibrated value for water at 1500 m/s. Trials with the water-filled core liner on the PWL and discrete contact probe suggested that core liner parameters were not being used in the PWL's processing computations. This has now been confirmed, and previously recorded PWL velocity data have been corrected by subtracting 2.617 µs (the time taken for a *P*-wave to move through two layers of 2.8 mm thick core liner with a velocity of 2140 m/s) from the traveltime given by the PWL. Velocity was then recalculated using the time provided (corrected data have been uploaded into the database). This section discusses the corrected PWL data.

Corrected whole-core and split-core data follow similar trends, with key features occurring at similar locations (Fig. **F30**). An excellent correlation between PWL and *y*-axis values is observed from 0 to 80 m CSF. *Z*-axis measurements show good correlation in this interval with some values underestimated by ~40 m/s. Below 80 m CSF no *z*-axis measurements were obtained and the *y*-axis values significantly underestimate velocity (~1400 m/s) because the sediments are predominantly radiolarian ooze that is poorly cemented and so splits/fractures easily when the transducers are inserted. *X*-axis measurements are generally ~80 m/s faster than PWL values throughout the succession; this is expected to be related to the pressure applied to the sediments by the contact probes—increased sediment compactness, and thus traveltime.

PWL data show a limited relationship between velocity and lithology downhole (Fig. **F30**); the general trend is a slight velocity increase with depth. More information on the relationship between downhole trends in velocity and lithology can be detailed using the cross-plot of velocity (PWL) and wet bulk density (GRA) (Fig. **F31**). At low densities (<1.2 g/cm³) all units show considerable variability in velocity. All units apart from Unit III show a very slight decrease in velocity (from 1600 to ~1520 m/s) with increased density (from 1.2 to 1.45 g/cm³). Unit III shows a correlation where density and velocity increase together and may relate to the increased carbonate content of this unit.

Postcruise correction

During the initial sampling of Hole U1337A, it was observed that *x*-direction velocities are consistently higher than other velocities and that PWL velocities are consistently low for Hole U1337A and all holes drilled at Sites U1331–U1336. It was determined that the high *x*-directed velocities are the result of using an incorrect value for the system delay associated with the contact probe (see **"Physical properties"** in the "Site U1337" chapter). Critical parameters used in this correction are system delay = 19.811 µs, liner thickness = 2.7 mm, and liner delay = 1.26 µs. PWL velocities were corrected for Hole U1337A by adding a constant value that would produce a reasonable velocity of water (~1495 m/s) for the quality assurance/quality control (QA/QC) liner (see **"Physical properties"** in the "Site U1337" chapter). These corrections have not been applied to the velocity data presented in this chapter.

Natural gamma radiation

NGR was measured on all whole cores at Site U1332 (Fig. **F27**). The highest NGR values are present at the seafloor (~130 counts per second [cps]) and decrease rapidly, reaching 15 cps at 5 m CSF. NGR increases in

Unit I to 22 cps at 11 m CSF and then decreases to ~9 cps at 15 m CSF. This feature appears in all three holes and is a useful independent check on stratigraphic correlation based on magnetic susceptibility and GRA measurements. NGR is relatively uniform throughout the remainder of the section; however, relatively small variations (5–10 cps) occur at various locations downhole and can be identified in all three holes. At the top boundary of Subunit IVa, NGR values increase sharply to 9 cps (at 75 m CSF) and decrease gradually to 6 cps at ~84 m CSF. A prominent shift of NGR in the gamma ray pass of the Hole U1332A borehole log at 131 m WSF (see **"Downhole measurements"**) is not observed in the cores. NGR is slightly higher in the basal intervals recovered from Cores 320-U1332A-17X and 320-U1332B-18X.

Thermal conductivity

Thermal conductivity was measured on the third section of each core from Hole U1332A (Table **T32**). Thermal conductivity measurements show a strong dependence on porosity in intervals containing >20% calcium carbonate (see **"Geochemistry"**). Thermal conductivity is ~0.8 W/(m·K) in Units I and II (Fig. **F32**). In Unit III, values increase to between 1 and 1.2 W/(m·K). In Subunit IVa, values return to 0.8 W/(m·K). A single measurement in Subunit IVb suggests thermal conductivity is higher in this unit. Thermal conductivity has been used with borehole temperature to investigate heat flow (see **"Downhole measurements"**).

Reflectance spectroscopy

Spectral reflectance was measured on split archive section halves from Holes U1332A–U1332C using the SHMSL (Fig. **F33**). The parameters L* (black–white), a* (green–red), and b* (blue–yellow) follow changes in lithology, with variations in L* and b* correlating very well to carbonate content, density, and magnetic susceptibility. The parameter a* has a slightly more limited relationship with lithologic variation downhole. Carbonate-rich sediments are found in Unit III and Subunit IVb; these intervals are represented by a distinct increase in the L* and b* values in these sections. This feature is less obvious in the a* record. The upper half of Unit I is marked by high L*, a*, and b* values (averaging 62, 5.1, and 16, respectively); this high is related to the presence of clay in the upper part of this succession. L* and b* values increase around the middle of Subunit IVa (~96–102 m CSF). These increases in L*, a*, and b* are clearly responding to lithology, where carbonate-rich sections are light brown-gray and radiolarian-rich sections are darker brown.

Stratigraphic correlation and composite section

Special Task Multisensor Logger (STMSL) data were collected at 5 cm intervals from Holes U1332B and U1332C and compared to the WRMSL data obtained from Hole U1332A. In this way we monitored drilling in Holes U1332B and U1332C in real time to recover and construct a stratigraphically complete composite section. Several intervals between Holes U1332A and U1332B did not overlap sufficiently to cover gaps between cores. Thus, coring of Hole U1332C was designed to cover the missing intervals, as well as to provide additional material for high-resolution studies. Coring in Hole U1332C was successful at covering gaps between cores in Holes U1332A and U1332B to a depth of ~125.46 m CSF (140.38 m CCSF-A) (Fig. **F34**). Below ~140 m CCSF-A, recovery was poor and it was not possible to correlate features in the track data between different holes. The position of Core 320-U1332C-10H was designed to cover a gap in the composite section between the bottom of Core 320-U1332A-9H and the undisturbed part of Core 320-U1332B-10H (~83 m CCSF-A) (Fig. **F34**). However, the coring line parted during retrieval of the core and the impact of the subsequent fall and fishing operations left the physical properties of the entire core unsuitable for stratigraphic correlation. The correlation between the three holes for the chosen parameters was adequate to good and, in some depth intervals, excellent. The gaps between successive cores in any of the holes are on the order of 1 to 2 m, with a maximum of 3.5 m between Cores 320-U1332A-13H and 14H.

The correlation was refined once magnetic susceptibility and GRA density were available at 2.5 cm resolution from the WRMSL and NGR and color reflectance data were available from the NGR track and the SHMSL (see **"Physical properties"**). Magnetic susceptibility and GRA density proved most useful for correlating between holes at Site U1332. Features in the magnetic susceptibility are well aligned between Holes U1332A–U1332C to ~140 m CCSF-A, although the section below ~100 m CCSF-A is difficult to correlate because of the scarcity of characteristic features (Fig. **F34**). Offsets and composite depths are listed in Table **T33.** Strong winds and swells caused 3 m heave, which had a negative effect on the quality of the APC cores, especially on the core tops (see **"Paleomagnetism;"** Table **T11**). Chert and porcellanite layers in lithologic Unit IV (see **"Lithostratigraphy"**) below ~130 m CSF were the main reason for poor core recovery in this interval.

Following construction of the composite depth section for Site U1332, a single spliced record was assembled for the aligned cores to 140 m CCSF-A with a gap at 83 m CCSF-A (Fig. F34). Detailed correlation and comparison with the Site 1220 magnetic susceptibility record (Shipboard Scientific Party, 2002b) suggests that the gap spans <50 cm, indicating that only a very small part of the section is missing. The sections of core used for the splice are identified in Table T34 and displayed in Figure F34. The spliced composite section consists of almost equal proportions from all three holes (Fig. F34).

Biostratigraphic and magnetostratigraphic evidence (see "Biostratigraphy" and "Paleomagnetism") suggests repetition of nannofossil Zones NP21 and NP22 (and Chrons C12r and C13n) in the early Oligocene sediments. Superposition of the duplicated section and comparison with the Site 1220 susceptibility record (Shipboard Scientific Party, 2002b) (Fig. F35) shows very good agreement and supports the hypothesis of a duplication of this sequence over a 5–7 m interval in all three drilled holes. Hole U1332A is duplicated between 73.2 and 78.1 m CCSF-A, Hole U1332B between 71.2 and 77.3 m CCSF-A, and Hole U1332C between 68.2 and 75.7 m CCSF-A (see also corresponding intervals in Fig. F34B).

We avoided intervals with significant disturbance or distortion and intervals where whole-round samples for interstitial water chemistry and microbiology were taken (see "Paleomagnetism;" Table T11). The Site U1332 splice can be used as a sampling guide to recover a single sedimentary sequence between 0 and 140 m CCSF-A, although it is advisable to overlap a few decimeters from different holes when sampling to accommodate anticipated ongoing development of the depth scale. Stretching and compression of sedimentary features in aligned cores indicates distortion of the cored sequence. Because much of the distortion occurs within individual cores on depth scales of <9 m, it was not possible to align every single feature in the magnetic susceptibility, GRA, NGR, and color reflectance records. However, at crossover points along the splice (Table T34), care was taken to align highly identifiable features from cores in each hole.

A growth factor of 1.10 is calculated by linear regression for all holes at Site U1332, indicating a 10% increase in CCSF-A relative to CSF depth (Fig. F36). We used this value to calculate the CCSF-B (see "Corrected core composite depth scale" in the "Methods" chapter) depth presented in Table T33 to aid in the calculation of mass accumulation rates.

Sedimentation rates

All the principal biostratigraphies, plus a set of ~72 paleomagnetic reversals, are defined in Holes U1332A–U1332C (Table T35; see "Biostratigraphy" and "Paleomagnetism") and were used in establishing age control (Fig. F11). Only the paleomagnetic reversals are used to calculate the average linear sedimentation rates (LSRs) for Site U1332 as depicted in Figure F11 using the CCSF-B depth scale.

Based on a simple linear interpolation from the sediment surface (assumed to be zero age) and the onset of Chron C2An.3n (Table T35), the clays of lithologic Unit I (see "Lithostratigraphy") have an LSR of 2.7 m/m.y.

The LSR at Site U1332 in the radiolarian and nannofossil oozes of lithologic Units II and III decreases from ~7 m/m.y. in the middle Eocene to 4.5 m/m.y. in the late Eocene to early Oligocene and to ~3 m/m.y. in the remainder of the section. A hiatus is present between ~20.4 and 3.6 Ma (Fig. F11) at the location of the major susceptibility peak at 11–13 m CCSF-A in Figure F34A.

Downhole measurements

Logging operations

Downhole logging measurements in Hole U1332A were made after completion of APC/XCB coring to a total depth of 152.9 m DSF. In preparation for logging, the hole was flushed with a 65 bbl sweep of high viscosity mud and the go-devil was dropped to open the lockable flapper valve. The hole was then displaced with 80 bbl of mud, and the bit was pulled up to ~80 m DSF. No tight spots were encountered while raising the drill string. The deployment of two tool strings (modified triple combo and FMS-sonic) was planned for Hole U1332A.

On 24 March 2009, the modified triple combo tool string (magnetic susceptibility, density, and NGR) was lowered and logged down to ~150 m WSF, almost to the bottom of the hole. Two upward logging passes were made up to the base of the pipe (Fig. F37). The tools provided continuous and good quality log data, but they are affected by ship heave (typically 2 m peak to peak) because the wireline heave compensator (WHC) was not working. The borehole diameter ranged from ~33 cm (13 inches) near the base of the hole to >50 cm (20 inches) above 127 m WMSF. Logging results gave information on the porcellanite-bearing sediment interval below 136 m WMSF that was only partially recovered in the cores.

At the end of the second upward pass we encountered difficulties when attempting to pull the tool string back into the pipe. Four attempts were made to enter the pipe, and each time increasing cable tension indicated that the head of the tool was obstructed at the base of the pipe, likely near the LFV.

The pipe was raised 5 m and then another 5 m, and four more unsuccessful attempts were made to enter the pipe. The pipe was rotated, and then seawater was pumped down to attempt to remove any obstructions and push open the LFV. During this procedure communications with the tool string were partially lost, and shortly after that the wireline lost ~800 lb of weight, corresponding to the weight of the tool string. At 0600 h (HST) on 25 March, the wireline was retrieved and it was confirmed that the tool string was severed from the wireline. The end of the wireline had suffered an apparently clean cut, making the most likely culprit the LFV. Fishing attempts were made to retrieve the tool string over ~18 h, using two kinds of grapple on the end of an APC core barrel; however, these were unsuccessful. Hole U1332A was cemented and abandoned on 26 March.

Logging units

Hole U1332A was divided into three units on the basis of the logs (Fig. F38).

Logging Unit 1: base of drill pipe to 136 m WMSF

Unit 1 is characterized by mostly low gamma ray values (between 3 and 9 gAPI), low density values varying between 1.25 and 1.5 g/cm³, and low magnetic susceptibility. Unit 1 has been divided into seven subunits (1A–1G). Subunits 1A, 1C, and 1E are characterized by low gamma, photoelectric effect (PEF), and density, with slightly higher magnetic susceptibility and electrical conductivity than the surrounding subunits. The low bulk density (~1.3 g/cm³) of these subunits is consistent with the lithostratigraphy of high-porosity radiolarian ooze (radiolarian opal has a density of ~2.15 g/cm³, whereas calcite and most clays have densities around 2.7 g/cm³). In comparison, Subunits 1B and 1D have higher density and PEF, most likely indicative of higher carbonate content. Electrical conductivity is lower, indicating lower porosity, and magnetic susceptibility is also low, indicating probably lower terrigenous content than in the radiolarian oozes.

Subunit 1F is characterized by high density (~1.8 g/cm³) and high PEF (~3 capture units), consistent with the recovered porcellanite in this zone (see "Lithostratigraphy"). Magnetic susceptibility is higher in Subunit 1F, and conductivity is low.

The lowermost subunit (1G) includes a peak in total gamma ray to 45 gAPI units (Fig. F39), which is mostly made up of contributions from uranium and potassium. Its origin is unclear at the moment. It seems likely that an increased proportion of clays would account for the potassium but not the uranium.

Logging Unit 2: 136–146 m WMSF

Unit 2 is characterized by a series of peaks reaching densities of 2.0 g/cm³ and lower electrical conductivity, indicating harder and less porous sediment overall (Fig. F38). PEF values higher than 4 capture units indicate that high PEF elements such as Mn or Fe may also be present in addition to calcium carbonate (PEF = ~5). The corresponding lithostratigraphy only partially recovered in this interval, however, is a mixture of radiolarian oozes and porcellanites.

Logging Unit 3: 146–151 m WMSF

The only log data for Unit 3 is magnetic susceptibility and conductivity measured at the base of the tool string. Magnetic susceptibility sharply increases to higher values at the top of the unit. These are identified in the lithostratigraphy as dark brown zeolitic clays.

Heat flow

Seven APCT-3 temperature measurements in Holes U1332B and U1332C ranged from 1.77°C at 11.6 m to 9.11°C at 100.6 m (Table T36), giving a geothermal gradient of 75.0°C/km (Fig. F40). The seafloor temperature was 1.46°C, based on the average temperature minima of the eight temperature profiles (one APCT-3 deployment, on Core 320-U1332B-5H, did not result in a valid in situ temperature). Thermal conductivity under in situ conditions was estimated from laboratory-determined thermal conductivity using the method of Hyndman et al. (1974) (see "Physical properties" in the "Methods" chapter). The calculated in situ values are within 2.2% of the measured laboratory values. Thermal resistance was then calculated by cumulatively adding the inverse of the in situ thermal conductivity values over depth intervals downhole (Fig. F40). Heat flow was obtained from the linear fit between temperature and thermal resistance (Fig. F40) (Pribnow et al., 2000). The heat flow estimate for Site 1332 is 70.7 mW/m², which is similar to heat flow values from nearby Sites 1218 and 1219.

References

Adkins, J.F., and Schrag, D.P., 2003. Reconstructing Last Glacial Maximum bottom water salinities from deep-sea sediment pore fluid profiles. *Earth Planet Sci. Lett.,* 216:109–123. doi:10.1016/S0012-821X(03)00502-8

Amante, C., and Eakins, B.W., 2008. *ETOPO1 1 Arc-Minute Global Relief Model: Procedures, Data Sources and Analysis:* Washington, DC (DOC/NOAA/NESDIS/NGDC).

Barron, J.A., 1985. Late Eocene to Holocene diatom biostratigraphy of the equatorial Pacific Ocean, Deep Sea Drilling Project Leg 85. *In* Mayer, L., Theyer, F., Thomas, E., et al., *Init. Repts. DSDP,* 85: Washington, DC (U.S. Govt. Printing Office), 413–456. doi:10.2973/dsdp.proc.85.108.1985

Barron, J.A. 2006. Diatom biochronology for the early Miocene of the equatorial Pacific. *Stratigraphy,* 2(4):281–30.

Barron, J.A., Fourtanier, E., and Bohaty, S.M., 2004. Oligocene and earliest Miocene diatom biostratigraphy of ODP Leg 199 Site 1220, equatorial Pacific. *In* Wilson, P.A., Lyle, M., Janecek, T.R., and Firth, J.V. (Eds.), *Proc. ODP, Sci. Results,* 199: College Station (Ocean Drilling Program), 1–25. doi:10.2973/odp.proc.sr.199.204.2004

Busch, W.H., Vanden Berg, M.D., and Masau, P.E., 2006. Velocity and density of Paleogene equatorial sediments: variation with sediment composition. *In* Wilson, P.A., Lyle, M., and Firth, J.V. (Eds.), *Proc. ODP, Sci. Results,* 199: College Station, TX (Ocean Drilling Program), 1–31. doi:10.2973/odp.proc.sr.199.226.2006

Cande, S.C., and Kent, D.V., 1995. Revised calibration of the geomagnetic polarity timescale for the Late Cretaceous and Cenozoic. *J. Geophys. Res.,* 100(B4):6093–6095. doi:10.1029/94JB03098

Cande, S.C., LaBrecque, J.L., Larson, R.L., Pitmann, W.C., III, Golovchenko, X., and Haxby, W.F., 1989. *Magnetic Lineations of the World's Ocean Basins.* AAPG Map Ser., 13.

Coxall, H.K., Wilson, P.A., Pälike, H., Lear, C.H., and Backman, J., 2005. Rapid stepwise onset of Antarctic glaciation and deeper calcite compensation in the Pacific Ocean. *Nature (London, U. K.),* 433(7021):53–57. doi:10.1038/nature03135

Engebretson, D.C., Cox, A., and Gordon, R.G., 1985. *Relative Motions between Oceanic and Continental Plates in the Pacific Basin.* Spec. Pap.—Geol. Soc. Am., 206.

Hyndman, R.D., Erickson, A.J., and Von Herzen, R.P., 1974. Geothermal measurements on DSDP Leg 26. *In* Davies, T.A., Luyendyk, B.P., et al., *Init. Repts. DSDP,* 26: Washington, DC (U.S. Govt. Printing Office), 451–463. doi:10.2973/dsdp.proc.26.113.1974

Knappenberger, M., 2000. Sedimentation rates and Pacific plate motion calculated using seismic cross sections of the Neogene equatorial sediment bulge [M.Sc. thesis]. Boise State Univ., Idaho.

Koppers, A.A.P., Phipps Morgan, J., Morgan, J.W., and Staudigel, H., 2001. Testing the fixed hotspot hypothesis using $^{40}Ar/^{39}Ar$ age progressions along seamount trails. *Earth Planet. Sci. Lett.,* 185(3–4):237–252. doi:10.1016/S0012-821X(00)00387-3

Lyle, M., 2003. Neogene carbonate burial in the Pacific Ocean. *Paleoceanography,* 18(3):1059. doi:10.1029/2002PA000777

Lyle, M., Liberty, L., Moore, T.C., Jr., and Rea, D.K., 2002. Development of a seismic stratigraphy for the Paleogene sedimentary section, central tropical Pacific Ocean. *In* Lyle, M., Wilson, P.A., Janecek, T.R., et al., *Proc. ODP, Init. Repts.,* 199: College Station, TX (Ocean Drilling Program), 1–21. doi:10.2973/odp.proc.ir.199.104.2002

Lyle, M., Wilson, P.A., Janecek, T.R., et al., 2002. *Proc. ODP, Init. Repts.,* 199: College Station, TX (Ocean Drilling Program). doi:10.2973/odp.proc.ir.199.2002

Lyle, M., Olivarez Lyle, A., Backman, J., and Tripati, A., 2005. Biogenic sedimentation in the Eocene equatorial Pacific—the stuttering greenhouse and Eocene carbonate compensation depth. *In* Lyle, M., Wilson, P.A., Janecek, T.R., et al., *Proc. ODP, Init. Repts.,* 199: College Station, TX (Ocean Drilling Program), 1–35. doi:10.2973/odp.proc.sr.199.219.2005

Lyle, M.W., Pälike, H., Moore, T.C., Mitchell, N., and Backman, J., 2006. *Summary Report of R/V Roger Revelle Site Survey AMAT03 to the IODP Environmental Protection and Safety Panel (EPSP) in Support for Proposal IODP626:* Southampton, U.K. (Univ. Southampton). http://eprints.soton.ac.uk/45921/

Lowenstein, T.K., and Demicco, R.V., 2007. Elevated Eocene atmospheric CO_2 and subsequent decline. *Science,* 313(5795):1928. doi:10.1126/science.1129555

Moore, T.C., Jr., 2008. Biogenic silica and chert in the Pacific Ocean. *Geology,* 36(12):975–978. doi:10.1130/G25057A.1

Müller, R.D., Roest, W.R., Royer, J.-Y., Gahagan, L.M., and Sclater, J.G., 1997. Digital isochrons of the world's ocean floor. *J. Geophys. Res.,* 102(B2):3211–3214. doi:10.1029/96JB01781

Nomura, R., and Takata, H., 2005. Data report: Paleocene/Eocene benthic foraminifers, ODP Leg 199 Sites 1215, 1220, and 1221, equatorial central Pacific Ocean. *In* Wilson, P.A., Lyle, M., and Firth, J.V. (Eds.), *Proc. ODP, Sci. Results,* 199: College Station, TX (Ocean Drilling Program), 1–34. doi:10.2973/odp.proc.sr.199.223.2005

Nuñes, F., and Norris, R.D., 2006. Abrupt reversal in ocean overturning during the Palaeocene/Eocene warm period. *Nature (London, U. K.),* 439(7072):60–63. doi:10.1038/nature04386

Olsson, R.K., Hemleben, C., and Pearson, P.N., 2006. Taxonomy, biostratigraphy, and phylogeny of Eocene *Dentoglobigerina. In* Pearson, P.N., Olsson, R.K., Huber, B.T., Hemleben, C., and Berggren, W.A. (Eds.), *Atlas of Eocene Planktonic Foraminifera.* Spec. Publ.—Cushman Found. Foraminiferal Res., 41:401–412.

Pälike, H., Lyle, M.W., Ahagon, N., Raffi, I., Gamage, K., and Zarikian, C.A., 2008. Pacific equatorial age transect. *IODP Sci. Prosp.,* 320/321. doi:10.2204/iodp.sp.320321.2008

Pälike, H., Norris, R.D., Herrle, J.O., Wilson, P.A., Coxall, H.K., Lear, C.H., Shackleton, N.J., Tripati, A.K., and Wade, B.S., 2006. The heartbeat of the Oligocene climate system. *Science,* 314(5807):1894–1898. doi:10.1126/science.1133822

Petronotis, K.E., 1991. Paleomagnetic studies of the skewness of Pacific plate marine magnetic anomalies 25–32R: implications for anomalous skewness and the motion of the Pacific plate and hotspots [Ph.D. thesis]. Northwestern Univ., Evanston, IL.

Petronotis, K.E., Gordon, R.G., and Acton, G.D., 1994. A 57 Ma Pacific plate paleomagnetic pole determined from a skewness analysis of crossings of marine magnetic anomaly 25r. *Geophys. J. Int.,* 118(3):529–554. **doi:10.1111/j.1365-246X.1994.tb03983.x**

Pribnow, D.F.C., Kinoshita, M., and Stein, C.A., 2000. *Thermal Data Collection and Heat Flow Recalculations for ODP Legs 101–180:* Hanover, Germany (Inst. Joint Geosci. Res., Inst. Geowiss. Gemeinschaftsauf. [GGA]). **http://www-odp.tamu.edu/publications/heatflow/ODPReprt.pdf**

Raffi, I., Backman, J., and Pälike, H., 2005. Changes in calcareous nannofossil assemblages across the Paleocene/Eocene transition from the paleo-equatorial Pacific Ocean. *Palaeogeogr., Palaeoclimatol., Palaeoecol.,* 226(1–2):93–126. **doi:10.1016/j.palaeo.2005.05.006**

Rea, D.K., and Lyle, M.W., 2005. Paleogene calcite compensation depth in the eastern subtropical Pacific: answers and questions. *Paleoceanography,* 20(1):PA1012. **doi:10.1029/2004PA001064**

Sager, W.W., and Pringle, M.S., 1988. Mid-Cretaceous to early Tertiary apparent polar wander path of the Pacific plate. *J. Geophys. Res., [Solid Earth],* 93(B10):11753–11771. **doi:10.1029/JB093iB10p11753**

Shackleton, N.J., Hall, M.A., Raffi, I., Tauxe, L., and Zachos, J., 2000. Astronomical calibration age for the Oligocene–Miocene boundary. *Geology,* 28(5):447–450. **doi:10.1130/0091-7613(2000)28<447:ACAFTO>2.0.CO;2**

Shipboard Scientific Party, 2002. Leg 199 summary. *In* Lyle, M., Wilson, P.A., Janecek, T.R., et al., *Proc. ODP, Init. Repts.,* 199: College Station, TX (Ocean Drilling Program), 1–87. **doi:10.2973/odp.proc.ir.199.101.2002**

Shipboard Scientific Party, 2002. Site 1220. *In* Lyle, M., Wilson, P.A., Janecek, T.R., et al., *Proc. ODP, Init. Repts.,* 199: College Station, TX (Ocean Drilling Program), 1–92. **doi:10.2973/odp.proc.ir.199.113.2002**

Shipboard Scientific Party, 2003. Site 1223. *In* Stephen, R.A., Kasahara, J., Acton, G.D., et al., *Proc. ODP, Init. Repts.,* 200: College Station, TX (Ocean Drilling Program), 1–159. **doi:10.2973/odp.proc.ir.200.103.2003**

Shipboard Scientific Party, 2004. Leg 208 summary. *In* Zachos, J.C., Kroon, D., Blum, P., et al., *Proc. ODP, Init. Repts.,* 208: College Station, TX (Ocean Drilling Program), 1–112. **doi:10.2973/odp.proc.ir.208.101.2004**

Tanaka, H., 1999. Circular asymmetry of the paleomagnetic directions observed at low latitude volcanic sites. *Earth, Planets Space,* 51(12):1279–1286.

Thomas, E., 1985. Late Eocene to Recent deep-sea benthic foraminifers from the central equatorial Pacific Ocean. *In* Mayer, L., Theyer, F., Thomas, E., et al., *Init. Repts. DSDP,* 85: Washington, DC (U.S. Govt. Printing Office), 655–694. **doi:10.2973/dsdp.proc.85.117.1985**

van Andel, T.H., 1975. Mesozoic/Cenozoic calcite compensation depth and the global distribution of calcareous sediments. *Earth Planet. Sci. Lett.,* 26(2):187–194. **doi:10.1016/0012-821X(75)90086-2**

van Morkhoven, F.P.C.M., Berggren, W.A., and Edwards, A.S., 1986. *Cenozoic Cosmopolitan Deep-Water Benthic Foraminifera.* Bull. Cent. Rech. Explor.—Prod. Elf-Aquitaine, Mem. 11.

Zachos, J., Pagani, M., Sloan, L., Thomas, E., and Billups, K., 2001. Trends, rhythms, and aberrations in global climate 65 Ma to present. *Science,* 292(5517):686–693. **doi:10.1126/science.1059412**

Publication: 30 October 2010
MS 320321-104

Figure F1. A. ETOPO1 (Amante and Eakins, 2008) bathymetric overview map of Site U1332 and PEAT drilling locations, with previous ODP and DSDP sites. **B.** Swath map bathymetry for Site U1332 region from the AMAT-03 site survey. Black labels = seismic shotpoints, white labels = bathymetric contours. Yellow line = north–south trending survey line for Site U1332. F.Z. = fracture zone.

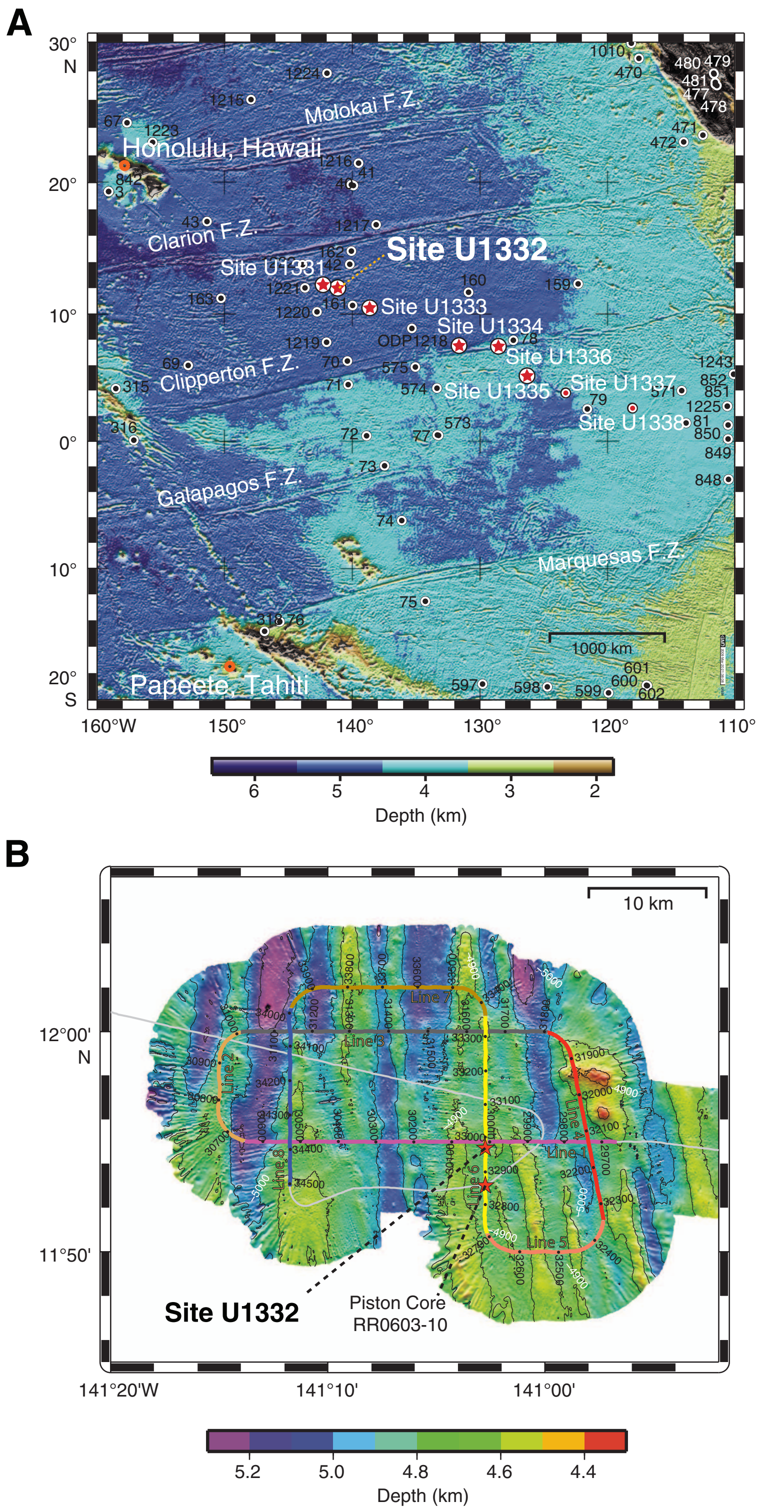

Figure F2. Seismic reflection profile PEAT-2C (Site U1332) Line 6 from the 48-channel seismic reflection survey, annotated in shotpoints (Lyle et al., 2006). Data are filtered, stacked, and migrated. Site was located where basal reflections appeared less strong to minimize possible cherts. Tentative conversion from two-way traveltime to depth uses velocity model of Busch et al. (2006). P2, P3 = seismic reflectors of Lyle et al., (2002). All times are Universal Time Coordinated (UTC). TD = total depth.

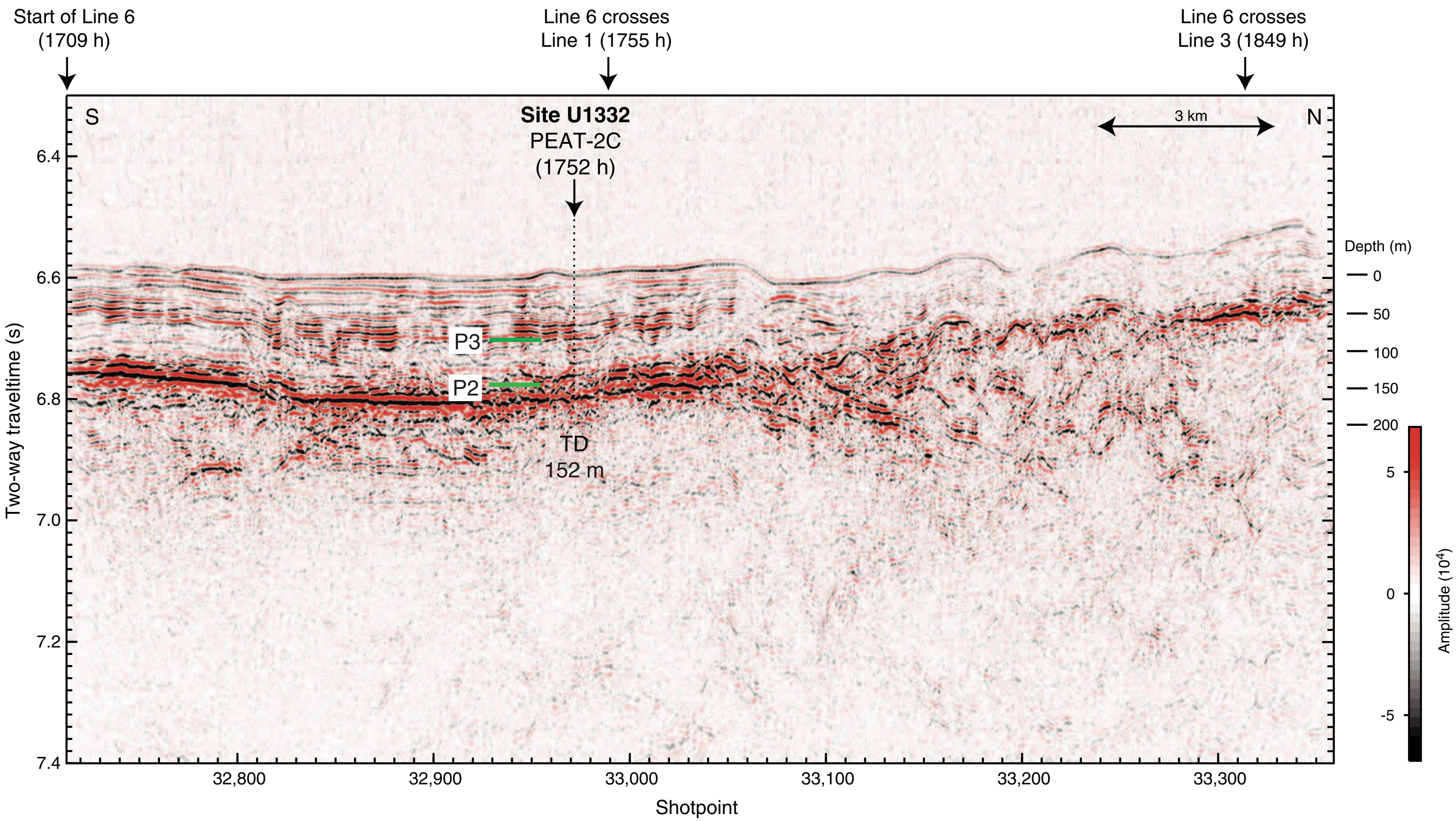

Figure F3. Lithologic summary, Site U1332. A +5 m adjustment is added to the downhole logging magnetic susceptibility depths to convert from WMSF to CSF. L* = reflectance value of sediment as defined in the LAB color model. Chron/Polarity: green wavy line = slump, red wavy line = hiatus.

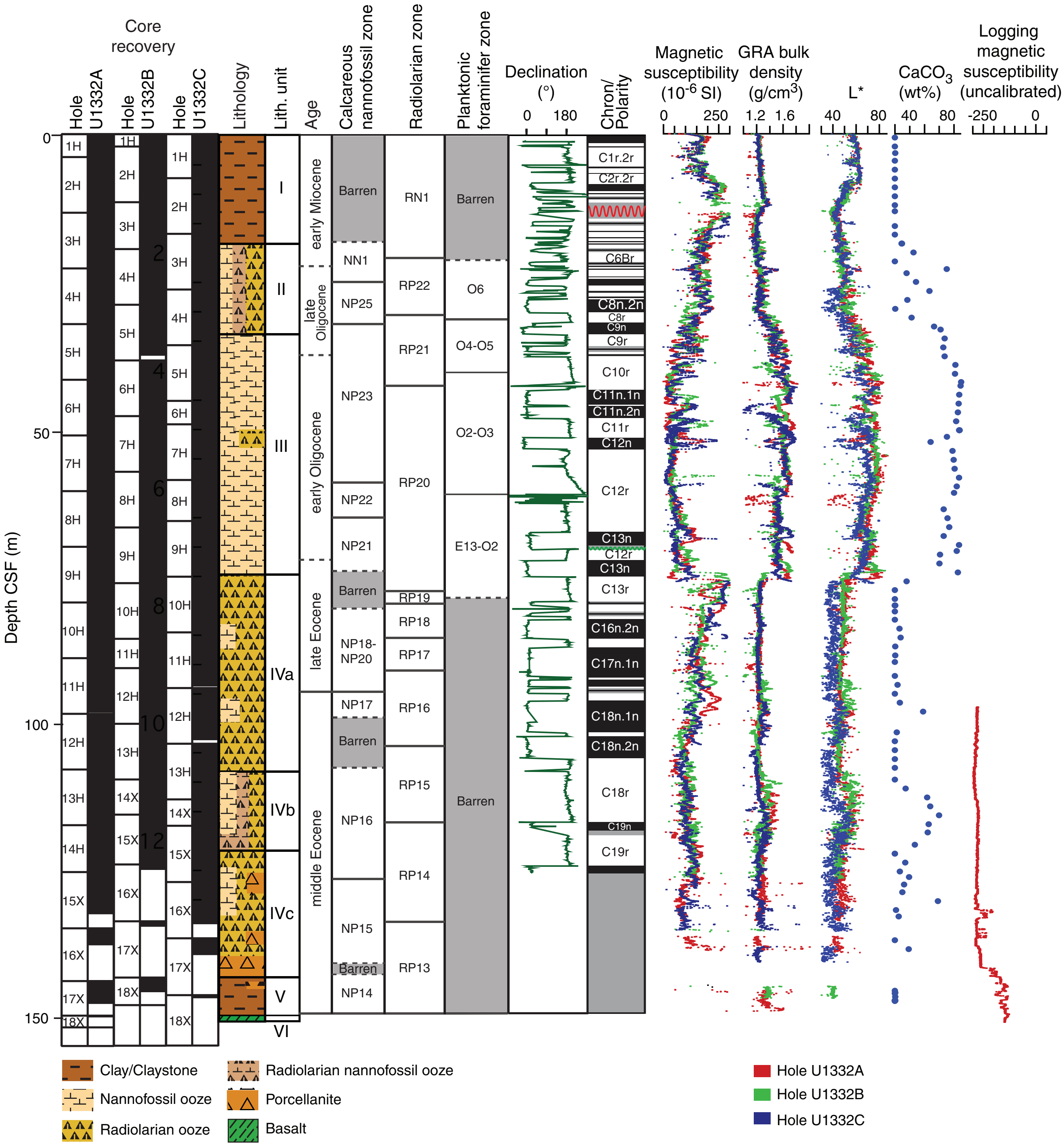

Figure F4. Site U1332 summary.

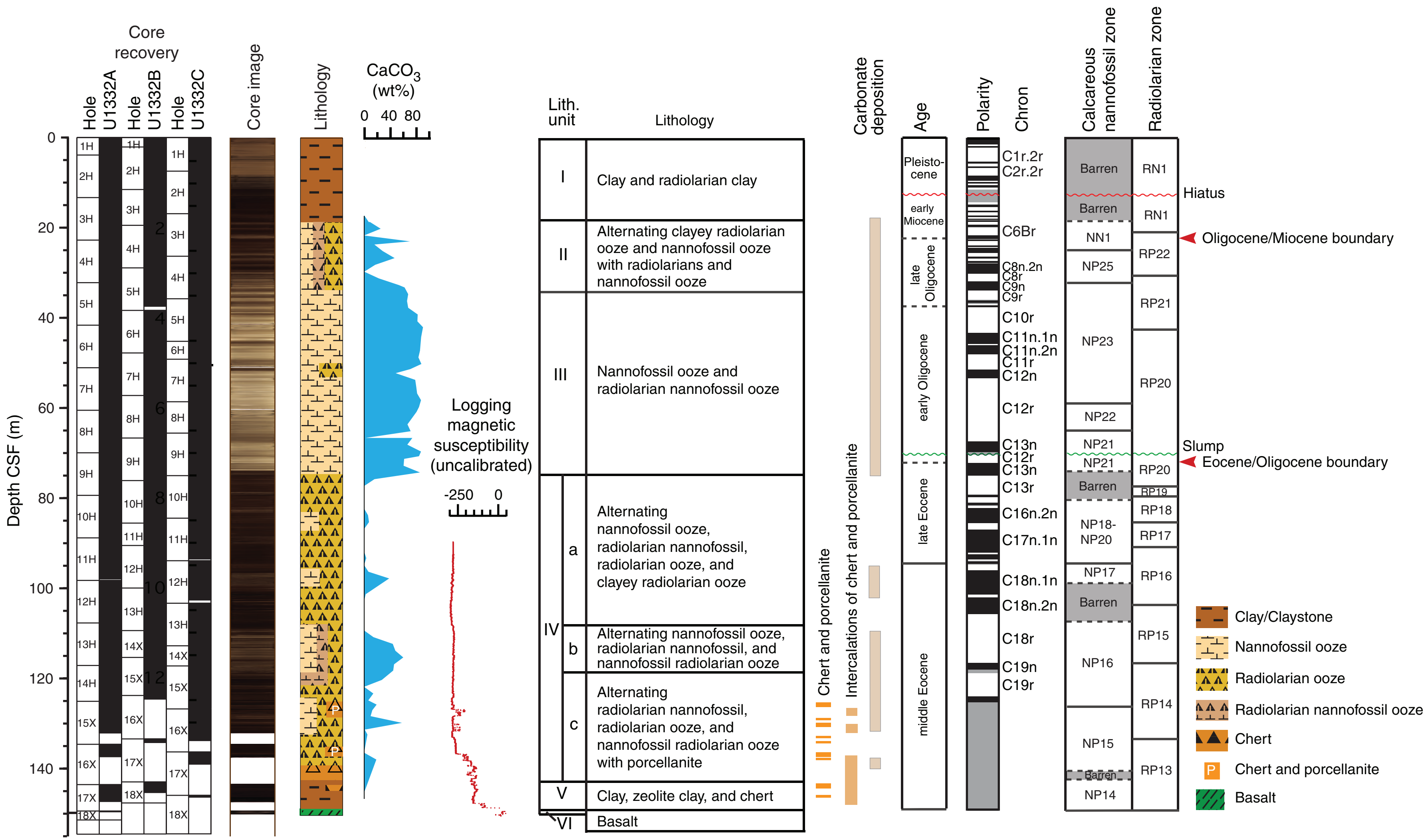

Figure F5. Smear slide photomicrographs of selected representative lithologies, Site U1332. Left image = plane-polarized light, right image = cross-polarized light. **A.** Zeolite clay (Sample 320-U1332C-2H-3, 100 cm). **B.** Nannofossil ooze (Sample 320-U1332C-5H-2, 14 cm). **C.** Radiolarian nannofossil ooze with diatoms (Sample 320-U1332C-8H-5, 18 cm). **D.** Radiolarian ooze (Sample 320-U1332C-11H-4, 75 cm).

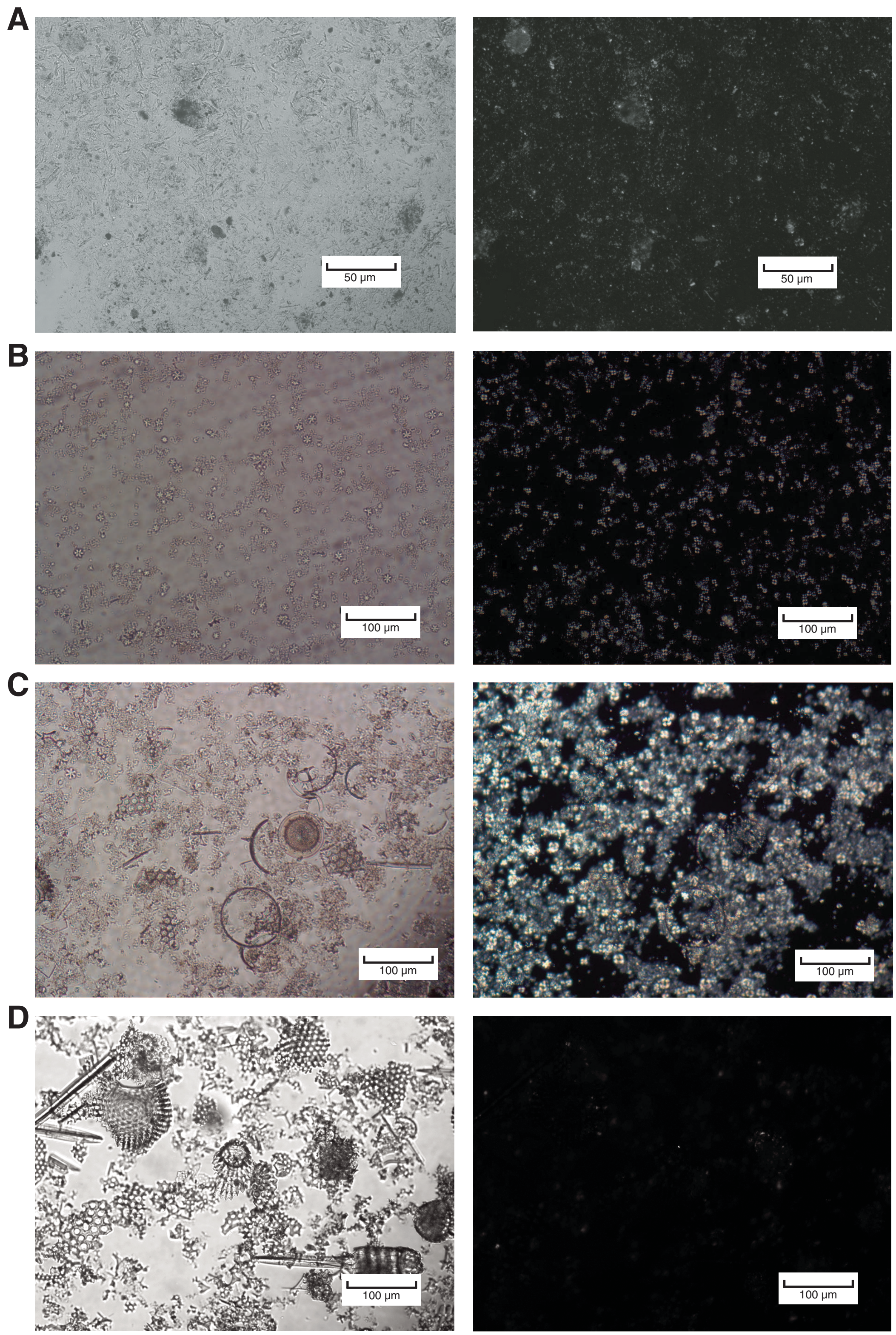

Figure F6. Thin section photomicrographs of porcellanites, Site U1332. Left image = plane-polarized light, right image = cross-polarized light. **A, B.** Porcellanite with foraminifers and coarse basal layers (Sample 320-U1332A-15X-2, 112–114 cm). **C, D.** Porcellanite with veins of recrystalized silica (Sample 320-U1332A-17X-1, 0–4 cm). Large radial crystals of chalcedony are visible in D.

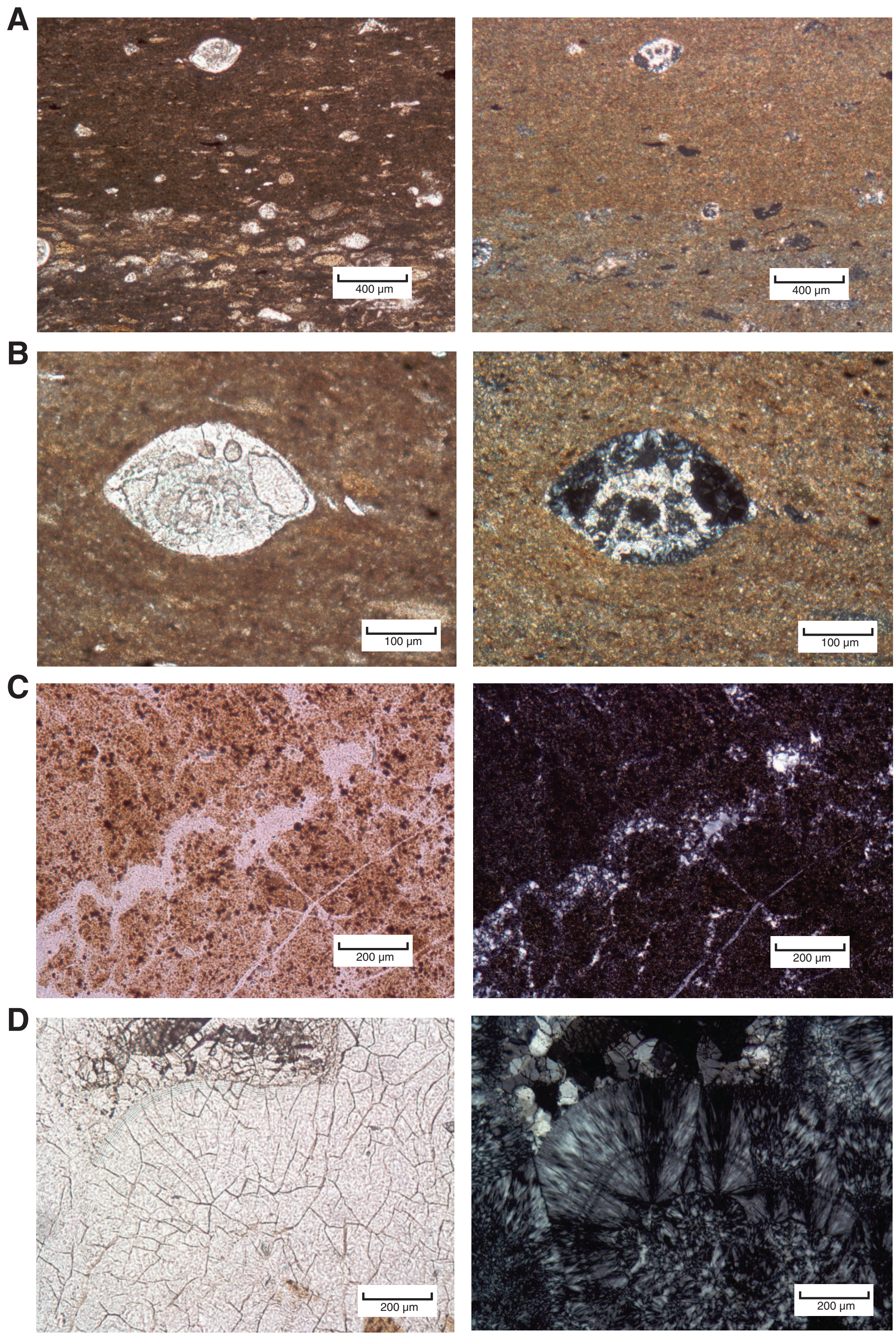

Figure F7. Thin section photomicrographs of basalt, Site U1332. Left image = plane-polarized light, right image = cross-polarized light. **A.** Very fine grained sparsely plagioclase phyric basalt (fresh chilled margin = subhedral clinopyroxene, lath plagioclases, and glass in groundmass) (Sample 320-U1332A-18X-CC, 12–16 cm). **B.** Fine-grained plagioclase phyric basalt (calcite vein and highly altered groundmass) (Sample 320-U1332A-18X-CC, 16–19 cm).

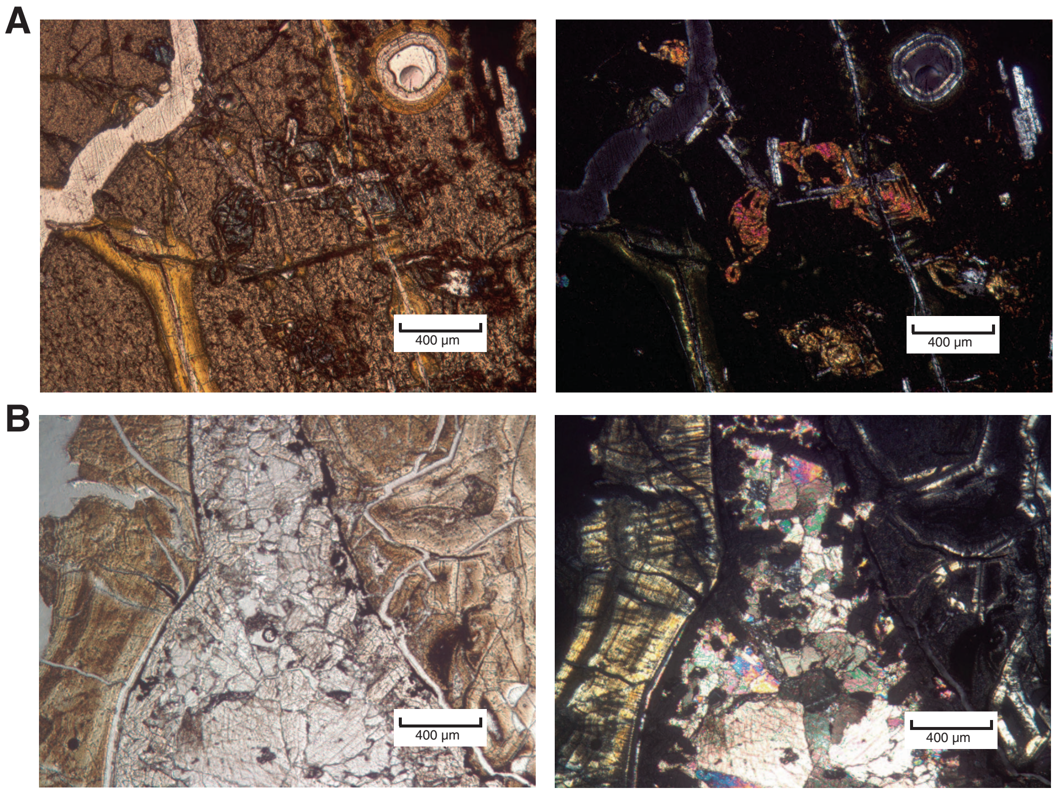

Figure F8. Line scan images, magnetic susceptibility, and lightness reflectance of Eocene–Oligocene transition. **A.** Hole U1332A. **B.** Hole U1332B. L* = reflectance value of sediment as defined in the LAB color model.

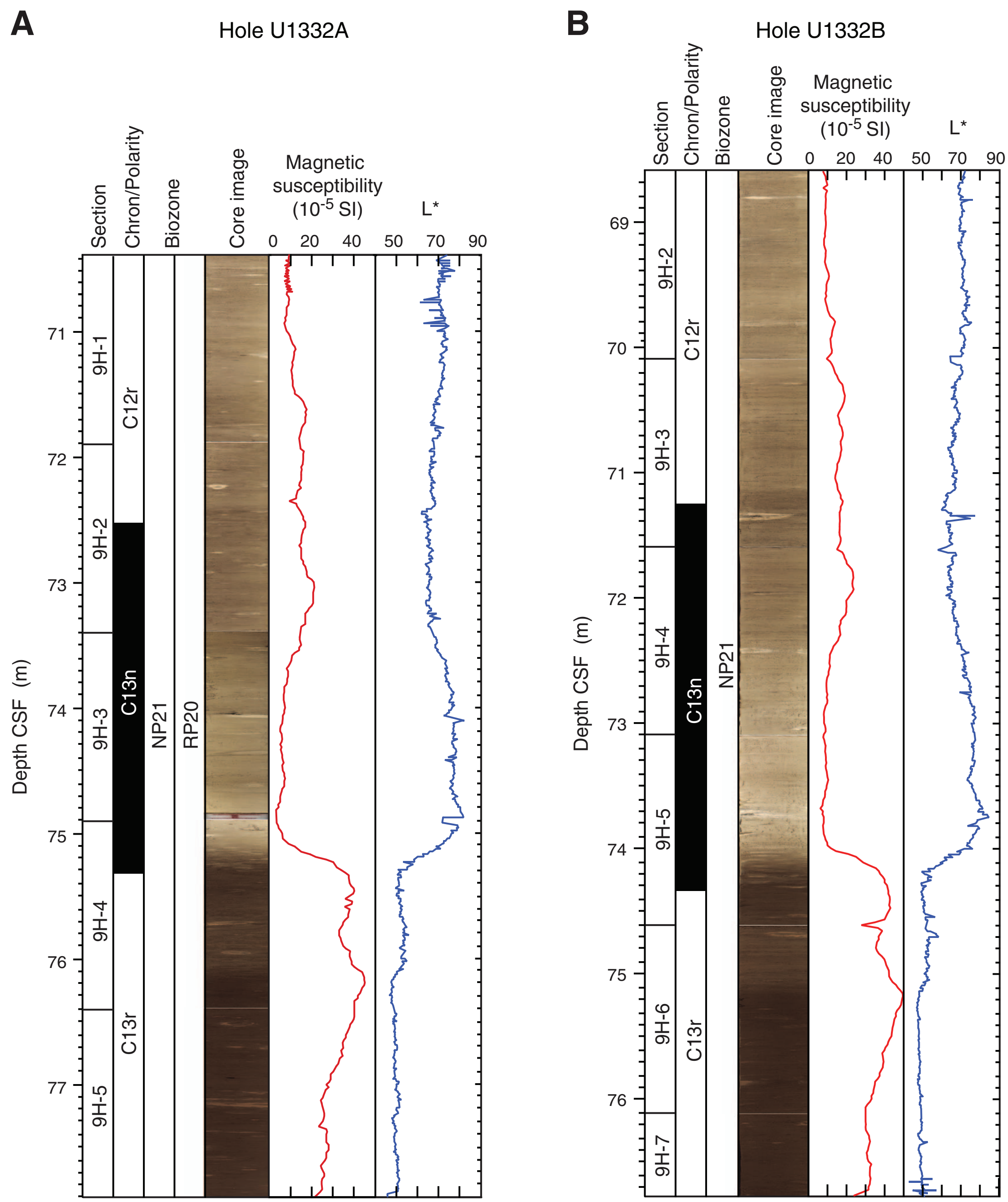

Figure F9. Line scan images of duplicated latest Eocene early Oligocene sequences with sharp contact (close-up images) recovered well above the Eocene–Oligocene transition. **A.** Sections 320-U1332B-8H-7 and 8H-CC. **B.** Section 320-U1332B-9H-2. Depths do not account for core gaps or core expansion (note overlap in depth between the bottom of Cores 320-U1332C-8H and 9H). In composite depth the sharp basal contact of the inferred slump or sliding shown in the close-up images falls ~8 m above the Eocene–Oligocene transition (red arrows).

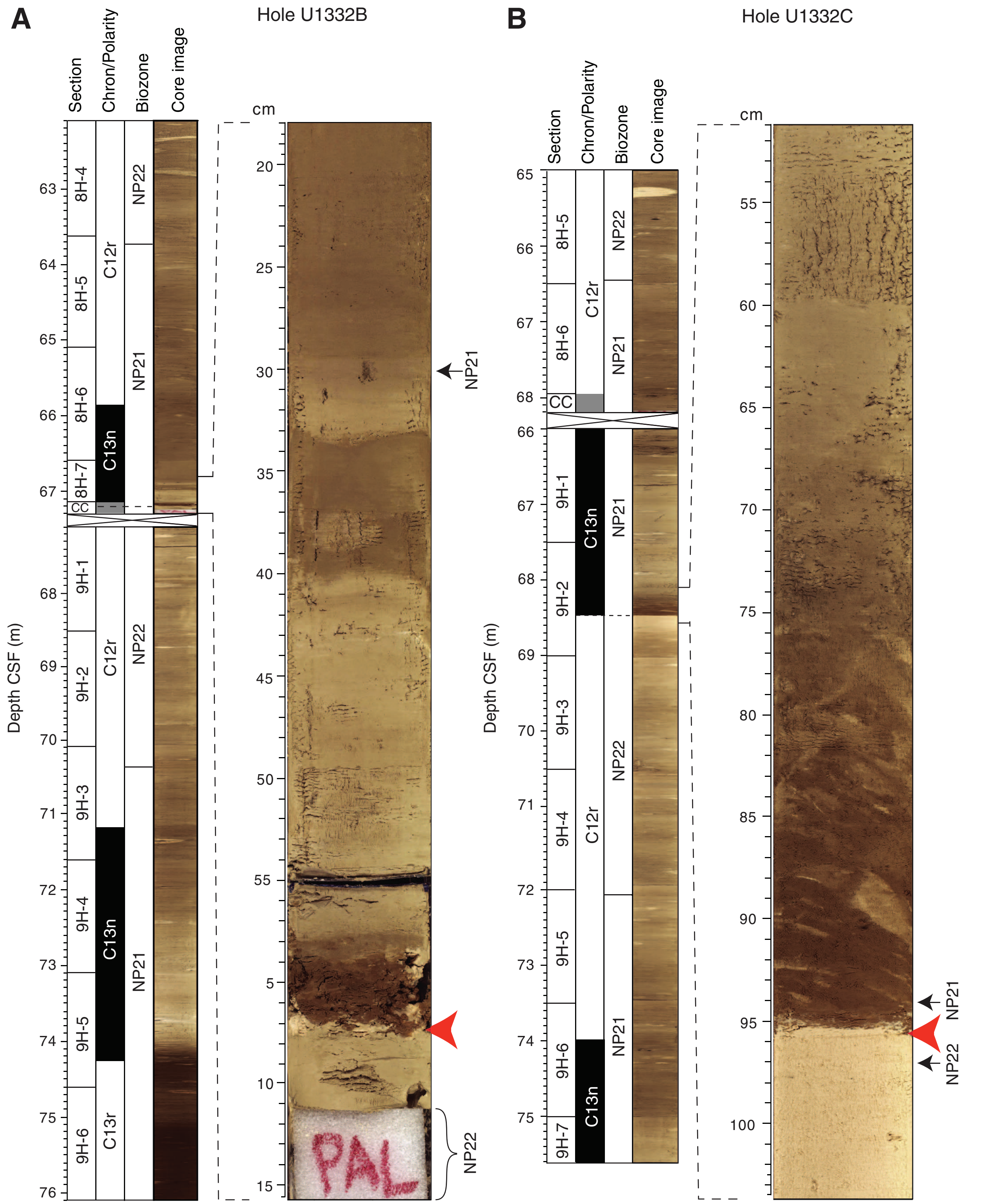

Figure F10. Integrated calcareous and siliceous microfossil biozonation, Site U1332. Calcareous microfossil zonation was limited by the presence of barren intervals; dashed zonal boundaries indicate stratigraphic extent of calcareous microfossil assemblages consistent with a particular zonal assignment.

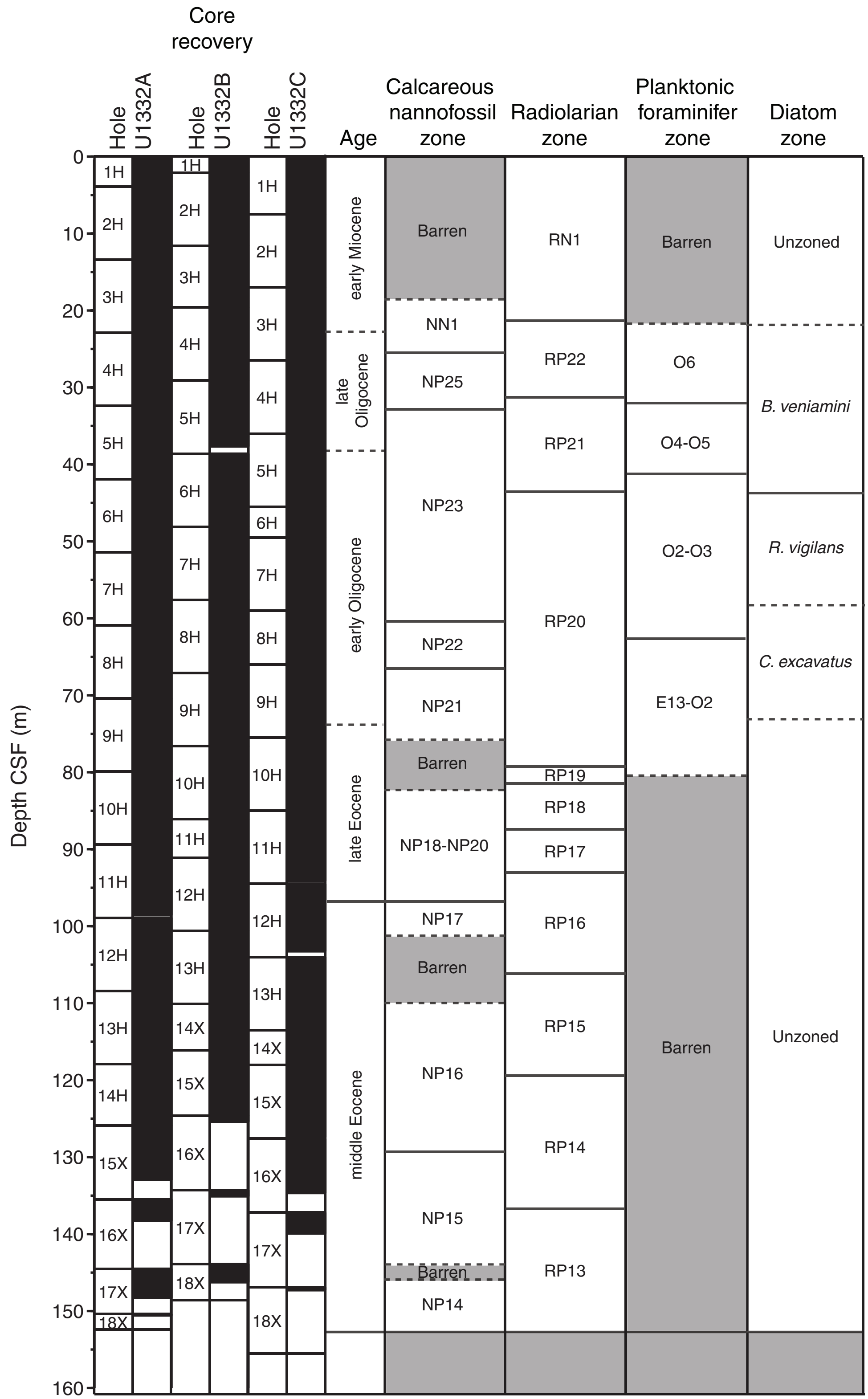

Figure F11. Linear sedimentation rates and chronostratigraphic markers, Site U1332.

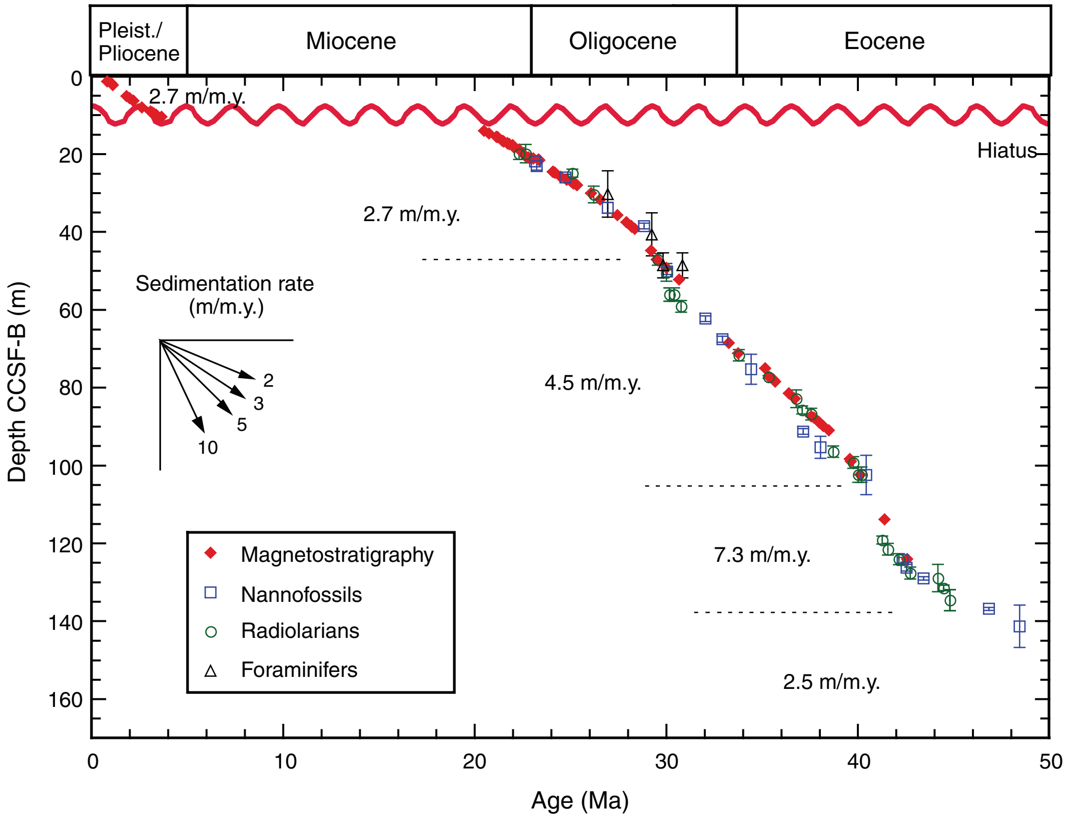

Figure F12. Summary of magnetic susceptibility and paleomagnetic results, Hole U1332A. Declinations are shown in sample coordinates (not reoriented to geographical coordinates). PCA = principal component analysis.

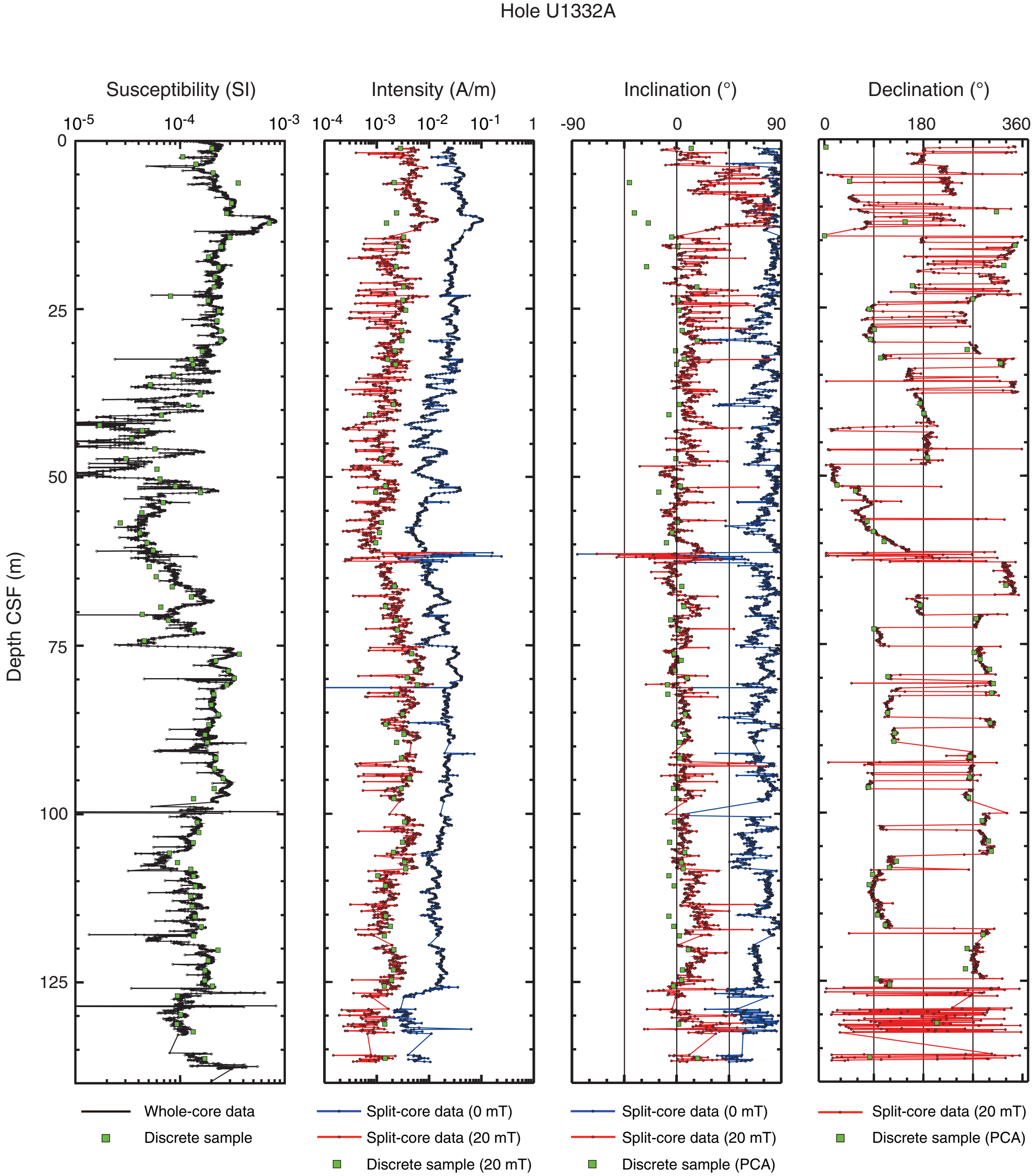

Figure F13. Summary of magnetic susceptibility and paleomagnetic results, Hole U1332B. Declinations are shown in sample coordinates (not reoriented to geographical coordinates).

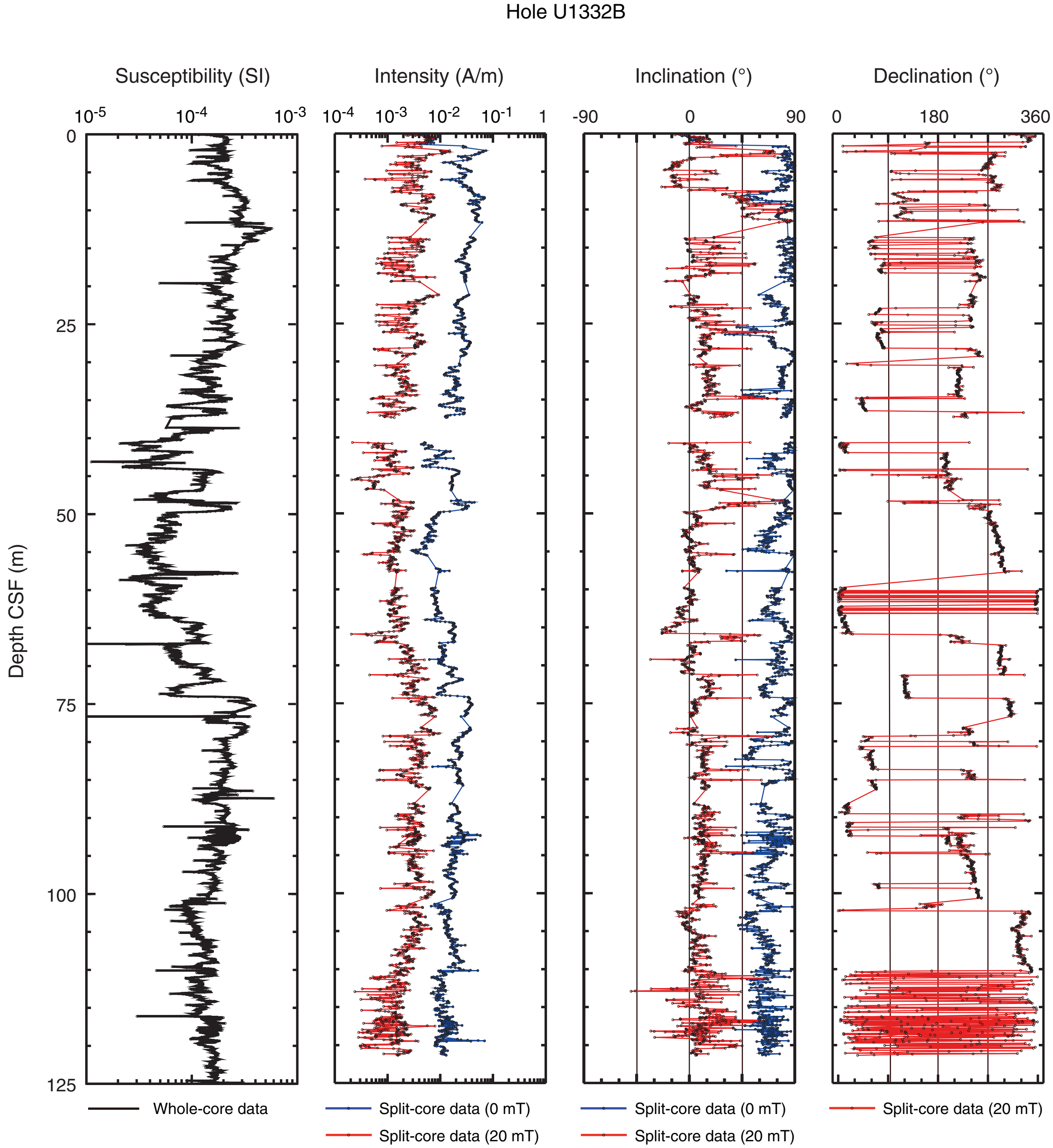

Figure F14. Summary of magnetic susceptibility and paleomagnetic results, Hole U1332C. Declinations are shown in sample coordinates (not reoriented to geographical coordinates).

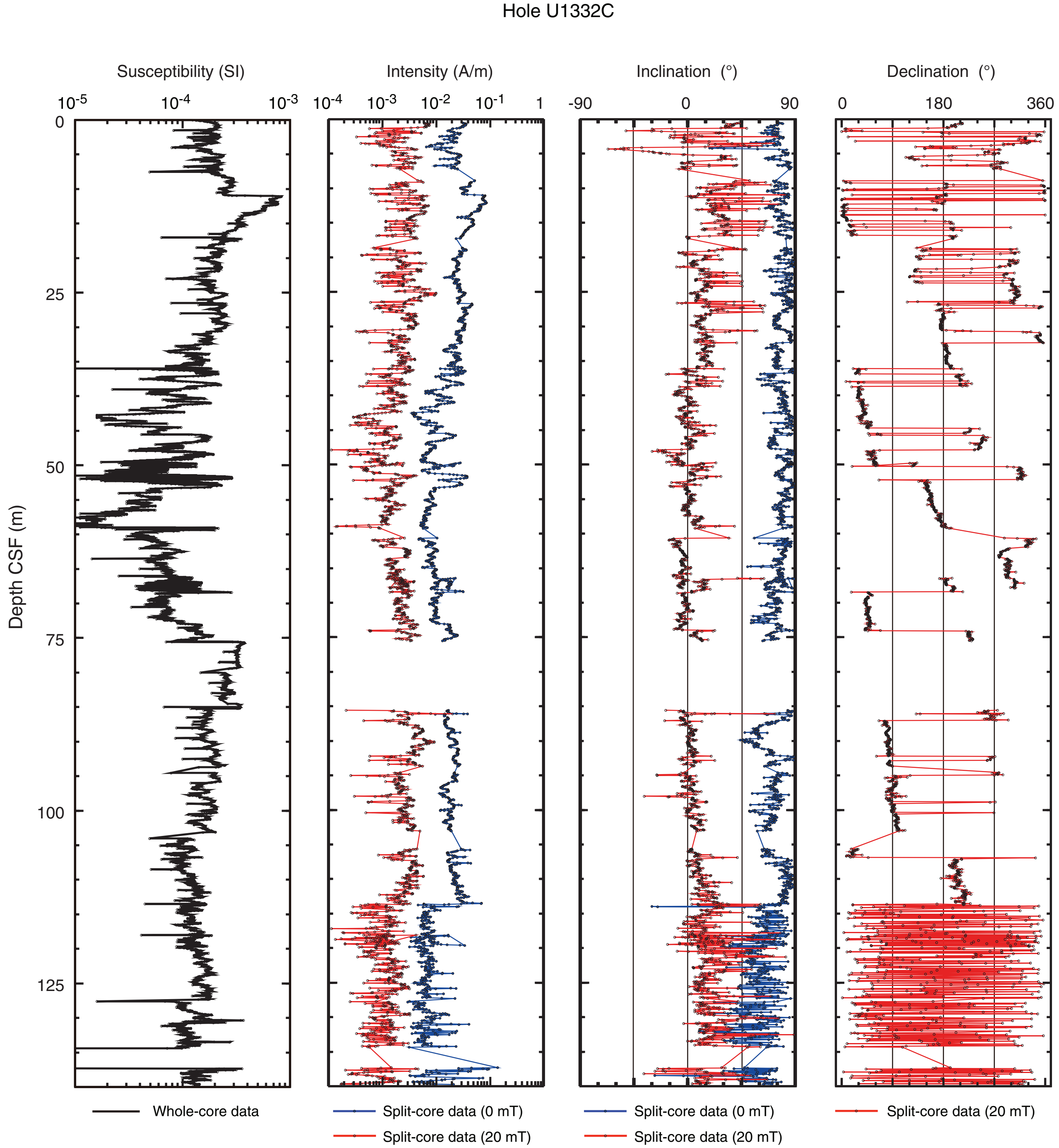

Figure F15. Alternating-field demagnetization (demag) results for four discrete samples. Larger plot shows vector endpoints of paleomagnetic directions on vector demagnetization diagrams or modified Zijderveld plots (solid circles = horizontal projections, open circles = vertical projections, gray circles = data not used in computing ChRM, black dashed line = ChRM direction), smaller plot shows intensity variation with progressive demagnetization. Data illustrate removal of a steep drilling overprint by ~10–15 mT, with the remaining magnetization providing a well-resolved characteristic remanent magnetization. **A.** Sample 320-U1332A-4H-2, 85 cm (25.25 m CSF). **B.** Sample 320-U1332A-5H-5, 85 cm (39.25 m CSF). **C.** Sample 320-U1332A-9H-7, 45 cm (79.85 m CSF). **D.** Sample 320-U1332A-12H-6, 85 cm (107.25 m CSF). NRM = natural remanent magnetization. Inc = inclination, Dec = declination, MAD = maximum angular deviation.

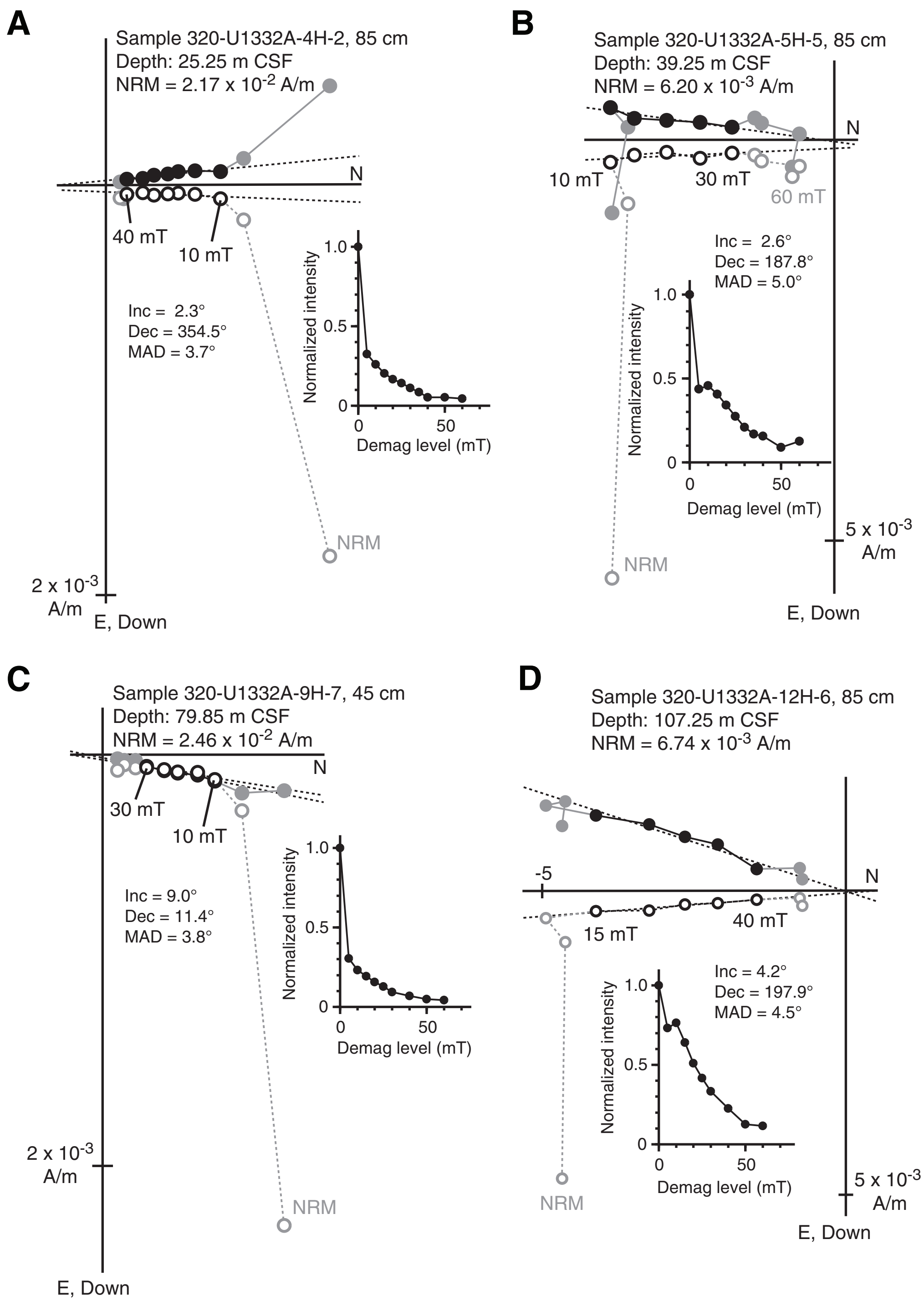

Figure F16. Variations of virtual geomagnetic pole (VGP) latitude and geographic declination, Hole U1332A. Variations computed using paleomagnetic data after 20 mT demagnetization. Geographic declinations calculated by subtracting mean paleomagnetic declination of each core (indicated in Table T23) from raw declination values. North latitudes = normal polarity, south latitudes = reversed polarity. O/M = Oligocene/Miocene boundary, E/O = Eocene/Oligocene boundary.

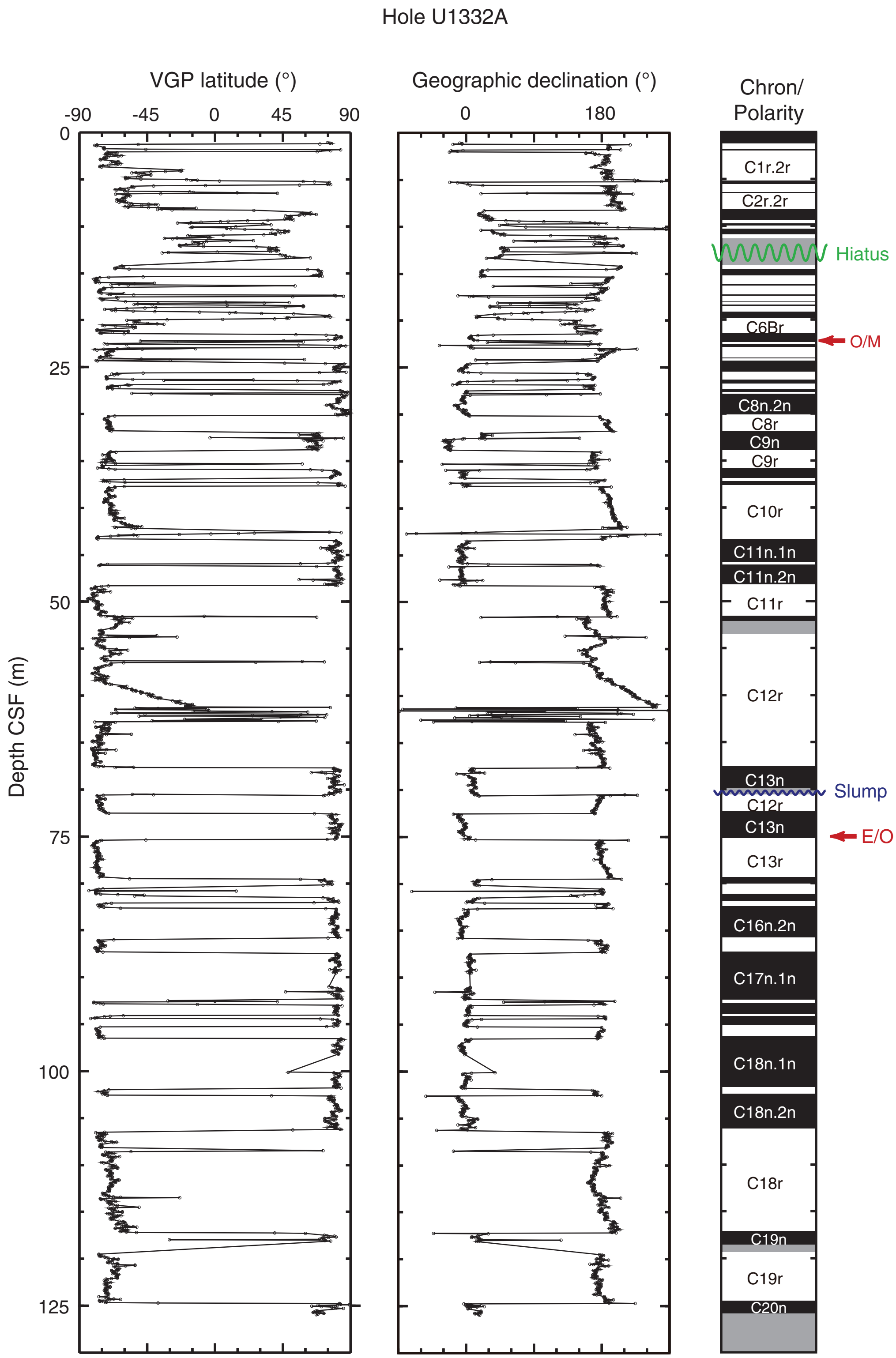

Figure F17. Variations of virtual geomagnetic pole (VGP) latitude and geographic declination, Hole U1332B. Variations computed using paleomagnetic data after 20 mT demagnetization. Geographic declinations calculated by subtracting mean paleomagnetic declination of each core (indicated in Table T23) from raw declination values. North latitudes = normal polarity, south latitudes = reversed polarity. O/M = Oligocene/Miocene boundary, E/O = Eocene/Oligocene boundary.

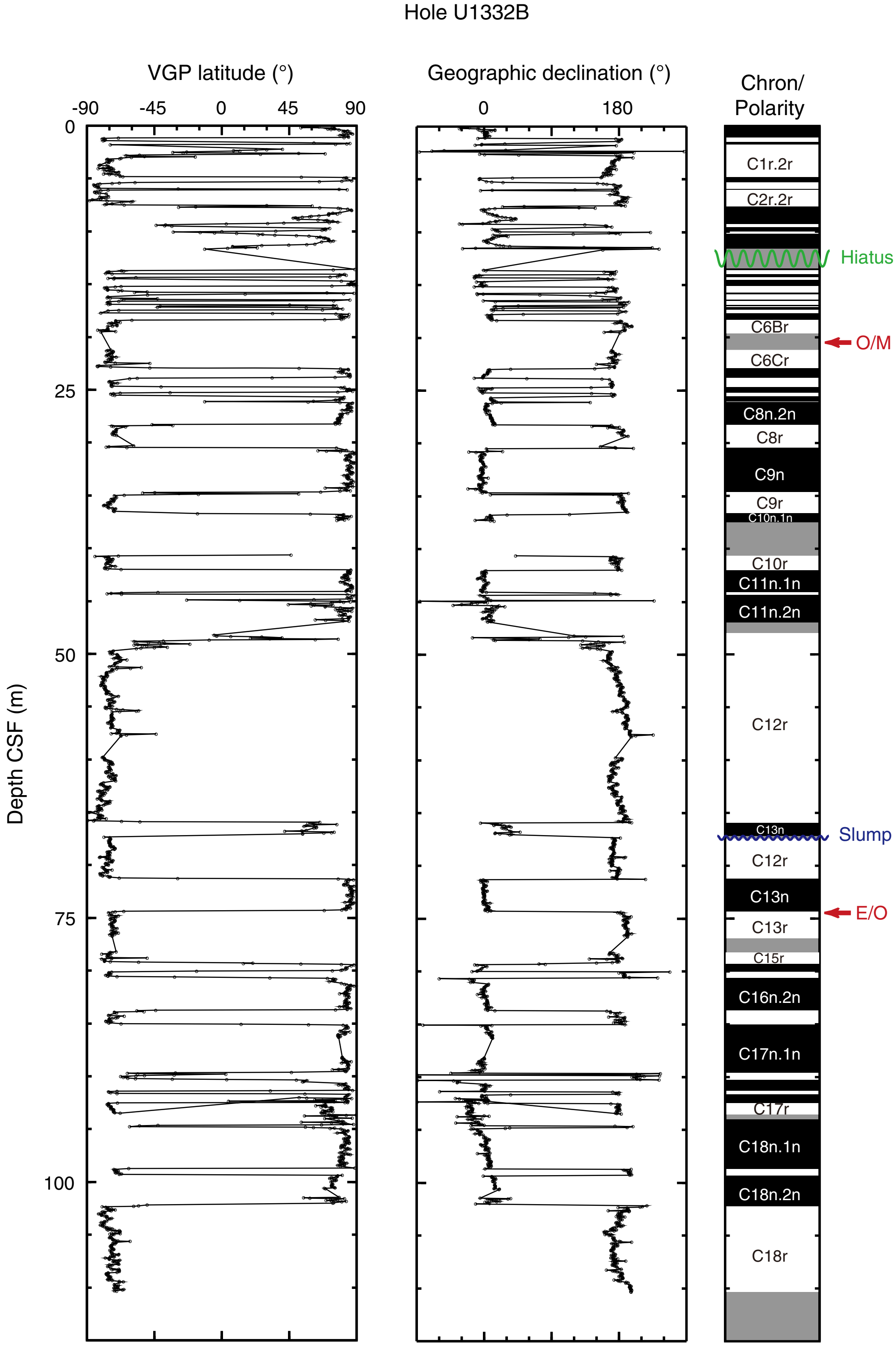

Figure F18. Variations of virtual geomagnetic pole (VGP) latitude and geographic declination, Hole U1332C. Variations computed using paleomagnetic data after 20 mT demagnetization. Geographic declinations calculated by subtracting mean paleomagnetic declination of each core (indicated in Table T23) from raw declination values. North latitudes = normal polarity, south latitudes = reversed polarity. O/M = Oligocene/Miocene boundary, E/O = Eocene/Oligocene boundary.

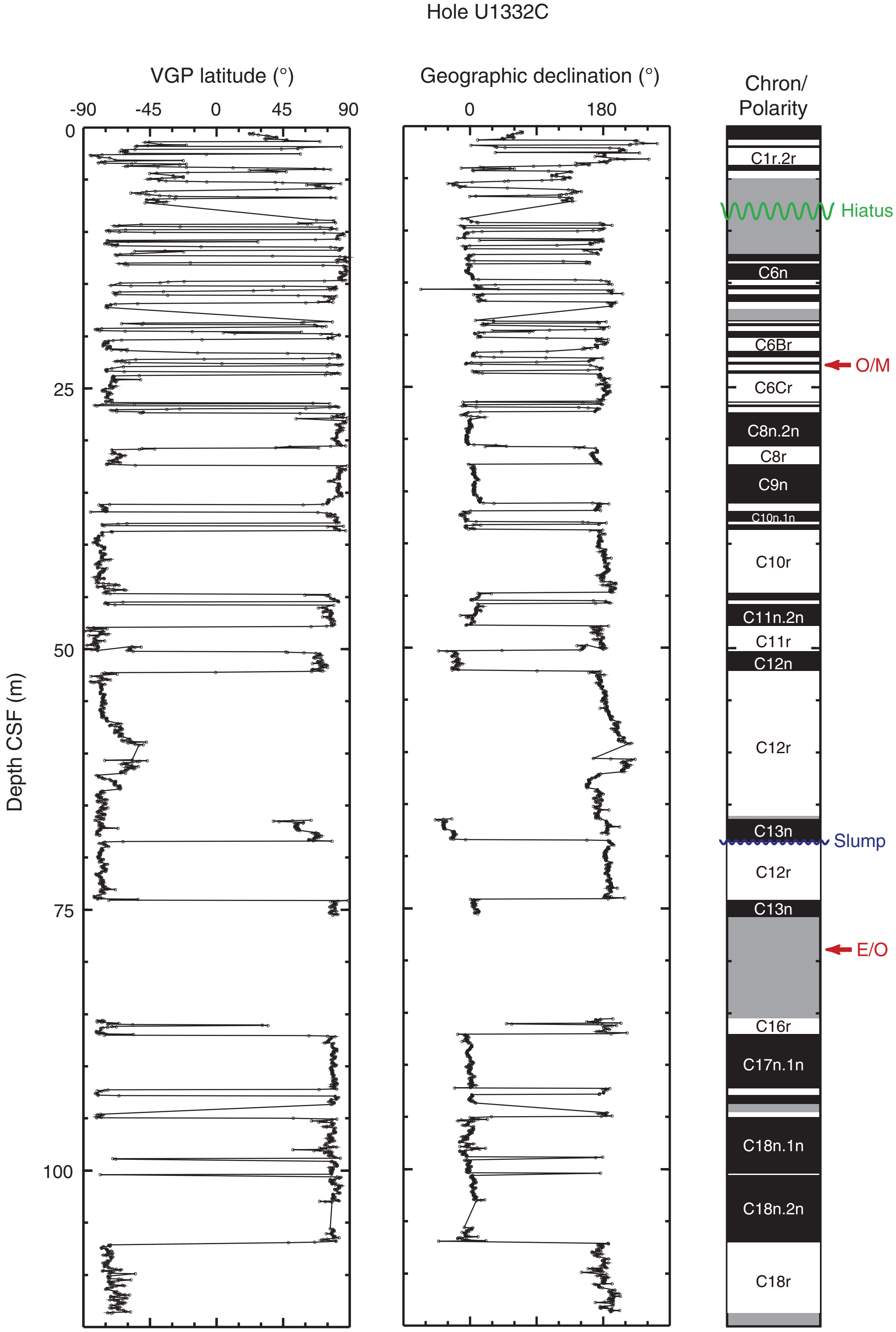

Figure F19. Comparison of magnetostratigraphy determined from each hole. Dotted lines = some representative iso-boundaries of geomagnetic chrons, solid lines = Oligocene/Miocene (O/M) and Eocene/Oligocene (E/O) boundaries.

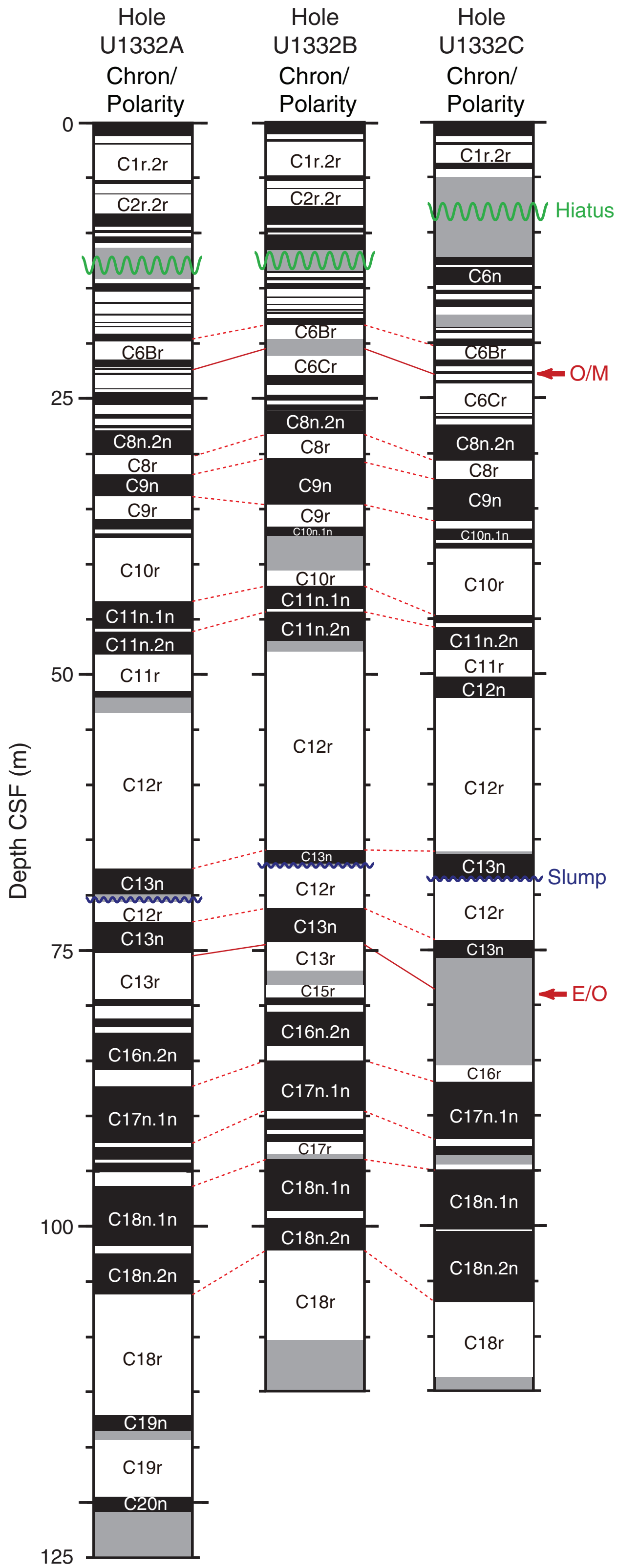

Figure F20. Variations of geographic declinations and remanent magnetization (after 20 mT demagnetization) for the slump interval in Cores 320-U1332A-8H and 9H. Correlatable variations in intensity are marked by letters a–i.

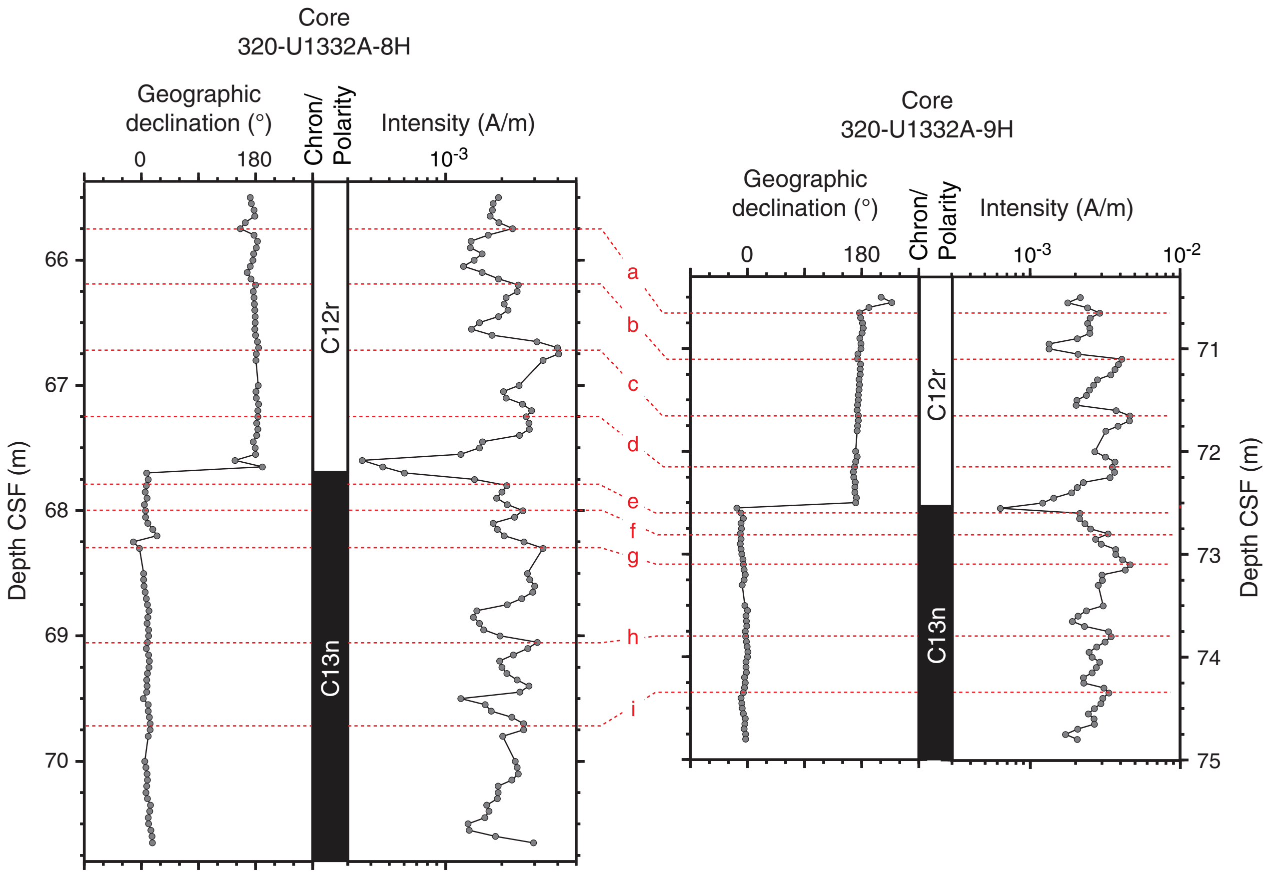

Figure F21. Variations of geographic declinations and remanent magnetization (after 20 mT demagnetization) for the slump interval in Cores 320-U1332B-8H and 9H. Features marked by letters a–d, g, and h can be correlated to those in Figure F20.

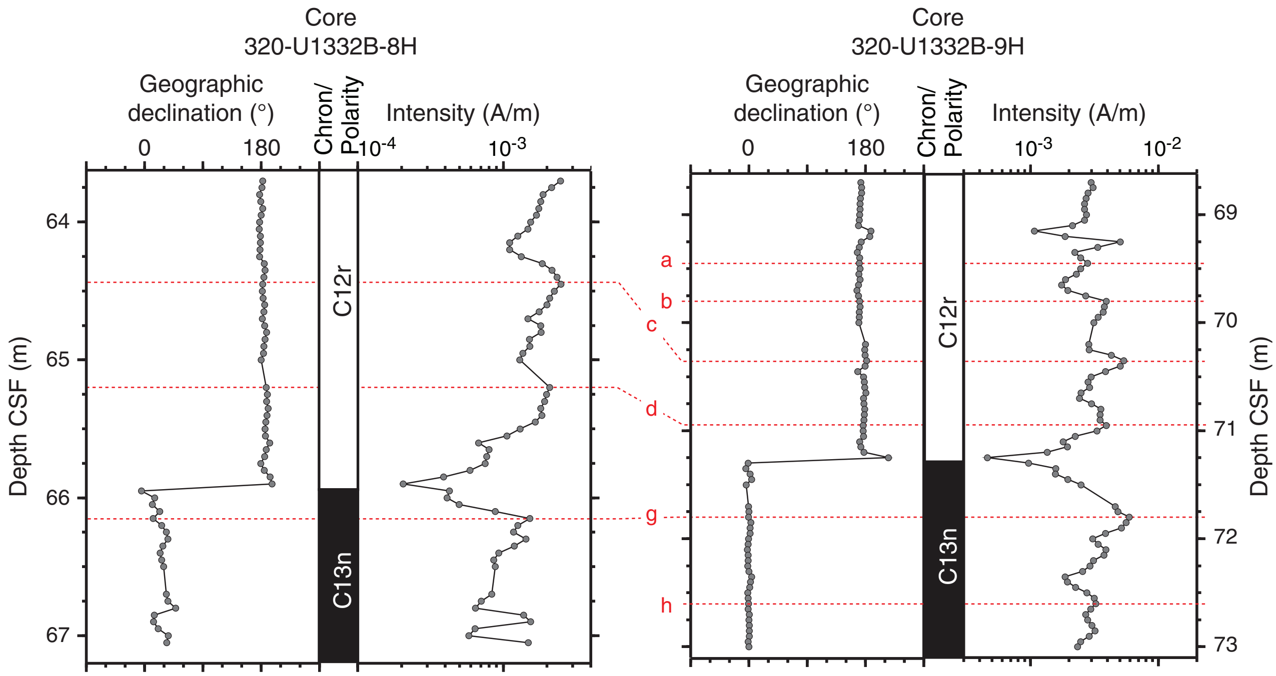

Figure F22. Variations of geographic declinations and remanent magnetization (after 20 mT demagnetization) for the slump interval in Core 320-U1332C-9H. Features marked by letters a–d, g, and h can be correlated to those in Figure F20.

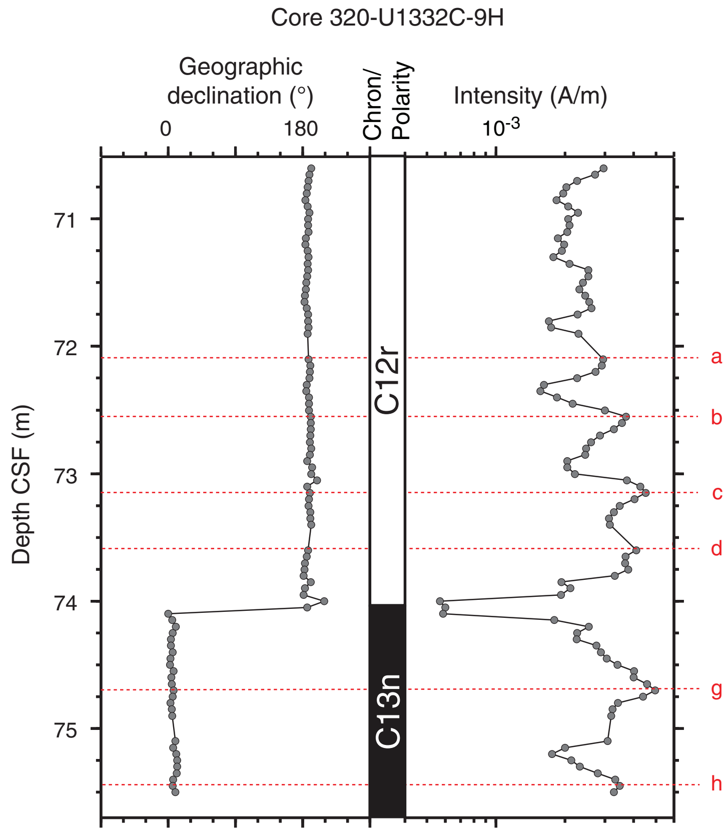

Figure F23. Interstitial water chemistry, Hole U1332A. Values below the detection limit (see Table T26) are plotted as zero. (See "Lithostratigraphy" for information on unit boundaries.) (Continued on next page.)

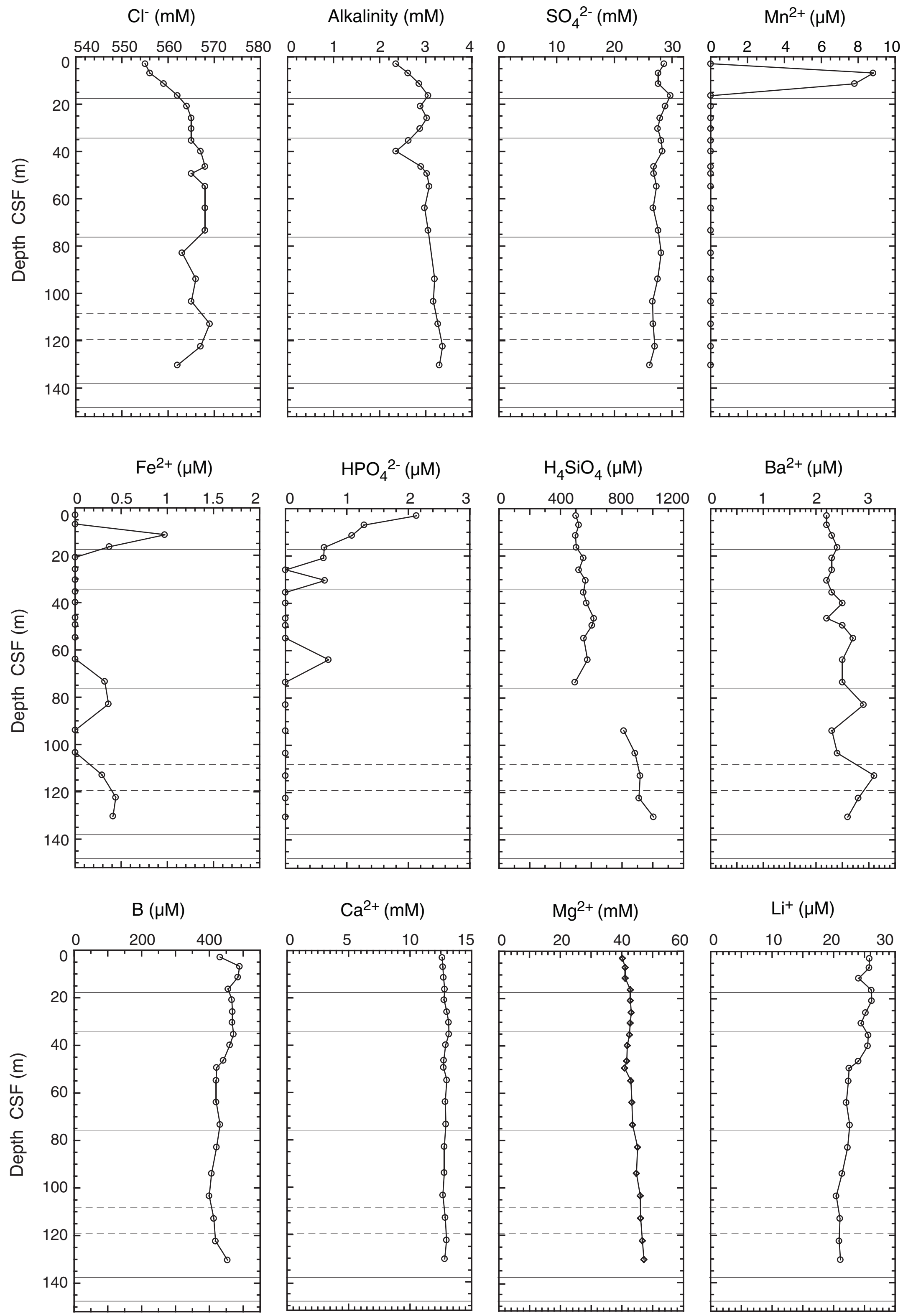

Figure F23 (continued). Interstitial water chemistry, Hole U1332A.

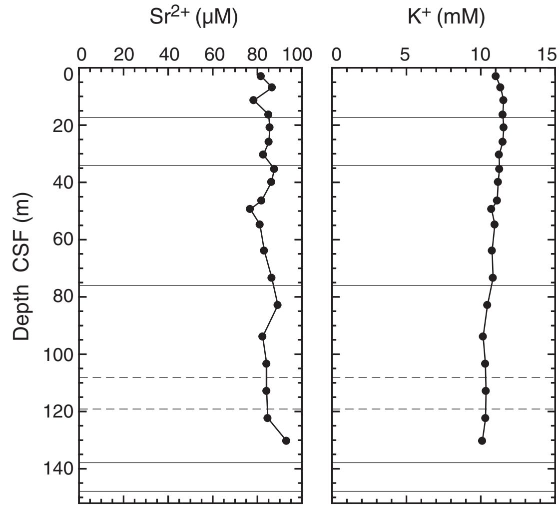

Figure F24. Interstitial water chemistry data from Rhizon samples, Hole U1332C. Values below the detection limit (see Table T27) are plotted as zero.

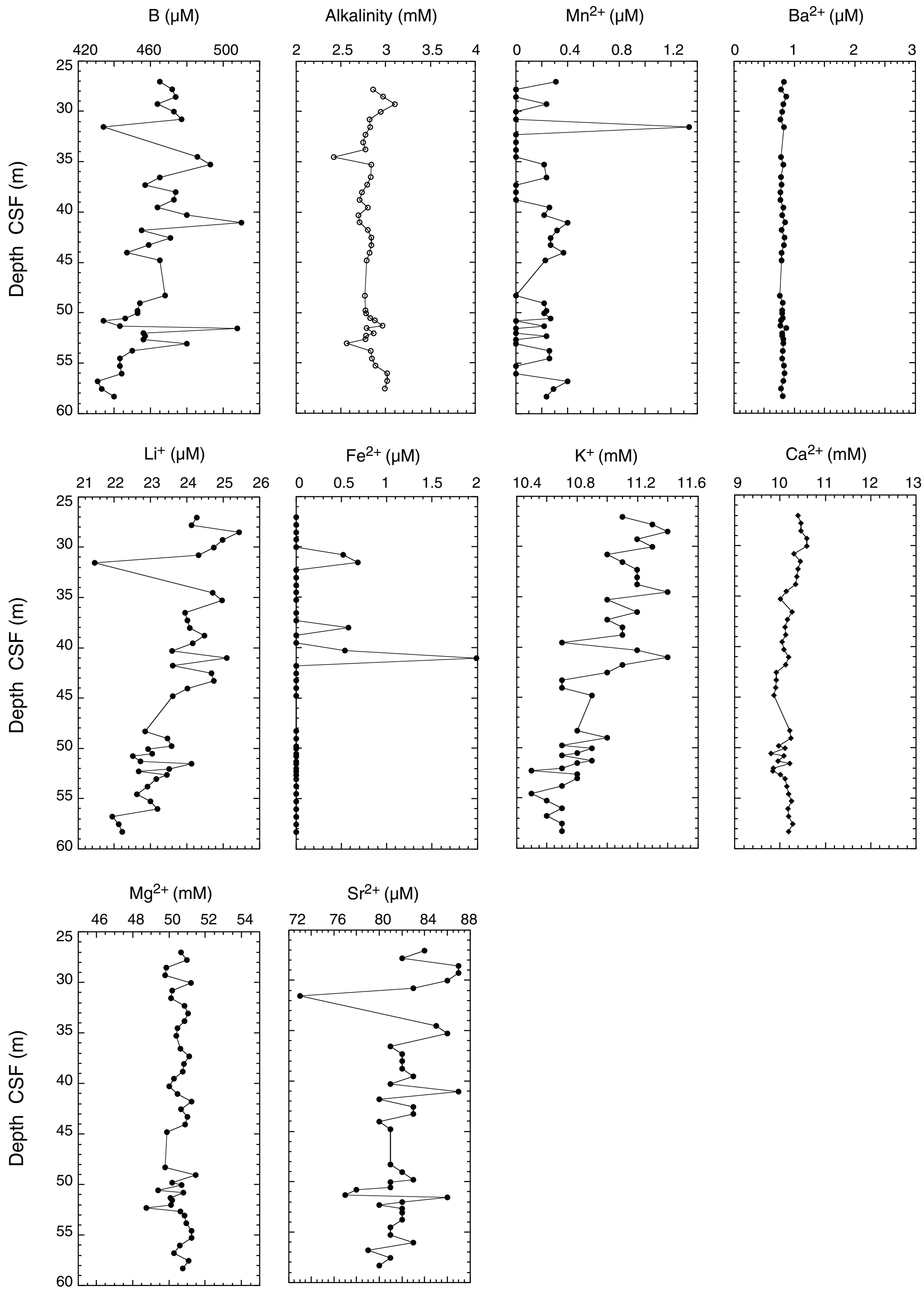

Figure F25. Interstitial water chemistry, Site U1332. Values below the detection limit (see Tables T26, T27) are plotted as zero. Note offsets in concentration scales for Ca^{2+} and Mg^{2+} for whole-round and Rhizon samples. Rhizon samples are from Hole U1332C; whole-round (WR) samples are from Hole U1332A.

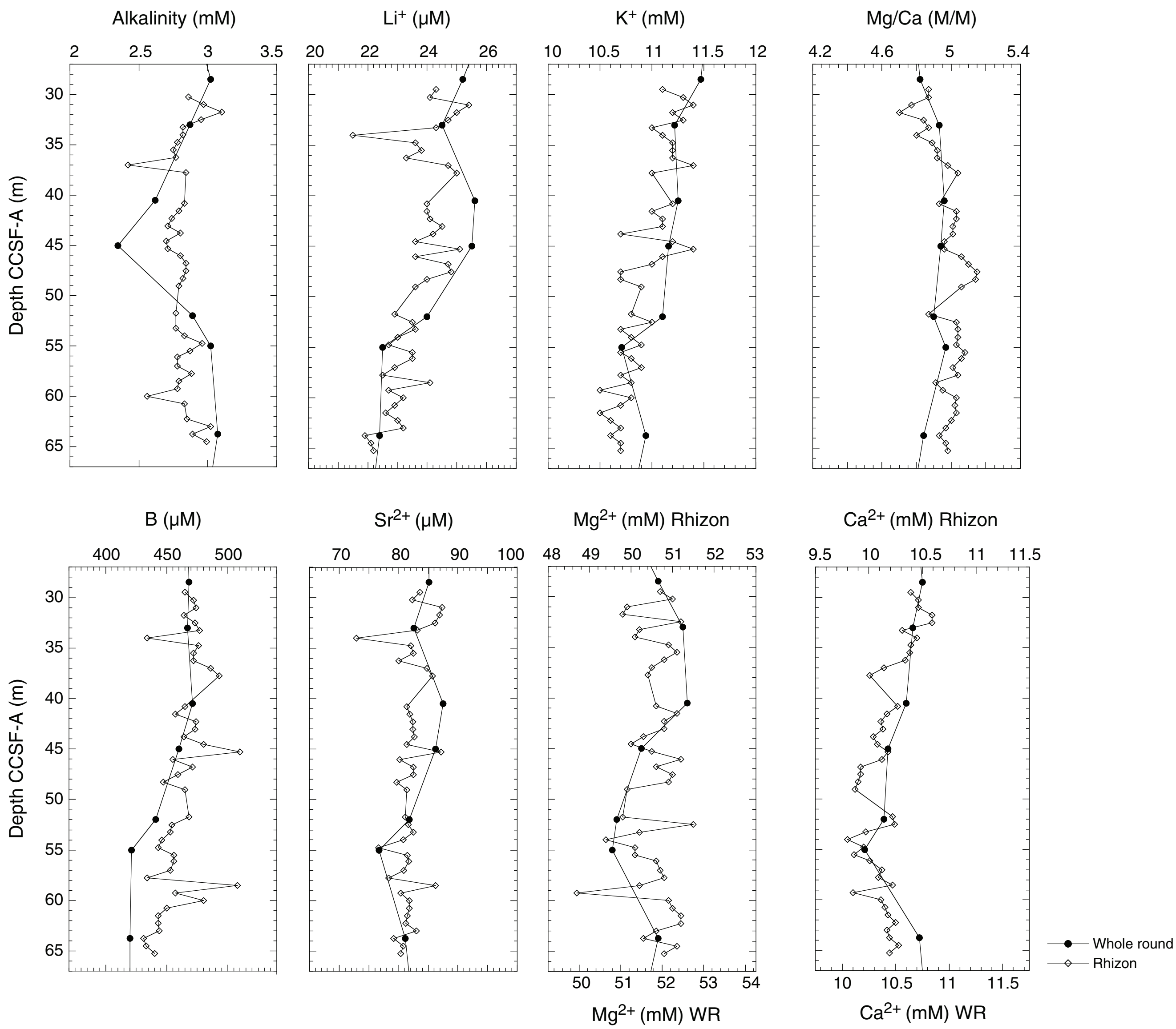

Figure F26. Calcium carbonate ($CaCO_3$), total carbon (TC), inorganic carbon (IC), and total organic carbon (TOC) determined by difference and acidification methods in sediments from Hole U1332A. (See **"Lithostratigraphy"** for information on unit boundaries.)

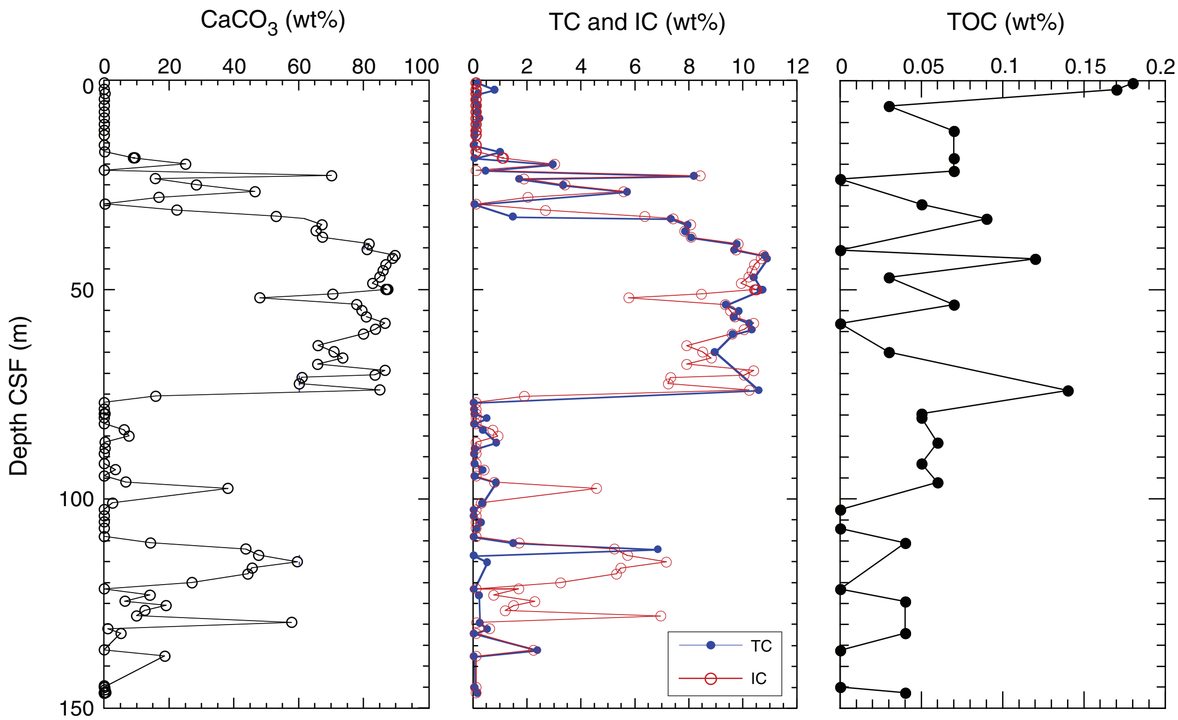

Figure F27. Whole-Round Multisensor Logger (WRMSL) and natural gamma radiation (NGR) data, Holes U1332A–U1332C. Hole U1332B and U1332C data are plotted using offsets (0.5 and 1 g/cm³ for gamma ray attenuation [GRA] bulk density; 10 and 20 × 10^{-5} SI for magnetic susceptibility; 100 and 200 m/s for *P*-wave velocity; 10 and 20 cps for NGR).

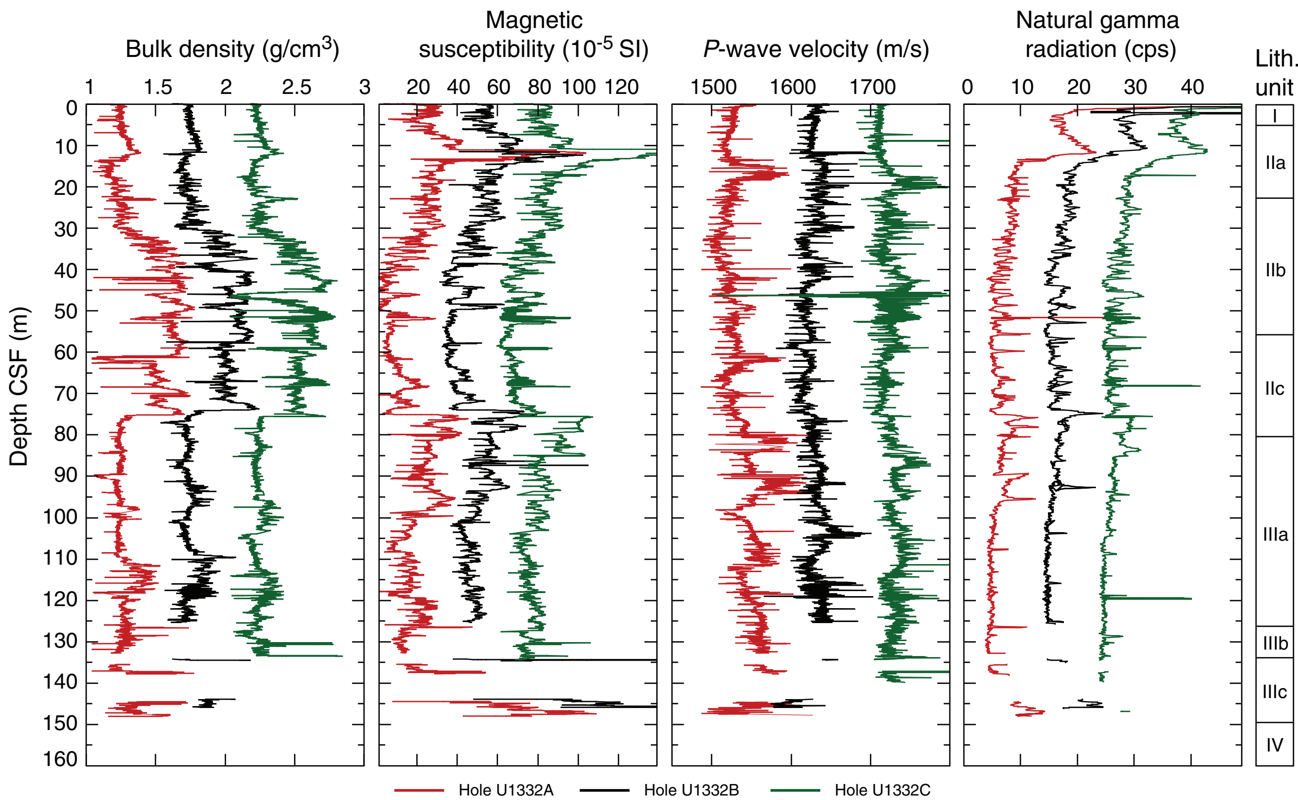

Figure F28. Moisture and density measurements, Hole U1332A. GRA = gamma ray attenuation.

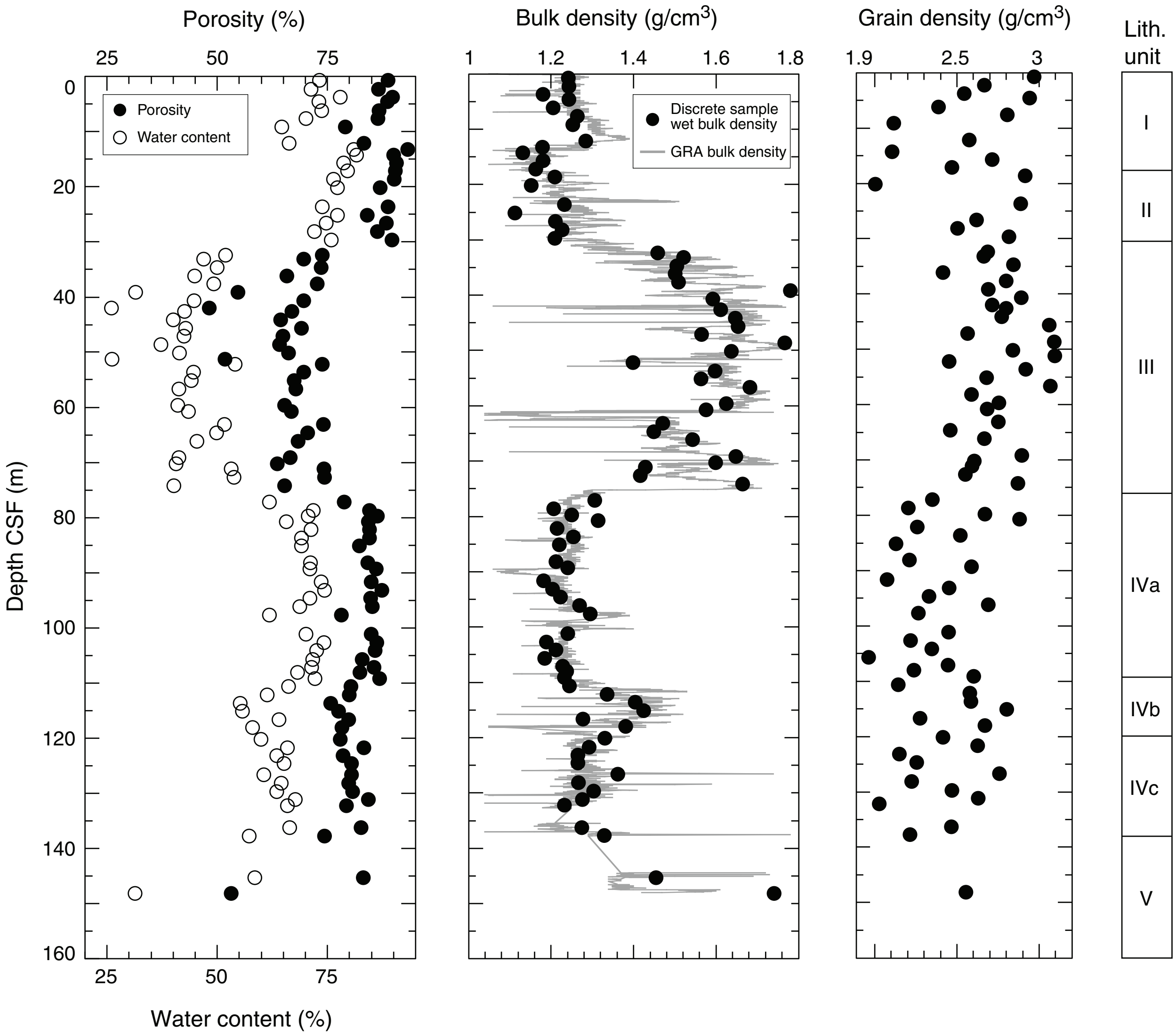

Figure F29. Moisture and density (MAD) analysis of discrete samples, Hole U1332A. Gamma ray attenuation (GRA) density interpolated with a 20 cm wide Gaussian window.

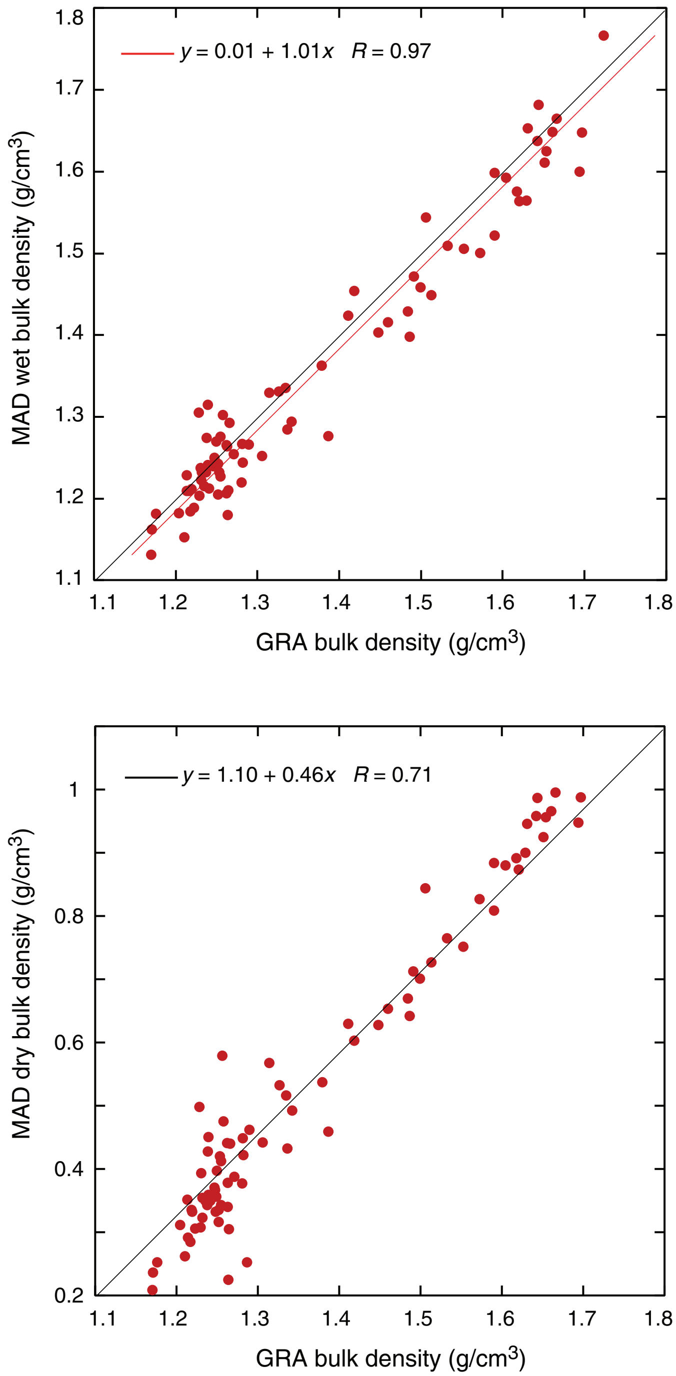

Figure F30. Compressional wave velocity from the *P*-wave logger (PWL) and discrete velocity measurements on split core from Hole U1332A, using the contact probe for *x*-axis measurements and insertion probes for *y*- and *z*-axis measurements. (see **"Compressional wave velocity"** for note on postcruise velocity correction.)

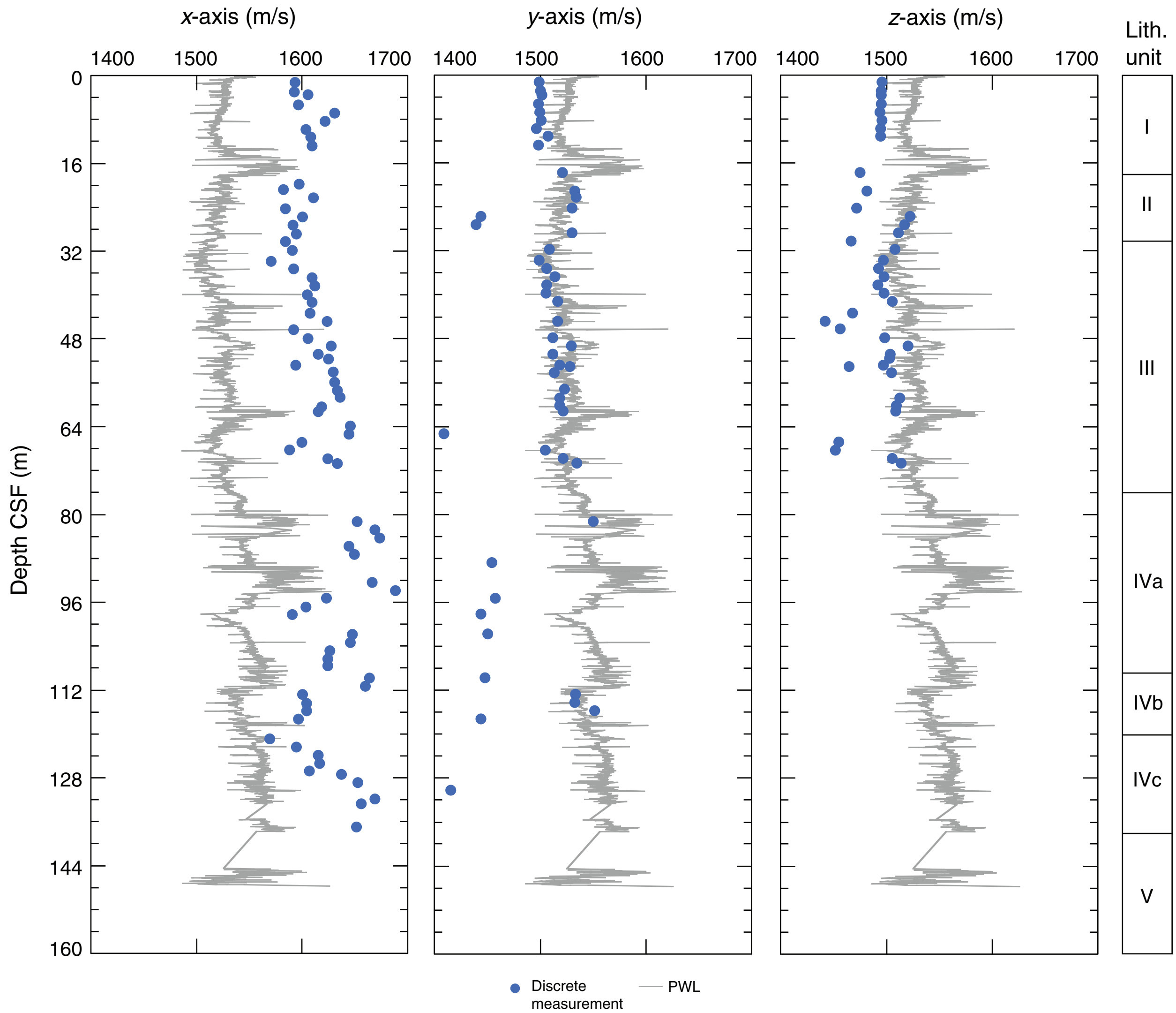

Figure F31. Compressional wave velocity from the *P*-wave logger (PWL) plotted with wet bulk density (MAD measurements).

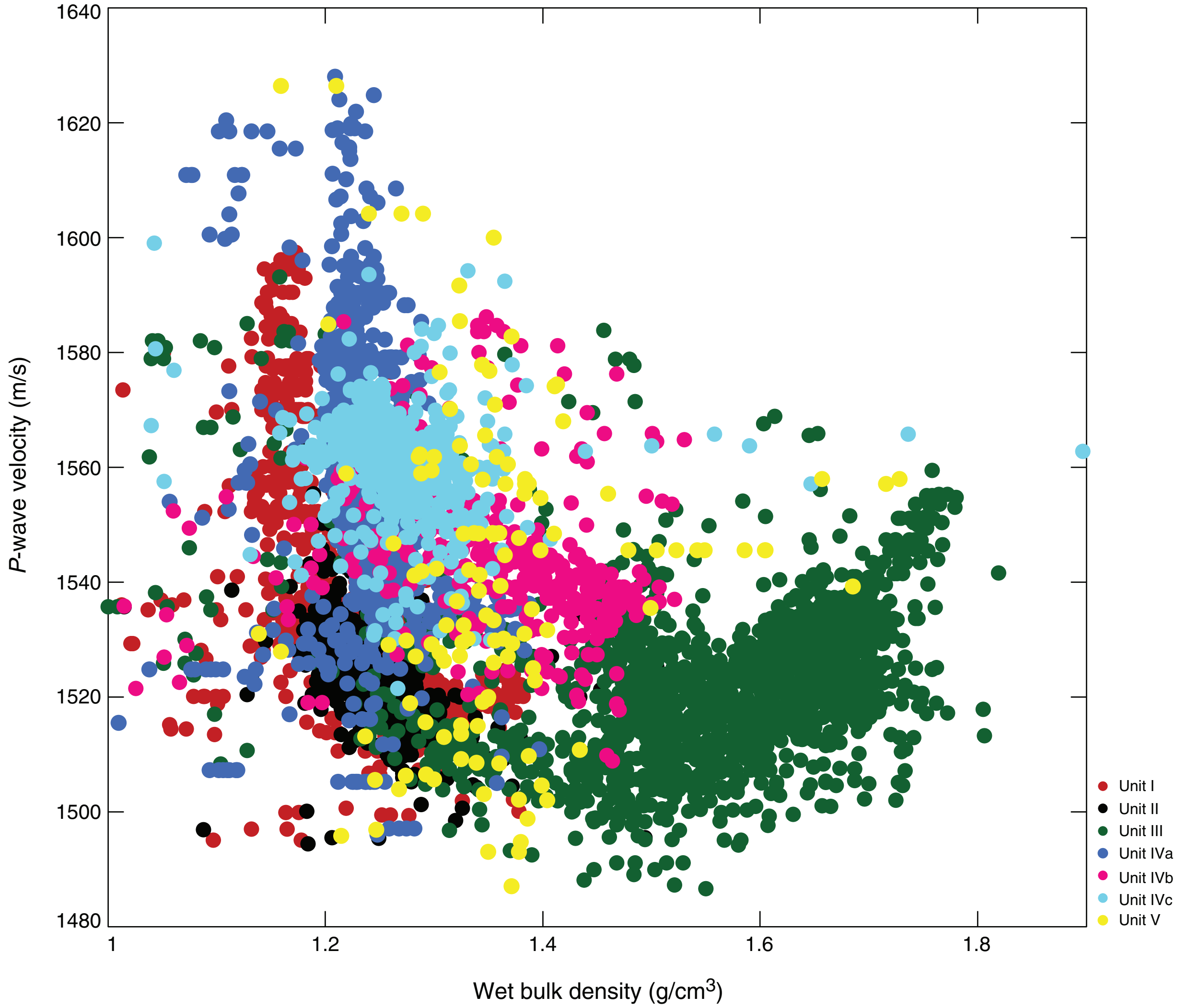

Figure F32. Thermal conductivity measurements, Hole U1332A.

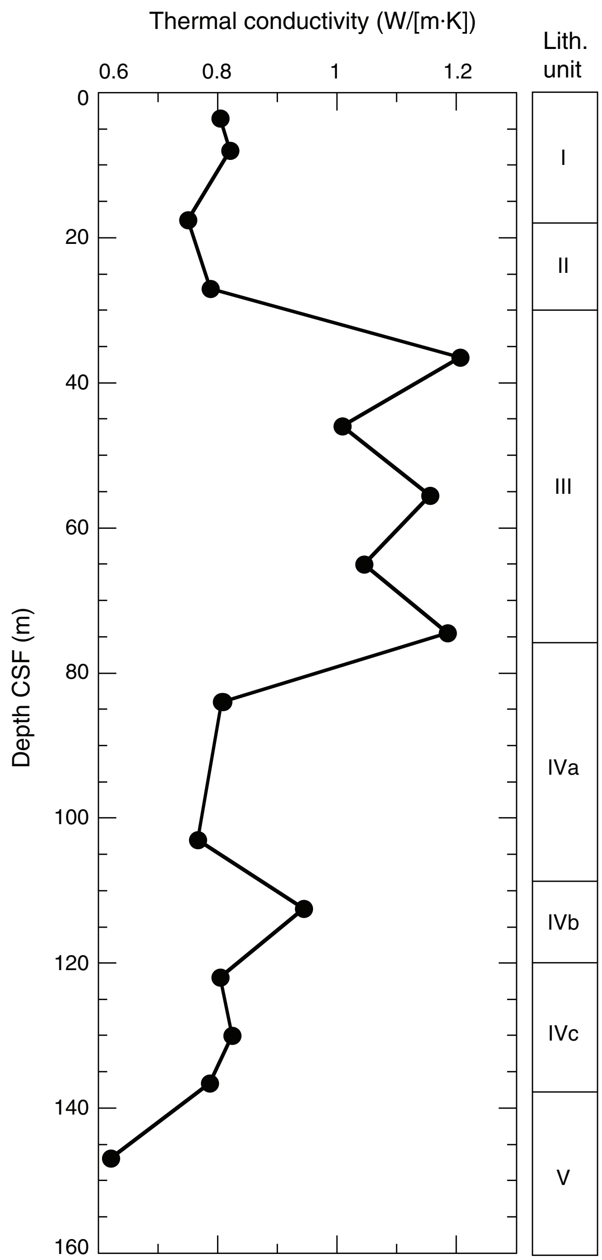

Figure F33. Reflectance spectrophotometer (RSC) data, Holes U1332A–U1332C. RSC for Holes U1332B and U1332C have been offset (20 and 40 for L*; 5 and 10 for a*; 10 and 20 for b*) for core to core comparison. L*, a*, b* = reflectance value of sediment as defined in the LAB color model.

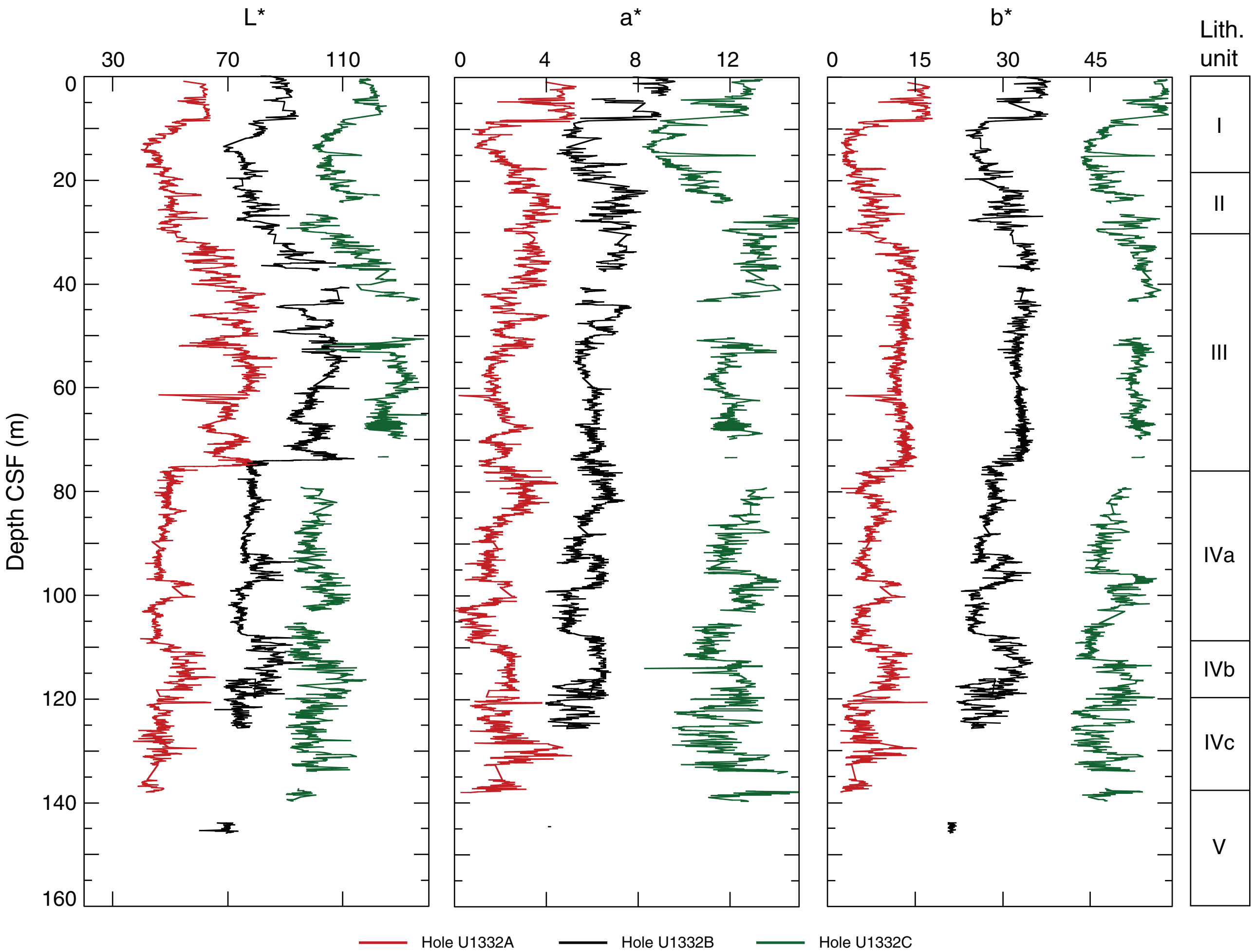

Figure F34. Magnetic susceptibility data, Site U1332. Top panel = spliced section with core breaks (triangles) and hole designations, bottom panel = Holes U1332A (red), U1332B (blue), and U1332C (green), offset from each other by a constant (300 × 10^{-6} SI). **A.** 0–50 CCSF-A. (**Continued on next three pages.**)

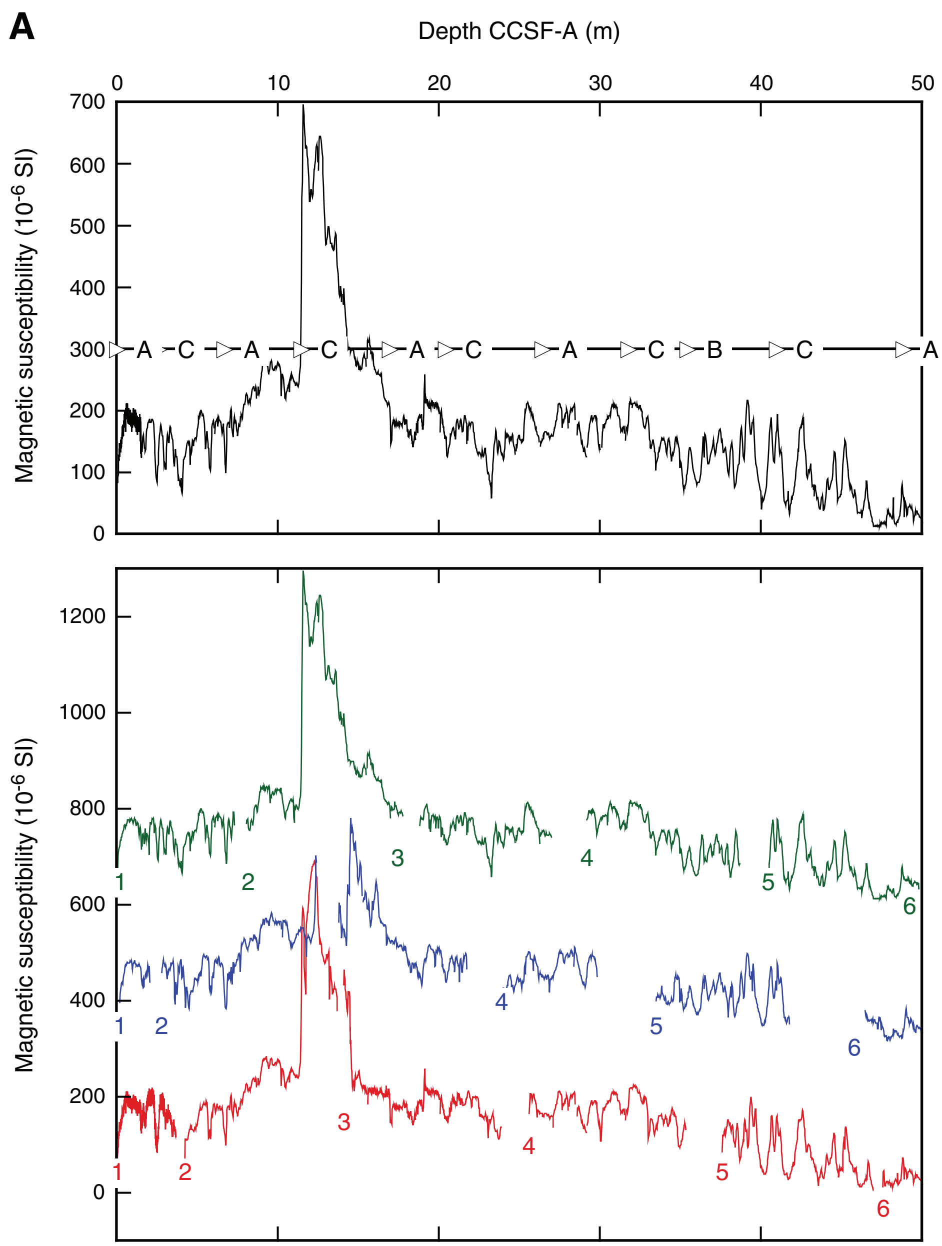

Figure F34 (continued). B. 50–100 CCSF-A. (Continued on next page.)

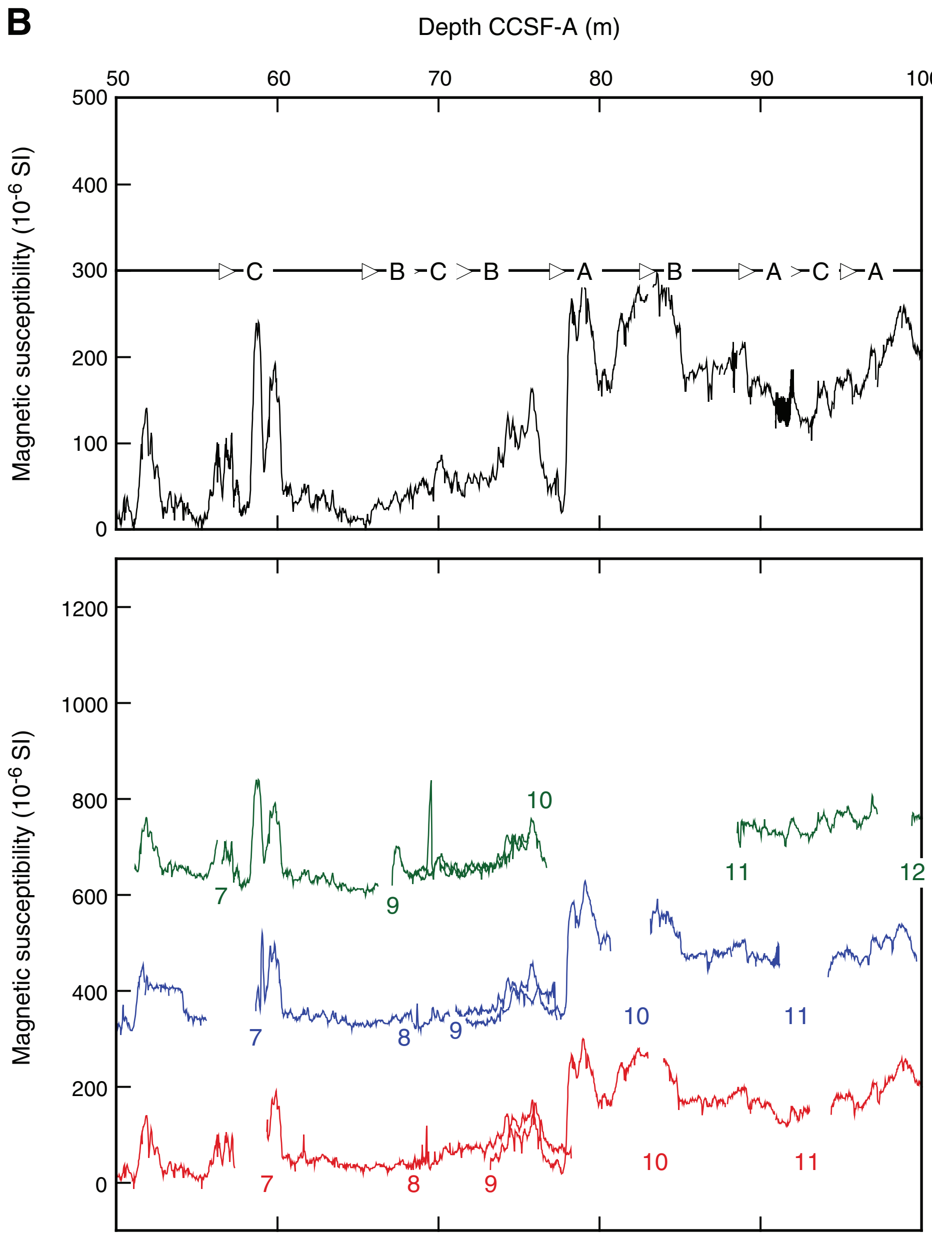

Figure F34 (continued). C. 100–150 CCSF-A. (**Continued on next page.**)

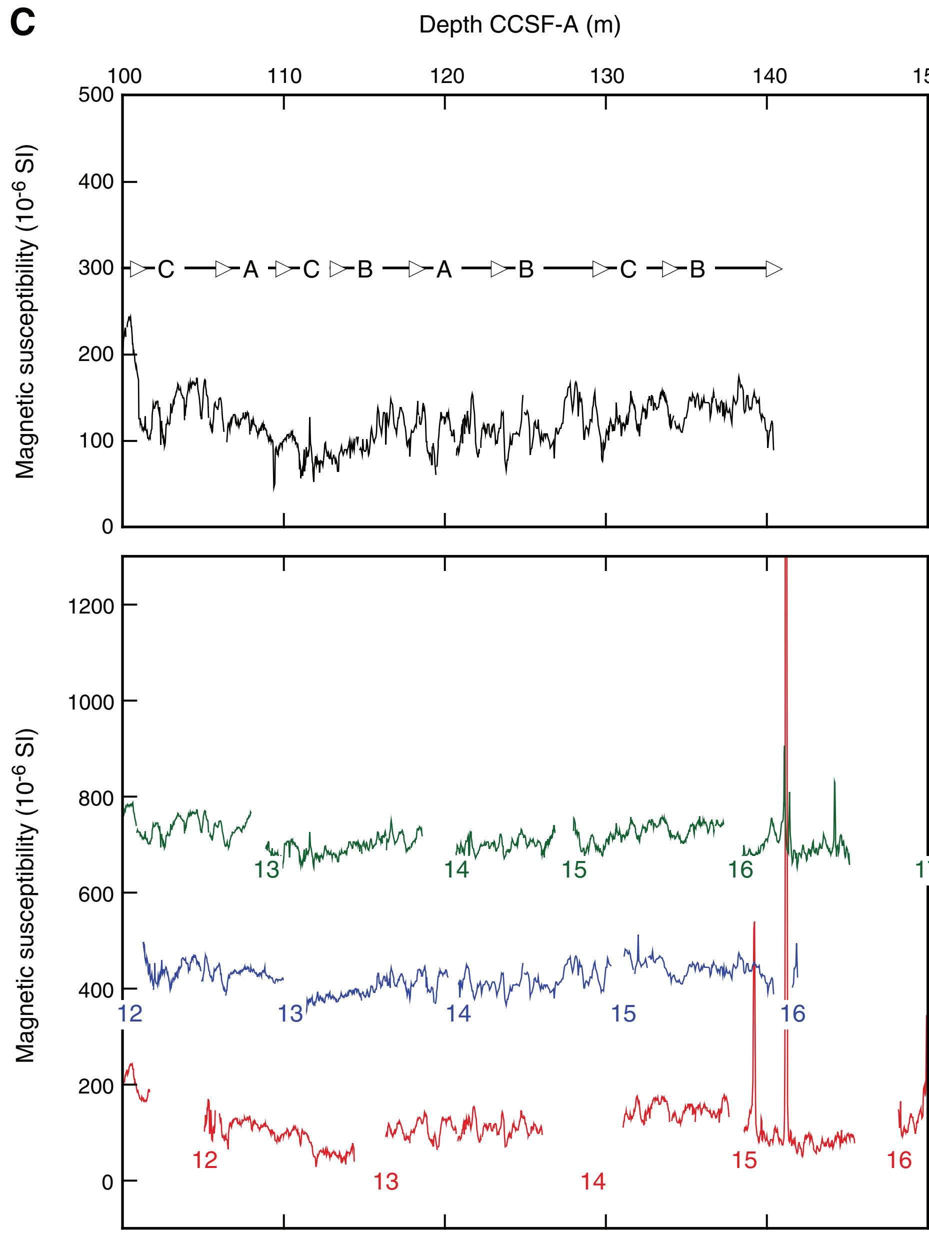

Figure F34 (continued). D. 150–200 CCSF-A.

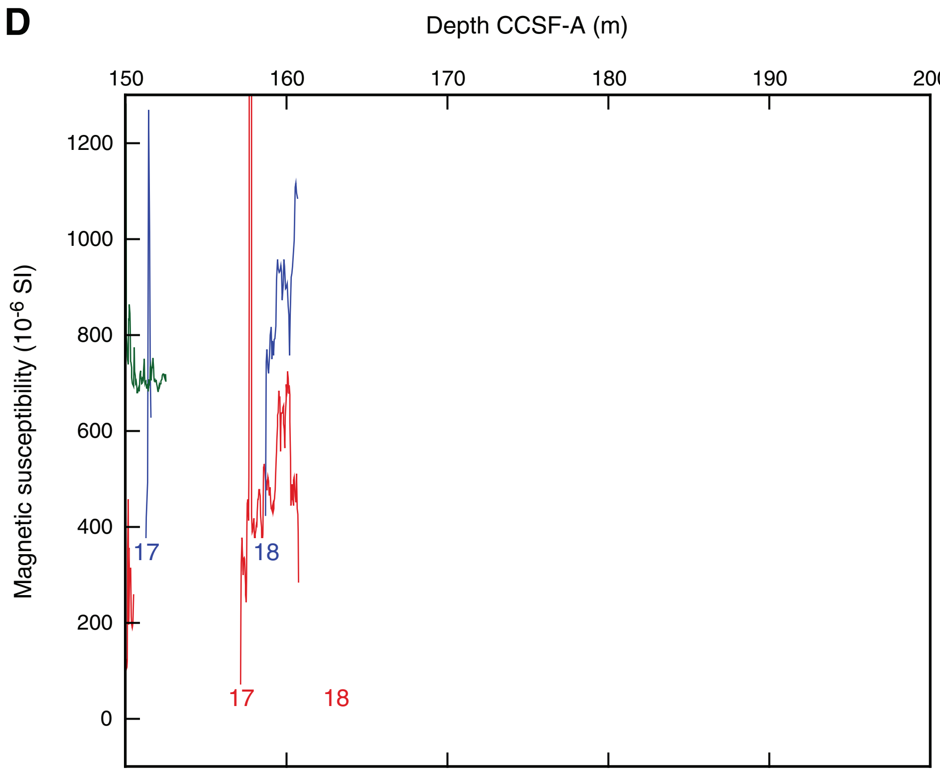

Figure F35. Magnetic susceptibility data, Site U1332. **A.** Magnetic susceptibility data from Cores 320-U1332A-7H through 9H, 320-U1332B-7H through 9H, and 320-U1332C-7H through 9H. Note similar pattern in Cores 8H and 9H of each hole. **B.** Correlation of magnetic susceptibility data from Cores 320-U1332B-7H through 9H and 320-U1332C-7H through 9H to Cores 320-U1332A-7H through 9H, illustrating the actual sequence of sediment at U1332. Note gaps between Cores 320-U1332A-7H through 9H have been expanded artificially for straightforward correlation. **C.** Correlation of magnetic susceptibility data from Cores 320-U1332A-7H through 9H, 320-U1332B-7H through 9H, and 320-U1332C-7H through 9H to ODP Site 1220. The strong similarity between observed patterns allows for detailed correlation between all three holes and confirms duplication of sediments and recovery of a complete stratigraphic record. The sharp contact observed in Section 320-U1332C-9H-2 (core image) marks the base of the duplicated interval.

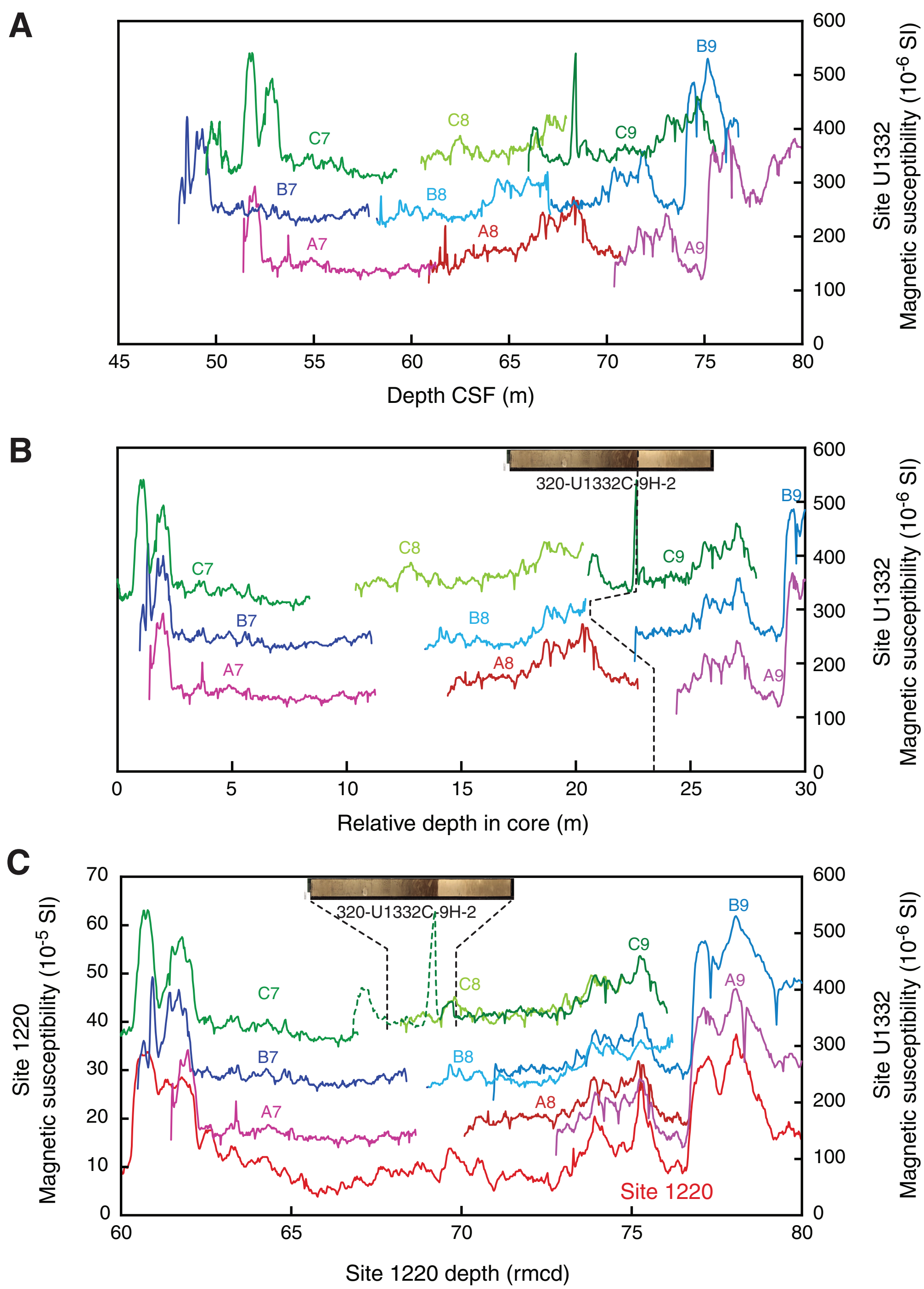

Figure F36. CSF depth vs. CCSF-A depth for tops of cores, Site U1332. Growth factor = slope of the regression line. On average, CCSF-A depth of spliced section is 10% greater than CSF depth.

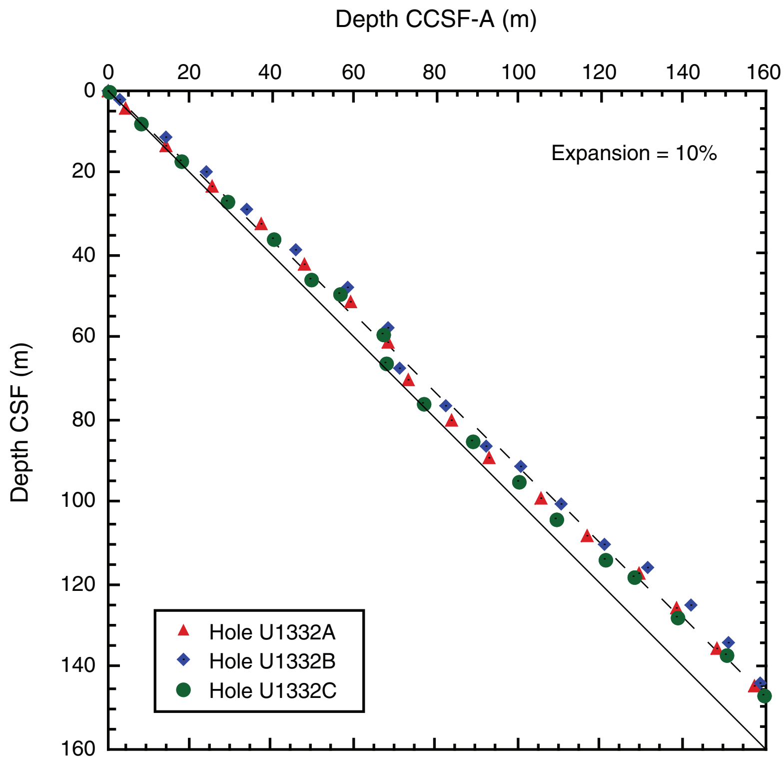

Figure F37. Logging operations summary diagram. **A.** Modified triple combination tool string run in Hole 1332A. **B.** Depth intervals of downlog and two upward passes. HNGS = Hostile Environment Gamma Ray Sonde, HLDS = Hostile Environment Litho-Density Sonde, MSS = Magnetic Susceptibility Sonde.

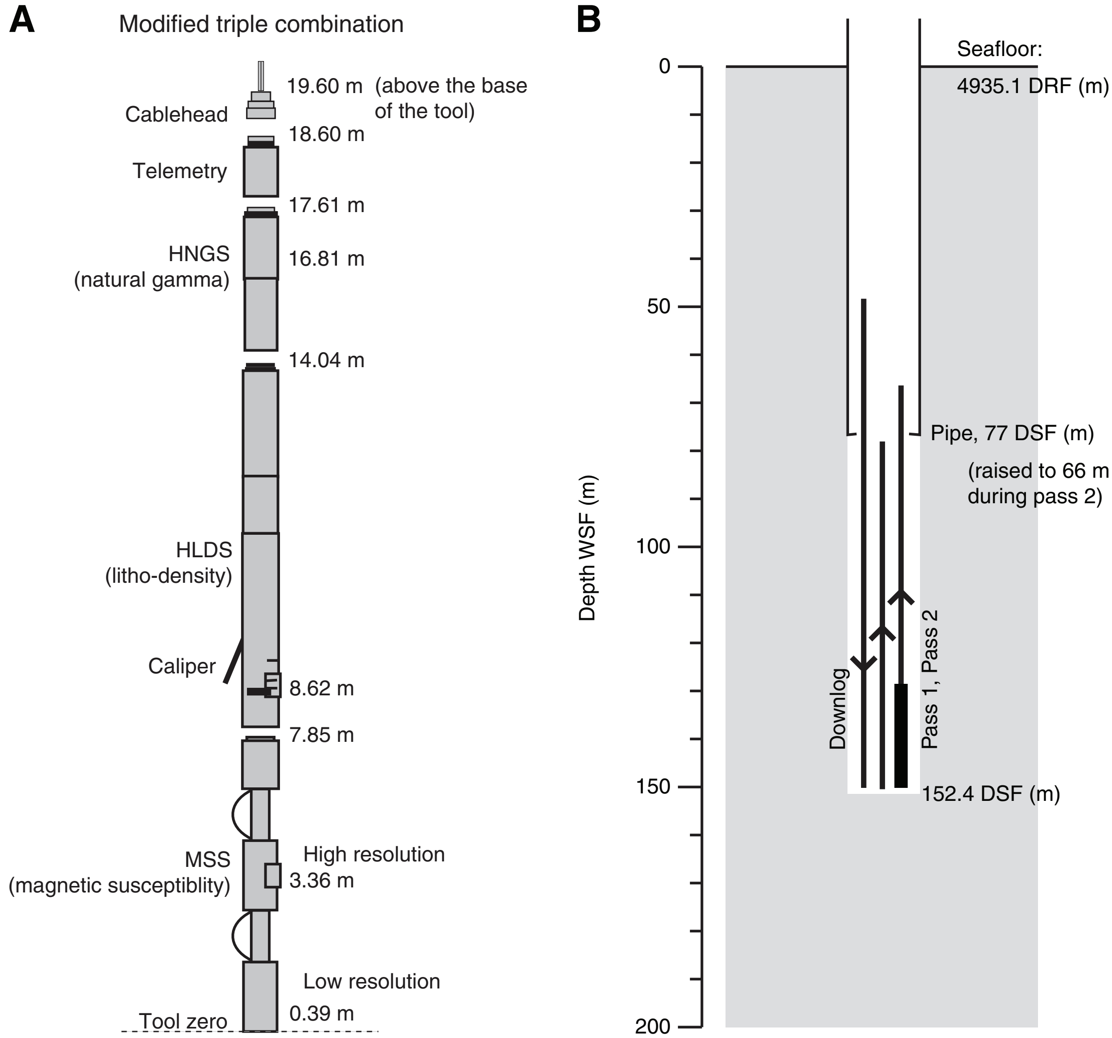

Figure F38. Downhole logs, Hole U1332A. Logging units are described in text. Unit 1 is characterized by alternating radiolarian and nannofossil oozes with higher density and photoelectric effect (PEF) in the nannofossil oozes. Uncal. = uncalibrated.

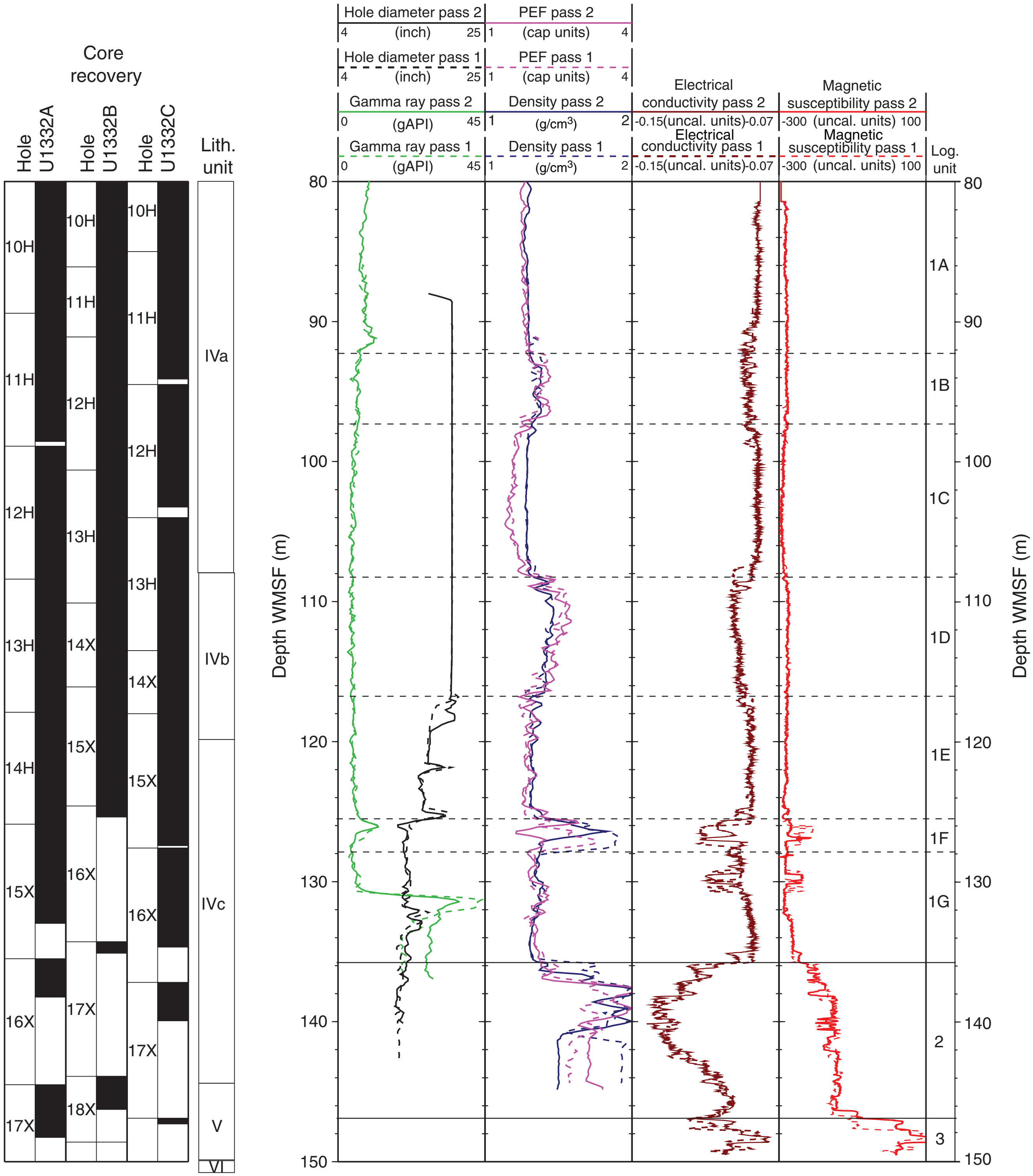

Figure F39. Natural gamma radiation data, Hole U1332A. A large peak in uranium and potassium occurs at ~130 m WMSF.

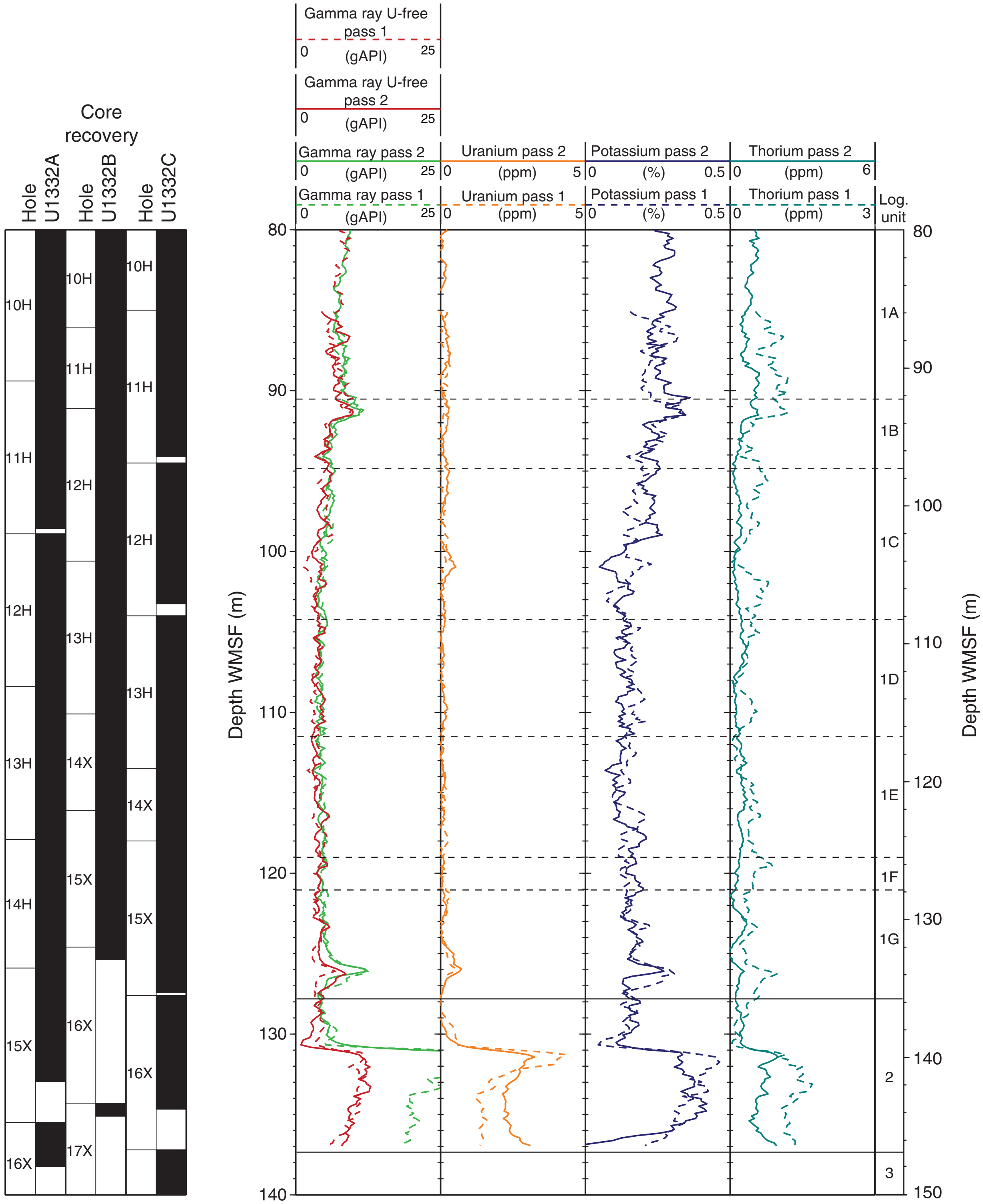

Figure F40. Heat flow calculation, Hole U1332A. **A.** Sediment temperatures. **B.** Thermal resistance based on laboratory thermal conductivity data. **C.** Bullard plot where heat flow is calculated from a linear fit of the temperature data. APCT-3 = advanced piston corer temperature tool.

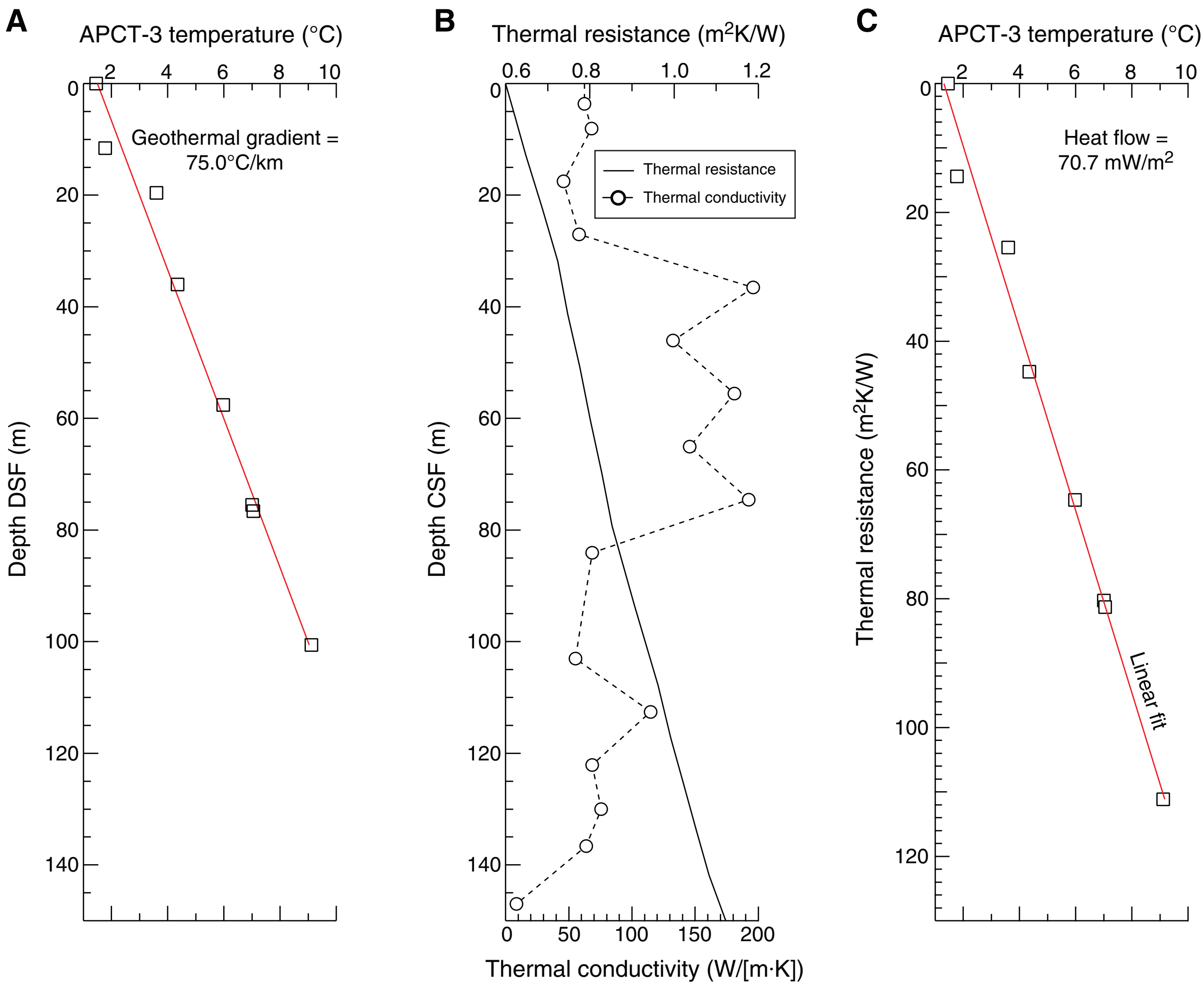

Table T1. Coring summary, Site U1332. (See table notes.) (Continued on next page.)

Site U1332
Time on site (h): 172.8 (1445 h, 22 March–1930 h, 29 March 2009)

Hole U1332A
Latitude: 11°54.710′N
Longitude: 141°2.743′W
Time on hole (h): 89.3 (1445 h, 22 March–0800 h, 26 March 2009)
Seafloor (drill pipe measurement below rig floor, m DRF): 4935.1
Distance between rig floor and sea level (m): 11.2
Water depth (drill pipe measurement from sea level, mbsl): 4923.9
Total depth (drill pipe measurement from rig floor, m DRF): 5087.5
Total penetration (drilling depth below seafloor, m DSF): 152.4
Total length of cored section (m): 152.4
Total core recovered (m): 145.6
Core recovery (%): 96
Total number of cores: 18

Hole U1332B
Latitude: 11°54.721′N
Longitude: 141°2.743′W
Time on hole (h): 38.5 (0800 h, 26 March–2230 h, 27 March 2009)
Seafloor (drill pipe measurement below rig floor, m DRF): 4936.9
Distance between rig floor and sea level (m): 11.2
Water depth (drill pipe measurement from sea level, mbsl): 4925.7
Total depth (drill pipe measurement from rig floor, m DRF): 5089.5
Total penetration (drilling depth below seafloor, m DSF): 148.6
Total length of cored section (m): 148.6
Total core recovered (m): 141.3
Core recovery (%): 94
Total number of cores: 18

Hole U1332C
Latitude: 11°54.737′N
Longitude: 141°2.740′W
Time on hole (h): 45.0 h (2230 h, 27 March–1930 h, 29 March 2009)
Seafloor (drill pipe measurement below rig floor, m DRF): 4934.0
Distance between rig floor and sea level (m): 11.2
Water depth (drill pipe measurement from sea level, mbsl): 4922.8
Total depth (drill pipe measurement from rig floor, m DRF): 5089.5
Total penetration (drilling depth below seafloor, m DSF): 155.5
Total length of cored section (m): 155.5
Total core recovered (m): 148.1
Core recovery (%): 95
Total number of cores: 18

			Depth DSF (m)			Depth CSF (m)			
Core	Date (2009)	Local time (h)	Top of cored interval	Bottom of cored interval	Interval advanced (m)	Top of cored interval	Bottom of cored interval	Length of core recovered (m)	Recovery (%)
320-U1332A-									
1H	23 Mar	1125	0.0	3.9	3.9	0.0	3.91	3.91	100
2H	23 Mar	1245	3.9	13.4	9.5	3.9	13.67	9.77	103
3H	23 Mar	1440	13.4	22.9	9.5	13.4	23.56	10.16	107
4H	23 Mar	1550	22.9	32.4	9.5	22.9	33.00	10.10	106
5H	23 Mar	1710	32.4	41.9	9.5	32.4	42.52	10.12	107
6H	23 Mar	1835	41.9	51.4	9.5	41.9	52.02	10.12	107
7H	23 Mar	1950	51.4	60.9	9.5	51.4	61.54	10.14	107
8H	23 Mar	2110	60.9	70.4	9.5	60.9	71.05	10.15	107
9H	23 Mar	2220	70.4	79.9	9.5	70.4	80.52	10.12	107
10H	23 Mar	2335	79.9	89.4	9.5	79.9	89.94	10.04	106
11H	24 Mar	0100	89.4	98.9	9.5	89.4	98.57	9.17	97
12H	24 Mar	0240	98.9	108.4	9.5	98.9	108.50	9.60	101
13H	24 Mar	0410	108.4	117.9	9.5	108.4	118.43	10.03	106
14H	24 Mar	0610	117.9	125.9	8.0	117.9	126.33	8.43	105
15X	24 Mar	0835	125.9	135.5	9.6	125.9	132.98	7.08	74
16X	24 Mar	1045	135.5	144.5	9.0	135.5	138.25	2.75	31
17X	24 Mar	1300	144.5	150.4	5.9	144.5	148.26	3.76	64
18X	24 Mar	1515	150.4	152.4	2.0	150.4	150.56	0.16	8
				Advanced total:	152.4			145.6	96
				Total interval cored:	152.4				

Table T1 (continued).

Core	Date (2009)	Local time (h)	Depth DSF (m) Top of cored interval	Depth DSF (m) Bottom of cored interval	Interval advanced (m)	Depth CSF (m) Top of cored interval	Depth CSF (m) Bottom of cored interval	Length of core recovered (m)	Recovery (%)
320-U1332B-									
1H	26 Mar	1300	0.0	2.10	2.1	0.00	2.10	2.10	100
2H	26 Mar	1500	2.1	11.60	9.5	2.10	12.14	10.04	106
3H	26 Mar	1630	11.6	19.60	8.0	11.60	21.52	8.42	124
4H	26 Mar	1800	19.6	29.10	9.5	19.60	29.66	10.06	106
5H	26 Mar	1930	29.1	38.60	9.5	29.10	37.68	8.58	90
6H	26 Mar	2235	38.6	48.10	9.5	38.60	48.55	9.95	105
7H	27 Mar	0025	48.1	57.60	9.5	48.10	58.10	10.00	105
8H	27 Mar	0310	57.6	67.10	9.5	57.60	67.30	9.70	102
9H	27 Mar	0530	67.1	76.60	9.5	67.10	77.12	10.02	105
10H	27 Mar	0700	76.6	86.10	9.5	76.60	86.69	10.09	106
11H	27 Mar	0830	86.1	91.10	5.0	86.10	93.87	7.77	155
12H	27 Mar	1020	91.1	100.60	9.5	91.10	101.06	9.96	105
13H	27 Mar	1215	100.6	110.10	9.5	100.60	110.81	10.21	107
14X	27 Mar	1345	110.1	116.10	6.0	110.10	119.83	9.73	162
15X	27 Mar	1515	116.1	124.60	8.5	116.10	125.82	9.72	114
16X	27 Mar	1645	124.6	134.30	9.7	124.60	125.39	0.79	8
17X	27 Mar	1850	134.3	143.90	9.6	134.30	135.11	0.78	8
18X	27 Mar	2055	143.9	148.60	4.7	143.90	146.26	2.36	50
				Advanced total:	148.6			140.28	94
				Total interval cored:	148.6				
320-U1332C-									
1H	28 Mar	0135	0.0	7.50	7.5	0.00	7.49	7.49	100
2H	28 Mar	0300	7.5	17.00	9.5	7.50	17.48	9.98	105
3H	28 Mar	0415	17.0	26.50	9.5	17.00	26.96	9.96	105
4H	28 Mar	0550	26.5	36.00	9.5	26.50	36.55	10.05	106
5H	28 Mar	0730	36.0	45.50	9.5	36.00	45.79	9.79	103
6H	28 Mar	0850	45.5	49.50	4.0	45.50	53.07	7.57	189
7H	28 Mar	1000	49.5	59.00	9.5	49.50	59.46	9.96	105
8H	28 Mar	1115	59.0	66.00	7.0	59.00	68.22	9.22	132
9H	28 Mar	1255	66.0	75.50	9.5	66.00	75.96	9.96	105
10H	28 Mar	1815	75.5	85.00	9.5	75.50	85.58	10.08	106
11H	28 Mar	2030	85.0	94.50	9.5	85.00	94.10	9.10	96
12H	28 Mar	2150	94.5	104.00	9.5	94.50	103.25	8.75	92
13H	28 Mar	2315	104.0	113.50	9.5	104.00	114.13	10.13	107
14X	29 Mar	0040	113.5	118.00	4.5	113.50	119.88	6.38	142
15X	29 Mar	0215	118.0	127.60	9.6	118.00	127.43	9.43	98
16X	29 Mar	0350	127.6	137.20	9.6	127.60	134.67	7.07	74
17X	29 Mar	0600	137.2	146.90	9.7	137.20	139.94	2.74	28
18X	29 Mar	0810	146.9	155.50	8.6	146.90	147.30	0.40	5
				Advanced total:	155.5			148.06	95
				Total interval cored:	155.5				

Notes: DRF = drilling depth below rig floor, DSF = drilling depth below seafloor, CSF = core depth below seafloor. H = APC core, X = XCB core. Local time = UTC – 10 h.

Table T2. Lithologic unit boundaries, Site U1332. (**See table notes.**)

Unit	Core, section, interval (cm)	Depth CSF (m)	Core, section, interval (cm)	Depth CSF (m)	Core, section, interval (cm)	Depth CSF (m)
	320-U1331A-		320-U1331B-		320-U1331C-	
I	3H-3, 130	17.7	3H-4, 150	17.6	3H-1, 70	17.7
II	5H-1, 150	33.9	5H-1, 150	30.6	4H-7, 30	35.8
III	9H-4, 124	76.14	9H-6, 50	75.1	10H-1, 41	75.91
IVa	13H-1, 20	108.6	13H-5, 120	107.8	13H-2, 150	107
IVb	14H-1, 150	119.4	15H-4, 40	121	15H-2, 50	120
IVc	16X-CC, 42*	138.29*	17X-CC, 40*	135.08*	17X-2, 7*	138.77*
V	17X-CC, 3	148.15	18X-CC, 16	146.09	18X-CC, 46	147.36
VI	18X-CC, 52*	150.56*	18X-CC, 34*	146.27*	18X-CC, 62*	147.52*

Notes: Interval/depth are given for basal boundary of each unit. * = unit extends through at least given interval and depth, but boundary was not cored.

Table T3. Calcareous nannofossil datums, Site U1332. (See table note.)

Core, section, interval (cm)				Depth CSF (m)			
Top	Bottom	Marker species	Age (Ma)	Top	Bottom	Midpoint	±
320-U1332A-	320-U1332A-						
3H-4, 100	3H-5, 100	T *Triquetrorhabdulus carinatus*	18.28	18.90	20.40	19.65	0.75
3H-7, 60	3H-CC	T *Sphenolithus delphix*	23.1	23.00	23.51	23.26	0.26
3H-CC	4H-2, 60	B *Sphenolithus delphix*	23.2	23.51	23.50	23.51	0.01
4H-2, 60	4H-3, 60	X *T. longus/T. carinatus*	24.7	25.00	26.50	25.75	0.75
4H-2, 60	4H-3, 60	Tc *C. abisectus*	24.7	25.00	26.50	25.75	0.75
4H-CC	5H-1, 80	T *Sphenolithus predistentus*	26.9	32.95	33.20	33.08	0.13
5H-3, 80	5H-4, 80	T *Sphenolithus pseudoradians*	28.8	36.20	37.70	36.95	0.75
6H-5, 70	6H-6, 70	B *Sphenolithus distentus*	30.0	48.60	50.10	49.35	0.75
7H-6, 80	7H-7, 80	T *Reticulofenestra umbilicus*	32.0	59.69	61.18	60.44	0.75
8H-4, 50	8H-5, 50	T *Coccolithus formosus*	32.9	65.90	67.40	66.65	0.75
9H-4, 110	10H-3, 80	T *Discoaster saipanensis*	34.4	76.00	83.70	79.85	3.85
11H-5, 70	11H-6, 70	T *Chiasmolithus grandis*	37.1	96.10	97.60	96.85	0.75
11H-CC	12H-2, 100	B *Dictyococcites bisectus*	38.0	98.52	101.40	99.96	1.44
12H-2, 100	13H-1, 140	T *Chiasmolithus solitus*	40.4	101.40	109.80	105.60	4.20
14H-5, 40	14H-6, 35	T *Nannotetrina*	42.3	124.30	125.74	125.02	0.72
14H-CC	15X-1, 113	B *Reticulofenestra umbilicus* >14 µm	42.5	126.28	127.03	126.66	0.38
15X-2, 137	15X-3, 66	T *Nannotetrina fulgens*	43.4	128.77	129.56	129.17	0.39
16X-2, 39	16X-CC	B *Nannotetrina fulgens*	46.8	137.39	138.20	137.80	0.41
320-U1332B-	320-U1332B-						
17X-CC	18X-2, 48	T *Discoaster lodoensis*	48.4	135.06	145.88	140.47	5.41

Note: T = top, B = bottom, X = abundance crossover, Tc = top common.

Table T4. Preservation and relative abundance of radiolarians, Hole U1332A. This table is available in an oversized format.

Table T5. Preservation and relative abundance of radiolarians, Hole U1332B. (See table notes.) (Continued on next page.)

Core, section, interval (cm)	Radiolarian zone	Abundance	Preservation	Mixing	*Anthocyrtoma* spp.	*Artophormis barbadensis*	*Artophormis gracilis*	*Calocyclas bandyca*	*Calocyclas hispida*	*Calocyclas turris*	*Calocycletta anekathen*	*Calocycletta robusta*	*Calocycloma ampulla*	*Calocycloma castum*	*Carpocanopsis bramlettei*	*Carpocanopsis cingulata*	*Centrobotrys gravida*	*Cryptocarpium azyx*	*Cryptocarpium ornatum*
320-U1332B-																			
1H-CC		R	P	3															
2H-CC		B																	
3H-CC	RN1	C	M									R			R	R			
4H-CC		C	M				R												
5H-CC	RP21	A	G	2															
6H-CC		A	M																
7H-CC		A	M	1			R												
8H-CC		A	G	2			F										R		
9H-5, 15–23	RP20	C	G	I			R												
9H-5, 45–53		C	G	1			R										R		
9H-5, 75–83		A	G				R				R								
9H-5, 112–120		A	M	3					R		R								R
9H-5, 135–143	RP19	A	M	3					R		R								R
9H-6, 15–23		A	M	3					R		R								R
9H-CC		A	G	2		R					C								F
10H-CC	RP18	A	G	1				R			R							F	R
11H-CC		A	G	1					R				R					VR	R
12H-CC	RP16	A	G	1		VR								R					R
13H-CC		C	M											R					R
14H-CC		A	G											R					
15H-CC	RP14	A	G		R									R					
16H-CC		A	G											R					
17H-CC	RP12	A	G											R					
18H-CC	B																		

Core, section, interval (cm)	*Dictyophimus craticula*	*Dictyoprora armadillo*	*Dictyoprora mongolfieri*	*Didymocyrtis laticonus*	*Didymocyrtis tubaria*	*Didymocyrtis violina*	*Dorcadospyris anastasis*	*Dorcadospyris ateuchus*	*Dorcadospyris circulus*	*Dorcadospyris copelata*	*Dorcadospyris ombros* (upper)	*Dorcadospyris pseudopapilio*	*Dorcadospyris quadripes*	*Dorcadospyris riedeli*	*Dorcadospyris scambos*
320-U1332B-															
1H-CC															
2H-CC															
3H-CC				R	R	R		R							R
4H-CC								R	R					R	R
5H-CC									R						
6H-CC									R						
7H-CC													R		
8H-CC										R		R	R		
9H-5, 15–23										R					
9H-5, 45–53										R					
9H-5, 75–83										R					
9H-5, 112–120		R													
9H-5, 135–143		R								VR	R				
9H-6, 15–23		R													
9H-CC		VR	R							R	R				
10H-CC		R	R							R	R				
11H-CC		R									R				
12H-CC		R					R				R				
13H-CC											R				
14H-CC	R														
15H-CC	R														
16H-CC	R														
17H-CC	R														
18H-CC															

Core, section, interval (cm)	*Dorcadospyris spinosa*	*Eucyrtidium diaphanes*	*Eucyrtidium mitodes*	*Eucyrtidium plesiodiaphanes*	*Eusyringium fistuligerum*	*Eusyringium lagena*	*Lithochytris vespertilio*	*Lithocyclia angusta*	*Lithocyclia aristotelis* gr.	*Lithocyclia crux*	*Lithocyclia ocellus* gr.	*Lophocyrtis exitelus*	*Lophocyrtis hadra*	*Lophocyrtis jacchia*	*Lophocyrtis milowi*
320-U1332B-															
1H-CC															
2H-CC															
3H-CC		R	R												
4H-CC			R												
5H-CC			R	R				R							
6H-CC				R				R							
7H-CC	R							R		R					R
8H-CC					VR			R		R					R
9H-5, 15–23								R	R						R
9H-5, 45–53								R							R
9H-5, 75–83								R							
9H-5, 112–120								R	R			R	R	R	
9H-5, 135–143					—			R	R			R	R	R	
9H-6, 15–23								R	R		VR		R	R	
9H-CC									R			R	R	R	
10H-CC					R				R		R			R	
11H-CC					R		R		R						
12H-CC					R		R								
13H-CC					R		R								
14H-CC					R		R								
15H-CC					R	R	R								
16H-CC					R	R	R								
17H-CC					—	F	R								
18H-CC															

Notes: Abundance: A = abundant, C = common, F = frequent, R = rare, VR = very rare, B = barren, — = undetermined. Preservation: G = good, M = moderate, P = poor. Mixing: blank = no mixing of older specimens detected, 1 = 1–3 reworked specimens detected, 2 = 3–10 reworked specimens detected, 3 = >10 reworked specimens detected.

Table T5 (continued).

Core, section, interval (cm)	Radiolarian zone	Abundance	Preservation	Mixing	*Lophocyrtis oberhaensliae*	*Lophocyrtis pegetrum*	*Lychnocanoma amphitrite*	*Lychnocanoma babylonis*	*Lychnocanoma elongata*	*Lychnocanoma turgidum*	*Podocyrtis ampla*	*Podocyrtis apeza*	*Podocyrtis chalara*	*Podocyrtis diamesa*	*Podocyrtis fasciolata*	*Podocyrtis goetheana*	*Podocyrtis helenae*	*Podocyrtis mitra*	*Podocyrtis papalis*	*Podocyrtis sinuosa*	*Podocyrtis trachodes*	*Rhopalocanium ornatum*	*Sethochytris triconiscus*	*Spongatractus pachystylus*	*Theocorys puriri*	*Theocotylissa ficus*	*Theocyrtis annosa*	*Theocyrtis careotuberosa*	*Theocyrtis perpumila*	*Theocyrtis perysinos*	*Theocyrtis setanios*	*Theocyrtis tuberosa*	*Thyrsocyrtis bromia*	*Thyrsocyrtis krooni*	*Thyrsocyrtis lochites*	*Thyrsocyrtis orthotenes*	*Thyrsocyrtis robusta*	*Thyrsocyrtis tetracantha*	*Thyrsocyrtis triacantha*	*Tristylospyris triceros*	*Zealithapium mitra*	*Zealithapium plegmacantha*	*Zygocircus cimelium*
320-U1332B-																																											
1H-CC		R	P	3																																							
2H-CC		B																																									
3H-CC	RN1	C	M						R																			R															
4H-CC	RP21	C	M			R																						R															
5H-CC		A	G	2																							VR			—	R									—			
6H-CC		A	M																												R									R			
7H-CC	RP20	A	M	1	R																									R	R	C							VR	R			
8H-CC		A	G	2	R																							R		R	R	C								R			
9H-5, 15–23		C	G	I	R																				R			R				F								R			
9H-5, 45–53		C	G	1																								R				F								R			
9H-5, 75–83		A	G		R																							R												R			
9H-5, 112–120	RP19	A	M	3				R																				R							VR			VR	VR	R	R		
9H-5, 135–143		A	M	3				R																				R							VR	R		VR	VR	R			
9H-6, 15–23		A	M	3				R																				R							VR			VR	VR	R			
9H-CC		A	G	2			R			R																		R					VR						VR	R	R		
10H-CC	RP18	A	G	1						R																		R					R	R	F			R	R	R	R		
11H-CC	RP16	A	G	1															F			R						R	R					R		R			F				
12H-CC		A	G	1						R		R	F			F		R	R			R		R		R		R	R					R			VR		F				R
13H-CC		C	M									R	R						R			R	R	R		R		R	R										R				R
14H-CC	RP14	A	G							R								F	R		R		R	R															R		R		R
15H-CC		A	G							R	R				R			F	R		F			R		R			R										R				
16H-CC		A	G							R	F				R		R	F	R	R	F	R		R															R			R	
17H-CC	RP12	A	G								—			R	—		—	—	R	R	—	R		R		R													R			R	R
18H-CC	B																																										

Table T6. Preservation and relative abundance of radiolarians, Hole U1332C. (See table notes.) (Continued on next page.)

Core, section, interval (cm)	Radiolarian zone	Abundance	Preservation	Mixing	*Anthocyrtoma* spp.	*Artophormis barbadensis*	*Artophormis gracilis*	*Calocyclas bandyca*	*Calocyclas turris*	*Calocycletta anekathen*	*Calocycletta robusta*	*Calocycletta serrata*	*Calocycloma castum*	*Cryptocarpium azyx*	*Cryptocarpium ornatum*	*Cyrtocapsella cornuta*	*Cyrtocapsella tetrapera*	*Dictyophimus craticula*	*Dictyoporaa armadillo*
320-U1332C-																			
1H-CC		F	P																
2H-CC	RN1	C	M	1							F	R				F	F		
3H-CC	RP22	C	M	1			R				F								
4H-CC	RP21	C	M	3			R				R								
5H-CC		C	M	3			R												
6H-CC	RP20	A	G	2			R												
7H-CC		A	G				R												
8H-CC		A	G				R												
9H-CC		A	G						—	R				—	R				R
10H-CC	RP18	A	G				—	R	R	R				R	R				R
11H-CC	RP17	A	G			R	—	—	R	—				R	R				R
12H-CC	RP16	A	G						—					—	R				R
13H-CC	RP15				R										R				
14H-CC	RP14	A	G										R						
15H-CC		A	G																
16H-CC	RP13	A	G																
17H-CC	RP12	A	G										R					R	
18H-CC	B	B																	

Core, section, interval (cm)	*Didymocyrtis bassanii*	*Didymocyrtis prismatica*	*Dorcadospyris ateuchus*	*Dorcadospyris circulus*	*Dorcadospyris copelata*	*Dorcadospyris papilio*	*Dorcadospyris praeforcipata*	*Dorcadospyris pseudopapilio*	*Dorcadospyris quadripes*	*Dorcadospyris scambos*	*Dorcadospyris spinosa*	*Eucyrtidium diaphanes*	*Eucyrtidium mitodes*	*Eusyringium fistuligerum*	*Eusyringium lagena*
320-U1332C-															
1H-CC															
2H-CC	R	R	R				R			R		R			
3H-CC		R	R			R	R			F		R	R		
4H-CC		R	R		R							R			
5H-CC		R	R		R										
6H-CC		R	R	R					R						
7H-CC									R		R				
8H-CC															
9H-CC														—	
10H-CC														R	
11H-CC														R	
12H-CC														R	
13H-CC														R	R
14H-CC														R	VR
15H-CC														R	
16H-CC														R	R
17H-CC														VR	R
18H-CC															

Core, section, interval (cm)	*Lithochytris vespertilio*	*Lithocyclia angusta*	*Lithocyclia aristotelis* gr.	*Lithocyclia crux*	*Lophocyrtis pegetrum*	*Lophocyrtis hadra*	*Lophocyrtis jacchia*	*Lophocyrtis milowi*	*Lychnocanoma amphitrite*	*Lychnocanoma elongata*	*Lychnocanoma turgidum*	*Podocyrtis ampla*	*Podocyrtis chalara*	*Podocyrtis diamesa*	*Podocyrtis helenae*
320-U1332C-															
1H-CC															
2H-CC					R					R					
3H-CC					R					F					
4H-CC					R										
5H-CC					R										
6H-CC		R			R										
7H-CC		R		R				R							
8H-CC		R													
9H-CC		R					R								
10H-CC						R	R		R		R				
11H-CC						R					R				
12H-CC											R				
13H-CC			—								R		F		
14H-CC	R										R				VR
15H-CC	R										R	R			R
16H-CC	R											R		R	
17H-CC	R											R		R	
18H-CC															

Notes: Abundance: A = abundant, C = common, F = frequent, B = barren, R = rare, VR = very rare, — = undetermined. Preservation: G = good, M = moderate, P = poor. Mixing: blank = no mixing of older specimens detected, 1 = 1–3 reworked specimens detected, 2 = 3–10 reworked specimens detected, 3 = >10 reworked specimens detected.

Table T6 (continued).

Core, section, interval (cm)	Radiolarian zone	Abundance	Preservation	Mixing	*Podocyrtis mitra*	*Podocyrtis papalis*	*Podocyrtis phyxis*	*Podocyrtis sinuosa*	*Podocyrtis trachodes*	*Rhopalocanium ornatum*	*Sethochytris triconiscus*	*Spongatractus pachystylus*	*Theocorys puriri*	*Theocotylissa ficus*	*Theocyrtis annosa*	*Theocyrtis careotuberosa*	*Theocyrtis perpumila*	*Theocyrtis perysinos*	*Theocyrtis setanios*	*Theocyrtis tuberosa*	*Thyrsocyrtis bromia*	*Thyrsocyrtis lochites*	*Thyrsocyrtis orthotenes*	*Thyrsocyrtis tetracantha*	*Thyrsocyrtis triacantha*	*Tristylospyris triceros*	*Zealithapium mitra*	*Zealithapium plegmacantha*
320-U1332C-																												
1H-CC		F	P																									
2H-CC	RN1	C	M	1																								
3H-CC	RP22	C	M	1											R													
4H-CC	RP21	C	M	3											R													
5H-CC		C	M	3											R													
6H-CC	RP20	A	G	2									R					R	R									
7H-CC		A	G													R				C								
8H-CC		A	G													R				C								
9H-CC		A	G													R						R		VR	VR	R		
10H-CC	RP18	A	G													R					R	R	—	F	R	R		
11H-CC	RP17	A	G													R					R	R	R	F	R	—		
12H-CC	RP16	A	G													—					—		R	F	R			
13H-CC	RP15				VR					R		R		R			R						R		R			
14H-CC	RP14	A	G		R	R			R	R	R	R					R								R		VR	
15H-CC		A	G		R	R		R	F	R		R		R			R								R			
16H-CC	RP13	A	G		R	R	VR	R		R		R		R											R			R
17H-CC	RP12	A	G			R	VR	R		R		R		R											R			R
18H-CC	B	B																										

Table T7. Radiolarian datums, Site U1332. (See table notes.) (Continued on next page.)

Geologic age	Zone	Marker species	Age (Ma)	Core, section, interval (cm) Top	Core, section, interval (cm) Bottom	Depth CSF (m) Top	Depth CSF (m) Bottom	Depth CSF (m) Midpoint	±
lower Miocene	RN1			320-U1332A-	320-U1332A-				
		B *C. cornuta*	22.26	3H-2, 93–95	3H-4, 93–95	15.87	18.83	17.35	1.48
		B *C. tetrapera*	22.35	3H-4, 93–95	3H-CC	18.83	23.52	21.18	2.35
upper Oligocene	RP22	T *A. gracilis*	22.62	3H-4, 93–95	3H-CC	18.83	23.52	21.18	2.35
		B *D. bassanii*	22.93	3H-4, 93–95	3H-CC	18.83	23.52	21.18	2.35
		B *E. diaphanes*	22.95	3H-4, 93–95	3H-CC	18.83	23.52	21.18	2.35
		T *D. cyclacantha*	22.98	3H-4, 93–95	3H-CC	18.83	23.52	21.18	2.35
		T *D. riedeli*	23.01	3H-4, 93–95	3H-CC	18.83	23.52	21.18	2.35
		B *D. cyclacantha*	23.29	3H-CC	4H-2, 105–107	23.52	25.50	24.51	0.99
		L *L. longicornuta*	24.12	4H-2, 105–107	4H-4, 105–107	25.50	28.45	26.98	1.47
		L *A. octopylus*	24.38	—	—				
		L *L. apodora*	24.5	—	—				
		B *L. elongata*	25.05	4H-4, 105–107	4H-CC	28.45	32.96	30.71	2.26
	RP21	B *A. octopylus*	25.09	—	—				
		B *D. praeforcipata*	25.27	4H-4, 105–107	4H-CC	28.45	32.96	30.71	2.26
		B *C. robusta*	25.27	4H-4, 105–107	4H-CC	28.45	32.96	30.71	2.26
		B *D. tubaria*	25.27	4H-4, 105–107	4H-CC	28.45	32.96	30.71	2.26
		B *L. longicornuta*	25.29	4H-4, 105–107	4H-CC	28.45	32.96	30.71	2.26
		B *D. scambos*	25.33	4H-4, 105–107	4H-CC	28.45	32.96	30.71	2.26
		B *L. apodora*	25.55	—	—				
		T *D. circulus*	26.17	4H-4, 105–107	4H-CC	28.45	32.96	30.71	2.26
		B *D. riedeli*	26.2						
		T *E. plesiodiaphanes*	26.4	4H-CC	5H-2, 110–112	32.96	35.04	34.00	1.04
		T *L. angusta*	27.68	5H-2, 110–112	5H-4, 105–107	35.04	37.94	36.49	1.45
		T *T. setanios*	28.21	5H-4, 105–107	5H-CC	37.94	42.48	40.21	2.27
		B *T. annosa*	28.33	6H-2, 105–107	6H-4, 105–107	44.46	47.46	45.96	1.50
		T. triceros > *D. ateuchus*	28.60	6H-2, 105–107	6H-4, 105–107	44.46	47.46	45.96	1.50
lower Oligocene	RP20	B *D. ateuchus*	29.50	6H-2, 105–107	6H-4, 105–107	44.46	47.46	45.96	1.50
		B *E. mitodes*	29.41	6H-4, 105–107	6H-CC	47.46	51.98	49.72	2.26
		B *D. circulus*	29.96	6H-4, 105–107	6H-CC	47.46	51.98	49.72	2.26
		T *T. tuberosa*	30.13	6H-CC	7H-3, 100–102	51.98	55.40	53.69	1.71
		T *L. crux*	30.13	6H-CC	7H-3, 100–102	51.98	55.40	53.69	1.71
		B *E. plesiodiaphanes*	30.37	6H-CC	7H-3, 100–102	51.98	55.40	53.69	1.71
		T *L. oberhaensliae*	30.74	7H-3, 100–102	7H-5, 100–102	55.40	58.41	56.91	1.50
		B *D. spinosa*	30.84	7H-5, 100–102	7H-CC	58.41	61.50	59.96	1.55
		T *D. pseudopaplilio*	30.84	7H-CC	8H-2, 105–107	61.50	63.45	62.48	0.98
		T *C. gravida*	30.89	7H-CC	8H-2, 105–107	61.50	63.45	62.48	0.98
		B *L. crux*	31.00	8H-4, 105–107	8H-CC	66.45	71.01	68.73	2.28
		B *T. tuberosa*	31.00	8H-4, 105–107	8H-CC	66.45	71.01	68.73	2.28
		B *D. pseudopaplilio*	31.00	9H-1, 92–98	9H-3, 92–98	71.35	74.38	72.87	1.52
		B *C. gravida*	31.01	8H-4, 105–107	8H-CC	66.45	71.01	68.73	2.28
		T *T. triacantha*	33.34	9H-3, 92–98 (8H-4,105)	9H-5, 92–98 (8H-CC)	74.37	77.34	75.86	1.49
		T *L. aristotelis* gr.	33.51	9H-3, 92–98	9H-5, 92–98	74.37	77.34	75.86	1.49
		T *C. hispida*	33.62	9H-3, 92–98	9H-5, 92–98	74.37	77.34	75.86	1.49
		T *C. ornatum*	33.62	9H-3, 92–98	9H-5, 92–98	74.37	77.34	75.86	1.49
		T *L. babylonis*	33.75	9H-3, 92–98	9H-5, 92–98	74.37	77.34	75.86	1.49
upper Eocene		*L. aristotelis* > *L. angusta*	33.82	9H-5, 92–98	9H-CC	77.34	81.68	79.51	2.17
	RP19	T *D. copetata*	33.84	9H-5, 92–98	9H-CC	77.34	81.68	79.51	2.17
		B *L. angusta*	34.13	9H-CC	10H-2, 94–96	81.68	82.34	82.01	0.33
		T *C. bandyca*	34.62	9H-CC	10H-2, 94–96	81.68	82.34	82.01	0.33
		T *T. tetracantha*	35.30	9H-CC	10H-2, 94–96	81.68	82.34	82.01	0.33
	RP18	B *L. hadra*	35.34	10H-2, 94–96	10H-4, 94–96	82.34	85.34	83.84	1.50
		B *C. bandyca*	36.74	10H-4, 94–96	10H-CC	85.34	89.90	87.62	2.28
middle Eocene	RP17	B *L. jacchia*	37.06	10H-CC	11H-2, 105–107	89.90	91.94	90.92	1.02
		B *C. azyx*	37.52	11H-2, 105–107	11H-4, 105–107	91.94	94.94	93.44	1.50
	RP16	T *Anthocyrtoma* spp.	37.92	11H-4, 105–107	12H-CC	94.94	98.53	96.74	1.80
		B *T. bromia*	38.07	11H-4, 105–107	12H-CC	94.94	98.53	96.74	1.80
		B *T. tetracantha*	38.12	11H-4, 105–107	12H-CC	94.94	98.53	96.74	1.80
		T *D. anastasis*	38.45	12H-2, 105–107	12H-4, 105–107	101.46	104.46	102.96	1.50
		B *C. turris*	38.67	11H-CC	12H-2, 105–107	98.53	101.46	100.00	1.46
		B *L. aristotelis* gr.	39.73	12H-2, 105–107	12H-4, 105–107	101.46	104.46	102.96	1.50
		B *D. anastasis*	39.98	12H-4, 105–107	13H-CC	104.46	108.46	106.46	2.00
		B *P. goetheana*	40.16	12H-4, 105–107	13H-CC	104.46	108.46	106.46	2.00
	RP15	T *L. biaurita*	40.36	12H-4, 105–107	13H-CC	104.46	108.46	106.46	2.00
		P. mitra > *P. chalara*	40.70	13H-CC	14H-2, 104–106	118.39	120.44	119.42	1.03

Table T7 (continued).

Geologic age	Zone	Marker species	Age (Ma)	Core, section, interval (cm) Top	Bottom	Depth CSF (m) Top	Bottom	Midpoint	±
middle Eocene	RP14	T *P. trachodes*	41.23	13H-CC	14H-2, 104–106	118.39	120.44	119.42	1.03
		B *P. chalara*	41.54	14H-2, 104–106	14H-4, 104–106	120.44	123.45	121.95	1.51
		B *C. ornatum*	42.10	14H-4, 104–106	14H-CC	123.45	126.29	124.87	1.42
		B *S. triconiscus*	42.40	14H-CC	15X-3, 42–44	126.29	129.36	127.83	1.53
		T *E. lagena*	42.69	14H-CC	15X-3, 42–44	126.29	129.36	127.83	1.53
		B *T. perpumila*	42.97	14H-CC	15X-3, 42–44	126.29	129.36	127.83	1.53
		T *P. helenae*	43.05	14H-2, 104–106	14H-4, 104–106	120.44	123.45	121.95	1.51
		B *P. trachodes*	43.22	16X-1, 41–49	16X-1, 112–120	135.94	136.66	136.30	0.36
		B *Z. cimelium*	43.35	15X-5, 40–42	15X-CC	132.30	132.93	132.62	0.31
		P. sinuosa > *P. mitra*	43.84	16X-1, 112–120	16X-2, 37–44	136.66	137.36	137.01	0.35
				320-U1332C-	320-U133C-				
	RP13	B *P. helenae*	44.14	15X-CC	16X-CC	132.93	138.20	135.57	2.63
		T *P. phyxis*	44.44	15X-CC	16X-CC	132.93	138.20	135.57	2.63
		T *P. diamesa*	44.44	15X-CC	16X-CC	132.93	138.20	135.57	2.63
		T *S. balbis*	44.77	16X-CC	17X-CC	138.20	146.90	142.55	4.35
		B *P. mitra*	44.77	16X-CC	17X-CC	138.20	146.90	142.55	4.35
		B *P. ampla*	44.77	16X-CC	17X-CC	138.20	146.90	142.55	4.35
		P. phyxis > *P. ampla*	44.77	16X-CC	17X-CC	138.20	146.90	142.55	4.35

Notes: B = bottom, T = top, L = last. — = not encountered.

Table T8. Planktonic foraminifer datums, Site U1332. (See table note.)

Core, section, interval (cm) Top	Bottom	Marker species	Age (Ma)	Depth CSF (m) Top	Bottom	Midpoint	±
320-U1331A-	320-U1331A-						
4H-CC, 26–31	5H-2, 100–101	T *Paragloborotalia opima*	26.9	32.95	34.90	33.93	0.97
6H-CC, 27–32	7H-4, 38–40	T *Subbotina angiporoides*	29.8	51.97	56.28	54.13	4.76
6H-CC, 27–32	7H-2-38–40	B *Paragloborotalia opima*	30.8	51.97	53.28	52.63	0.66
320-U1331B-	320-U1331B-						
4H-CC, 23–28	5H-CC, 21–26	T *Paragloborotalia opima*	26.9	29.61	37.63	33.62	4.01
5H-CC, 21–26	6H-CC, 9–14	T *Subbotina angiporoides*	29.8	37.63	48.50	43.07	5.44
7H-CC, 23–26	8H-CC, 33–36	B *Paragloborotalia opima*	30.8	58.07	67.47	62.77	4.70
320-U1331C-	320-U1331C-						
3H-CC, 18–21	4H-CC, 28–31	T *Paragloborotalia opima*	26.9	26.93	36.52	31.73	4.80
4H-CC, 28–31	5H-CC, 22–25	B *Globigerina angulisuturalis*	29.2	36.52	45.76	41.14	4.62
5H-CC, 22–25	6H-CC, 22–25	T *Subbotina angiporoides*	29.8	45.76	53.04	49.40	3.64
5H-CC, 22–25	6H-CC, 22–25	B *Paragloborotalia opima*	30.8	45.76	53.04	49.40	3.64

Note: T = top, B = bottom.

Table T9. Distribution of planktonic foraminifers, Site U1332. (See table notes.) (Continued on next page.)

Core, section, interval (cm)	Depth CSF (m)	Zone	Abundance (%)	Preservation	*Catapsydrax dissimilis*	*Catapsydrax* cf. *howei*	*Catapsydrax unicavus*	*Catapsydrax* sp.	*Dentoglobigerina galavisi*	*Dentoglobigerina pseudovenezuelana*	*Dentoglobigerina tripartita*	*Dentoglobigerina* spp.	*Globigerina angulisuturalis*	*Globigerina officinalis*	*Globigerina ouachitensis*	*Globigerina praesepsis*	*Globoquadrina euapertura*	*Globoquadrina* sp.	*Globoquadrina tapuriensis*	*Globoquadrina venezuelana*	*Globorotaloides suteri*	*Paragloborotalia nana*	*Paragloborotalia opima*	*Paragloborotalia opima-mayeri* transition	*Paragloborotalia pseudocontinuosa*	*Paragloborotalia semivera*	*Paragloborotalia* spp.	*Subbotina angiporoides*	*Subbotina patagonica*	*Subbotina utilisindex*	*Subbotina* sp.	*Turborotalia ampliapertura*	*Turborotalia increbescens*
320-U1332A-																																	
1H-2, 38–40	1.88	B	0	B																													
1H-CC	3.86	B	0	B																													
2H-CC	13.62	B	0	B																													
3H-5, 47–49	19.87	B	0	B																													
3H-7, 75–77	23.15	O6	<1	P							P																						
3H-CC	23.51	O3–Plio.	<1	P																P													
4H-3, 40–42	26.30	E13–O6	1	M							P																						
4H-7, 38–40	32.28	O6	<1	M			A			P	F						P		P	F	A	P				P							
4H-CC	32.95	O6	5	M			P			P	P					P				R	P	P	P			P							
5H-2, 100–101	34.90	O2–O5	<5	M			A				P	P										A	F										
5H-5, 28–29	38.68	O2–O5	5	M			A															D											
5H-CC	42.47	O2–O5	50	M	P		A		P		P	P					P			P		A	D	P									
6H-2, 38–40	43.78	O2–O5	<1	M			F		P		R									R	P	F	P										
6H-4, 38–40	46.78	O2–O5	<5	M			D															A	R				P						R
6H-CC	51.97	O2–O5	5	P	P		A	P	P							P				F	F	A	F		P					P	P		
7H-2, 38–40	53.28	O2–O5	<1	P			P															P											
7H-4, 38–40	56.28	E14–O2	1	M	R	P	A		F											P	F	P						P		F			
7H-CC	61.49	O1–O2	5	M	P		A		A	P	P										A							P		R			
8H-2, 48–50	62.88	Olig.	<1	P			P									P		P															
8H-4, 38–40	65.78	E13–O6	<1	P							P																						
8H-CC	71.00	B	0	B																													
9H-1, 15–22	70.55	E13–Olig.	<1	P																		P											
9H-2, 15–22	72.05		<1	P																		P											
9H-3, 15–22	73.55	E13–early Olig.	2	P			P		P																								P
9H-4, 15–22	75.05	E13–O6	<1	P			P					P																			P		
9H-4, 70–77	75.60	B	0	B																													
9H-4, 130–137	76.20	B	0	B																													
9H-5, 15–22	76.55	B	0	B																													
9H-6, 15–22	78.05	B	0	B																													
9H-7, 15–22	79.55	B	0	B																													
9H-CC	81.67	B	0	B																													
10H-3, 108–110	83.98	B	0	B																													
10H-CC	89.89	B	0	B																													
11H-6, 99–101	97.89	B	0	B																													
11H-CC	98.52	B	0	B																													
12H-1, 140–142	100.30	B	0	B																													
12H-CC	108.45	B	0	B																													
13H-3, 30–32	111.70	B	0	B																													
13H-5, 144–146	115.84	B	0	B																													
13H-CC	118.38	P4–E8	<1	P																									P				
14H-2, 38–40	119.78	B	0	B																													
14H-4, 38–40	122.78	B	0	B																													
14H-CC	126.28	B	0	B																													
15X-3, 58–60	129.48	B	0	B																													
15X-CC	132.98	B	0	B																													
16X-2, 38–40	137.38	B	0	B																													
16X-CC	138.25	B	0	B																													
17X-CC	148.21	B	0	B																													
320-U1332B-																																	
1H-CC	2.05	B	0	B																													
2H-CC	12.09	B	0	B																													
3H-CC	19.97	B	0	B																													
4H-CC	29.61	B	0	B			P																										
5H-CC	37.63	O6	<1	P	F		A	R	F	R	F									F	A	A											
6H-CC	48.50	O3–O5	5	M			D							P	P		D			P		F	P				P						

Table T9 (continued).

Core, section, interval (cm)	Depth CSF (m)	Zone	Abundance (%)	Preservation	*Catapsydrax dissimilis*	*Catapsydrax* cf. *howei*	*Catapsydrax unicavus*	*Catapsydrax* sp.	*Dentoglobigerina galavisi*	*Dentoglobigerina pseudovenezuelana*	*Dentoglobigerina tripartita*	*Dentoglobigerina* spp.	*Globigerina angulisuturalis*	*Globigerina officinalis*	*Globigerina ouachitensis*	*Globigerina prasepsis*	*Globoquadrina euapertura*	*Globoquadrina* sp.	*Globoquadrina tapuriensis*	*Globoquadrina venezuelana*	*Globorotaloides suteri*	*Paragloborotalia nana*	*Paragloborotalia opima*	*Paragloborotalia opima-mayeri* transition	*Paragloborotalia pseudocontinuosa*	*Paragloborotalia semivera*	*Paragloborotalia* spp.	*Subbotina angiporoides*	*Subbotina patagonica*	*Subbotina utilisindex*	*Subbotina* sp.	*Turborotalia ampliapertura*	*Turborotalia increbescens*
7H-CC	58.07	E11–O3	20	M			D	P																				P					
8H-CC	67.47	O1–O2	10	M			P				F																			P			
9H-CC	77.09	B	<3	M																													
10H-CC	86.66	B	0	B																													
11H-CC	93.84	B	0	B																													
12H-CC	101.03	B	0	B																													
13H-CC	110.76	B	0	B																													
14X-CC	119.78	B	0	B																													
15X-CC	125.77	B	0	B																													
16X-CC	125.34	B	0	B																													
17X-CC	0.00	B	0	B																													
320-U1332C-																																	
1H-CC	7.46	B	0	B																													
2H-CC	17.45	B	0	B																													
3H-CC	26.93	B	0	B																													
4H-CC	36.52	O4–O5	<5	M			R																F										
5H-CC	45.76	O4–O5	20	M			D				R		P				F			A			R										
6H-CC	53.04	E15–O2	<5	M			A				P											A						P					
7H-CC	59.43	E15–O2	3	M			A		R	P									P		A												
8H-CC	68.27	E15–O2	1	M	P		P														P							R					
9H-CC	75.91	E15–O2	2	M																												P	
10H-CC	85.53	B	0	B																													
11H-CC	94.05	B	0	B																													
12H-CC	103.20	B	0	B																													
13H-CC	114.08	B	0	B																													
14X-CC	119.69	B	0	B																													
15X-CC	127.38	B	0	B																													
16X-CC	134.64	B	0	B																													
17X-CC	139.91	B	0	B																													

Notes: Abundance: D = dominant, A = abundant, F = few, P = present, R = rare. Abundance estimated from total number of particles in the >250 µm size fraction. Preservation: M = moderate, P = poor, B = barren.

Table T10. Distribution of benthic foraminifers, Site U1332. (See table notes.) (Continued on next two pages.)

Core, section, interval (cm)	Depth CSF (m)	Preservation	Bathymetry	*Abyssamina poagi*	*Abyssamina quadrata*	*Alabamina dissonata*	*Amphicoryna* sp.	*Anomalinoides* sp.	*Astacolus* sp.	*Astrononion echolsi*	*Bigenerina* sp.	*Buliminella parvula*	*Chrysalogonium crassitestum*	*Chrysalogonium* sp. indet.	*Cibicidoides eocanus*	*Cibicidoides grimsdalei*	*Cibicidoides havanensis*	*Cibicidoides mundulus*	*Cibicidoides praemundulus*	*Cibicidoides* sp. A	*Cibicidoides* sp. indet.	*Cystammina pauciloculata*	*Dentalina* spp.	*Eggerella bradyi*	*Eggerella* sp.	*Favocassidulina spinifer*	*Gaudryina* sp. indet	*Glandulina* sp.	*Globocassidulina subglobosa*	*Globocassidulina* sp.	*Glomospira goldialis*	*Glomospira irregularis*	*Gyroidinoides soldanii*
320-U1332A-																																	
1H-CC, 12–17	3.86	—																															
2H-CC, 19–24	13.62	—																															
3H-CC, 29–34	23.51	M	LB-A									R				R	R	R								R			A				
4H-CC, 26–31	32.95	G	LB-A				R				R									F			R						F			R	R
5H-CC, 20–25	42.47	VG	LB-A										R			R	R			F	F											R	R
6H-CC, 27–32	51.97	VG	LB-A				R	R	R								F	F	R	R	F	R	R						R	R			
7H-CC, 21–26	61.49	G	LB-A					R								R		A		R	R								F				F
8H-CC, 28–33	71.00	M	LB-A																					F									A
9H-CC, 145–150	81.67	P																														—	
10H-CC, 32–37	89.89	P																															
11H-CC, 27–32	98.52	P																P														—	
12H-CC, 21–26	108.45	—																															
13H-CC, 20–25	118.38	P	LB-A	R											F						R						R		R			R	
14H-CC, 25–30	126.28	P		—											P						—												
15X-CC, 13–18	132.93	P																															
320-U1332B-																																	
1H-CC, 15–20	2.05	P																															
2H-CC, 35–40	12.09	—																															
3H-CC, 38–43	19.97	G	LB-A													R									R								
4H-CC, 23–28	29.61	G	LB-A											F		F	F				F			R					F				R
5H-CC, 21–26	37.63	G	LB-A					R		R				R		F	A	A		R	F												R
6H-CC, 9–14	48.50	G	LB-A					R									R	R		R	F		R					R	F			R	R
7H-CC, 23–26	58.07	G	LB-A					R									R	R		R	A								R				R
8H-CC, 33–36	67.47	G	LB-A													A		R			F								F				
9H-CC, 33–36	77.09	P																													A		
10H-CC, 21–24	86.66	P																															
11H-CC, 24–27	93.84	P		P												P					P												
12H-CC, 32–35	101.03	P																															
13H-CC, 31–36	110.76	P	LB-A																										F				
14H-CC, 16–21	119.78	P		P												P	P																
15X-CC, 37–42	125.77	P															P																
16X-CC, 29–34	125.34	P																			P												
17X-CC, 38–43	135.06	—																															
320-U1332C-																																	
1H-CC, 19–22	7.46	—																															
2H-CC, 14–17	17.45	P																															
3H-CC, 18–21	26.93	P																								A			R			R	R
4H-CC, 28–31	36.52	G	LB-A									R						F		R	F								R				R
6H-CC, 22–25	45.76	G	LB-A													R	R	A		A	R								R				F
8H-CC, 22–25	53.04	G	LB-A													F		F	R	R				R					F	R			R
7H-CC, 17–20	59.43	G	LB-A					R										R		R	F								F			R	R
8H-CC, 32–35	68.27	G	LB-A							R						R	R	F			R								A				
9H-CC, 32–37	75.91	G	LB-A				R	F		F						R		R		R	R		P					R	F	R		P	R
10H-CC, 29–34	85.53	P																															
11H-CC, 31–36	94.05	P																															
12H-CC, 7–12	103.21	P																															
13H-CC, 31–36	114.08	P	LB-A		F			F								F					F								F				
14H-CC, 0–3	119.69	P	LB-A																														R
15X-CC, 0–5	127.38	P	LB-A		P	P																											P
16X-CC, 23–26	134.64	P																			P												
17X-CC, 8–11	139.91	—																															

Notes: — = presence of specimens found during other observations (other size fractions or planktonic foraminifer analysis). Preservation: VG = very good, G = good, M = moderate, P = poor. LB = lower bathyal zone, A = abyssal zone. Abundance: D = dominant, A = abundant, F = frequent, R = rare, P = present.

Table T10 (continued). (Continued on next page.)

Core, section, interval (cm)	Depth CSF (m)	*Gyroidinoides* sp. A	*Gyroidinoides* sp. B	*Gyroidinoides* sp. C	*Gyroidinoides* sp. D	*Gyroidinoides* sp. indet.	*Haplophragmoides walteri*	*Haplophragmoides* sp. indet.	*Karreriella chapapotensis*	*Karrerulina coniformis*	*Lenticulina* spp.	*Martinottiella communis*	*Myllostomella* spp.	*Nodosaria* spp.	*Nonion affine*	*Nonion havanensis*	*Nuttallides truempyi*	*Nuttallides umbonifer*	*Oridorsalis umbonatus*	*Paratrochamminoides* spp.	*Pleurostomella* sp.	*Pseudoparrella exigua*	*Pseudopleurostomella* spp.	*Pullenia* sp. A	*Pullenia bulloides*	*Pullenia eocenica*	*Pullenia osloensis*	*Pullenia quinqueloba*	*Pullenia salisburyi*	*Pullenia subcarinata*	*Pyrulina* spp.	*Quadrimorphina profunda*	*Quinqueloculina* sp.	*Recurvoides* spp.	*Reophax* sp.	*Reticulophragmium amplectens*
320-U1332A-																																				
1H-CC, 12–17	3.86																																			
2H-CC, 19–24	13.62																																			
3H-CC, 29–34	23.51	F	R	R	R	R			R						R			A	F	R	R	R		R	R			R		R			R			
4H-CC, 26–31	32.95	F	R	F		R			R					F		R		A	F		F						R			R						
5H-CC, 20–25	42.47	R							F		R	R		R	R			F	A		R												R			
6H-CC, 27–32	51.97	R	R	R				R	R					R		R		R	A	R	R			R	R						R			R		
7H-CC, 21–26	61.49	R				R		R	R					R				R	A	R	F			R	R						F					
8H-CC, 28–33	71.00	F	F																A		F						F									
9H-CC, 145–150	81.67																																			
10H-CC, 32–37	89.89								—																											
11H-CC, 27–32	98.52					—								—			P		P																	
12H-CC, 21–26	108.45																																			
13H-CC, 20–25	118.38	F	R				R										A		A		R															
14H-CC, 25–30	126.28													P			—				P															
15X-CC, 13–18	132.93																																			
320-U1332B-																																				
1H-CC, 15–20	2.05																																	P		
2H-CC, 35–40	12.09																																			
3H-CC, 38–43	19.97																				R														A	
4H-CC, 23–28	29.61			F					R							R		A	F					F												R
5H-CC, 21–26	37.63		R						R			R				R		R	A		R										R					
6H-CC, 9–14	48.50	R		R		F								R					F		R						R				R			R		
7H-CC, 23–26	58.07	F				R							R	R		R			A						R			R						R		
8H-CC, 33–36	67.47	F					R								R				A					R							F					
9H-CC, 33–36	77.09																			P																
10H-CC, 21–24	86.66									P																										
11H-CC, 24–27	93.84														P		P								P											
12H-CC, 32–35	101.03							P																												
13H-CC, 31–36	110.76																D		F		F					F						A				
14H-CC, 16–21	119.78																																			
15X-CC, 37–42	125.77																																			
16X-CC, 29–34	125.34																																			
17X-CC, 38–43	135.06																																			
320-U1332C-																																				
1H-CC, 19–22	7.46																																			
2H-CC, 14–17	17.45																																		P	
3H-CC, 18–21	26.93			R				R										A	A																	
4H-CC, 28–31	36.52	R	R	R	R									R				F	R								R							R		
6H-CC, 22–25	45.76	R	R			R								R										R						R	R		R			
8H-CC, 22–25	53.04		R	F		R			R				R	R				F	A						R						R					R
7H-CC, 17–20	59.43	R	A						R							R			A				R						R		R					
8H-CC, 32–35	68.27	F				R												R	A		R			R							F	R		R		
9H-CC, 32–37	75.91	F		R		P		P	P				R			R		R	A		R			R				P			R	R		P		
10H-CC, 29–34	85.53																																			
11H-CC, 31–36	94.05							P																										P		
12H-CC, 7–12	103.21																																	P		
13H-CC, 31–36	114.08																A		A												F					
14H-CC, 0–3	119.69								R					R			F		R													R				
15X-CC, 0–5	127.38																		P																	
16X-CC, 23–26	134.64																														P					
17X-CC, 8–11	139.91																																			

Table T10 (continued).

Core, section, interval (cm)	Depth CSF (m)	*Siphonodosaria antillea*	*Siphonodosaria spinata*	*Siphonodosaria* sp. indet.	*Spheroidina bulloides*	*Spiroplectammina spectabilis*	*Textularia* sp.	*Trochamminoides?* sp.	*Valvulina spinosa*	Tube-shaped agglutinated foraminifer	Unilocular species	Agglutinated foram. gen. et sp. indet.	Calc. hyaline foram. gen. et sp. indet.
320-U1332A-													
1H-CC, 12–17	3.86												
2H-CC, 19–24	13.62												
3H-CC, 29–34	23.51	R	R	A	R		R				R	R	R
4H-CC, 26–31	32.95			F	R	R			R	R		R	R
5H-CC, 20–25	42.47	R		R	R			R	R	R	R		F
6H-CC, 27–32	51.97	R	R		R	R				R	R		
7H-CC, 21–26	61.49	R	R	R	F	R			R		R		F
8H-CC, 28–33	71.00			A						F			
9H-CC, 145–150	81.67									—		P	
10H-CC, 32–37	89.89					—				P			
11H-CC, 27–32	98.52	P				P				P			
12H-CC, 21–26	108.45												
13H-CC, 20–25	118.38	R							R		F		
14H-CC, 25–30	126.28												
15X-CC, 13–18	132.93												
320-U1332B-													
1H-CC, 15–20	2.05												
2H-CC, 35–40	12.09												
3H-CC, 38–43	19.97						R			D	R	A	F
4H-CC, 23–28	29.61				R							F	F
5H-CC, 21–26	37.63	F		F	R	R			R	R	R		R
6H-CC, 9–14	48.50		R	F	F	R			R	R	F	R	F
7H-CC, 23–26	58.07	F		R	F							R	F
8H-CC, 33–36	67.47			F					R	A			R
9H-CC, 33–36	77.09											P	
10H-CC, 21–24	86.66					P				P			
11H-CC, 24–27	93.84												
12H-CC, 32–35	101.03									P			
13H-CC, 31–36	110.76	F											A
14H-CC, 16–21	119.78	P											
15X-CC, 37–42	125.77												
16X-CC, 29–34	125.34												P
17X-CC, 38–43	135.06												
320-U1332C-													
1H-CC, 19–22	7.46												
2H-CC, 14–17	17.45									P			
3H-CC, 18–21	26.93					R				F	R		A
4H-CC, 28–31	36.52	F	R	R						A		R	F
6H-CC, 22–25	45.76	R	R	R	F					A	R		A
8H-CC, 22–25	53.04	R	R	R		R				R	R		R
7H-CC, 17–20	59.43	R	R	R	R						F	R	R
8H-CC, 32–35	68.27	R		R	R	R					R	R	F
9H-CC, 32–37	75.91	P		R	P	P	R		P	P	R		F
10H-CC, 29–34	85.53									P		P	
11H-CC, 31–36	94.05												
12H-CC, 7–12	103.21									P			
13H-CC, 31–36	114.08	F											
14H-CC, 0–3	119.69	R											
15X-CC, 0–5	127.38									P			
16X-CC, 23–26	134.64												P
17X-CC, 8–11	139.91												

Table T11. Coring-disturbed intervals and gaps, Site U1332. (See table notes.)

Core, section, interval (cm)	Type of disturbance
320-U1332A-	
1H-1, 0–100	Top of core
1H-2, 145–150	Interstitial water
2H-1, 0–5	Top of core
2H-2, 145–150	Interstitial water
2H-5, 145–150	Interstitial water
3H-1, 0–75	Top of core
3H-2, 145–150	Interstitial water
3H-5, 145–150	Interstitial water
4H-1, 0–8	Top of core
4H-2, 145–150	Interstitial water
4H-5, 145–150	Interstitial water
5H-2, 145–150	Interstitial water
5H-5, 145–150	Interstitial water
6H-1, 0–61	Top of core
6H-3, 145–150	Interstitial water
6H-5, 145–150	Interstitial water
7H-3, 32–37	Paleontology
7H-4, 138–150	Gamage sample
8H-1, 0–150	Top of core
8H-2, 0–32	Very soft
8H-2, 145–150	Interstitial water
8H-7, 145–150	Interstitial water
9H-2, 145–150	Interstitial water
9H-4, 0–8	Top of core
10H-1, 0–60	Top of core
10H-2, 145–150	Interstitial water
10H-3, 145–150	Interstitial water
11H-1, 0–137	Top of core
11H-3, 145–150	Interstitial water
12H-1, 0–118	Top of core
12H-3, 145–150	Interstitial water
12H-4, 0–10	Top of core
12H-5, 138–150	Gamage sample
13H-3, 145–150	Interstitial water
14H-1, 0–143	Top of core
14H-3, 145–150	Interstitial water
15X-1, 52–72	Disturbed
15X-2, 107–117	Disturbed
15X-3, 145–150	Interstitial water
16X-1, 0–32	Top of core
320-U1332B-	
2H-3, 140–150	Mills sample
3H-1, 0–150	Top of core
3H-2, 0–45	Top of core
4H-1, 0–148	Top of core
4H-3, 140–150	Mills sample
5H-1, 0–118	Top of core
6H-1, 0–150	Top of core
6H-2, 0–54	Top of core
6H-6, 84–150	Top of core
7H-1, 0–2	Top of core
8H-1, 0–150	Top of core
8H-2, 0–60	Top of core
9H-1, 0–24	Top of core
10H-1, 0–97	Top of core
11H-1, 0–150	Top of core
11H-2, 0–52	Top of core
12H-1, 0–86	Top of core
13H-1, 0–82	Top of core
15X-4, 79–150	Slightly brecciated
15X-5, 0–150	Slightly brecciated
15X-6, 0–150	Slightly brecciated
16X-1, 22–24	Slightly brecciated
17X-1, 25–150	Brecciated
320-U1332C-	
1H-1, 0–48	Top of core
2H-1, 0–130	Top of core
3H-1, 0–150	Top of core
3H-2, 62–65	Expansion
3H-2, 70–73	Expansion
4H-1, 0–15	Top of core
5H-1, 0–6	Top of core
6H-1, 0–150	Top of core
6H-2, 0–108	Top of core
7H-1, 0–20	Top of core
8H-1, 0–135	Top of core
9H-1, 0–35	Slightly disturbed
10H-1, 0–150	Core barrel dropped downhole (disturbed)
10H-2, 0–150	Core barrel dropped downhole (disturbed)
10H-3, 0–150	Core barrel dropped downhole (disturbed)
10H-4, 0–150	Core barrel dropped downhole (disturbed)
10H-5, 0–150	Core barrel dropped downhole (disturbed)
10H-6, 0–150	Core barrel dropped downhole (disturbed)
10H-7, 0–74	Core barrel dropped downhole (disturbed)
11H-1, 0–50	Top of core
13H-1, 0–130	Top of core

Notes: When interval listed is 0–150 cm, entire section is included even if true section length is <150 cm. Top of core = myriad forms of voids, disturbance, and debris from uphole that affect top portion of most cores. For that reason, probably the top 20 cm or so of all cores should be avoided. Gamage sample = whole-round sample taken for K. Gamage, Mills sample = whole-round sample taken for H. Mills.

Table T12. Paleomagnetic data from archive-half sections, Hole U1332A, at 0 mT AF demagnetization. (**See table notes.)**

Core, section	Offset (m)	Depth CSF (m)	Declination (°)	Inclination (°)	Intensity (A/m)	Time (s)
320-U1332A-						
1H-1	1.05	1.05	358.2	66.6	2.329E–02	3320732162.73437
1H-1	1.10	1.10	354.3	67.2	2.620E–02	3320732168.06250
1H-1	1.15	1.15	357.4	70.1	2.808E–02	3320732173.39062
1H-1	1.20	1.20	355.6	77.8	2.750E–02	3320732178.71875
1H-1	1.25	1.25	247.6	88.2	2.504E–02	3320732184.04687
1H-1	1.30	1.30	185.6	78.5	2.381E–02	3320732189.35937
1H-1	1.35	1.35	173.4	75.4	2.238E–02	3320732194.68750
1H-1	1.40	1.40	178.4	75.9	2.175E–02	3320732200.01562
1H-2	0.10	1.60	194.5	82.9	2.325E–02	3320733396.03125
1H-2	0.15	1.65	190.4	78.2	2.274E–02	3320733401.35937
1H-2	0.20	1.70	174.4	73.7	2.055E–02	3320733406.68750
1H-2	0.25	1.75	178.7	86.2	1.870E–02	3320733412.00000
1H-2	0.30	1.80	356.1	75.5	2.293E–02	3320733417.32812
1H-2	0.35	1.85	354.9	75.9	2.578E–02	3320733422.65625
1H-2	0.40	1.90	345.9	73.7	2.748E–02	3320733427.98437
1H-2	0.45	1.95	343.9	71.0	2.882E–02	3320733433.31250
1H-2	0.50	2.00	346.5	79.7	2.854E–02	3320733438.62500
1H-2	0.55	2.05	356.1	84.1	3.019E–02	3320733443.95312
1H-2	0.60	2.10	70.3	82.0	3.103E–02	3320733449.28125
1H-2	0.65	2.15	81.0	86.6	3.007E–02	3320733454.60937
1H-2	0.70	2.20	102.6	87.5	3.007E–02	3320733459.93750
1H-2	0.75	2.25	145.3	88.5	2.864E–02	3320733465.26562
1H-2	0.80	2.30	229.3	89.3	2.531E–02	3320733470.57812
1H-2	0.85	2.35	218.3	86.1	2.059E–02	3320733475.90625
1H-2	0.90	2.40	187.2	84.7	1.502E–02	3320733481.23437
1H-2	0.95	2.45	215.8	85.1	1.108E–02	3320733486.56250
1H-2	1.00	2.50	143.6	85.2	1.118E–02	3320733491.87500
1H-2	1.05	2.55	122.9	84.4	1.472E–02	3320733497.20312
1H-2	1.10	2.60	205.3	87.9	2.111E–02	3320733502.53125
1H-2	1.15	2.65	203.6	85.7	2.704E–02	3320733507.85937
1H-2	1.20	2.70	202.2	86.2	2.791E–02	3320733513.18750
1H-2	1.25	2.75	214.4	87.6	2.867E–02	3320733518.51562
1H-2	1.30	2.80	198.6	85.7	2.897E–02	3320733523.82812
1H-2	1.35	2.85	168.2	84.3	2.906E–02	3320733529.15625
1H-2	1.40	2.90	135.6	86.2	2.508E–02	3320733534.48437
1H-3	0.10	3.10	211.5	88.5	2.562E–02	3320736022.75000
1H-3	0.15	3.15	204.3	89.3	2.687E–02	3320736028.07812
1H-3	0.20	3.20	223.8	87.1	2.834E–02	3320736033.40625
1H-3	0.25	3.25	149.5	88.2	2.814E–02	3320736038.71875
1H-3	0.30	3.30	185.2	84.4	2.826E–02	3320736044.04687
1H-3	0.35	3.35	172.8	59.2	3.137E–02	3320736049.37500
1H-3	0.40	3.40	159.0	42.9	3.185E–02	3320736054.70312
1H-3	0.45	3.45	147.7	48.9	2.242E–02	3320736060.01562
1H-3	0.50	3.50	151.9	61.2	2.085E–02	3320736065.34375
1H-3	0.55	3.55	151.5	65.9	1.957E–02	3320736070.67187
1H-3	0.60	3.60	155.2	60.6	1.781E–02	3320736076.00000
1H-3	0.65	3.65	163.6	54.2	1.465E–02	3320736081.32812
2H-1	0.10	4.00	223.8	82.0	3.708E–02	3320744157.64062
2H-1	0.15	4.05	201.1	83.8	3.778E–02	3320744162.96875
2H-1	0.20	4.10	216.6	85.3	3.577E–02	3320744168.29687
2H-1	0.25	4.15	215.6	84.9	3.407E–02	3320744173.60937
2H-1	0.30	4.20	231.6	81.9	3.413E–02	3320744178.93750
2H-1	0.35	4.25	217.9	79.8	3.423E–02	3320744184.26562
2H-1	0.40	4.30	219.9	79.5	3.364E–02	3320744189.59375
2H-1	0.45	4.35	229.3	81.5	3.236E–02	3320744194.92187
2H-1	0.50	4.40	216.8	83.3	3.111E–02	3320744200.25000
2H-1	0.55	4.45	224.9	83.0	3.274E–02	3320744205.56250
2H-1	0.60	4.50	241.3	85.6	3.403E–02	3320744210.89062
2H-1	0.65	4.55	233.6	84.9	3.384E–02	3320744216.21875
2H-1	0.70	4.60	222.7	88.7	3.559E–02	3320744221.54687
2H-1	0.75	4.65	262.3	84.1	3.718E–02	3320744226.87500
2H-1	0.80	4.70	219.4	84.3	3.803E–02	3320744232.18750
2H-1	0.85	4.75	236.3	83.9	4.059E–02	3320744237.51562

Notes: Time = since 1 January 1904. Only a portion of this table appears here. The complete table is available in **ASCII.**

Table T13. Paleomagnetic data from archive-half sections, Hole U1332A, at 5 mT AF demagnetization. (**See table note.**)

Core, section	Offset (m)	Depth CSF (m)	Declination (°)	Inclination (°)	Intensity (A/m)	Time (s)
320-U1332A-						
1H-2	0.10	1.60	183.2	10.2	5.582E–03	3320733923.20312
1H-2	0.15	1.65	179.9	11.7	6.416E–03	3320733928.51562
1H-2	0.20	1.70	180.7	11.9	6.317E–03	3320733933.84375
1H-2	0.25	1.75	182.1	28.7	2.370E–03	3320733939.17187
1H-2	0.30	1.80	356.1	21.3	3.417E–03	3320733944.50000
1H-2	0.35	1.85	342.1	22.9	4.687E–03	3320733949.82812
1H-2	0.40	1.90	341.3	18.0	6.552E–03	3320733955.15625
1H-2	0.45	1.95	343.3	15.9	5.840E–03	3320733960.46875
1H-2	0.50	2.00	354.4	46.1	2.064E–03	3320733965.79687
1H-2	0.55	2.05	126.9	78.9	2.335E–03	3320733971.12500
1H-2	0.60	2.10	120.6	29.8	4.442E–03	3320733976.45312
1H-2	0.65	2.15	151.2	24.3	3.816E–03	3320733981.78125
1H-2	0.70	2.20	160.3	21.7	5.435E–03	3320733987.09375
1H-2	0.75	2.25	161.2	24.2	4.893E–03	3320733992.42187
1H-2	0.80	2.30	171.8	32.3	3.631E–03	3320733997.75000
1H-2	0.85	2.35	186.4	32.4	3.481E–03	3320734003.07812
1H-2	0.90	2.40	184.5	35.7	2.585E–03	3320734008.40625
1H-2	0.95	2.45	183.3	50.7	2.003E–03	3320734013.71875
1H-2	1.00	2.50	179.3	41.6	1.854E–03	3320734019.04687
1H-2	1.05	2.55	177.9	33.0	2.326E–03	3320734024.37500
1H-2	1.10	2.60	179.5	25.1	4.169E–03	3320734029.70312
1H-2	1.15	2.65	182.1	24.2	5.281E–03	3320734035.03125
1H-2	1.20	2.70	181.5	26.8	4.681E–03	3320734040.34375
1H-2	1.25	2.75	186.0	31.8	4.413E–03	3320734045.67187
1H-2	1.30	2.80	183.6	21.9	5.797E–03	3320734051.00000
1H-2	1.35	2.85	176.5	18.8	6.540E–03	3320734056.32812
1H-2	1.40	2.90	174.9	21.5	5.148E–03	3320734061.64062
1H-3	0.10	3.10	191.2	47.9	4.452E–03	3320736407.10937
1H-3	0.15	3.15	182.6	49.2	4.377E–03	3320736412.43750
1H-3	0.20	3.20	173.7	36.6	5.797E–03	3320736417.76562
1H-3	0.25	3.25	172.9	40.0	5.881E–03	3320736423.09375
1H-3	0.30	3.30	179.8	54.6	5.298E–03	3320736428.42187
1H-3	0.35	3.35	178.2	52.3	5.857E–03	3320736433.73437
1H-3	0.40	3.40	164.2	36.6	6.893E–03	3320736439.06250
1H-3	0.45	3.45	155.4	35.1	5.112E–03	3320736444.39062
1H-3	0.50	3.50	161.8	25.1	4.291E–03	3320736449.71875
1H-3	0.55	3.55	165.1	12.6	5.924E–03	3320736455.03125
1H-3	0.60	3.60	162.5	6.2	6.891E–03	3320736460.35937
1H-3	0.65	3.65	160.5	1.7	6.215E–03	3320736465.68750

Note: Time = since 1 January 1904. This table is available in **ASCII.**

Table T14. Paleomagnetic data from archive-half sections, Hole U1332A, at 10 mT AF demagnetization. (See table note.) (Continued on next page.)

Core, section	Offset (m)	Depth CSF (m)	Declination (°)	Inclination (°)	Intensity (A/m)	Time (s)
320-U1332A-						
1H-1	1.05	1.05	350.3	–6.0	6.767E–03	3320732579.18750
1H-1	1.10	1.10	351.3	–3.4	6.873E–03	3320732584.50000
1H-1	1.15	1.15	354.6	–1.5	6.071E–03	3320732589.82812
1H-1	1.20	1.20	351.4	3.1	4.114E–03	3320732595.15625
1H-1	1.25	1.25	211.1	–15.5	1.428E–03	3320732600.48437
1H-1	1.30	1.30	172.8	–9.8	5.619E–03	3320732605.79687
1H-1	1.35	1.35	167.7	–13.4	7.773E–03	3320732611.12500
1H-1	1.40	1.40	173.4	–13.9	7.200E–03	3320732616.45312
1H-2	0.10	1.60	181.3	1.5	6.282E–03	3320734549.45312
1H-2	0.15	1.65	178.9	3.0	7.041E–03	3320734554.76562
1H-2	0.20	1.70	180.5	2.8	6.684E–03	3320734560.09375
1H-2	0.25	1.75	180.7	4.3	2.932E–03	3320734565.42187
1H-2	0.30	1.80	352.7	10.9	1.415E–03	3320734570.75000
1H-2	0.35	1.85	347.6	8.9	2.402E–03	3320734576.07812
1H-2	0.40	1.90	343.7	9.1	4.289E–03	3320734581.39062
1H-2	0.45	1.95	342.1	7.0	3.940E–03	3320734586.71875
1H-2	0.50	2.00	126.1	17.5	5.085E–04	3320734592.04687
1H-2	0.55	2.05	145.4	5.4	2.478E–03	3320734597.37500
1H-2	0.60	2.10	135.8	6.0	4.352E–03	3320734602.70312
1H-2	0.65	2.15	156.9	2.4	4.140E–03	3320734608.01562
1H-2	0.70	2.20	159.8	6.4	5.866E–03	3320734613.34375
1H-2	0.75	2.25	162.1	7.3	5.889E–03	3320734618.67187
1H-2	0.80	2.30	170.8	10.5	3.922E–03	3320734624.00000
1H-2	0.85	2.35	181.8	11.7	3.817E–03	3320734629.32812
1H-2	0.90	2.40	179.4	26.3	2.233E–03	3320734634.64062
1H-2	0.95	2.45	178.0	30.8	1.539E–03	3320734639.96875
1H-2	1.00	2.50	177.6	16.9	1.568E–03	3320734645.29687
1H-2	1.05	2.55	177.5	11.2	2.257E–03	3320734650.62500
1H-2	1.10	2.60	178.5	7.7	4.655E–03	3320734655.95312
1H-2	1.15	2.65	178.7	4.8	6.262E–03	3320734661.26562
1H-2	1.20	2.70	178.1	6.8	4.722E–03	3320734666.59375
1H-2	1.25	2.75	181.0	7.7	4.851E–03	3320734671.92187
1H-2	1.30	2.80	180.1	3.6	7.279E–03	3320734677.25000
1H-2	1.35	2.85	174.7	2.5	7.325E–03	3320734682.57812
1H-2	1.40	2.90	173.7	5.9	5.776E–03	3320734687.90625
1H-3	0.10	3.10	185.9	21.4	4.298E–03	3320736746.87500
1H-3	0.15	3.15	179.6	23.2	4.110E–03	3320736752.20312
1H-3	0.20	3.20	174.0	17.6	5.880E–03	3320736757.53125
1H-3	0.25	3.25	172.8	20.9	5.794E–03	3320736762.84375
1H-3	0.30	3.30	177.2	31.0	4.521E–03	3320736768.17187
1H-3	0.35	3.35	177.3	27.2	4.866E–03	3320736773.50000
1H-3	0.40	3.40	172.1	23.1	4.719E–03	3320736778.82812
1H-3	0.45	3.45	167.2	21.8	3.429E–03	3320736784.14062
1H-3	0.50	3.50	163.9	5.3	4.768E–03	3320736789.46875
1H-3	0.55	3.55	164.4	–3.8	5.939E–03	3320736794.79687
1H-3	0.60	3.60	161.1	–5.6	6.744E–03	3320736800.12500
1H-3	0.65	3.65	161.7	–8.3	6.728E–03	3320736805.45312
7H-1	0.10	51.50	10.9	68.3	3.465E–03	3320801263.79687
7H-1	0.15	51.55	36.2	25.0	2.320E–03	3320801269.12500
7H-1	0.20	51.60	58.9	16.0	2.784E–03	3320801274.45312
7H-1	0.25	51.65	62.2	13.6	3.232E–03	3320801279.78125
7H-1	0.30	51.70	51.0	11.8	1.817E–03	3320801285.10937
7H-1	0.35	51.75	58.2	19.6	1.420E–03	3320801290.42187
7H-1	0.40	51.80	53.1	14.1	2.387E–03	3320801295.75000
7H-1	0.45	51.85	61.0	19.6	2.833E–03	3320801301.07812
7H-1	0.50	51.90	65.1	17.5	3.367E–03	3320801306.40625
7H-1	0.55	51.95	56.5	16.0	3.804E–03	3320801311.71875
7H-1	0.60	52.00	60.4	16.3	3.370E–03	3320801317.04687
7H-1	0.65	52.05	58.6	15.3	3.262E–03	3320801322.37500
7H-1	0.70	52.10	62.3	23.1	3.191E–03	3320801327.70312
7H-1	0.75	52.15	62.6	26.6	2.964E–03	3320801333.03125
7H-1	0.80	52.20	57.8	23.3	2.474E–03	3320801338.35937
7H-1	0.85	52.25	56.9	19.2	2.120E–03	3320801343.67187
7H-1	0.90	52.30	85.6	13.9	1.541E–03	3320801349.00000
7H-1	0.95	52.35	59.2	7.6	1.571E–03	3320801354.32812
7H-1	1.00	52.40	59.3	6.0	1.571E–03	3320801359.65625

Table T14 (continued).

Core, section	Offset (m)	Depth CSF (m)	Declination (°)	Inclination (°)	Intensity (A/m)	Time (s)
7H-1	1.05	52.45	59.6	2.9	1.825E–03	3320801364.96875
7H-1	1.10	52.50	59.1	1.3	2.259E–03	3320801370.29687
7H-1	1.15	52.55	58.4	1.5	2.113E–03	3320801375.62500
7H-1	1.20	52.60	59.4	1.1	2.508E–03	3320801380.95312
7H-1	1.25	52.65	59.1	2.4	2.614E–03	3320801386.31250
7H-1	1.30	52.70	60.3	4.0	2.166E–03	3320801391.64062
7H-1	1.35	52.75	61.3	3.7	2.292E–03	3320801396.96875
7H-1	1.40	52.80	63.4	6.7	2.800E–03	3320801402.29687
7H-2	0.10	53.00	67.0	1.1	3.007E–03	3320802506.79687
7H-2	0.15	53.05	73.5	1.4	2.651E–03	3320802512.12500
7H-2	0.20	53.10	74.2	2.9	2.124E–03	3320802517.45312
7H-2	0.25	53.15	71.5	5.1	1.512E–03	3320802522.78125
7H-2	0.30	53.20	71.4	5.3	1.786E–03	3320802528.10937
7H-2	0.35	53.25	76.3	3.3	3.252E–03	3320802533.42187
7H-2	0.40	53.30	72.3	3.8	3.006E–03	3320802538.75000
7H-2	0.45	53.35	73.8	4.8	2.637E–03	3320802544.07812
7H-2	0.50	53.40	67.3	7.3	1.479E–03	3320802549.39062
7H-2	0.55	53.45	75.4	5.5	1.483E–03	3320802554.71875
7H-2	0.60	53.50	75.6	5.3	1.468E–03	3320802560.04687
7H-2	0.65	53.55	75.6	5.0	1.601E–03	3320802565.35937
7H-2	0.70	53.60	70.0	9.9	1.151E–03	3320802570.68750
7H-2	0.75	53.65	72.4	22.2	3.333E–03	3320802576.01562
7H-2	0.80	53.70	101.0	39.7	6.749E–03	3320802581.34375
7H-2	0.85	53.75	197.5	27.9	4.614E–03	3320802586.65625
7H-2	0.90	53.80	34.1	47.4	6.003E–04	3320802591.98437
7H-2	0.95	53.85	70.7	6.8	1.538E–03	3320802597.31250
7H-2	1.00	53.90	75.3	2.4	1.506E–03	3320802602.64062
7H-2	1.05	53.95	82.2	–3.5	1.067E–03	3320802607.96875
7H-2	1.10	54.00	86.3	3.4	9.267E–04	3320802613.29687
7H-2	1.15	54.05	83.3	11.5	1.010E–03	3320802618.60937
7H-2	1.20	54.10	83.6	10.5	1.393E–03	3320802623.93750
7H-2	1.25	54.15	85.0	8.3	1.408E–03	3320802629.26562
7H-2	1.30	54.20	83.2	3.5	1.407E–03	3320802634.59375
7H-2	1.35	54.25	82.5	1.8	1.367E–03	3320802639.92187
7H-2	1.40	54.30	83.4	1.5	1.487E–03	3320802645.25000

Note: Time = since 1 January 1904. This table is available in **ASCII.**

Table T15. Paleomagnetic data from archive-half sections, Hole U1332A, at 15 mT AF demagnetization. (See table note.)

Core, section	Offset (m)	Depth CSF (m)	Declination (°)	Inclination (°)	Intensity (A/m)	Time (s)
320-U1332A-						
1H-2	0.10	1.60	182.8	–1.7	5.588E-03	3320734978.60937
1H-2	0.15	1.65	179.0	1.6	6.292E-03	3320734983.93750
1H-2	0.20	1.70	179.8	3.0	6.296E-03	3320734989.25000
1H-2	0.25	1.75	181.0	2.9	3.816E-03	3320734994.57812
1H-2	0.30	1.80	198.0	34.5	3.315E-04	3320734999.90625
1H-2	0.35	1.85	348.2	8.9	1.677E-03	3320735005.23437
1H-2	0.40	1.90	336.5	9.6	2.695E-03	3320735010.56250
1H-2	0.45	1.95	340.6	7.6	3.652E-03	3320735015.87500
1H-2	0.50	2.00	326.6	11.3	8.375E-04	3320735021.20312
1H-2	0.55	2.05	141.3	–1.0	2.542E-03	3320735026.53125
1H-2	0.60	2.10	142.7	1.9	3.626E-03	3320735031.85937
1H-2	0.65	2.15	152.4	1.2	4.258E-03	3320735037.18750
1H-2	0.70	2.20	161.2	4.7	4.927E-03	3320735042.50000
1H-2	0.75	2.25	161.8	7.0	5.740E-03	3320735047.82812
1H-2	0.80	2.30	171.3	7.7	4.718E-03	3320735053.15625
1H-2	0.85	2.35	182.4	10.3	3.660E-03	3320735058.48437
1H-2	0.90	2.40	180.7	13.9	2.924E-03	3320735063.81250
1H-2	0.95	2.45	177.8	30.6	1.432E-03	3320735069.12500
1H-2	1.00	2.50	176.8	24.1	1.377E-03	3320735074.45312
1H-2	1.05	2.55	176.7	11.0	1.830E-03	3320735079.78125
1H-2	1.10	2.60	178.0	7.0	3.900E-03	3320735085.10937
1H-2	1.15	2.65	179.4	4.9	5.412E-03	3320735090.42187
1H-2	1.20	2.70	178.5	4.4	5.219E-03	3320735095.75000
1H-2	1.25	2.75	179.7	6.4	4.443E-03	3320735101.07812
1H-2	1.30	2.80	182.1	4.3	5.401E-03	3320735106.40625
1H-2	1.35	2.85	177.3	1.8	7.127E-03	3320735111.73437
1H-2	1.40	2.90	174.2	3.2	6.568E-03	3320735117.06250
1H-3	0.10	3.10	186.5	20.2	4.027E-03	3320737088.90625
1H-3	0.15	3.15	179.3	22.0	3.837E-03	3320737094.23437
1H-3	0.20	3.20	174.1	16.2	5.646E-03	3320737099.56250
1H-3	0.25	3.25	173.0	19.7	5.350E-03	3320737104.87500
1H-3	0.30	3.30	177.5	28.2	4.398E-03	3320737110.20312
1H-3	0.35	3.35	177.0	26.3	4.518E-03	3320737115.53125
1H-3	0.40	3.40	172.4	22.0	4.274E-03	3320737120.85937
1H-3	0.45	3.45	168.0	18.5	3.203E-03	3320737126.18750
1H-3	0.50	3.50	162.0	5.5	4.718E-03	3320737131.50000
1H-3	0.55	3.55	165.2	–1.8	5.609E-03	3320737136.82812
1H-3	0.60	3.60	159.9	–3.7	6.212E-03	3320737142.15625
1H-3	0.65	3.65	162.2	–8.4	6.117E-03	3320737147.48437

Note: Time = since 1 January 1904. This table is available in ASCII.

Table T16. Paleomagnetic data from archive-half sections, Hole U1332A, at 20 mT AF demagnetization. (See table notes.)

Core, section	Offset (m)	Depth CSF (m)	Declination (°)	Inclination (°)	Intensity (A/m)	Time (s)	Declination: Core mean (°)	Declination: Geographical coordinates 0°–360°	Declination: Geographical coordinates –90°–270°	VGP (°) Latitude	VGP (°) Longitude
320-U1332A-											
1H-1	1.05	1.05	343.5	–1.5	5.12E–03	3320733002.92187	352.1	351.4	–8.6	74.7	73.5
1H-1	1.10	1.10	346.6	–1.3	5.19E–03	3320733008.23437	352.1	354.5	–5.5	76.3	62.8
1H-1	1.15	1.15	346.6	1.3	4.53E–03	3320733013.56250	352.1	354.5	–5.5	77.5	65.2
1H-1	1.20	1.20	334.5	2.2	2.61E–03	3320733018.89062	352.1	342.4	–17.6	69.5	98.5
1H-1	1.25	1.25	209.7	–0.8	2.36E–03	3320733024.21875	352.1	217.6	217.6	–50.9	–216.7
1H-1	1.30	1.30	180.9	–8.3	4.64E–03	3320733029.54687	352.1	188.8	188.8	–78.3	–190.2
1H-1	1.35	1.35	180.3	–11.4	6.30E–03	3320733034.85937	352.1	188.2	188.2	–79.8	–194.6
1H-1	1.40	1.40	182.2	–12.7	5.56E–03	3320733040.18750	352.1	190.1	190.1	–78.6	–203.2
1H-2	0.10	1.60	183.3	0.4	4.52E–03	3320735404.89062	352.1	191.2	191.2	–73.6	–184.4
1H-2	0.15	1.65	179.6	4.1	5.50E–03	3320735410.21875	352.1	187.5	187.5	–74.2	–169.7
1H-2	0.20	1.70	180.3	4.0	5.49E–03	3320735415.54687	352.1	188.2	188.2	–73.9	–172.0
1H-2	0.25	1.75	181.1	3.9	3.96E–03	3320735420.87500	352.1	189.0	189.0	–73.5	–174.5
1H-2	0.30	1.80	197.5	42.5	4.06E–04	3320735426.20312	352.1	205.4	205.4	–45.9	–175.1
1H-2	0.35	1.85	347.6	14.0	1.48E–03	3320735431.51562	352.1	355.5	–4.5	83.5	82.0
1H-2	0.40	1.90	332.3	15.2	2.61E–03	3320735436.84375	352.1	340.2	–19.8	70.1	118.7
1H-2	0.45	1.95	340.5	10.1	3.22E–03	3320735442.17187	352.1	348.4	–11.6	76.7	99.2
1H-2	0.50	2.00	329.8	17.9	7.11E–04	3320735447.50000	352.1	337.7	–22.3	67.9	124.0
1H-2	0.55	2.05	159.6	3.5	2.23E–03	3320735452.82812	352.1	167.5	167.5	–71.5	–98.0
1H-2	0.60	2.10	150.9	3.1	3.14E–03	3320735458.14062	352.1	158.8	158.8	–65.0	–82.3
1H-2	0.65	2.15	151.3	3.6	3.35E–03	3320735463.46875	352.1	159.2	159.2	–65.2	–83.3
1H-2	0.70	2.20	163.7	7.5	4.82E–03	3320735468.79687	352.1	171.6	171.6	–72.2	–112.5
1H-2	0.75	2.25	163.2	8.9	5.00E–03	3320735474.12500	352.1	171.1	171.1	–71.4	–112.2
1H-2	0.80	2.30	168.5	9.9	4.28E–03	3320735479.45312	352.1	176.4	176.4	–72.7	–128.9
1H-2	0.85	2.35	182.5	13.3	3.12E–03	3320735484.76562	352.1	190.4	190.4	–68.7	–170.6
1H-2	0.90	2.40	180.5	19.6	2.11E–03	3320735490.09375	352.1	188.4	188.4	–66.5	–162.2
1H-2	0.95	2.45	178.4	28.5	1.46E–03	3320735495.42187	352.1	186.3	186.3	–62.2	–154.2
1H-2	1.00	2.50	176.5	25.5	1.22E–03	3320735500.75000	352.1	184.4	184.4	–64.3	–151.0
1H-2	1.05	2.55	177.3	12.9	1.60E–03	3320735506.07812	352.1	185.2	185.2	–70.8	–157.0
1H-2	1.10	2.60	178.2	9.8	2.88E–03	3320735511.40625	352.1	186.1	186.1	–72.1	–161.2
1H-2	1.15	2.65	179.5	6.3	4.65E–03	3320735516.71875	352.1	187.4	187.4	–73.2	–167.6
1H-2	1.20	2.70	178.4	5.9	4.52E–03	3320735522.04687	352.1	186.3	186.3	–73.9	–164.3
1H-2	1.25	2.75	180.0	8.0	3.93E–03	3320735527.37500	352.1	187.9	187.9	–72.2	–167.8
1H-2	1.30	2.80	180.9	5.0	5.41E–03	3320735532.70312	352.1	188.8	188.8	–73.1	–172.9
1H-2	1.35	2.85	176.5	2.2	6.18E–03	3320735538.01562	352.1	184.4	184.4	–76.3	–160.0
1H-2	1.40	2.90	174.0	4.0	5.85E–03	3320735543.34375	352.1	181.9	181.9	–76.0	–148.9
1H-3	0.10	3.10	182.1	23.0	3.32E–03	3320740103.17187	352.1	190.0	190.0	–64.1	–164.0
1H-3	0.15	3.15	177.9	23.5	3.80E–03	3320740108.50000	352.1	185.8	185.8	–65.1	–154.7
1H-3	0.20	3.20	172.6	17.9	4.94E–03	3320740113.82812	352.1	180.5	180.5	–68.9	–142.4
1H-3	0.25	3.25	173.1	23.2	4.57E–03	3320740119.14062	352.1	181.0	181.0	–66.0	–143.5
1H-3	0.30	3.30	177.4	28.2	3.95E–03	3320740124.46875	352.1	185.3	185.3	–62.6	–152.2
1H-3	0.35	3.35	176.1	25.3	4.02E–03	3320740129.79687	352.1	184.0	184.0	–64.5	–150.1
1H-3	0.40	3.40	170.7	23.6	3.25E–03	3320740135.12500	352.1	178.6	178.6	–65.7	–137.7
1H-3	0.45	3.45	167.9	14.1	2.84E–03	3320740140.45312	352.1	175.8	175.8	–70.5	–128.5
1H-3	0.50	3.50	163.2	1.9	4.80E–03	3320740145.76562	352.1	171.1	171.1	–74.4	–106.0

Notes: Time = since 1 January 1904. VGP = virtual geomagnetic pole. Only a portion of this table appears here. The complete table is available in ASCII.

Table T17. Paleomagnetic data from archive-half sections, Hole U1332B, at 0 mT AF demagnetization. (See table notes.)

Core, section	Offset (m)	Depth CSF (m)	Declination (°)	Inclination (°)	Intensity (A/m)	Time (s)
320-U1332B-						
1H-1	0.100	0.10	288.2	–3.9	5.674E–03	3321020940.82812
1H-1	0.150	0.15	276.0	–6.9	5.347E–03	3321020946.15625
1H-1	0.200	0.20	287.0	–7.0	4.067E–03	3321020951.48437
1H-1	0.250	0.25	309.1	–6.9	3.350E–03	3321020956.81250
1H-1	0.300	0.30	326.4	–6.2	5.799E–03	3321020962.12500
1H-1	0.350	0.35	327.0	–1.9	6.460E–03	3321020967.45312
1H-1	0.400	0.40	315.3	4.4	5.510E–03	3321020972.78125
1H-1	0.450	0.45	313.9	3.0	6.664E–03	3321020978.10937
1H-1	0.500	0.50	317.1	–0.7	7.573E–03	3321020983.43750
1H-1	0.550	0.55	315.6	0.5	6.765E–03	3321020988.76562
1H-1	0.600	0.60	315.2	5.9	6.488E–03	3321020994.07812
1H-1	0.650	0.65	321.4	8.6	8.175E–03	3321020999.40625
1H-1	0.700	0.70	316.7	11.0	8.355E–03	3321021004.73437
1H-1	0.750	0.75	307.9	9.4	6.519E–03	3321021010.06250
1H-1	0.800	0.80	313.6	4.1	6.353E–03	3321021015.39062
1H-1	0.850	0.85	321.9	1.5	7.192E–03	3321021020.70312
1H-1	0.900	0.90	312.0	2.6	5.855E–03	3321021026.03125
1H-1	0.950	0.95	311.8	5.7	6.303E–03	3321021031.35937
1H-1	1.000	1.00	313.2	7.8	6.802E–03	3321021036.68750
1H-1	1.050	1.05	312.2	10.0	6.694E–03	3321021042.01562
1H-1	1.100	1.10	289.2	14.2	4.063E–03	3321021047.32812
1H-1	1.150	1.15	208.1	8.7	4.497E–03	3321021052.65625
1H-1	1.200	1.20	190.1	–1.0	7.541E–03	3321021057.98437
1H-1	1.250	1.25	190.2	–1.9	6.572E–03	3321021063.31250
1H-1	1.300	1.30	193.1	–1.0	5.616E–03	3321021068.62500
1H-1	1.350	1.35	201.8	–2.8	4.052E–03	3321021073.95312
1H-1	1.400	1.40	202.3	–3.4	3.260E–03	3321021079.28125
1H-2	0.100	1.60	30.3	82.1	2.700E–02	3320985450.07812
1H-2	0.150	1.65	359.1	77.7	2.756E–02	3320985455.40625
1H-2	0.200	1.70	344.8	71.1	2.969E–02	3320985460.73437
1H-2	0.250	1.75	335.3	75.5	3.076E–02	3320985466.04687
1H-2	0.300	1.80	18.2	84.7	2.745E–02	3320985471.37500
2H-1	0.100	2.20	103.3	85.4	7.306E–02	3321019643.37500
2H-1	0.150	2.25	33.8	81.4	6.623E–02	3321019648.70312
2H-1	0.200	2.30	24.2	81.1	6.554E–02	3321019654.03125
2H-1	0.250	2.35	358.5	82.5	6.600E–02	3321019659.35937
2H-1	0.300	2.40	24.5	83.2	6.121E–02	3321019664.68750
2H-1	0.350	2.45	341.2	83.1	5.445E–02	3321019670.00000
2H-1	0.400	2.50	308.3	81.6	5.684E–02	3321019675.32812
2H-1	0.450	2.55	309.6	86.8	5.561E–02	3321019680.65625
2H-1	0.500	2.60	81.0	80.5	5.481E–02	3321019685.98437
2H-1	0.550	2.65	87.0	79.4	5.213E–02	3321019691.31250
2H-1	0.600	2.70	62.9	88.5	4.792E–02	3321019696.62500
2H-1	0.650	2.75	300.6	82.7	4.519E–02	3321019701.95312
2H-1	0.700	2.80	296.8	79.1	4.422E–02	3321019707.28125
2H-1	0.750	2.85	296.1	83.1	3.924E–02	3321019712.60937
2H-1	0.800	2.90	277.5	85.6	2.955E–02	3321019717.93750
2H-1	0.850	2.95	298.7	85.3	2.200E–02	3321019723.26562
2H-1	0.900	3.00	327.3	83.0	2.681E–02	3321019728.57812
2H-1	0.950	3.05	288.0	82.2	2.472E–02	3321019733.90625
2H-1	1.000	3.10	295.0	79.7	2.588E–02	3321019739.23437
2H-1	1.050	3.15	287.8	75.4	3.243E–02	3321019744.56250
2H-1	1.100	3.20	285.4	80.6	3.354E–02	3321019749.87500
2H-1	1.150	3.25	292.9	81.7	3.595E–02	3321019755.20312
2H-1	1.200	3.30	277.4	84.5	3.773E–02	3321019760.53125
2H-1	1.250	3.35	279.6	85.8	3.574E–02	3321019765.85937
2H-1	1.300	3.40	292.7	86.1	3.315E–02	3321019771.18750
2H-1	1.350	3.45	274.0	80.9	3.238E–02	3321019776.50000
2H-1	1.400	3.50	279.3	79.0	2.717E–02	3321019781.82812
2H-2	0.100	3.70	280.8	83.7	1.622E–02	3321023792.68750
2H-2	0.150	3.75	337.4	87.6	1.243E–02	3321023798.01562
2H-2	0.200	3.80	326.4	86.8	1.143E–02	3321023803.34375

Notes: Time = since 1 January 1904. Only a portion of this table appears here. The complete table is available in ASCII.

Table T18. Paleomagnetic data from archive-half sections, Hole U1332B, at 20 mT AF demagnetization. (See table notes.)

Core, section	Offset (m)	Depth CSF (m)	Declination (°)	Inclination (°)	Intensity (A/m)	Time (s)	Declination: Core mean (°)	Declination: Geographical coordinates 0°–360°	Declination: Geographical coordinates –90°–270°	VGP (°) Latitude	VGP (°) Longitude
320-U1332B-											
1H-1	0.10	0.10	321.1	–8.0	4.43E–03	3321021828.39062	340.9	340.3	–19.8	64.7	91.1
1H-1	0.15	0.15	308.0	–12.1	3.50E–03	3321021833.71875	340.9	327.2	–32.9	52.7	101.8
1H-1	0.20	0.20	332.6	–4.9	2.30E–03	3321021839.04687	340.9	351.8	–8.3	73.5	69.2
1H-1	0.25	0.25	334.4	–2.7	2.46E–03	3321021844.35937	340.9	353.6	–6.5	75.3	65.2
1H-1	0.30	0.30	355.3	–1.5	4.73E–03	3321021849.6875	340.9	14.4	14.4	70.9	–10.6
1H-1	0.35	0.35	355.0	4.2	5.88E–03	3321021855.01562	340.9	14.1	14.1	72.9	–17.2
1H-1	0.40	0.40	350.4	9.6	5.50E–03	3321021860.34375	340.9	9.5	9.5	78.2	–15.0
1H-1	0.45	0.45	338.5	12.3	5.68E–03	3321021865.67187	340.9	357.7	–2.4	83.9	61.3
1H-1	0.50	0.50	343.8	8.9	6.66E–03	3321021870.98437	340.9	2.9	2.9	82.0	17.3
1H-1	0.55	0.55	344.5	7.6	6.09E–03	3321021876.3125	340.9	3.6	3.6	81.1	14.6
1H-1	0.60	0.60	345.8	12.3	5.68E–03	3321021881.64062	340.9	4.9	4.9	82.5	–2.1
1H-1	0.65	0.65	344.3	16.0	6.48E–03	3321021886.96875	340.9	3.4	3.4	84.9	–3.5
1H-1	0.70	0.70	343.1	17.2	7.85E–03	3321021892.29687	340.9	2.3	2.3	86.2	3.3
1H-1	0.75	0.75	341.3	17.8	6.10E–03	3321021897.625	340.9	0.4	0.4	87.2	29.9
1H-1	0.80	0.80	341.9	10.1	5.35E–03	3321021902.9375	340.9	1.0	1.0	83.1	30.2
1H-1	0.85	0.85	345.0	7.0	5.95E–03	3321021908.26562	340.9	4.1	4.1	80.7	12.5
1H-1	0.90	0.90	347.8	6.5	5.77E–03	3321021913.59375	340.9	6.9	6.9	78.9	–0.1
1H-1	0.95	0.95	344.6	8.5	5.21E–03	3321021918.92187	340.9	3.8	3.8	81.5	12.7
1H-1	1.00	1.00	341.5	12.6	5.79E–03	3321021924.23437	340.9	0.6	0.6	84.4	32.3
1H-1	1.05	1.05	341.9	13.0	5.73E–03	3321021929.5625	340.9	1.0	1.0	84.6	27.8
1H-1	1.10	1.10	332.4	19.6	3.62E–03	3321021934.89062	340.9	351.6	–8.5	81.5	117.4
1H-1	1.15	1.15	156.5	16.8	1.48E–03	3321021940.21875	340.9	175.7	175.7	–69.1	–128.9
1H-1	1.20	1.20	164.3	–2.0	5.02E–03	3321021945.54687	340.9	183.5	183.5	–78.6	–158.7
1H-1	1.25	1.25	164.0	–4.1	5.43E–03	3321021950.875	340.9	183.2	183.2	–79.7	–158.9
1H-1	1.30	1.30	159.9	0.8	4.34E–03	3321021956.1875	340.9	179.1	179.1	–77.7	–136.6
1H-1	1.35	1.35	161.6	–0.7	4.15E–03	3321021961.51562	340.9	180.8	180.8	–78.4	–144.8
1H-1	1.40	1.40	159.3	–2.6	2.39E–03	3321021966.84375	340.9	178.5	178.5	–79.3	–132.7
1H-2	0.10	1.60	8.4	40.3	7.77E–04	3320985786.48437	340.9	27.5	27.5	61.6	–77.7
1H-2	0.15	1.65	337.8	17.1	2.57E–03	3320985791.79687	340.9	357.0	–3.1	85.6	82.7
1H-2	0.20	1.70	337.4	12.4	4.40E–03	3320985797.125	340.9	356.6	–3.5	83.4	70.4
1H-2	0.25	1.75	328.7	9.4	3.05E–03	3320985802.45312	340.9	347.9	–12.2	76.0	99.1
1H-2	0.30	1.80	157.1	6.5	2.16E–03	3320985807.78125	340.9	176.3	176.3	–74.4	–127.0
2H-1	0.10	2.20	130.7	71.4	1.52E–02	3321020505.46875	101.8	28.9	28.9	40.5	–120.3
2H-1	0.15	2.25	48.6	71.1	1.02E–02	3321020510.79687	101.8	306.8	–53.2	30.1	–172.6
2H-1	0.20	2.30	32.4	64.6	1.04E–02	3321020516.125	101.8	290.6	–69.4	22.7	–185.4
2H-1	0.25	2.35	9.0	69.1	1.36E–02	3321020521.4375	101.8	267.2	267.2	7.7	–178.8
2H-1	0.30	2.40	15.5	72.9	1.51E–02	3321020526.76562	101.8	273.7	–86.3	12.0	–173.4
2H-1	0.35	2.45	301.5	69.0	1.21E–02	3321020532.09375	101.8	199.7	199.7	–23.4	–154.0
2H-1	0.40	2.50	283.0	63.7	1.24E–02	3321020537.42187	101.8	181.2	181.2	–32.7	–142.0
2H-1	0.45	2.55	277.7	68.9	1.13E–02	3321020542.73437	101.8	175.9	175.9	–25.7	–138.3
2H-1	0.50	2.60	95.8	67.5	1.07E–02	3321020548.0625	101.8	354.0	–6.0	51.2	–147.2
2H-1	0.55	2.65	102.2	52.2	1.08E–02	3321020553.39062	101.8	0.4	0.4	69.1	–140.2
2H-1	0.60	2.70	147.7	79.2	6.12E–03	3321020558.71875	101.8	45.9	45.9	25.8	–124.5

Notes: Time = since 1 January 1904. VGP = virtual geomagnetic pole. Only a portion of this table appears here. The complete table is available in ASCII.

Table T19. Paleomagnetic data from archive-half sections, Hole U1332C, at 0 mT AF demagnetization. (See table notes.)

Core, section	Offset (m)	Depth CSF (m)	Declination (°)	Inclination (°)	Intensity (A/m)	Time (s)
320-U1332C-						
1H-1	0.500	0.50	212.2	77.4	3.224E–02	3321179655.34912
1H-1	0.550	0.55	202.2	79.2	3.339E–02	3321179660.67725
1H-1	0.600	0.60	196.8	80.1	3.558E–02	3321179666.00537
1H-1	0.650	0.65	201.1	76.1	3.663E–02	3321179671.31787
1H-1	0.700	0.70	190.0	75.7	3.533E–02	3321179676.64600
1H-1	0.750	0.75	183.4	75.3	3.513E–02	3321179681.97412
1H-1	0.800	0.80	183.5	75.1	3.598E–02	3321179687.30225
1H-1	0.850	0.85	176.8	75.6	3.642E–02	3321179692.63037
1H-1	0.900	0.90	168.4	73.3	3.517E–02	3321179697.94287
1H-1	0.950	0.95	164.6	70.2	3.253E–02	3321179703.27100
1H-1	1.000	1.00	159.5	71.5	3.111E–02	3321179708.59912
1H-1	1.050	1.05	167.3	72.4	3.265E–02	3321179713.92725
1H-1	1.100	1.10	170.2	70.4	3.285E–02	3321179719.25537
1H-1	1.150	1.15	161.9	67.2	2.987E–02	3321179724.56787
1H-1	1.200	1.20	157.9	68.0	2.894E–02	3321179729.89600
1H-1	1.250	1.25	153.2	72.6	2.774E–02	3321179735.22412
1H-1	1.300	1.30	146.9	74.0	2.458E–02	3321179740.55225
1H-1	1.350	1.35	142.1	76.2	2.086E–02	3321179745.88037
1H-1	1.400	1.40	107.4	76.5	2.037E–02	3321179751.19287
1H-2	0.100	1.60	139.9	65.5	1.798E–02	3321181317.13037
1H-2	0.150	1.65	127.2	71.8	1.676E–02	3321181322.44287
1H-2	0.200	1.70	102.4	72.2	1.889E–02	3321181327.77100
1H-2	0.250	1.75	87.1	74.2	1.893E–02	3321181333.09912
1H-2	0.300	1.80	126.8	76.1	2.085E–02	3321181338.42725
1H-2	0.350	1.85	154.6	71.0	2.237E–02	3321181343.75537
1H-2	0.400	1.90	158.4	66.9	2.211E–02	3321181349.06787
1H-2	0.450	1.95	156.4	62.5	2.559E–02	3321181354.39600
1H-2	0.500	2.00	157.7	64.2	2.870E–02	3321181359.72412
1H-2	0.550	2.05	135.9	75.6	2.672E–02	3321181365.05225
1H-2	0.600	2.10	120.7	76.3	2.738E–02	3321181370.38037
1H-2	0.650	2.15	116.0	72.9	2.810E–02	3321181375.69287
1H-2	0.700	2.20	117.2	67.6	2.735E–02	3321181381.02100
1H-2	0.750	2.25	119.8	72.5	2.241E–02	3321181386.34912
1H-2	0.800	2.30	112.6	74.9	2.129E–02	3321181391.67725
1H-2	0.850	2.35	116.1	71.6	1.958E–02	3321181397.00537
1H-2	0.900	2.40	121.7	72.9	1.623E–02	3321181402.31787
1H-2	0.950	2.45	114.1	75.0	1.317E–02	3321181407.64600
1H-2	1.000	2.50	103.0	77.5	1.193E–02	3321181412.97412
1H-2	1.050	2.55	103.3	78.9	1.779E–02	3321181418.30225
1H-2	1.100	2.60	107.5	80.8	2.193E–02	3321181423.63037
1H-2	1.150	2.65	95.9	80.7	2.420E–02	3321181428.94287
1H-2	1.200	2.70	103.5	80.2	2.506E–02	3321181434.27100
1H-2	1.250	2.75	114.9	80.2	2.284E–02	3321181439.59912
1H-2	1.300	2.80	109.5	77.0	2.166E–02	3321181444.92725
1H-2	1.350	2.85	116.5	73.3	1.795E–02	3321181450.23975
1H-2	1.400	2.90	97.7	72.7	1.451E–02	3321181455.56787
1H-3	0.100	3.10	113.0	66.7	2.046E–02	3321182222.66162
1H-3	0.150	3.15	120.1	70.3	1.948E–02	3321182227.98975
1H-3	0.200	3.20	104.0	76.2	2.169E–02	3321182233.31787
1H-3	0.250	3.25	96.2	67.8	2.405E–02	3321182238.63037
1H-3	0.300	3.30	107.5	58.0	2.464E–02	3321182243.95850
1H-3	0.350	3.35	111.5	53.3	2.178E–02	3321182249.28662
1H-3	0.400	3.40	111.4	57.9	1.667E–02	3321182254.59912
1H-3	0.450	3.45	105.6	66.1	1.209E–02	3321182259.92725
1H-3	0.500	3.50	103.6	77.7	1.080E–02	3321182265.25537
1H-3	0.550	3.55	97.2	72.8	1.300E–02	3321182270.56787
1H-3	0.600	3.60	106.4	72.3	1.361E–02	3321182275.89600
1H-3	0.650	3.65	109.9	73.5	1.277E–02	3321182281.22412
1H-3	0.700	3.70	137.0	78.0	9.873E–03	3321182286.55225
1H-3	0.750	3.75	139.1	75.3	8.195E–03	3321182291.86475

Notes: Time = since 1 January 1904. Core 320-U1332C-6H overlaps Core 7H by about 3 m CSF because Core 6H was advanced 4 m but recovered >7 m of core. The upper 2.6 m was slurry (cement and water with mixed sediments). To partially fix the overlap, we have subtracted 2.6 m from the Core 6H depths. This brings the top of the good core from Core 6H up to the base of Core 5H and reduces the overlap between Cores 6H and 7H to about 50 cm. Only a portion of this table appears here. The complete table is available in ASCII.

Table T20. Paleomagnetic data from archive-half sections, Hole U1332C, at 20 mT AF demagnetization. (See table notes.)

Core, section	Offset (m)	Depth CSF (m)	Declination (°)	Inclination (°)	Intensity (A/m)	Time (s)	Declination: Core mean (°)	Declination: Geographical coordinates 0°–360°	Declination: Geographical coordinates –90°–270°	VGP (°) Latitude	VGP (°) Longitude
320-U1332C-											
1H-1	0.50	0.50	210.8	42.4	6.01E–03	3321180839.55225	142.9	67.9	67.9	24.9	–72.8
1H-1	0.55	0.55	213.7	40.5	5.97E–03	3321180844.88037	142.9	70.8	70.8	22.1	–71.4
1H-1	0.60	0.60	213.4	43.7	6.25E–03	3321180850.19287	142.9	70.5	70.5	22.6	–74.0
1H-1	0.65	0.65	211.0	38.8	7.17E–03	3321180855.52100	142.9	68.1	68.1	24.6	–69.9
1H-1	0.70	0.70	206.7	31.7	7.15E–03	3321180860.84912	142.9	63.8	63.8	28.3	–64.3
1H-1	0.75	0.75	201.1	35.5	6.59E–03	3321180866.17725	142.9	58.2	58.2	33.7	–66.8
1H-1	0.80	0.80	200.1	37.3	7.07E–03	3321180871.50537	142.9	57.2	57.2	34.7	–68.3
1H-1	0.85	0.85	198.8	38.2	7.41E–03	3321180876.81787	142.9	55.9	55.9	35.9	–69.1
1H-1	0.90	0.90	193.9	37.2	7.33E–03	3321180882.14600	142.9	51.0	51.0	40.5	–68.3
1H-1	0.95	0.95	193.7	31.2	6.78E–03	3321180887.47412	142.9	50.8	50.8	40.7	–63.1
1H-1	1.00	1.00	195.5	31.0	6.17E–03	3321180892.80225	142.9	52.6	52.6	38.9	–63.0
1H-1	1.05	1.05	202.0	32.6	6.27E–03	3321180898.13037	142.9	59.1	59.1	32.8	–64.6
1H-1	1.10	1.10	201.3	35.3	6.52E–03	3321180903.44287	142.9	58.4	58.4	33.5	–66.7
1H-1	1.15	1.15	186.5	34.0	5.90E–03	3321180908.77100	142.9	43.6	43.6	47.5	–65.7
1H-1	1.20	1.20	186.2	31.3	4.53E–03	3321180914.09912	142.9	43.3	43.3	47.8	–63.2
1H-1	1.25	1.25	188.7	27.4	3.37E–03	3321180919.42725	142.9	45.8	45.8	45.4	–59.8
1H-1	1.30	1.30	153.0	48.9	9.38E–04	3321180924.75537	142.9	10.1	10.1	69.8	–114.9
1H-1	1.35	1.35	7.8	–13.9	5.65E–04	3321180930.06787	142.9	224.9	224.9	–45.5	–229.0
1H-1	1.40	1.40	5.7	–30.3	2.45E–03	3321180935.39600	142.9	222.8	222.8	–48.3	117.8
1H-2	0.10	1.60	17.0	–28.9	1.60E–03	3321181846.00537	142.9	234.1	234.1	–37.4	118.5
1H-2	0.15	1.65	36.3	–52.1	10.00E–04	3321181851.31787	142.9	253.4	253.4	–20.3	98.2
1H-2	0.20	1.70	7.7	–30.5	3.47E–03	3321181856.64600	142.9	224.8	224.8	–46.4	117.6
1H-2	0.25	1.75	0.1	–22.5	4.05E–03	3321181861.97412	142.9	217.2	217.2	–53.6	125.3
1H-2	0.30	1.80	358.2	–11.4	3.42E–03	3321181867.30225	142.9	215.3	215.3	–54.6	–224.2
1H-2	0.35	1.85	144.2	32.4	7.54E–04	3321181872.63037	142.9	1.3	1.3	84.2	–128.8
1H-2	0.40	1.90	176.0	26.4	3.54E–03	3321181877.94287	142.9	33.1	33.1	57.7	–58.4
1H-2	0.45	1.95	178.5	23.3	5.21E–03	3321181883.27100	142.9	35.6	35.6	55.2	–55.3
1H-2	0.50	2.00	179.0	25.6	5.19E–03	3321181888.59912	142.9	36.1	36.1	54.8	–57.6
1H-2	0.55	2.05	190.2	37.5	1.68E–03	3321181893.92725	142.9	47.3	47.3	43.9	–68.8
1H-2	0.60	2.10	331.9	38.8	7.08E–04	3321181899.25537	142.9	189.0	189.0	–55.1	–155.7
1H-2	0.65	2.15	344.3	5.7	1.28E–03	3321181904.56787	142.9	201.4	201.4	–64.1	–197.6
1H-2	0.70	2.20	349.3	2.2	1.33E–03	3321181909.89600	142.9	206.4	206.4	–60.7	–206.4
1H-2	0.75	2.25	350.5	–3.0	1.36E–03	3321181915.22412	142.9	207.6	207.6	–60.7	–212.3
1H-2	0.80	2.30	347.1	–11.0	2.10E–03	3321181920.55225	142.9	204.2	204.2	–65.3	–218.2
1H-2	0.85	2.35	353.2	–15.1	1.32E–03	3321181925.88037	142.9	210.3	210.3	–59.9	–225.8
1H-2	0.90	2.40	345.1	8.6	5.78E–04	3321181931.19287	142.9	202.2	202.2	–62.6	–196.0
1H-2	0.95	2.45	345.3	11.3	5.60E–04	3321181936.52100	142.9	202.4	202.4	–61.6	–193.9
1H-2	1.00	2.50	177.1	28.2	8.08E–04	3321181941.84912	142.9	34.2	34.2	56.6	–60.3
1H-2	1.05	2.55	11.8	75.0	3.26E–04	3321181947.17725	142.9	228.9	228.9	–7.0	–162.1
1H-2	1.10	2.60	315.5	–3.5	1.67E–03	3321181952.50537	142.9	172.6	172.6	–77.5	–104.7
1H-2	1.15	2.65	325.4	–15.5	2.58E–03	3321181957.81787	142.9	182.5	182.5	–85.3	–172.8
1H-2	1.20	2.70	324.0	–12.4	2.93E–03	3321181963.14600	142.9	181.1	181.1	–84.3	–152.0

Notes: Time = since 1 January 1904. VGP = virtual geomagnetic pole. Core 320-U1332C-6H overlaps Core 7H by about 3 m CSF because Core 6H was advanced 4 m but recovered >7 m of core. The upper 2.6 m was slurry (cement and water with mixed sediments). To partially fix the overlap, we have subtracted 2.6 m from the Core 6H depths. This brings the top of the good core from Core 6H up to the base of Core 5H and reduces the overlap between Cores 6H and 7H to about 50 cm. Only a portion of this table appears here. The complete table is available in ASCII.

Table T21. Paleomagnetic results for discrete samples, Hole U1332A. (See table notes.)

Core, section, interval (cm)	Depth CSF (m)	Demag (mT)	Declination Azimuthally unoriented (°)	Declination Geographical coordinates 0°–360°	Declination Geographical coordinates –90°–270°	Inclination (°)	Intensity (A/m)
320-U1332A-							
1H-1, 115	1.15	0	2.7	10.6	10.6	69.9	1.640E–02
1H-1, 115	1.15	5	3.2	11.1	11.1	27.7	4.998E–03
1H-1, 115	1.15	10	–2.6	5.3	5.3	21.4	3.622E–03
1H-1, 115	1.15	15	0.7	8.6	8.6	20.8	3.232E–03
1H-1, 115	1.15	20	7.7	15.6	15.6	22.8	2.835E–03
1H-1, 115	1.15	25	–1.7	6.2	6.2	24.1	2.476E–03
1H-1, 115	1.15	30	–3.9	4.0	4.0	29.4	2.013E–03
1H-1, 115	1.15	35	–4.7	3.2	3.2	31.6	1.460E–03
1H-1, 115	1.15	40	–13.6	–5.7	–5.7	33.4	1.282E–03
1H-1, 115	1.15	50	9.6	17.5	17.5	47.7	1.095E–03
1H-1, 115	1.15	60	–16.4	–8.5	–8.5	68.0	8.940E–04
1H-2, 85	2.35	0	166.2	174.2	174.2	78.5	2.939E–03
1H-2, 85	2.35	5	134.4	142.3	142.3	13.3	7.681E–04
1H-2, 85	2.35	10	–175.7	–167.8	192.2	–11.0	6.415E–04
1H-2, 85	2.35	15	154.5	162.4	162.4	–5.1	7.006E–04
1H-2, 85	2.35	20	134.5	142.4	142.4	–7.7	7.736E–04
1H-2, 85	2.35	25	161.9	169.8	169.8	–5.0	4.870E–04
1H-2, 85	2.35	30	163.3	171.2	171.2	9.8	4.524E–04
1H-2, 85	2.35	35	155.6	163.5	163.5	6.6	3.140E–04
1H-2, 85	2.35	40	169.3	177.2	177.2	21.6	3.722E–04
1H-2, 85	2.35	50	105.1	113.0	113.0	30.5	3.404E–04
1H-2, 85	2.35	60	146.0	153.9	153.9	50.0	3.473E–04
2H-1, 85	4.75	0	0.1	332.2	–27.8	77.9	9.503E–03
2H-1, 85	4.75	5	–10.6	321.4	–38.6	–12.2	1.416E–03
2H-1, 85	4.75	10	–29.0	303.0	–57.0	–48.7	2.130E–03
2H-1, 85	4.75	15	–16.8	315.2	–44.8	–49.2	1.917E–03
2H-1, 85	4.75	20	11.8	343.8	–16.2	–43.9	1.559E–03
2H-1, 85	4.75	25	–5.3	326.7	–33.3	–42.7	1.205E–03
2H-1, 85	4.75	30	–20.7	311.4	–48.6	–29.4	9.272E–04
2H-1, 85	4.75	35	–23.5	308.6	–51.4	–20.1	6.954E–04
2H-1, 85	4.75	40	–15.4	316.6	–43.4	20.7	5.720E–04
2H-1, 85	4.75	50	71.3	43.4	43.4	43.2	2.982E–04
2H-1, 85	4.75	60	20.5	352.6	–7.4	67.6	1.244E–03
2H-2, 85	6.25	0	18.5	350.5	–9.5	83.6	1.540E–02
2H-2, 85	6.25	5	50.2	22.3	22.3	14.2	1.677E–03
2H-2, 85	6.25	10	46.6	18.6	18.6	–27.1	1.978E–03
2H-2, 85	6.25	15	55.6	27.6	27.6	–25.6	2.178E–03
2H-2, 85	6.25	20	54.2	26.3	26.3	–22.3	2.145E–03
2H-2, 85	6.25	25	44.0	16.0	16.0	–24.9	1.440E–03
2H-2, 85	6.25	30	39.6	11.7	11.7	–16.7	9.639E–04
2H-2, 85	6.25	35	47.1	19.1	19.1	–9.3	6.947E–04
2H-2, 85	6.25	40	22.4	354.5	–5.5	12.2	3.298E–04
2H-2, 85	6.25	50	43.8	15.9	15.9	54.2	4.785E–04
2H-2, 85	6.25	60	55.3	27.3	27.3	78.5	7.408E–04
2H-5, 85	10.75	0	–63.7	268.4	268.4	–61.6	2.171E–02
2H-5, 85	10.75	5	–47.7	284.4	–75.6	–48.6	7.862E–03
2H-5, 85	10.75	10	–50.8	281.2	–78.8	–26.0	4.105E–03
2H-5, 85	10.75	15	–45.0	287.0	–73.0	–25.7	2.998E–03
2H-5, 85	10.75	20	–47.2	284.8	–75.2	–23.4	2.406E–03
2H-5, 85	10.75	25	–48.0	284.0	–76.0	–15.5	1.954E–03
2H-5, 85	10.75	30	–50.1	281.9	–78.1	–1.8	1.577E–03
2H-5, 85	10.75	35	–49.1	283.0	–77.0	2.5	9.856E–04
2H-5, 85	10.75	40	–64.1	267.9	267.9	20.2	6.986E–04
2H-5, 85	10.75	50	–42.0	290.0	–70.0	51.6	7.502E–04
2H-5, 85	10.75	60	–42.7	289.3	–70.7	71.9	1.015E–03
2H-6, 85	12.25	0	150.0	122.1	122.1	–72.2	1.208E–02
2H-6, 85	12.25	5	139.8	111.8	111.8	–27.4	3.612E–03
2H-6, 85	12.25	10	148.2	120.2	120.2	–16.7	2.335E–03
2H-6, 85	12.25	15	148.2	120.2	120.2	–10.8	1.845E–03
2H-6, 85	12.25	20	143.6	115.6	115.6	–5.8	1.549E–03
2H-6, 85	12.25	25	146.2	118.3	118.3	3.1	1.115E–03
2H-6, 85	12.25	30	156.8	128.8	128.8	14.8	6.562E–04

Notes: Only a portion of this table appears here. The complete table is available in ASCII.

Table T22. Principal component analysis (PCA) results for paleomagnetic data, Hole U1332A. (See table notes.) (Continued on next page.)

Core, section, interval (cm)	Depth CSF (m)	PCA: Declination: Azimuthally unoriented (°)	PCA: Declination: Geographical coordinates (0°–360°)	PCA: Inclination (°)	PCA: MAD (°)	PCA: Range (mT)	Archive-half section at 20 mT AF demagnetization (°): Declination	Archive-half section at 20 mT AF demagnetization (°): Inclination
320-U1332A-								
1H-1, 115	1.15	2.8	10.7	12.8	13.1	10–35	346.6	1.3
1H-2, 85	2.35	NA	NA	NA	NA	NA	182.5	13.3
2H-1, 85	4.75	NA	NA	NA	NA	NA	209.6	34.0
2H-2, 85	6.25	45.8	17.8	–40.5	10.3	25–50	211.0	36.2
2H-5, 85	10.75	312.9	284.9	–36.1	7.7	10–40	77.8	61.9
2H-6, 85	12.25	146.8	118.9	–24.2	9.9	10–35	74.6	67.6
3H-1, 95	14.35	0.6	204.3	–4.0	7.8	10–35	0.1	–2.1
3H-2, 85	15.75	346.1	189.8	0.9	8.6	10–35	344.2	–8.8
3H-4, 85	18.75	325.9	169.6	–25.6	10.0	10–30	306.5	–2.3
3H-5, 85	20.25	NA	NA	NA	NA	NA	300.1	4.6
3H-6, 85	21.75	159.8	3.5	17.5	10.1	5–40	161.3	14.8
3H-7, 65	23.05	NA	NA	NA	NA	NA	332.9	7.9
4H-1, 85	23.75	269.8	183.2	0.9	7.5	10–30	269.7	12.2
4H-2, 85	25.25	81.2	354.5	2.3	3.7	10–40	78.7	11.2
4H-4, 85	28.25	91.2	4.6	4.9	3.6	10–35	83.0	14.1
4H-5, 85	29.75	83.8	357.1	17.7	9.5	5–35	83.2	22.5
4H-6, 85	31.25	259.3	172.6	–0.8	9.6	10–30	273.1	15.5
4H-7, 60	32.50	102.4	15.7	6.6	5.3	10–35	107.7	20.2
5H-1, 85	33.25	319.9	334.0	0.1	11.8	10–50	323.0	15.8
5H-2, 85	34.75	NA	NA	NA	NA	NA	161.8	17.3
5H-4, 85	37.75	NA	NA	NA	NA	NA	167.6	21.9
5H-5, 85	39.25	173.7	187.8	2.6	5.0	10–30	177.5	5.3
5H-6, 85	40.75	180.8	194.9	–6.6	8.7	10–30	183.5	6.7
5H-7, 83	42.23	NA	NA	NA	NA	10–30		
6H-1, 115	43.05	NA	NA	NA	NA	15–60	12.0	0.6
6H-2, 85	44.25	NA	NA	NA	NA	10–50	203.9	–8.9
6H-4, 85	47.25	186.9	354.3	–0.4	4.0	10–30	187.6	11.8
6H-5, 85	48.75	NA	NA	NA	NA	NA	21.4	0.6
6H-6, 85	50.25	NA	NA	NA	NA	NA	13.9	3.6
6H-7, 45	51.35	23.3	190.7	3.5	9.8	10–40	20.3	–3.7
7H-1, 85	52.25	57.0	155.9	–15.1	13.7	15–40	57.4	6.2
7H-2, 85	53.75	NA	NA	NA	NA	NA	139.7	31.8
7H-4, 85	56.75	77.4	176.3	0.8	8.4	5–50	67.0	–2.6
7H-5, 85	58.25	89.1	188.0	–3.7	9.9	15–35	93.0	0.0
7H-6, 85	59.75	108.7	207.6	–8.6	8.4	20–40	122.7	9.8
7H-7, 45	60.85	NA	NA	NA	NA	NA	148.6	16.9
8H-2, 85	63.25	NA	NA	NA	NA	NA	332.2	–4.0
8H-4, 85	66.25	330.0	167.7	4.5	8.1	10–40	338.7	–4.5
8H-5, 85	67.75	NA	NA	NA	NA	NA	172.8	14.4
8H-6, 85	69.25	174.0	11.8	6.4	13.6	10–35	174.2	17.7
8H-7, 45	70.35	NA	NA	NA	NA	NA	176.5	18.3
9H-1, 85	71.25	275.8	171.3	–5.1	4.4	10–30	282.0	–1.7
9H-2, 85	72.75	90.0	345.5	1.4	4.9	10–40	94.8	9.2
9H-4, 135	76.25	271.9	167.4	–2.1	2.3	10–30	283.4	–2.7
9H-5, 85	77.25	283.1	178.6	3.9	3.1	10–40	283.5	–0.1
9H-6, 85	78.75	299.7	195.2	–1.1	5.1	10–30	291.6	–5.3
9H-7, 45	79.85	115.9	11.4	9.0	3.8	10–30	116.6	9.4
10H-1, 95	80.85	307.19	185.7	–7.63	3.6	10–30	304.5	1.1
10H-2, 85	82.25	303.95	182.5	–7.37	7.8	10–30	306	2
10H-4, 85	85.25	115.1	353.6	7.5	3.8	10–30	115.4	10.3
10H-5, 85	86.75	301.2	179.7	–1.8	6.4	10–30	306.5	2.7
10H-6, 85	88.25	127.6	6.1	7.1	5.8	10–30	128.5	9.3
10H-7, 50	89.40	126.71	5.2	2.82	6.9	10–30	127	6
11H-2, 85	91.75	264.37	1.1	2.68	2.7	10–30	269.2	8.5
11H-4, 85	94.75	264.05	0.7	0.68	4.3	15–35	263.8	8.2
11H-5, 85	96.25	79.96	176.7	–2.50	7.4	10–30	77.50	5.20
11H-6, 85	97.75	261.9	358.6	0.0	4.9	10–40	256.5	10.2
12H-2, 85	101.25	286.4	353.3	–1.8	3.0	20–50	292.3	2.4
12H-4, 85	104.25	297.8	4.6	–6.0	3.9	15–40	290.2	9.7
12H-5, 85	105.75	303.4	10.3	6.9	5.6	10–40	296.4	7.6
12H-6, 85	107.25	131.0	197.9	4.2	4.5	15–40	123.1	–0.5
12H-7, 50	108.20	118.35	185.2	5.83	4.1	10–40		
13H-1, 85	109.25	88.0	169.0	–6.5	6.7	20–40	102.7	18.3

Table T22 (continued).

Core, section, interval (cm)	Depth CSF (m)	PCA Declination Azimuthally unoriented (°)	PCA Declination Geographical coordinates (0°–360°)	PCA Inclination (°)	PCA MAD (°)	PCA Range (mT)	Archive-half section at 20 mT AF demagnetization (°) Declination	Archive-half section at 20 mT AF demagnetization (°) Inclination
13H-2, 85	110.75	81.4	162.3	–1.9	8.6	15–35	89.3	12.8
13H-4, 85	113.75	NA	NA	NA	NA	NA	100.5	10.6
13H-5, 85	115.25	96.5	177.4	–6.4	12.5	15–50	102.9	18.2
13H-6, 85	116.75	110.8	191.7	–2.3	9.5	10–30	112.8	14.9
13H-7, 75	118.15	288.1	9.1	2.5	6.4	10–30		
14H-2, 85	120.25	259.4	160.4	10.3	11.8	10–50	276.9	15.4
14H-4, 85	123.25	256.3	157.3	5.3	8.8	10–35	271.6	8.2
14H-5, 85	124.75	94.9	356.0	4.4	6.5	25–50	95.7	10.3
14H-6, 20	125.60	118.6	19.7	–2.5	11.0	10–40	115.0	–2.4
15X-1, 115	127.05	NA	NA	NA	NA	NA	238.8	5.7
15X-4, 85	131.25	204.1	NA	2.0	12.4	5–60	204.2	39.2
15X-5, 50	132.40	NA	NA	NA	NA	NA	113.70	23.20
16X-1, 85	136.35	82.5	NA	18.0	6.3	15–40		

Notes: MAD = maximum angular deviation. NA = not applicable.

Table T23. Mean paleomagnetic direction for each core, Site U1332. (See table notes.)

Core	Inclination (°)	Declination (°)	*N*	α95 (°)
320-U1332A-				
1H	–6.6	352.1	47	4.4
2H	–76.1	28.0	170	8.4
3H	3.4	156.3	162	4.7
4H	3.7	86.7	174	3.0
5H	–4.7	345.9	177	2.6
6H	7.6	192.5	164	2.1
7H	–2.3	261.1	175	4.0
8H	8.6	162.3	171	2.9
9H	3.3	104.5	176	1.4
10H	4.9	121.5	162	1.5
11H	5.7	263.3	132	2.0
12H	3.2	293.1	143	1.5
13H	–14.8	279.0	175	2.2
14H	–11.6	99.0	118	2.2
320-U1332B-				
1H	6.9	340.9	32	4.4
2H	30.0	101.8	170	6.9
3H	5.9	68.1	107	4.0
4H	6.0	68.6	147	3.0
5H	12.4	219.9	127	3.0
6H	13.6	194.1	114	3.2
7H	–5.9	105.0	174	2.9
8H	7.9	188.8	132	2.8
9H	3.6	120.6	170	1.8
10H	7.4	57.9	148	2.8
11H	4.6	18.7	99	3.8
12H	10.4	238.2	156	2.4
13H	–3.2	152.1	161	1.8
320-U1332C-				
1H	21.9	142.9	151	15.6
2H	17.4	5.8	151	5.0
3H	–1.7	125.7	145	3.6
4H	9.1	179.8	172	2.7
5H	3.5	215.4	169	1.4
6H	5.4	240.2	85	2.2
7H	–0.1	335.5	172	2.5
8H	5.8	120.6	134	2.5
9H	6.4	219.8	165	2.4
11H	2.2	82.4	148	1.4
12H	3.0	92.8	155	1.4
13H	–8.4	25.2	148	2.0

Notes: Mean paleomagnetic directions and statistics calculated using Bingham statistics for each core. Inclination = mean paleomagnetic inclination from stable polarity intervals in core, declination = mean paleomagnetic declination from stable polarity intervals in core. By subtracting this value from observed paleomagnetic declinations measured along core, core can be approximately reoriented back into geographic coordinates. After reorientation, normal polarity intervals will have ~0° declination and reversed polarity intervals will have ~180° declination. *N* = number of paleomagnetic observations used in calculating mean, α95 = 95% confidence angle for mean direction.

Table T24. Magnetic susceptibility of discrete samples, Hole U1332A. (See table notes.) (Continued on next page.)

Core, section	Depth CSF (m)	LIMS ID	Susceptibility (SI)	Total mass (g)	Bulk density (g/cm^3)	Volume (cm^3)	Susceptibility: Volume normalized (SI)	Susceptibility: Mass normalized (m^3/kg)	Whole core (raw values)	Scale factor
320-U1332A-										
1H-1	1.14	CUBE582661	1.370E–04	10.51	1.25	4.75	2.021E–04	9.125E–08	28.2	7.166E–06
1H-2	2.37	CUBE582671	5.981E–05	9.50	1.24	3.97	1.054E–04	4.407E–08	19.0	5.549E–06
1H-3	3.43	CUBE582681	1.119E–04	11.48	1.25	5.53	1.417E–04	6.823E–08	17.7	8.005E–06
2H-1	4.73	CUBE583611	1.495E–04	10.97	1.25	5.09	2.058E–04	9.540E–08	23.3	8.831E–06
2H-2	6.27	CUBE583621	1.782E–04	12.46	2.25	3.49	3.574E–04	1.001E–07	24.0	1.489E–05
2H-4	9.24	CUBE583631	2.792E–04	12.63	1.27	6.33	3.088E–04	1.547E–07	42.0	7.352E–06
2H-5	10.77	CUBE583651	2.393E–04	12.60	1.33	6.01	2.786E–04	1.329E–07	36.3	7.676E–06
2H-6	12.24	CUBE583671	2.382E–04	7.69	1.32	2.36	7.078E–04	2.168E–07	81.4	8.695E–06
3H-1	14.34	CUBE584901	2.533E–04	11.71	1.20	5.96	2.977E–04	1.514E–07	37.5	7.938E–06
3H-2	15.77	CUBE584911	2.256E–04	12.07	1.16	6.42	2.458E–04	1.308E–07	31.3	7.854E–06
3H-3	17.24	CUBE584921	1.623E–04	12.06	1.23	6.09	1.865E–04	9.420E–08	27.0	6.908E–06
3H-4	18.73	CUBE584941	2.105E–04	12.14	1.20	6.30	2.341E–04	1.214E–07	31.0	7.551E–06
3H-5	20.27	CUBE584961	1.781E–04	11.59	1.20	5.83	2.138E–04	1.076E–07	29.4	7.272E–06
3H-6	21.73	CUBE584981	1.810E–04	11.89	1.22	5.99	2.116E–04	1.066E–07	30.0	7.054E–06
3H-7	23.03	CUBE585001	6.580E–05	11.19	1.16	5.67	8.119E–05	4.116E–08	30.3	2.680E–06
4H-1	23.74	CUBE586061	1.490E–04	11.45	1.22	5.61	1.859E–04	9.109E–08	25.0	7.434E–06
4H-2	25.28	CUBE586071	2.111E–04	12.60	1.28	6.27	2.358E–04	1.173E–07	30.4	7.758E–06
4H-3	26.73	CUBE586081	1.984E–04	12.34	1.25	6.20	2.239E–04	1.125E–07	27.4	8.171E–06
4H-4	28.23	CUBE586091	2.150E–04	12.25	1.24	6.16	2.445E–04	1.229E–07	31.0	7.887E–06
4H-5	29.77	CUBE586101	2.115E–04	11.92	1.21	6.04	2.451E–04	1.242E–07	31.3	7.830E–06
4H-6	31.24	CUBE586111	1.485E–04	12.84	1.30	6.37	1.632E–04	8.096E–08	23.0	7.096E–06
4H-7	32.48	CUBE586121	1.137E–04	12.91	1.34	6.20	1.283E–04	6.165E–08	18.0	7.129E–06
5H-1	33.24	CUBE587081	1.186E–04	14.38	1.58	6.21	1.336E–04	5.773E–08	15.2	8.789E–06
5H-2	34.77	CUBE587101	6.177E–05	12.43	1.58	4.98	8.689E–05	3.479E–08	10.3	8.436E–06
5H-3	36.23	CUBE587111	4.914E–05	15.08	1.59	6.61	5.202E–05	2.281E–08	7.0	7.431E–06
5H-4	37.73	CUBE587121	1.368E–04	13.97	1.52	6.17	1.552E–04	6.855E–08	14.7	1.056E–05
5H-5	39.26	CUBE587131	1.028E–04	13.90	1.56	5.96	1.208E–04	5.177E–08	13.3	9.080E–06
5H-6	40.73	CUBE587141	3.744E–05	10.82	1.57	3.96	6.624E–05	2.422E–08	8.0	8.280E–06
5H-7	42.22	CUBE587091	1.685E–05	15.97	1.65	6.91	1.707E–05	7.386E–09	3.1	5.508E–06
6H-1	43.03	CUBE587781	3.609E–05	14.30	1.67	5.81	4.346E–05	1.767E–08	5.0	8.692E–06
6H-2	44.24	CUBE587791	3.019E–05	14.87	1.68	6.13	3.448E–05	1.421E–08	4.1	8.410E–06
6H-3	45.76	CUBE587811	6.392E–05	14.38	1.26	7.79	5.742E–05	3.112E–08	8.5	6.755E–06
6H-4	47.23	CUBE587821	2.600E–05	14.60	1.66	6.02	3.022E–05	1.247E–08	2.0	1.511E–05
6H-5	48.76	CUBE587831	5.422E–05	15.51	1.73	6.32	6.004E–05	2.447E–08	4.7	1.277E–05
6H-6	50.25	CUBE587841	5.287E–05	14.15	1.66	5.76	6.424E–05	2.615E–08	6.2	1.036E–05
6H-7	51.34	CUBE587801	7.530E–05	14.15	1.64	5.84	9.028E–05	3.725E–08	10.3	8.765E–06
7H-1	52.24	CUBE588081	1.151E–04	12.18	1.47	5.16	1.561E–04	6.615E–08	19.8	7.883E–06
7H-2	53.73	CUBE588101	5.998E–05	14.10	1.56	6.11	6.871E–05	2.978E–08	12.0	5.726E–06
7H-3	55.23	CUBE588111	3.176E–05	13.19	1.67	5.15	4.313E–05	1.686E–08	7.2	5.990E–06
7H-4	56.74	CUBE588121	2.345E–05	14.85	1.67	6.14	2.672E–05	1.105E–08	5.0	5.345E–06
7H-5	58.24	CUBE588131	3.774E–05	15.17	1.65	6.40	4.128E–05	1.741E–08	5.9	6.997E–06
7H-6	59.73	CUBE588141	4.253E–05	14.80	1.66	6.14	4.847E–05	2.012E–08	6.4	7.574E–06
7H-7	60.83	CUBE588091	4.894E–05	14.62	1.62	6.21	5.517E–05	2.343E–08	7.0	7.882E–06
8H-2	63.23	CUBE588401	4.564E–05	13.80	1.46	6.33	5.048E–05	2.315E–08	9.2	5.487E–06
8H-3	64.76	CUBE588421	5.316E–05	14.13	1.52	6.28	5.926E–05	2.633E–08	11.7	5.065E–06
8H-4	66.23	CUBE588431	7.562E–05	14.10	1.51	6.30	8.407E–05	3.754E–08	14.8	5.680E–06
8H-5	67.73	CUBE588441	1.173E–04	13.70	1.42	6.41	1.281E–04	5.993E–08	21.4	5.986E–06
8H-6	69.24	CUBE588451	6.113E–05	15.49	1.66	6.58	6.502E–05	2.762E–08	12.3	5.286E–06
8H-7	70.33	CUBE588411	3.856E–05	15.21	1.72	6.19	4.360E–05	1.775E–08	9.5	4.589E–06
9H-1	71.24	CUBE588941	6.490E–05	13.55	1.52	5.88	7.729E–05	3.353E–08	11.0	7.026E–06
9H-2	72.74	CUBE588951	1.060E–04	12.64	1.47	5.47	1.357E–04	5.870E–08	15.0	9.048E–06
9H-3	74.27	CUBE588961	4.696E–05	15.17	1.47	7.21	4.562E–05	2.167E–08	5.7	8.003E–06
9H-4	76.24	CUBE588971	3.174E–04	12.31	1.28	6.05	3.670E–04	1.805E–07	44.0	8.342E–06
9H-5	77.23	CUBE588981	1.996E–04	12.45	1.24	6.36	2.198E–04	1.122E–07	26.0	8.453E–06
9H-6	78.73	CUBE588991	2.504E–04	12.22	1.26	6.06	2.893E–04	1.434E–07	33.3	8.688E–06
9H-7	79.83	CUBE589001	2.811E–04	12.08	1.25	5.97	3.295E–04	1.629E–07	40.0	8.238E–06
10H-1	80.84	CUBE589271	2.333E–04	11.80	1.23	5.85	2.794E–04	1.384E–07	34.0	8.217E–06
10H-2	82.23	CUBE589281	1.814E–04	12.04	1.23	6.06	2.095E–04	1.055E–07	26.0	8.059E–06
10H-3	83.76	CUBE589291	1.876E–04	13.15	1.29	6.64	1.978E–04	9.986E–08	25.7	7.696E–06
10H-4	85.23	CUBE589301	2.010E–04	12.33	1.28	6.07	2.318E–04	1.141E–07	29.0	7.994E–06
10H-5	86.73	CUBE589311	1.629E–04	12.04	1.23	6.06	1.882E–04	9.471E–08	25.0	7.527E–06
10H-6	88.23	CUBE589321	1.481E–04	11.99	1.23	6.00	1.729E–04	8.646E–08	18.7	9.247E–06
10H-7	89.38	CUBE589331	1.464E–04	11.65	1.25	5.66	1.811E–04	8.797E–08	23.0	7.872E–06
11H-2	91.73	CUBE589561	1.824E–04	11.66	1.21	5.84	2.186E–04	1.095E–07	26.7	8.174E–06

Table T24 (continued).

Core, section	Depth CSF (m)	LIMS ID	Susceptibility (SI)	Total mass (g)	Bulk density (g/cm³)	Volume (cm³)	Susceptibility: Volume normalized (SI)	Susceptibility: Mass normalized (m³/kg)	Susceptibility: Whole core (raw values)	Scale factor
11H-3	93.26	CUBE589571	1.819E–04	11.92	1.23	5.98	2.130E–04	1.068E–07	27.0	7.890E–06
11H-4	94.73	CUBE589581	2.270E–04	12.23	1.24	6.17	2.576E–04	1.299E–07	33.7	7.643E–06
11H-5	96.24	CUBE589591	1.950E–04	12.73	1.26	6.48	2.105E–04	1.072E–07	32.2	6.537E–06
11H-6	97.73	CUBE589601	1.082E–04	12.16	1.34	5.66	1.338E–04	6.229E–08	25.8	5.186E–06
12H-7	101.24	CUBE589951	1.334E–04	12.43	1.23	6.40	1.459E–04	7.512E–08	18.0	8.108E–06
12H-3	102.76	CUBE589981	1.371E–04	12.66	1.26	6.38	1.504E–04	7.581E–08	17.3	8.691E–06
12-H4	104.24	CUBE589991	1.163E–04	12.10	1.23	6.09	1.337E–04	6.728E–08	14.8	9.034E–06
12H-5	105.80	CUBE590001	6.721E–05	11.87	1.22	5.96	7.899E–05	3.964E–08	7.7	1.026E–05
12H-6	107.23	CUBE589961	8.106E–05	11.98	1.23	6.01	9.439E–05	4.736E–08	7.7	1.226E–05
12H-7	108.18	CUBE589971	1.138E–04	12.49	1.25	6.30	1.265E–04	6.378E–08	10.8	1.171E–05
13H-1	109.24	CUBE590231	1.193E–04	12.22	1.23	6.21	1.344E–04	6.834E–08	18.0	7.469E–06
13H-2	110.73	CUBE590251	1.129E–04	11.73	1.26	5.65	1.398E–04	6.737E–08	18.2	7.683E–06
13H-3	112.26	CUBE590261	1.331E–04	13.65	1.23	7.37	1.264E–04	6.826E–08	19.0	6.653E–06
13H-4	113.73	CUBE590271	1.042E–04	12.78	1.47	5.58	1.307E–04	5.707E–08	16.3	8.017E–06
13H-5	115.23	CUBE590281	1.060E–04	11.97	1.38	5.36	1.385E–04	6.199E–08	17.9	7.737E–06
13H-6	116.73	CUBE590291	1.337E–04	12.48	1.34	5.91	1.584E–04	7.499E–08	18.4	8.609E–06
13H-7	118.12	CUBE590241	1.101E–04	12.63	1.40	5.75	1.341E–04	6.102E–08	12.5	1.073E–05
14H-2	120.23	CUBE590651	1.976E–04	12.56	1.32	6.03	2.295E–04	1.101E–07	25.4	9.035E–06
14H-3	121.77	CUBE590671	1.791E–04	12.92	1.23	6.76	1.855E–04	9.704E–08	24.8	7.479E–06
14H-4	123.23	CUBE590681	1.265E–04	11.21	1.29	5.12	1.730E–04	7.899E–08	21.9	7.900E–06
14H-5	124.73	CUBE590691	1.436E–04	11.96	1.26	5.85	1.718E–04	8.405E–08	22.0	7.807E–06
14H-6	125.59	CUBE590661	1.718E–04	12.36	1.32	5.90	2.039E–04	9.730E–08	25.0	8.156E–06
15X-1	127.04	CUBE590791	8.267E–05	12.49	1.28	6.16	9.401E–05	4.633E–08	15.9	5.912E–06
15X-3	129.80	CUBE590801	9.385E–05	12.72	1.25	6.51	1.010E–04	5.165E–08	13.4	7.534E–06
15X-4	131.23	CUBE590811	8.111E–05	12.14	1.24	6.11	9.297E–05	4.677E–08	10.7	8.689E–06
15X-5	132.38	CUBE590821	1.131E–04	11.99	1.24	5.95	1.330E–04	6.603E–08	14.3	9.302E–06
16X-1	136.34	CUBE591041	1.475E–04	12.47	1.31	6.00	1.721E–04	8.280E–08	20.1	8.561E–06
									Mean scale factor:	7.96E–06

Notes: Depth = depth to middle of discrete sample measured in meters using the core depth below seafloor, method A (CSF), depth scale. LIMS ID = sample identification within the Laboratory Information Management System (LIMS) database. Susceptibility = volume magnetic susceptibility of discrete sample measured in KappaBridge with volume of cube assumed to be 7 cm³. Mass = mass of sample including mass of plastic cube, which has a mean of 4.5921 g. Bulk density = density from moisture and density (MAD) measurements. When these were not available or were obviously anomalous, we used a density of 1.2 m³/kg. Volume = volume of sediments, calculated by subtracting mass of plastic cube from total mass and then dividing by bulk density. Volume normalized susceptibility = susceptibility of discrete samples normalized by true sample volume. These are unitless in the SI unit system. Mass normalized susceptibility = susceptibility of discrete samples normalize by mass of sediments in each sample cube. Scale factor = factor whole-core raw susceptibility values would need to be multiplied by to convert them to SI volume normalized susceptibilities.

Table T25. Magnetostratigraphy, Site U1332. (See table note.) (Continued on next five pages.)

Polarity chron	Age (Ma)	Hole U1332A Range CSF (m)	Best estimate CSF (m)	Best estimate core, section, interval (cm)	Measurement type
	0.000	0.00–0.00	0.000	Mudline	Split core
C1n–C1r.1r	0.781	1.25–1.25	1.250	1H-1, 125.0	Split core
C1r.1r–C1r.1n	0.988	1.80–1.85	1.825	1H-2, 32.5	Split core
C1r.1n–C1r.2r	1.072	2.00–2.05	2.025	1H-2, 52.5	Split core
C1r.2r–C2n	1.778	5.00–5.30	5.150	2H-1, 125.0	Split core
C2n–C2r.1r	1.945	5.60–5.60	5.600	2H-2, 20.0	Split core
C2r.1r–C2r.1n	2.128	6.40–6.40	6.400	2H-2, 100.0	Split core
C2r.1n–C2r.2r	2.148	6.45–6.50	6.475	2H-2, 107.5	Split core
C2r.2r–C2An.1n	2.581	8.25–8.30	8.275	2H-3, 137.5	Split core
C2An.1n–C2An.1r	3.032	9.35–9.50	9.425	2H-4, 102.5	Split core
C2An.1r–C2An.2n	3.116	9.70–9.75	9.725	2H-4, 132.5	Split core
C2An.2n–C2An.2r	3.207	10.00–10.05	10.025	2H-5, 12.5	Split core
C2An.2r–C2An.3n	3.330	10.30–10.35	10.325	2H-5, 42.5	Split core
C2An.3n–C2Ar	3.596	10.95–10.95	10.950	2H-5, 105.0	Split core
Hiatus				Hiatus	
C5En–C5Er	18.524			Not identified	
C5Er–C6n	18.748			Not identified	
C6n–C6r	19.722			Not identified	
C6r–C6An.1n	20.040			Not identified	
C6An.1n–C6An.1r	20.213		Above 14.20	Above 3H-1, 80.0	Split core
C6An.1r–C6An.2n	20.439	14.55–14.60	14.575	3H-1, 117.5	Split core
C6An.2n–C6Ar	20.709	15.30–15.35	15.325	3H-2, 42.5	Split core
C6Ar–C6AAn	21.083	16.25–16.30	16.275	3H-2, 137.5	Split core
C6AAn–C6AAr.1r	21.159	16.30–16.50	16.400	Between Sections 3H-2 and 3	Split core
C6AAr.1r–C6AAr.1n	21.403	17.30–17.35	17.325	3H-3, 92.5	Split core
C6AAr.1n–C6AAr.2r	21.483	17.50–17.55	17.525	3H-3, 112.5	Split core
C6AAr.2r–C6AAr.2n	21.659	18.05–18.05	18.050	3H-4, 15.0	Split core
C6AAr.2n–C6AAr.3r	21.688	18.15–18.20	18.175	3H-4, 27.5	Split core
C6AAr.3r–C6Bn.1n	21.767	18.40–18.40	18.400	3H-4, 50.0	Split core
C6Bn.1n–C6Bn.1r	21.936	18.60–18.65	18.625	3H-4, 72.5	Split core
C6Bn.1r–C6Bn.2n	21.992	19.10–19.30	19.200	3H-4, 130.0	Split core
C6Bn.2n–C6Br	22.268	19.70–19.95	19.825	3H-5, 42.5	Split core
C6Br–C6Cn.1n	22.564	21.50–21.50	21.500	3H-6, 60.0	Split core
C6Cn.1n–C6Cn.1r	22.754	22.15–22.15	22.150	3H-6, 125.0	Split core
C6Cn.1r–C6Cn.2n	22.902	22.25–22.25	22.250	3H-6, 135.0	Split core
C6Cn.2n–C6Cn.2r	23.030	22.30–22.50	22.400	Between Sections 3H-6 and 7	Split core
C6Cn.2r–C6Cn.3n	23.278	22.65–22.65	22.650	3H-7, 25.0	Split core
C6Cn.3n–C6Cr	23.340	22.90–22.95	22.925	3H-7, 52.5	Split core
C6Cr–C7n.1n	24.022	24.10–24.10	24.100	4H-1, 120.0	Split core
C7n.1n–C7n.1r	24.062	24.20–24.20	24.200	4H-1, 130.0	Split core
C7n.1r–C7n.2n	24.147	24.30–24.60	24.450	Between Sections 4H-1 and 2	Split core
C7n.2n–C7r	24.459	25.55–25.60	25.575	4H-2, 117.5	Split core
C7r–C7An	24.756	26.30–26.50	26.400	4H-3, 50.0	Split core
C7An–C7Ar	24.984	26.80–26.85	26.825	4H-3, 92.5	Split core
C7Ar–C8n.1n	25.110	27.30–27.50	27.400	Between Sections 4H-3 and 4	Split core
C8n.1n–C8n.1r	25.248	27.75–27.80	27.775	4H-4, 37.5	Split core
C8n.1r–C8n.2n	25.306	27.90–27.90	27.900	4H-4, 50.0	Split core
C8n.2n–C8r	26.032	30.15–30.20	30.175	4H-5, 127.5	Split core
C8r–C9n	26.508	31.80–32.00	31.900	Between Sections 4H-6 and 7	Split core
C9n–C9r	27.412	33.80–34.00	33.900	Between Sections 5H-1 and 2	Split core
C9r–C10n.1n	27.886	35.90–35.90	35.900	5H-3, 50.0	Split core
C10n.1n–C10n.1r	28.126	36.80–37.00	36.900	Between Sections 5H-3 and 4	Split core
C10n.1r–C10n.2n	28.164	37.25–37.30	37.275	5H-4, 37.5	Split core
C10n.2n–C10r	28.318	37.70–37.70	37.700	5H-4, 80.0	Split core
C10r–C11n.1n	29.166	43.30–43.50	43.400	Between Sections 6H-1 and 2	Split core
C11n.1n–C11n.1r	29.467	45.95–45.95	45.950	6H-3, 105.0	Split core
C11n.1r–C11n.2n	29.536	46.15–46.20	46.175	6H-3, 127.5	Split core
C11n.2n–C11r	29.957	48.25–48.30	48.275	6H-5, 37.5	Split core
C11r–C12n	30.617	51.55–51.60	51.575	6H-7, 67.5	Split core
C12n–C12r	31.021			Not identified	Split core
C12r–C13n	33.232	67.65–67.70	67.675	8H-5, 77.5	Split core
(repeated)	33.232	72.50–72.55	72.525	9H-2, 62.5	Split core
C13n–C13r	33.705	75.30–75.35	75.325	9H-4, 42.5	Split core
C13r–C15n	35.126	79.50–79.55	79.525	9H-7, 12.5	Split core
C15n–C15r	35.254		Below 80.15	Below 9H-7, 75.0	Split core
C15r–C16n.1n	35.328	81.20–81.30	81.250	10H-1, 135.0	Split core
C16n.1n–C16n.1r	35.554	82.05–82.05	82.050	10H-2, 65.0	Split core
C16n.1r–C16n.2n	35.643	82.60–82.65	82.625	10H-2, 122.5	Split core

Table T25 (continued). (Continued on next page.)

Polarity chron	Age (Ma)	Hole U1332B Range CSF (m)	Best estimate CSF (m)	Best estimate core, section, interval (cm)	Measurement type
	0.000				
C1n–C1r.1r	0.781	1.10–1.15	1.125	1H-1, 112.5	Split core
C1r.1r–C1r.1n	0.988	1.40–1.65	1.525	Between Sections 1H-1 and 2	Split core
C1r.1n–C1r.2r	1.072	1.75–1.80	1.775	1H-1, 27.5	Split core
C1r.2r–C2n	1.778	4.85–4.85	4.850	2H-2, 125.0	Split core
C2n–C2r.1r	1.945	5.30–5.35	5.325	2H-3, 22.5	Split core
C2r.1r–C2r.1n	2.128	5.95–5.95	5.950	2H-3, 85.0	Split core
C2r.1n–C2r.2r	2.148	6.05–6.05	6.050	2H-3, 95.0	Split core
C2r.2r–C2An.1n	2.581	7.50–7.75	7.625	2H-4, 102.5	Split core
C2An.1n–C2An.1r	3.032	9.25–9.30	9.275	2H-5, 117.5	Split core
C2An.1r–C2An.2n	3.116	9.50–9.70	9.600	Between Sections 2H-5 and 6	Split core
C2An.2n–C2An.2r	3.207	10.00–10.00	10.000	2H-6, 40.0	Split core
C2An.2r–C2An.3n	3.330	10.20–10.20	10.200	2H-6, 60.0	Split core
C2An.3n–C2Ar	3.596		Below 11.40	Below 2H-7, 30.0	Split core
Hiatus					
C5En–C5Er	18.524			Not identified	
C5Er–C6n	18.748		Above 13.60	Above 3H-2, 50.0	Split core
C6n–C6r	19.722	13.65–13.70	13.675	3H-2, 57.5	Split core
C6r–C6An.1n	20.040	14.00–14.05	14.025	3H-2, 92.5	Split core
C6An.1n–C6An.1r	20.213	14.30–14.35	14.325	3H-2, 122.5	Split core
C6An.1r–C6An.2n	20.439	14.50–14.70	14.600	Between Sections 3H-2 and 3	Split core
C6An.2n–C6Ar	20.709	15.15–15.20	15.175	3H-3, 57.5	Split core
C6Ar–C6AAn	21.083	15.75–15.80	15.775	3H-3, 117.5	Split core
C6AAn–C6AAr.1r	21.159	15.95–16.00	15.975	3H-3, 137.5	Split core
C6AAr.1r–C6AAr.1n	21.403	16.45–16.50	16.475	3H-4, 37.5	Split core
C6AAr.1n–C6AAr.2r	21.483	16.55–16.60	16.575	3H-4, 47.5	Split core
C6AAr.2r–C6AAr.2n	21.659	16.95–16.95	16.950	3H-4, 85.0	Split core
C6AAr.2n–C6AAr.3r	21.688	17.05–17.10	17.075	3H-4, 97.5	Split core
C6AAr.3r–C6Bn.1n	21.767	17.15–17.20	17.175	3H-4, 107.5	Split core
C6Bn.1n–C6Bn.1r	21.936	17.40–17.45	17.425	3H-4, 132.5	Split core
C6Bn.1r–C6Bn.2n	21.992	17.75–17.75	17.750	3H-5, 15.0	Split core
C6Bn.2n–C6Br	22.268	18.35–18.40	18.375	3H-5, 77.5	Split core
C6Br–C6Cn.1n	22.564		Below 19.50	Below 3H-6, 40.0	Split core
C6Cn.1n–C6Cn.1r	22.754			Not identified	
C6Cn.1r–C6Cn.2n	22.902			Not identified	
C6Cn.2n–C6Cn.2r	23.030			Not identified	
C6Cn.2r–C6Cn.3n	23.278			Not identified	
C6Cn.3n–C6Cr	23.340		Above 21.20	Above 4H-2, 10.0	Split core
C6Cr–C7n.1n	24.022	22.50–22.50	22.500	4H-2, 140.0	Split core
C7n.1n–C7n.1r	24.062	22.50–22.70	22.600	Between Sections 4H-2 and 3	Split core
C7n.1r–C7n.2n	24.147	22.90–22.95	22.925	4H-3, 32.5	Split core
C7n.2n–C7r	24.459	23.85–23.85	23.850	4H-3, 125.0	Split core
C7r–C7An	24.756	24.70–24.75	24.725	4H-4, 62.5	Split core
C7An–C7Ar	24.984	25.25–25.25	25.250	4H-4, 115.0	Split core
C7Ar–C8n.1n	25.110	25.50–25.70	25.600	Between Sections 4H-4 and 5	Split core
C8n.1n–C8n.1r	25.248	26.05–26.10	26.075	4H-5, 47.5	Split core
C8n.1r–C8n.2n	25.306	26.10–26.15	26.125	4H-5, 52.5	Split core
C8n.2n–C8r	26.032	28.25–28.30	28.275	4H-6, 117.5	Split core
C8r–C9n	26.508	30.45–30.45	30.450	5H-1, 135.0	Split core
C9n–C9r	27.412	34.65–34.70	34.675	5H-4, 107.5	Split core
C9r–C10n.1n	27.886	36.50–36.80	36.650	Between Sections 5H-5 and 6	Split core
C10n.1n–C10n.1r	28.126		Below 37.35	Below 5H-6, 75.0	Split core
C10n.1r–C10n.2n	28.164			Not identified	
C10n.2n–C10r	28.318		Above 47.50	Above 6H-2, 60.0	Split core
C10r–C11n.1n	29.166	42.00–42.05	42.025	6H-3, 42.5	Split core
C11n.1n–C11n.1r	29.467	44.10–44.15	44.125	6H-4, 102.5	Split core
C11n.1r–C11n.2n	29.536	44.35–44.40	44.375	6H-4, 127.5	Split core
C11n.2n–C11r	29.957		Below 46.90	Below 6H-6, 80.0	Split core
C11r–C12n	30.617			Not identified	
C12n–C12r	31.021		Above 48.80	Above 7H-1, 70.0	Split core
C12r–C13n	33.232	65.95–65.95	65.950	8H-6, 85.0	Split core
(repeated)	33.232	71.25–71.25	71.250	9H-3, 115.0	Split core
C13n–C13r	33.705	74.30–74.35	74.325	9H-5, 122.5	Split core
C13r–C15n	35.126		Below 76.00	Below 9H-6, 140.0	Split core
C15n–C15r	35.254		Above 78.20	Above 10H-2, 10.0	Split core
C15r–C16n.1n	35.328	79.20–79.30	79.250	10H-2 115.0	Split core
C16n.1n–C16n.1r	35.554	80.05–80.05	80.050	10H-3, 45.0	Split core
C16n.1r–C16n.2n	35.643	80.60–80.65	80.625	10H-3, 102.5	Split core

Table T25 (continued). (Continued on next page.)

Polarity chron	Age (Ma)	Hole U1332C Range CSF (m)	Best estimate CSF (m)	Best estimate core, section, interval (m)	Measurement type
	0.000				
C1n–C1r.1r	0.781	1.30–1.30	1.300	1H-1, 130.0	Split core
C1r.1r–C1r.1n	0.988	1.85–1.85	1.850	1H-2, 35.0	Split core
C1r.1n–C1r.2r	1.072	2.10–2.10	2.100	1H-2, 60.0	Split core
C1r.2r–C2n	1.778	3.55–3.85	3.700	1H-3, 70.0	Split core
C2n–C2r.1r	1.945	4.30–4.30	4.300	1H-3, 130.0	Split core
C2r.1r–C2r.1n	2.128			Not identified	
C2r.1n–C2r.2r	2.148			Not identified	
C2r.2r–C2An.1n	2.581			Not identified	
C2An.1n–C2An.1r	3.032			Not identified	
C2An.1r–C2An.2n	3.116			Not identified	
C2An.2n–C2An.2r	3.207			Not identified	
C2An.2r–C2An.3n	3.330			Not identified	
C2An.3n–C2Ar	3.596			Not identified	
Hiatus					
C5En–C5Er	18.524	12.95–12.95	12.950	2H-4, 95.0	Split core
C5Er–C6n	18.748	13.15–13.20	13.175	2H-4, 117.5	Split core
C6n–C6r	19.722	14.75–14.75	14.750	2H-5, 125.0	Split core
C6r–C6An.1n	20.040	15.20–15.20	15.200	2H-6, 20.0	Split core
C6An.1n–C6An.1r	20.213	15.60–15.65	15.625	2H-6, 62.5	Split core
C6An.1r–C6An.2n	20.439	16.05–16.10	16.075	2H-6, 107.5	Split core
C6An.2n–C6Ar	20.709	16.80–16.85	16.825	2H-7, 32.5	Split core
C6Ar–C6AAn	21.083		Below 17.25	Below 2H-7, 75.0	Split core
C6AAn–C6AAr.1r	21.159			Not identified	
C6AAr.1r–C6AAr.1n	21.403			Not identified	
C6AAr.1n–C6AAr.2r	21.483			Not identified	
C6AAr.2r–C6AAr.2n	21.659		Above 18.60	Above 3H-2, 10.0	Split core
C6AAr.2n–C6AAr.3r	21.688	18.70–18.75	18.725	3H-2, 22.5	Split core
C6AAr.3r–C6Bn.1n	21.767	18.85–18.90	18.875	3H-2, 37.5	Split core
C6Bn.1n–C6Bn.1r	21.936	19.10–19.25	19.175	3H-2, 67.5	Split core
C6Bn.1r–C6Bn.2n	21.992	19.55–19.70	19.625	3H-2, 112.5	Split core
C6Bn.2n–C6Br	22.268	20.30–20.30	20.300	3H-3, 30.0	Split core
C6Br–C6Cn.1n	22.564	21.40–21.70	21.550	Between Sections 3H-3 and 4	Split core
C6Cn.1n–C6Cn.1r	22.754	22.15–22.20	22.175	3H-4, 67.5	Split core
C6Cn.1r–C6Cn.2n	22.902	22.60–22.60	22.600	3H-4, 110.0	Split core
C6Cn.2n–C6Cn.2r	23.030	22.85–22.90	22.875	3H-4, 137.5	Split core
C6Cn.2r–C6Cn.3n	23.278	23.40–23.40	23.400	3H-5, 40.0	Split core
C6Cn.3n–C6Cr	23.340	23.70–23.75	23.725	3H-5, 72.5	Split core
C6Cr–C7n.1n	24.022	26.35–26.40	26.375	3H-7, 37.5	Split core
C7n.1n–C7n.1r	24.062	26.50–26.50	26.500	3H-7, 50.0	Split core
C7n.1r–C7n.2n	24.147		Below 26.65	Below 3H-7, 65.0	Split core
C7n.2n–C7r	24.459			Not identified	
C7r–C7An	24.756		Above 26.70	Above 4H-1, 20.0	Split core
C7An–C7Ar	24.984	26.90–26.95	26.925	4H-1, 42.5	Split core
C7Ar–C8n.1n	25.110	27.40–27.40	27.400	4H-1, 90.0	Split core
C8n.1n–C8n.1r	25.248	27.90–28.10	28.000	Between 4H-1 and 2	Split core
C8n.1r–C8n.2n	25.306	27.90–28.10	28.000	Between 4H-1 and 2	Split core
C8n.2n–C8r	26.032	30.55–30.85	30.700	4H-3, 120.0	Split core
C8r–C9n	26.508	32.35–32.40	32.375	4H-4, 137.5	Split core
C9n–C9r	27.412		Below 36.15	Below 4H-7, 65.0	Split core
C9r–C10n.1n	27.886	36.85–36.90	36.875	5H-1, 87.5	Split core
C10n.1n–C10n.1r	28.126	37.90–37.95	37.927	5H-2, 42.5	Split core
C10n.1r–C10n.2n	28.164	38.15–38.20	38.175	5H-2, 67.5	Split core
C10n.2n–C10r	28.318	38.65–38.70	38.675	5H-2, 117.5	Split core
C10r–C11n.1n	29.166	44.70–44.75	44.725	5H-6, 122.5	Split core
C11n.1n–C11n.1r	29.467		Below 45.45	Below 5H-7, 45.0	Split core
C11n.1r–C11n.2n	29.536	45.75–45.80	45.775	6H-2, 137.5	Split core
C11n.2n–C11r	29.957	47.85–47.90	47.875	6H-4, 47.5	Split core
C11r–C12n	30.617	50.25–50.30	50.275	7H-1, 77.5	Split core
C12n–C12r	31.021	52.20–52.20	52.200	7H-2, 120.0	Split core
C12r–C13n	33.232		Below 67.85	Between Cores 8H and 9H	Split core
(repeated)	33.232	74.05–74.10	74.075	9H-6, 57.5	Split core
C13n–C13r	33.705		Below 75.50	Below 9H-7, 50.0	Split core
C13r–C15n	35.126			Not identified	
C15n–C15r	35.254			Not identified	
C15r–C16n.1n	35.328			Not identified	
C16n.1n–C16n.1r	35.554			Not identified	
C16n.1r–C16n.2n	35.643			Not identified	

Table T25 (continued). (Continued on next page.)

Polarity chron	Age (Ma)	Hole U1332A Range CSF (m)	Best estimate CSF (m)	Best estimate core, section, interval (cm)	Measurement type
C16n.2n–C16r	36.355	85.80–86.00	85.900	Between Sections 10H-4 and 5	Split core
C16r–C17n.1n	36.668	87.30–87.50	87.400	Between Sections 10H-5 and 6	Split core
C17n.1n–C17n.1r	37.520	92.50–92.60	92.550	11H-3, 15.0	Split core
C17n.1r–C17n.2n	37.656	92.90–92.95	92.925	11H-3, 52.5	Split core
C17n.2n–C17n.2r	37.907	94.05–94.10	94.075	11H-4, 17.5	Split core
C17n.2r–C17n.3n	37.956	94.35–94.40	94.375	11H-4, 47.5	Split core
C17n.3n–C17r	38.159	95.25–95.30	95.275	11H-4, 137.5	Split core
C17r–C18n.1n	38.449	96.50–96.55	96.525	11H-5, 112.5	Split core
C18n.1n–C18n.1r	39.554	101.80–102.00	101.900	Between Sections 12H-2 and 3	Split core
C18n.1r–C18n.2n	39.602	102.60–102.60	102.600	12H-3, 70.0	Split core
C18n.2n–C18r	40.084	106.20–106.50	106.350	Between Sections 12H-5 and 6	Split core
C18r–C19n	41.358	117.25–117.25	117.250	13H-6, 135.0	Split core
C19n–C19r	41.510		Above 119.50	Above 14H-2, 10.0	Split core
C19r–C20n	42.536	124.70–124.70	124.700	14H-5, 80.0	Split core

Note: When the location of a reversal is listed as between sections, it could occur anywhere within 10 cm of the juxtaposing ends of the two sections listed.

Table T25 (continued). (Continued on next page.)

Polarity chron	Age (Ma)	Hole U1332B Range CSF (m)	Best estimate CSF (m)	Best estimate core, section, interval (cm)	Measurement type
C16n.2n–C16r	36.355	83.70–83.75	83.725	10H-5, 112.5	Split core
C16r–C17n.1n	36.668	85.05–85.05	85.050	10H-6, 95.0	Split core
C17n.1n–C17n.1r	37.520	89.60–89.65	89.625	11H-3, 52.5	Split core
C17n.1r–C17n.2n	37.656	90.25–90.30	90.275	11H-3, 117.5	Split core
C17n.2n–C17n.2r	37.907	91.35–91.35	91.350	11H-4, 75.0	Split core
C17n.2r–C17n.3n	37.956	91.65–91.65	91.650	11H-4, 105.0	Split core
C17n.3n–C17r	38.159	92.45–92.50	92.475	11H-5, 37.5	Split core
C17r–C18n.1n	38.449		Below 93.50	Below 11H-5, 140.0	Split core
C18n.1n–C18n.1r	39.554	98.70–98.75	98.725	12H-6, 12.5	Split core
C18n.1r–C18n.2n	39.602	99.30–99.35	99.325	12H-6 72.5	Split core
C18n.2n–C18r	40.084	102.20–102.30	102.250	13H-2, 15.0	Split core
C18r–C19n	41.358		Below 110.35	Below 13H-7, 75.0	Split core
C19n–C19r	41.510			Not identified	
C19r–C20n	42.536			Not identified	

Table T25 (continued).

Polarity chron	Age (Ma)	Hole U1332C Range CSF (m)	Best estimate CSF (m)	Best estimate core, section, interval (m)	Measurement type
C16n.2n–C16r	36.355		Above 86.15	Above 11H-1, 115.0	Split core
C16r–C17n.1n	36.668	86.95–87.05	87.000	11H-2, 50.0	Split core
C17n.1n–C17n.1r	37.520	92.20–92.20	92.200	11H-5, 120.0	Split core
C17n.1r–C17n.2n	37.656	92.80–92.85	92.825	11H-6, 32.5	Split core
C17n.2n–C17n.2r	37.907		Below 93.65	Below 11H-6, 115.0	Split core
C17n.2r–C17n.3n	37.956			Not identified	
C17n.3n–C17r	38.159		Above 94.60	Above 12H-1, 10.0	Split core
C17r–C18n.1n	38.449	94.95–95.00	94.975	Below 12H-1, 47.5	Split core
C18n.1n–C18n.1r	39.554	100.35–100.40	100.375	12H-4, 137.5	Split core
C18n.1r–C18n.2n	39.602	100.40–100.60	100.500	12H-5, 10.0	Split core
C18n.2n–C18r	40.084	106.80–107.10	106.950	Between Sections 13H-2 and 3	Split core
C18r–C19n	41.358		Below 113.70	Below 13H-7, 70.0	Split core
C19n–C19r	41.510			Not identified	
C19r–C20n	42.536			Not identified	

Table T26. Interstitial water data from squeezed whole-round samples, Site U1332. (**See table notes.**)

Core, section, interval (cm)	Depth (m) CSF	Depth (m) CCSF-A	pH	Alkalinity (mM)	Salinity	Cl^- (mM)	Na^+ (mM)	SO_4^{2-} (mM)	HPO_4^{2-} (µM)	H_4SiO_4 (µM)	Mn^{2+} (µM)	Fe^{2+} (µM)	Ca^{2+} (mM)	Mg^{2+} (mM)	B (µM)	Sr^{2+} (µM)	Ba^{2+} (µM)	Li^+ (µM)	K^+ (mM)
320-U1332A-																			
1H-2, 145–150	2.95	2.95	7.57	2.35	34.0	555	483	28.6	2.13	499	BDL	BDL	10.0	50.4	431	81.6	2.2	25.8	11.01
2H-2, 145–150	6.85	7.16	7.40	2.61	34.0	556	481	27.6	1.28	518	8.8	BDL	10.3	50.6	489	86.5	2.2	25.8	11.32
2H-5, 145–150	11.35	11.66	7.36	2.85	34.0	559	483	27.6	1.08	497	7.8	0.97	10.3	50.8	484	78.3	2.3	24.0	11.53
3H-2, 145–150	16.35	17.00	7.52	3.05	—	562	489	29.7	0.63	502	BDL	0.37	10.7	51.2	455	84.9	2.4	26.1	11.47
3H-5, 145–150	20.85	21.50	7.43	2.88	—	564	490	28.8	0.62	548	BDL	BDL	10.7	51.0	466	85.5	2.3	26.2	11.54
4H-2, 145–150	25.85	28.50	7.43	3.02	34.5	565	487	27.9	BDL	518	BDL	BDL	10.8	51.9	468	85.1	2.3	25.2	11.47
4H-5, 145–150	30.35	33.00	7.44	2.87	—	565	485	27.5	0.64	562	BDL	BDL	10.7	52.5	467	82.6	2.2	24.5	11.22
5H-2, 145–150	35.35	40.50	7.58	2.62	34.5	565	486	28.1	BDL	548	BDL	BDL	10.6	52.6	471	87.5	2.3	25.6	11.25
5H-5, 145–150	39.85	45.00	7.41	2.35	34.5	567	491	28.3	BDL	568	BDL	BDL	10.4	51.5	460	86.2	2.5	25.5	11.16
6H-3, 145–150	46.35	52.00	7.41	2.89	34.5	568	491	26.8	BDL	616	BDL	BDL	10.4	50.9	441	81.8	2.2	24.0	11.10
6H-5, 145–150	49.35	55.00	7.39	3.02	34.5	565	489	26.8	BDL	604	BDL	BDL	10.2	50.8	421	76.7	2.5	22.5	10.71
7H-3, 145–150	55.85	63.75	7.40	3.07	—	568	489	27.3	BDL	550	BDL	BDL	10.7	51.9	420	81.1	2.7	22.4	10.94
8H-3, 145–150	65.35	72.85	7.40	2.97	34.5	568	489	26.7	0.70	575	BDL	BDL	10.8	51.4	420	83.0	2.5	22.0	10.75
9H-3, 145–150	74.85	77.63	7.39	3.05	34.5	568	490	27.6	BDL	493	BDL	0.32	10.9	51.6	431	86.4	2.5	22.6	10.82
10H-3, 145–150	84.35	87.83	—	—	34.0	563	484	28.1	BDL	374	BDL	0.36	11.3	51.1	421	89.1	2.9	22.3	10.44
11H-3, 145–150	93.85	97.17	7.51	3.19	34.0	566	489	27.5	BDL	810	BDL	BDL	11.2	51.1	406	82.3	2.3	21.4	10.15
12H-3, 145–150	103.35	109.37	7.58	3.16	34.5	565	487	26.6	BDL	883	BDL	BDL	11.5	50.6	399	84.1	2.4	20.4	10.30
13H-3, 145–150	112.85	120.62	7.41	3.26	34.0	569	489	26.7	BDL	917	BDL	0.29	11.5	51.4	413	84.1	3.1	21.0	10.34
14H-3, 145–150	122.35	133.87	7.56	3.36	34.5	567	487	27.0	BDL	909	BDL	0.44	11.7	51.8	418	84.6	2.8	20.9	10.31
15X-3, 140–150	130.30	142.82	7.51	3.29	34.5	562	481	26.1	BDL	1004	BDL	0.41	11.8	51.2	453	93.0	2.6	21.1	10.10

Notes: — = no data. BDL = below detection limit (HPO_4^{2-} = 0.6 µM, Mn^{2+} = 0.4 µM, Fe^{2+} = 0.4 µM, B = 4 µM, Sr^{2+} = 0.6 µM, Ba^{2+} = 0.1 µM, Li^+ = 1.4 µM) calculated as three times the standard deviation of multiple measures of a blank. H_4SiO_4 values measured by different techniques during Expeditions 320 and 321 disagree significantly, especially for low values. Therefore, caution should be used concerning the H_4SiO_4 data and comparison between the different expeditions.

Table T27. Interstitial water data from rhizon samples, Sections 320-U1332C-4H-1 through 7H-6. (See table notes.)

Core, section, interval (cm)	Depth (m) CSF	Depth (m) CCSF-A	pH	Alkalinity (mM)	Salinity	Cl^- (mM)	Na^+ (mM)	SO_4^{2-} (mM)	HPO_4^{2-} (µM)	H_4SiO_4 (µM)	Mn^{2+} (µM)	Fe^{2+} (µM)	Ca^{2+} (mM)	Mg^{2+} (mM)	B (µM)	Sr^{2+} (µM)	Ba^{2+} (µM)	Li^+ (µM)	K^+ (mM)
320-U1332C-																			
4H-1, 55	27.05	29.50	ND	ND	ND	ND	ND	ND	ND	ND	0.31	BDL	10.4	50.7	465	83.6	0.83	24.3	11.1
4H-1, 130	27.80	30.25	7.48	2.86	ND	ND	ND	ND	ND	ND	BDL	BDL	10.5	51.0	472	82.3	0.78	24.1	11.3
4H-2, 55	28.55	31.00	7.54	2.97	ND	ND	ND	ND	ND	ND	BDL	BDL	10.5	49.9	474	87.3	0.87	25.4	11.4
4H-2, 130	29.30	31.75	7.64	3.10	ND	ND	ND	ND	ND	ND	0.24	BDL	10.6	49.8	464	86.9	0.82	25.0	11.2
4H-3, 55	30.05	32.50	7.54	2.95	ND	ND	ND	ND	ND	ND	BDL	BDL	10.6	51.2	473	86.1	0.80	24.7	11.3
4H-3, 130	30.80	33.25	7.49	2.82	ND	ND	ND	ND	ND	ND	BDL	0.52	10.3	50.2	477	83.2	0.77	24.3	11.0
4H-4, 55	31.55	34.00	7.50	2.82	ND	ND	ND	ND	ND	ND	1.34	0.68	10.5	50.1	434	72.9	0.83	21.5	11.1
4H-4, 130	32.30	34.75	7.34	2.78	ND	ND	ND	ND	ND	ND	BDL	0.69	10.4	50.9	476	82.1	1.02	23.6	11.2
4H-5, 55	33.05	35.50	7.47	2.75	ND	ND	ND	ND	ND	ND	BDL	BDL	10.4	51.1	472	82.5	1.03	23.8	11.2
4H-5, 130	33.80	36.25	7.41	2.77	ND	ND	ND	ND	ND	ND	BDL	BDL	10.3	50.8	472	80.0	1.00	23.3	11.2
4H-6, 55	34.55	37.00	7.46	2.42	ND	ND	ND	ND	ND	ND	BDL	BDL	10.1	50.5	486	84.8	0.78	24.7	11.4
4H-6, 130	35.30	37.75	7.85	2.84	ND	ND	ND	ND	ND	ND	0.22	BDL	10.0	50.4	493	85.7	0.82	25.0	11.0
5H-1, 55	36.55	40.80	7.43	2.83	ND	ND	ND	ND	ND	ND	0.24	BDL	10.3	50.6	465	81.4	0.78	24.0	11.2
5H-1, 130	37.30	41.55	7.46	2.79	ND	ND	ND	ND	ND	ND	BDL	BDL	10.2	51.1	457	81.9	0.79	24.0	11.0
5H-2, 55	38.05	42.30	7.47	2.74	ND	ND	ND	ND	ND	ND	BDL	0.58	10.1	50.8	474	82.4	0.77	24.1	11.1
5H-2, 130	38.80	43.05	7.42	2.71	ND	ND	ND	ND	ND	ND	BDL	BDL	10.1	50.8	473	82.4	0.77	24.5	11.1
5H-3, 55	39.55	43.80	7.43	2.80	ND	ND	ND	ND	ND	ND	0.26	BDL	10.0	50.3	464	82.7	0.82	24.2	10.7
5H-3, 130	40.30	44.55	7.46	2.70	ND	ND	ND	ND	ND	ND	0.22	0.54	10.1	50.0	480	81.4	0.80	23.6	11.2
5H-4, 55	41.05	45.30	7.50	2.71	ND	ND	ND	ND	ND	ND	0.40	1.99	10.2	50.5	510	87.2	0.85	25.1	11.4
5H-4, 130	41.80	46.05	7.44	2.80	ND	ND	ND	ND	ND	ND	0.32	BDL	10.1	51.2	455	80.2	0.79	23.6	11.1
5H-5, 55	42.55	46.80	7.42	2.84	ND	ND	ND	ND	ND	ND	0.27	BDL	9.9	50.6	471	82.5	0.84	24.7	11.0
5H-5, 130	43.30	47.55	7.46	2.84	ND	ND	ND	ND	ND	ND	0.27	BDL	9.9	51.0	459	82.5	0.83	24.8	10.7
5H-6, 55	44.05	48.30	7.41	2.82	ND	ND	ND	ND	ND	ND	0.37	BDL	9.9	50.9	447	79.7	0.79	24.0	10.7
5H-6, 130	44.80	49.05	7.44	2.79	ND	ND	ND	ND	ND	ND	0.23	BDL	9.9	49.9	465	81.4	0.79	23.6	10.9
6H-2, 130	48.30	51.75	7.47	2.77	ND	ND	ND	ND	ND	ND	BDL	BDL	10.2	49.8	468	81.1	0.76	22.9	10.8
6H-3, 55	49.05	52.50	7.45	ND	ND	ND	ND	ND	ND	ND	0.22	BDL	10.2	51.5	454	81.6	0.81	23.5	11.0
6H-3, 130	49.80	53.25	7.45	2.77	ND	ND	ND	ND	ND	ND	0.24	BDL	10.0	50.2	453	82.5	0.80	23.6	10.7
7H-1, 55	50.05	57.00	7.43	2.78	ND	ND	ND	ND	ND	ND	0.22	BDL	10.1	50.7	453	80.9	0.80	22.9	10.9
6H-4, 55	50.55	54.00	7.45	2.83	ND	ND	ND	ND	ND	ND	0.27	BDL	9.8	49.4	446	80.8	0.81	23.0	10.8
7H-1, 130	50.80	57.75	7.47	2.88	ND	ND	ND	ND	ND	ND	BDL	BDL	10.1	50.8	434	78.3	0.78	22.5	10.7
6H-4, 130	51.30	54.75	7.47	2.96	ND	ND	ND	ND	ND	ND	0.22	BDL	10.0	50.1	443	76.6	0.77	22.7	10.9
7H-2, 55	51.55	58.50	7.45	2.79	ND	ND	ND	ND	ND	ND	BDL	BDL	10.2	50.2	508	86.2	0.87	24.1	10.8
6H-5, 55	52.05	55.50	7.46	2.87	ND	ND	ND	ND	ND	ND	BDL	BDL	9.9	50.1	456	81.5	0.80	23.5	10.7
7H-2, 130	52.30	59.25	7.48	2.78	ND	ND	ND	ND	ND	ND	0.24	BDL	9.9	48.7	457	80.4	0.80	22.7	10.5
6H-5, 115	52.65	56.10	7.51	2.78	ND	ND	ND	ND	ND	ND	BDL	BDL	10.0	50.6	456	81.7	0.82	23.5	10.8
7H-3, 55	53.05	60.00	7.44	2.56	ND	ND	ND	ND	ND	ND	BDL	BDL	10.1	50.9	480	81.8	0.82	23.2	10.8
7H-3, 130	53.80	60.75	7.55	2.83	ND	ND	ND	ND	ND	ND	0.26	BDL	10.2	51.0	450	81.8	0.81	22.9	10.7
7H-4, 55	54.55	61.50	ND	ND	ND	ND	ND	ND	ND	ND	0.26	BDL	10.2	51.2	443	81.5	0.80	22.6	10.5
7H-4, 130	55.30	62.25	7.38	2.85	ND	ND	ND	ND	ND	ND	BDL	BDL	10.3	51.2	443	81.2	0.83	23.0	10.6
7H-5, 55	56.05	63.00	7.38	3.02	ND	ND	ND	ND	ND	ND	BDL	BDL	10.2	50.6	444	83.0	0.84	23.2	10.7
7H-5, 130	56.80	63.75	7.36	2.89	ND	ND	ND	ND	ND	ND	0.4	BDL	10.2	50.3	431	79.2	0.82	21.9	10.6
7H-6, 55	57.55	64.50	7.31	2.99	ND	ND	ND	ND	ND	ND	0.29	BDL	10.3	51.1	433	80.8	0.78	22.1	10.7
7H-6, 130	58.30	65.25	ND	ND	ND	ND	ND	ND	ND	ND	0.24	BDL	10.2	50.8	440	80.4	0.81	22.2	10.7

Notes: ND = not determined. BDL = below detection limit (Mn^{2+} = 0.2 µM, Fe^{2+} = 0.5 µM, B = 4 µM, Sr^{2+} = 0.6 µM, Ba^{2+} = 0.1 µM, Li^+ = 1 µM) calculated as three times the standard deviation of multiple measures of a blank. H_4SiO_4 values measured by different techniques during Expeditions 320 and 321 disagree significantly, especially for low values. Therefore, caution should be used concerning the H_4SiO_4 data and comparison between the different expeditions.

Table T28. Inorganic geochemistry of solid samples, Hole U1332A. (See table notes.)

Core, section, interval (cm)	Depth CSF (m)	Major element oxide (wt%)										Trace element (ppm)							
		SiO_2	Al_2O_3	Fe_2O_3 T	MnO	MgO	CaO	Na_2O	K_2O	TiO_2	P_2O_5	Ba	Cr	Cu	Sc	Sr	V	Y	Zr
320-U1332A-																			
1H-3, 25–26	3.25	53.62	12.89	6.57	0.06	3.37	1.00	4.67	2.43	0.62	0.42	3230	54.8	772	29.8	212.5	86.9	189.3	204.9
3H-4, 65–66	18.55	59.20	8.57	4.62	0.86	2.97	7.37	5.22	1.59	0.37	0.89	4719	23.9	693	29.6	504.1	51.7	244.4	160.8
4H-6, 65–66	31.05	50.71	5.78	3.04	0.59	2.09	16.85	4.30	1.21	0.25	0.77	3992	15.9	382	18.8	803	28.3	168.5	112.4
5H-4, 65–66	37.55	19.04	2.74	1.36	0.27	1.00	36.62	2.14	0.68	0.12	0.41	1691	6.6	173	7.2	1744	9.1	74.2	56.2
7H-4, 64–65	56.54	12.09	0.45	0.40	0.03	0.31	39.14	1.45	0.24	0.01	BDL	885	20.9	53	1.4	1811	BDL	16.4	20.2
9H-2, 65–66	72.55	27.47	1.95	1.22	0.19	0.77	30.57	2.06	0.54	0.08	0.34	1216	7.6	145	5.9	1360	7.9	44.8	44.9
10H-1, 74–75	80.64	66.46	5.62	4.10	0.51	2.18	1.25	4.45	1.09	0.25	0.50	2990	20.4	398	17.0	171.7	37.7	110.7	104.1
12H-6, 65–66	107.05	74.34	1.09	2.63	0.46	1.41	0.43	3.29	0.44	0.05	0.18	1042	6.2	200	4.1	59.6	33.7	28.4	35.3
13H-6, 65–66	116.55	40.26	0.79	2.03	0.43	1.16	25.98	2.13	0.33	0.04	0.24	1433	6.1	220	2.9	855	10.3	37.1	31.4
14H-3, 64–65	121.54	70.74	1.69	4.70	0.83	2.16	0.68	3.36	0.58	0.08	0.28	1727	5.3	334	7.0	90.9	34.4	61.7	52.0
15X-4, 64–65	131.04	74.94	0.62	2.16	0.55	1.34	1.03	3.26	0.35	0.03	0.19	2427	BDL	213	3.5	108.5	19.9	28.8	28.1
17X-2, 50–51	146.33	41.02	3.60	27.43	21.14	5.25	2.66	8.98	1.67	0.22	1.35	4093	22.7	1847	14.8	455.6	404.2	224.8	108.6

Notes: BDL = below detection limit (SiO_2 = 3.5 wt%, Al_2O_3 = 0.04 wt%, Fe_2O_3 T = 0.003 wt%, MnO = 0.0004 wt%, MgO = 0.007 wt%, CaO = 0.1 wt%, Na_2O = 0.02 wt%, K_2O = 0.004 wt%, TiO_2 = 0.001 wt%, P_2O_5 = 0.1 wt%, Ba = 28 wt%, Cr = 5 wt%, Cu = 16 wt%, Sc = 0.4 wt%, Sr = 3 wt%, V = 4 wt%, Y = 1.7 wt%, Zr = 4 wt%). See Table T9 in "Methods" for maximum values of calibration.

Table T29. Calcium carbonate and organic carbon data, Site U1332. (See table notes.)

Core, section, interval (cm)	Depth CSF (m)	$CaCO_3$ (wt%)	IC (wt%)	TC (wt%)	TOC (wt%)	
					Normal	Acid
320-U1332A-						
1H-1, 64–65	0.64	BDL	BDL	0.17	BDL	0.18
1H-2, 65–66	2.15	BDL	BDL	0.80	BDL	0.17
1H-3, 25–26	3.25	BDL	BDL	0.18	BDL	ND
2H-1, 64–65	4.54	BDL	BDL	0.07	BDL	ND
2H-2, 65–66	6.05	BDL	BDL	0.18	BDL	0.03
2H-3, 65–66	7.55	BDL	BDL	0.17	BDL	ND
2H-4, 65–66	9.05	BDL	BDL	0.24	BDL	ND
2H-5, 65–66	10.55	BDL	BDL	0.13	BDL	ND
2H-6, 65–66	12.05	BDL	BDL	0.06	BDL	0.07
2H-7, 20–21	13.10	BDL	BDL	0.06	BDL	ND
3H-2, 65–66	15.55	BDL	BDL	0.03	BDL	ND
3H-3, 65–66	17.05	BDL	BDL	1.01	BDL	ND
3H-4, 65–66	18.55	9.1	1.09	0.07	BDL	0.07
3H-4, 65–66	18.55	9.3	1.12	ND	BDL	ND
3H-4, 65–66	18.55	9.6	1.15	ND	BDL	ND
3H-4, 65–66	18.55	9.0	1.08	ND	BDL	ND
3H-5, 65–66	20.05	25.2	3.03	2.95	BDL	ND
3H-6, 65–66	21.55	BDL	BDL	0.46	BDL	0.07
3H-7, 45–46	22.85	70.2	8.42	8.19	BDL	ND
4H-1, 65–66	23.55	15.8	1.90	1.71	BDL	BDL
4H-2, 60–61	25.00	28.5	3.42	3.35	BDL	ND
4H-3, 65–66	26.55	46.6	5.59	5.71	0.12	ND
4H-4, 65–66	28.05	16.9	2.03	ND	ND	ND
4H-5, 65–66	29.55	BDL	BDL	0.07	BDL	0.05
4H-6, 65–66	31.05	22.4	2.69	ND	ND	ND
4H-7, 65–66	32.55	53.1	6.38	1.47	BDL	ND
5H-1, 65–66	33.05	61.8	7.42	7.33	BDL	0.09
5H-2, 65–66	34.55	67.2	8.06	7.96	BDL	ND
5H-3, 65–66	36.05	65.4	7.85	7.87	0.01	ND
5H-4, 65–66	37.55	67.3	8.08	8.08	BDL	ND
5H-5, 65–66	39.05	81.8	9.82	9.77	BDL	ND
5H-6, 65–66	40.55	81.2	9.75	9.68	BDL	BDL
5H-7, 49–50	41.89	89.7	10.77	10.82	0.05	ND
6H-1, 65–66	42.55	89.0	10.69	10.90	0.21	0.12
6H-2, 65–66	44.05	86.9	10.43	ND	ND	ND
6H-3, 65–66	45.55	86.1	10.34	ND	ND	ND
6H-4, 65–66	47.05	85.1	10.22	10.39	0.18	0.03
6H-5, 65–66	48.55	82.8	9.94	ND	ND	ND
6H-6, 65–66	50.05	87.3	10.48	10.70	0.22	ND
6H-6, 65–66	50.05	87.4	10.49	10.65	0.16	ND
6H-6, 65–66	50.05	87.1	10.45	10.69	0.24	ND
6H-6, 65–66	50.05	87.6	10.52	10.73	0.21	ND
6H-6, 65–66	50.05	86.9	10.43	10.71	0.28	ND
6H-7, 24–25	51.14	70.6	8.47	ND	ND	ND
7H-1, 64–65	52.04	48.1	5.78	ND	ND	ND
7H-2, 64–65	53.54	78.0	9.36	9.37	0.00	0.07
7H-3, 64–65	55.04	79.5	9.55	9.84	0.29	ND
7H-4, 64–65	56.54	80.9	9.71	9.66	BDL	ND
7H-5, 64–65	58.04	86.7	10.40	10.24	BDL	BDL
7H-6, 64–65	59.54	83.8	10.06	10.32	0.27	ND
7H-7, 24–25	60.64	80.0	9.61	9.62	0.02	ND
8H-2, 100–101	63.40	66.0	7.93	ND	ND	ND
8H-3, 100–101	64.90	70.9	8.51	8.95	0.44	0.03
8H-4, 100–101	66.40	73.5	8.83	ND	ND	ND
8H-5, 100–101	67.90	66.0	7.92	ND	ND	ND
8H-6, 100–101	69.40	86.7	10.41	ND	ND	ND
8H-7, 55–56	70.45	83.7	10.05	ND	ND	ND
9H-1, 65–66	71.05	61.0	7.32	ND	ND	ND
9H-2, 65–66	72.55	60.2	7.23	ND	ND	ND
9H-3, 65–66	74.05	85.2	10.23	10.59	0.36	0.14
9H-4, 65–66	75.55	15.8	1.90	ND	ND	ND
9H-5, 65–66	77.05	BDL	BDL	0.03	BDL	ND
9H-6, 65–66	78.55	BDL	BDL	0.05	BDL	ND
9H-7, 25–26	79.65	BDL	BDL	0.06	BDL	0.05
9H-7, 25–26	79.65	BDL	BDL	ND	ND	ND
9H-7, 25–26	79.65	BDL	BDL	ND	ND	ND
10H-1, 74–75	80.64	BDL	BDL	0.51	BDL	0.05
10H-2, 64–65	82.04	BDL	BDL	0.05	BDL	ND
10H-3, 64–65	83.54	6.1	0.73	0.38	BDL	ND
10H-4, 64–65	85.04	7.6	0.92	ND	ND	ND
10H-5, 64–65	86.54	BDL	BDL	0.87	BDL	0.06
10H-6, 64–65	88.04	BDL	BDL	0.07	BDL	ND
10H-7, 29–30	89.19	BDL	BDL	0.05	BDL	ND
11H-2, 65–66	91.55	BDL	BDL	0.06	BDL	0.05
11H-3, 65–66	93.05	3.5	0.42	0.36	BDL	ND
11H-4, 65–66	94.55	BDL	BDL	0.06	BDL	ND
11H-5, 65–66	96.05	6.6	0.80	0.84	0.05	0.06
11H-6, 65–66	97.55	38.2	4.59	ND	ND	ND
12H-2, 64–65	101.04	2.5	0.30	0.34	0.04	ND
12H-3, 65–66	102.55	BDL	BDL	0.03	BDL	BDL
12H-4, 65–66	104.05	BDL	BDL	BDL	BDL	ND
12H-5, 65–66	105.55	BDL	BDL	0.30	BDL	ND
12H-6, 65–66	107.05	BDL	BDL	0.14	BDL	BDL
13H-1, 65–66	109.05	BDL	BDL	BDL	BDL	ND
13H-2, 65–66	110.55	14.3	1.72	1.50	BDL	0.04
13H-3, 65–66	112.05	43.7	5.25	6.85	1.60	ND
13H-4, 65–66	113.55	47.7	5.73	BDL	BDL	ND
13H-5, 65–66	115.05	59.7	7.16	0.53	BDL	ND
13H-6, 65–66	116.55	45.7	5.49	ND	ND	ND
13H-7, 55–56	117.95	44.4	5.33	ND	ND	ND
14H-2, 64–65	120.04	27.1	3.25	ND	ND	ND
14H-3, 64–65	121.54	BDL	BDL	BDL	BDL	BDL
14H-4, 64–65	123.04	14.1	1.69	ND	ND	ND
14H-5, 64–65	124.54	6.4	0.77	0.23	BDL	0.04
14H-6, 9–10	125.49	19.1	2.30	ND	ND	ND
15X-1, 84–85	126.74	12.5	1.51	ND	ND	ND
15X-2, 64–65	128.04	10.0	1.20	ND	ND	ND
15X-3, 64–65	129.54	57.9	6.95	ND	ND	ND
15X-4, 64–65	131.04	1.2	0.15	0.25	0.10	ND
15X-5, 23–24	132.13	5.2	0.63	0.53	0.04	0.04
16X-1, 65–66	136.15	BDL	BDL	BDL	BDL	BDL
16X-2, 65–66	137.65	18.7	2.24	2.38	0.14	ND
17X-1, 50–51	145.00	BDL	BDL	BDL	BDL	BDL
17X-1, 60–61	145.10	BDL	BDL	0.05	BDL	ND
17X-2, 50–51	146.33	BDL	BDL	0.06	BDL	0.04
17X-2, 50–51	146.33	BDL	BDL	0.15	BDL	ND
17X-2, 50–51	146.33	BDL	BDL	ND	ND	ND
17X-2, 50–51	146.33	BDL	BDL	ND	ND	ND
17X-2, 50–51	146.33	BDL	BDL	ND	ND	ND
17X-2, 60–61	146.43	BDL	BDL	ND	ND	ND
320-U1332B-						
18X-1, 75–76	144.65	BDL	BDL	0.10	BDL	ND
18X-2, 30–31	145.70	BDL	BDL	0.08	BDL	ND

Notes: IC = inorganic carbon, TC = total carbon, TOC = total organic carbon, Acid = determined by acidification method. BDL = below detection limit ($CaCO_3$ = <1 wt%, TOC by either method = <0.03 wt%) as determined by three times the standard deviation of replicate measures of a low concentration sample. When $CaCO_3$ is BDL, TOC is reported as equal to TC. ND = not determined (negative TOC wt%).

Table T30. Moisture and density measurements, Site U1332.

Core, section, interval (cm)	Depth CSF (m)	Water content (%)	Density (g/cm³) Wet bulk	Dry bulk	Grain	Porosity (%)
320-U1332A-						
1H-1, 75–76	0.75	73.3	1.24	0.33	2.97	88.8
1H-2, 75–76	2.25	71.3	1.24	0.36	2.67	86.6
1H-3, 75–76	3.75	77.9	1.18	0.26	2.54	89.7
2H-1, 75–76	4.65	73.0	1.24	0.34	2.94	88.6
2H-2, 75–76	6.15	73.7	1.20	0.32	2.39	86.8
2H-3, 75–76	7.65	70.1	1.26	0.38	2.80	86.5
2H-4, 75–76	9.15	64.7	1.25	0.44	2.12	79.1
2H-6, 75–76	12.15	66.3	1.28	0.43	2.58	83.2
2H-7, 30–31	13.20	80.9	1.18	0.22	3.33	93.3
3H-1, 85–86	14.25	81.6	1.13	0.21	2.11	90.1
3H-2, 75–76	15.65	78.6	1.18	0.25	2.71	90.7
3H-3, 75–76	17.15	79.7	1.16	0.24	2.47	90.4
3H-4, 75–76	18.65	76.4	1.21	0.29	2.91	90.2
3H-5, 75–76	20.15	77.3	1.15	0.26	2.00	86.9
4H-1, 75–76	23.65	73.8	1.23	0.32	2.89	88.8
4H-3, 75–76	26.65	74.8	1.21	0.30	2.62	88.4
4H-4, 75–76	28.15	72.0	1.23	0.34	2.50	86.3
4H-5, 75–76	29.65	75.9	1.21	0.29	2.82	89.7
4H-7, 50–51	32.40	51.9	1.46	0.70	2.69	73.9
5H-1, 75–76	33.15	46.8	1.52	0.81	2.66	69.6
5H-2, 75–76	34.65	50.0	1.51	0.75	2.84	73.5
5H-3, 75–76	36.14	44.9	1.50	0.83	2.42	65.8
5H-4, 75–76	37.64	49.3	1.51	0.77	2.80	72.7
5H-5, 75–76	39.15	31.4	1.78	1.22	2.69	54.6
5H-6, 75–76	40.64	44.7	1.59	0.88	2.89	69.6
5H-7, 60–61	42.00	26.0	1.90	1.40	2.71	48.2
6H-1, 75–76	42.64	42.6	1.61	0.93	2.80	67.0
6H-2, 75–76	44.15	40.0	1.65	0.99	2.77	64.3
6H-3, 75–76	45.65	42.8	1.65	0.95	3.06	69.1
6H-4, 75–76	47.14	42.5	1.56	0.90	2.56	64.9
6H-5, 75–76	48.65	37.2	1.77	1.11	3.09	64.1
6H-6, 75–76	50.15	41.4	1.64	0.96	2.84	66.2
6H-7, 35–36	51.25	26.2	2.02	1.49	3.10	51.7
7H-1, 75–76	52.15	54.0	1.40	0.64	2.45	73.8
7H-2, 75–76	53.64	44.6	1.60	0.88	2.92	69.7
7H-3, 75–76	55.14	44.1	1.56	0.87	2.68	67.4
7H-4, 75–76	56.65	41.3	1.68	0.99	3.07	67.8
7H-6, 75–76	59.65	41.1	1.63	0.96	2.76	65.3
7H-7, 35–36	60.75	43.4	1.58	0.89	2.69	66.8
8H-2, 75–76	63.14	51.6	1.47	0.71	2.75	74.1
8H-3, 75–76	64.65	49.8	1.45	0.73	2.46	70.4
8H-4, 75–76	66.15	45.4	1.54	0.84	2.67	68.4
8H-6, 75–76	69.15	41.4	1.65	0.97	2.89	66.6
8H-7, 35–36	70.25	40.7	1.60	0.95	2.60	63.6
9H-1, 75–76	71.15	53.1	1.43	0.67	2.59	74.2
9H-2, 75–76	72.65	53.8	1.42	0.65	2.55	74.4
9H-3, 75–76	74.15	40.2	1.66	1.00	2.87	65.3
9H-5, 75–76	77.15	61.8	1.31	0.50	2.35	78.8
9H-6, 75–76	78.65	71.8	1.21	0.34	2.20	84.6
9H-7, 35–36	79.75	70.7	1.25	0.37	2.67	86.3
10H-1, 85–86	80.75	65.7	1.31	0.45	2.88	84.4
10H-2, 75–76	82.15	71.2	1.22	0.35	2.26	84.5
10H-3, 75–76	83.65	69.0	1.25	0.39	2.52	84.6
10H-4, 75–76	85.15	69.1	1.22	0.38	2.13	82.3
10H-6, 75–76	88.15	71.1	1.21	0.35	2.21	84.2
10H-7, 40–41	89.30	71.1	1.24	0.36	2.59	86.1
11H-2, 75–76	91.65	73.6	1.18	0.31	2.08	85.0
11H-3, 75–76	93.15	74.4	1.20	0.31	2.45	87.4
11H-4, 75–76	94.65	71.0	1.22	0.35	2.33	84.8
11H-5, 75–76	96.15	68.7	1.27	0.40	2.69	85.2
11H-6, 75–76	97.65	61.9	1.29	0.49	2.27	78.2
12H-2, 75–76	101.15	70.1	1.24	0.37	2.45	84.9
12H-3, 75–76	102.65	74.3	1.19	0.31	2.22	86.2
12H-4, 75–76	104.15	72.6	1.21	0.33	2.35	85.8
12H-5, 75–76	105.65	71.7	1.18	0.34	1.96	82.9
12H-6, 75–76	107.15	71.4	1.23	0.35	2.45	85.6
12H-7, 35–36	108.05	68.2	1.24	0.39	2.24	82.4
13H-1, 75–76	109.15	72.1	1.23	0.34	2.60	86.8
13H-2, 75–76	110.65	66.1	1.24	0.42	2.14	80.3
13H-3, 75–76	112.15	61.3	1.34	0.52	2.58	78.0
13H-4, 75–76	113.65	55.2	1.40	0.63	2.58	75.7
13H-5, 75–76	115.15	55.8	1.42	0.63	2.80	77.5
13H-6, 75–76	116.65	64.0	1.28	0.46	2.28	79.8
13H-7, 65–66	118.05	58.0	1.38	0.58	2.67	78.3
14H-2, 75–76	120.15	60.0	1.33	0.53	2.42	78.0
14H-3, 75–76	121.65	65.9	1.29	0.44	2.63	83.2
14H-4, 75–76	123.15	63.5	1.27	0.46	2.15	78.5
14H-5, 75–76	124.65	65.1	1.26	0.44	2.26	80.4
15X-1, 75–76	126.65	60.5	1.36	0.54	2.76	80.5
15X-2, 75–76	128.15	64.5	1.27	0.45	2.23	79.8
15X-3, 75–76	129.65	63.5	1.30	0.48	2.47	80.8
15X-4, 75–76	131.15	67.7	1.28	0.41	2.63	84.3
15X-5, 30–31	132.20	65.9	1.23	0.42	2.03	79.3
16X-1, 75–76	136.25	66.4	1.27	0.43	2.47	82.7
16X-2, 75–76	137.75	57.3	1.33	0.57	2.22	74.4
17X-1, 85–86	145.35	58.5	1.45	0.60	3.57	83.1
17X-3, 95–96	148.20	31.3	1.74	1.20	2.56	53.2
320-U1332B-						
18-X2, 30–31	145.70	59.6	1.38	0.56	2.89	80.6

Table T31. Split-core *P*-wave velocity measurements, Hole U1332A.

Core, section	Depth CSF (m)	Velocity (m/s)		
		x-axis	*y*-axis	*z*-axis
320-U1332A-				
1H-1	1.3		1499	
1H-1	1.3			1496
1H-1	1.21	1594		
1H-2	2.82		1500	
1H-2	2.82			1495
1H-2	2.89	1593		
1H-3	3.63		1502	
1H-3	3.63			1495
1H-3	3.54	1606		
2H-1	5.2		1499	
2H-1	5.2			1495
2H-1	5.31	1597		
2H-2	6.68		1500	
2H-2	6.68			1494
2H-2	6.77	1631		
2H-3	8.2		1501	
2H-3	8.2			1496
2H-3	8.28	1622		
2H-4	9.71		1497	
2H-4	9.71			1494
2H-4	9.8	1604		
2H-5	11.13		1508	
2H-5	11.13			1494
2H-5	11.21	1608		
2H-6	12.7		1499	
2H-6	12.7			1827
2H-6	12.79	1610		
3H-3	17.72		1521	
3H-3	17.72			1475
3H-4	19.73	1598		
3H-5	20.98		1533	
3H-5	20.98			1481
3H-5	20.75	1583		
3H-6	22.22		1534	
3H-6	22.3	1611		
4H-1	24.2		1530	
4H-1	24.2			1472
4H-1	24.28	1584		
4H-2	25.64		1444	
4H-2	25.64			1523
4H-2	25.73	1601		
4H-3	27.2		1439	
4H-3	27.2			1517
4H-3	27.29	1592		
4H-4	28.74		1530	
4H-4	28.74			1511
4H-4	28.83	1595		
4H-5	30.19			1467
4H-5	30.27	1585		
4H-6	31.74		1509	
4H-6	31.74			1508
4H-6	31.82	1591		
5H-1	33.74		1499	
5H-1	33.74			1497
5H-1	33.82	1571		
5H-2	35.13		1506	
5H-2	35.13			1493
5H-2	35.21	1592		
5H-3	36.73		1514	
5H-3	36.73			1498
5H-3	36.83	1609		
5H-4	38.25		1506	
5H-4	38.25			1492
5H-4	38.33	1613		
5H-5	39.94	1605		
5H-5	39.7		1505	
5H-5	39.7			1498
5H-6	41.24		1516	
5H-6	41.24			1505
5H-6	41.32	1610		
6H-1	43.26			1468
6H-1	43.34	1607		
6H-2	44.77		1516	
6H-2	44.77			1442
6H-2	44.85	1624		
6H-3	46.19			1456
6H-3	46.3	1592		
6H-4	47.78		1512	
6H-4	47.78			1498
6H-4	47.86	1606		
6H-5	49.21		1530	
6H-5	49.21			1520
6H-5	49.3	1628		
6H-6	50.77		1512	
6H-6	50.77			1503
6H-6	50.86	1615		
6H-7	51.55			1503
6H-7	51.65	1625		
7H-1	52.85		1518	
7H-1	52.85			1497
7H-1	52.76	1594		
7H-2	54.18		1514	
7H-2	54.18			1505
7H-2	54.08	1630		
7H-3	53.09		1528	
7H-3	53.09			1465
7H-3	55.8	1631		
7H-4	57.07		1523	
7H-4	57.23	1634		
7H-5	58.82		1519	
7H-5	58.82			1512
7H-5	58.68	1636		
7H-6	60.2		1519	
7H-6	60.2			1509
7H-6	60.35	1619		
7H-7	61.15		1521	
7H-7	61.15			1509
7H-7	61.23	1615		
8H-2	63.84	1646		
8H-3	65.23		1409	
8H-3	65.31	1645		
8H-4	66.75			1455
8H-4	66.85	1600		
8H-5	68.32		1505	
8H-5	68.32			1452
8H-5	68.23	1588		
8H-6	69.77		1522	
8H-6	69.77			1505
8H-6	69.84	1625		
8H-7	70.61		1535	
8H-7	70.61			1514
8H-7	70.69	1634		
10H-1	81.26		1550	
10H-1	81.34	1652		
10H-2	82.85	1669		
10H-3	84.28	1674		
10H-4	85.84	1645		
10H-5	87.33	1650		
10H-6	88.74		1454	
11H-2	92.34	1666		
11H-3	93.8	1689		
11H-4	95.23		1457	
11H-4	95.3	1623		
11H-5	96.81	1604		
11H-6	98.11		1444	
11H-6	98.19	1591		
12H-2	101.69		1450	
12H-2	101.82	1648		
12H-3	103.3	1646		
12H-4	104.8	1627		
12H-5	106.22	1625		
12H-6	107.63	1625		
13H-1	109.71		1448	
13H-1	109.81	1664		
13H-2	111.32	1660		
13H-3	112.7		1533	
13H-3	112.79	1600		
13H-4	114.25		1532	
13H-4	114.35	1605		
13H-5	115.73		1551	
13H-5	115.86	1604		
13H-6	117.22		1444	
13H-6	117.33	1597		
14H-2	120.85	1570		
14H-3	122.3	1595		
14H-4	123.86	1616		
14H-5	125.36	1617		
14H-6	126.84	1607		
15X-1	127.36	1637		
15X-2	128.85	1653		
15X-3	130.13		1416	
15X-4	131.86	1669		
15X-5	132.78	1656		
16X-1	136.94	1652		

Table T32. Thermal conductivity, Hole U1332A.

Core, section, interval (cm)	Depth CSF (m)	Thermal conductivity (W/[m·K])
320-U1332A-		
1H-3, 60	3.60	0.804
2H-3, 115	8.05	0.821
3H-3, 115	17.55	0.751
4H-3, 115	27.05	0.788
5H-3, 115	36.55	1.206
6H-3, 115	46.05	1.009
7H-3, 115	55.55	1.156
8H-3, 115	65.05	1.046
9H-3, 115	74.55	1.185
10H-3, 115	84.05	0.810
12H-3, 115	103.05	0.767
13H-3, 115	112.55	0.944
14H-3, 115	122.05	0.804
15X-3, 115	130.05	0.824
16X-1, 115	136.65	0.787
17X-2, 115	146.98	0.621

Table T33. Shipboard core top, composite, and corrected composite depths, Site U1332.

Core	Depth CSF (m)	Offset (m)	Top depth (m) CCSF-A	Top depth (m) CCSF-B
320-U1332A-				
1H	0	0.00	0.00	0.00
2H	3.9	0.31	4.21	3.79
3H	13.4	0.65	14.05	12.65
4H	22.9	2.65	25.55	23.00
5H	32.4	5.15	37.55	33.80
6H	41.9	5.65	47.55	42.80
7H	51.4	7.90	59.30	53.37
8H	60.9	7.50	68.40	61.56
9H	70.4	2.78	73.18	65.86
10H	79.9	3.48	83.38	75.04
11H	89.4	3.32	92.72	83.45
12H	98.9	6.02	104.92	94.43
13H	108.4	7.77	116.17	104.55
14H	117.9	11.52	129.42	116.48
15X	125.9	12.52	138.42	124.58
16X	135.5	12.52	148.02	133.22
17X	144.5	12.52	157.02	141.32
18X	150.4	12.52	162.92	146.63
320-U1332B-				
1H	0	0.15	0.15	0.14
2H	2.1	0.65	2.75	2.48
3H	11.6	2.15	13.75	12.38
4H	19.6	4.25	23.85	21.47
5H	29.1	4.35	33.45	30.11
6H	38.6	7.15	45.75	41.18
7H	48.1	10.50	58.60	52.74
8H	57.6	10.20	67.80	61.02
9H	67.1	3.90	71.00	63.90
10H	76.6	5.60	82.20	73.98
11H	86.1	6.07	92.17	82.95
12H	91.1	9.27	100.37	90.33
13H	100.6	9.72	110.32	99.29
14X	110.1	10.67	120.77	108.69
15X	116.1	14.92	131.02	117.92
16X	124.6	16.95	141.55	127.40
17X	134.3	16.95	151.25	136.13
18X	143.9	14.77	158.67	142.80
320-U1332C-				
1H	0	0.04	0.04	0.04
2H	7.5	0.49	7.99	7.19
3H	17	0.25	17.25	15.53
4H	26.5	2.45	28.95	26.06
5H	36	4.25	40.25	36.23
6H	45.5	3.45	48.95	44.06
7H	49.5	6.95	56.45	50.81
8H	59	7.66	66.66	59.99
9H	66	1.10	67.10	60.39
10H	75.5	0.70	76.20	68.58
11H	85	3.50	88.50	79.65
12H	94.5	4.84	99.34	89.41
13H	104	4.84	108.84	97.96
14X	113.5	7.14	120.64	108.58
15X	118	9.94	127.94	115.15
16X	127.6	10.69	138.29	124.46
17X	137.2	10.69	147.89	133.10
18X	146.9	12.69	159.59	143.63

Table T34. Splice tie points, Site U1332.

Hole, core, section, interval (cm)	Depth (m)			Hole, core, section, interval (cm)	Depth (m)	
	CSF	CCSF-A			CSF	CCSF-A
320-				320-		
U1332A-1H-2, 109	2.59	2.59	Tie to	U1332C-1H-2, 104	2.54	2.59
U1332C-1H-5, 63	6.63	6.67	Tie to	U1332A-2H-2, 96	6.36	6.67
U1332A-2H-5, 126	11.16	11.47	Tie to	U1332C-2H-3, 48	10.98	11.47
U1332C-2H-6, 146	16.46	16.95	Tie to	U1332A-3H-2, 140	16.30	16.95
U1332A-3H-5, 38	19.78	20.43	Tie to	U1332C-3H-3, 18	20.18	20.43
U1332C-3H-7, 17	26.17	26.42	Tie to	U1332A-4H-1, 87	23.77	26.42
U1332A-4H-5, 22	29.12	31.77	Tie to	U1332C-4H-2, 132	29.32	31.77
U1332C-4H-5, 47	32.97	35.42	Tie to	U1332B-5H-2, 47	31.07	35.42
U1332B-5H-5, 152	36.62	40.97	Tie to	U1332C-5H-1, 72	36.72	40.97
U1332C-5H-6, 110	44.60	48.85	Tie to	U1332A-6H-1, 130	43.20	48.85
U1332A-6H-7, 32	51.22	56.87	Tie to	U1332C-7H-1, 42	49.92	56.87
U1332C-7H-7, 28	58.78	65.73	Tie to	U1332B-7H-5, 113	55.23	65.73
U1332B-7H-7, 68	57.78	68.28	Tie to	U1332C-8H-2, 11	60.62	68.28
U1332C-8H-4, 34	63.84	71.50	Tie to	U1332B-9H-1, 50	67.60	71.50
U1332B-9H-5, 35	73.45	77.35	Tie to	U1332A-9H-3, 117	74.57	77.35
U1332A-9H-7, 74	80.14	82.92	Tie to	U1332B-10H-1, 72	77.32	82.92
U1332B-10H-5, 90	83.50	89.10	Tie to	U1332A-10H-4, 122	85.62	89.10
U1332A-10H-6, 110	88.50	91.98	Tie to	U1332C-11H-3, 48	88.48	91.98
U1332C-11H-5, 93	91.93	95.43	Tie to	U1332A-11H-2, 121	92.11	95.43
U1332A-11H-6, 72	97.62	100.94	Tie to	U1332C-12H-2, 10	96.10	100.94
U1332C-12H-5, 89	101.39	106.23	Tie to	U1332A-12H-1, 131	100.21	106.23
U1332A-12H-4, 57	103.97	109.99	Tie to	U1332C-13H-1, 115	105.15	109.99
U1332C-13H-3, 146	108.46	113.30	Tie to	U1332B-13H-2, 148	103.58	113.30
U1332B-13H-6, 44	108.54	118.26	Tie to	U1332A-13H-2, 59	110.49	118.26
U1332A-13H-5, 117	115.57	123.34	Tie to	U1332B-14X-2, 107	112.67	123.34
U1332B-14X-6, 140	119.00	129.67	Tie to	U1332C-15X-2, 23	119.73	129.67
U1332C-15X-5, 4	124.04	133.98	Tie to	U1332B-15X-2, 146	119.06	133.98

Table T35. Magnetostratigraphic and biostratigraphic datums, Site U1332. (See table note.)

Event	Age (Ma)	Depth CCSF-A (m)	Error (m)
C1n–C1r.1r	0.781	1.25	
C1r.1r–C1r.1n	0.988	1.83	
C1r.1n–C1r.2r	1.072	2.33	
C1r.2r–C2n	1.778	5.46	
C2n–C2r.1r	1.945	5.91	
C2r.1r–C2r.1n	2.128	6.71	
C2r.1n–C2r.2r	2.148	6.78	
C2r.2r–C2An.1n	2.581	8.58	
C2An.1n–C2An.1r	3.032	9.73	
C2An.1r–C2An.2n	3.116	10.03	
C2An.2n–C2An.2r	3.207	10.33	
C2An.2r–C2An.3n	3.330	10.63	
C2An.3n–C2Ar	3.596	11.26	
C6An.1r–C6An.2n	20.439	15.23	
C6An.2n–C6Ar	20.709	15.98	
C6Ar–C6AAn	21.083	16.93	
C6AAn–C6AAr.1r	21.159	17.05	
C6AAr.1r–C6AAr.1n	21.403	17.98	
C6AAr.1n–C6AAr.2r	21.483	18.18	
C6AAr.2r–C6AAr.2n	21.659	18.70	
C6AAr.2n–C6AAr.3r	21.688	18.83	
C6AAr.3r–C6Bn.1n	21.767	19.05	
C6Bn.1n–C6Bn.1r	21.936	19.28	
C6Bn.1r–C6Bn.2n	21.992	19.85	
C6Bn.2n–C6Br	22.268	20.48	
C6Br–C6Cn.1n	22.564	22.15	
C6Cn.1n–C6Cn.1r	22.754	22.80	
C6Cn.1r–C6Cn.2n	22.902	22.90	
C6Cn.2n–C6Cn.2r	23.030	23.05	
C6Cn.2r–C6Cn.3n	23.278	23.30	
C6Cn.3n–C6Cr	23.340	23.58	
C6Cr–C7n.1n	24.022	26.75	
C7n.1n–C7n.1r	24.062	26.85	
C7n.1r–C7n.2n	24.147	27.10	
C7n.2n–C7r	24.459	28.23	
C7r–C7An	24.756	29.05	
C7An–C7Ar	24.984	29.48	
C7Ar–C8n.1n	25.110	30.05	
C8n.1n–C8n.1r	25.248	30.43	
C8n.1r–C8n.2n	25.306	30.55	
C8n.2n–C8r	26.032	32.83	
C8r–C9n	26.508	34.55	
C9n–C9r	27.412	39.05	
C9r–C10n.1n	27.886	41.05	
C10n.1n–C10n.1r	28.126	42.05	
C10n.1r–C10n.2n	28.164	42.43	
C10n.2n–C10r	28.318	42.85	
C10r–C11n.1n	29.166	49.05	
C11n.1n–C11n.1r	29.467	51.60	
C11n.1r–C11n.2n	29.536	51.83	
C11n.2n–C11r	29.957	53.93	
C11r–C12n	30.617	57.23	
C12r–C13n	33.232	75.18	
C13n–C13r	33.705	78.11	
C13r–C15n	35.126	82.31	
C15r–C16n.1n	35.328	84.73	
C16n.1n–C16n.1r	35.554	85.53	
C16n.1r–C16n.2n	35.643	86.11	
C16n.2n–C16r	36.355	89.38	
C16r–C17n.1n	36.668	90.88	
C17n.1n–C17n.1r	37.520	95.87	
C17n.1r–C17n.2n	37.656	96.25	
C17n.2n–C17n.2r	37.907	97.40	
C17n.2r–C17n.3n	37.956	97.70	
C17n.3n–C17r	38.159	98.60	
C17r–C18n.1n	38.449	99.85	
C18n.1n–C18n.1r	39.554	107.92	
C18n.1r–C18n.2n	39.602	108.62	
C18n.2n–C18r	40.084	112.37	
C18r–C19n	41.358	125.02	
C19r–C20n	42.536	136.22	
Nannofossils			
T *Sphenolithus delphix*	23.1	23.91	0.26
B *Sphenolithus delphix*	23.2	25.16	0.01
X *T. longus/T. carinatus*	24.7	28.40	0.75
Tc *Cyclicargolithus abisectus*	24.7	28.40	0.75
T *Sphenolithus predistentus*	26.9	36.98	1.38
T *Sphenolithus pseudoradians*	28.8	42.10	0.75
B *Sphenolithus distentus*	30.0	55.00	0.75
T *Reticulofenestra umbilicus*	32.0	68.34	0.74
T *Coccolithus formosus*	32.9	74.15	0.75
T *Discoaster saipanensis*	34.4	82.63	4.20
T *Chiasmolithus grandis*	37.1	100.17	0.75
B *Dictyococcites bisectus*	38.0	104.63	2.79
T *Chiasmolithus solitus*	40.4	112.50	5.08
T *Nannotetrina*	42.3	136.54	0.72
B *Reticulofenestra umbilicus* >14 µm	42.5	138.68	0.88
T *Nannotetrina fulgens*	43.4	141.69	0.39
B *Nannotetrina fulgens*	46.8	150.32	0.41
T *Discoaster lodoensis*	48.4	155.24	4.32
Radiolarians			
B *Cyrtocapsella cornuta*	22.26	21.69	1.48
T *Artophormis gracilis*	22.62	21.69	2.35
B *Lychnocanoma elongata*	25.05	27.16	0.99
T *Dorcadospyris circulus*	26.17	33.24	2.13
B *Dorcadospyris ateuchus*	29.50	51.61	1.50
B *Dorcadospyris circulus*	29.96	55.24	2.26
T *Theocyrtis tuberosa*	30.13	61.46	1.71
T *Lithocyclia crux*	30.13	61.46	1.71
B *Eucyrtidium plesiodiaphanes*	30.37	61.46	1.71
T *Lophocyrtis oberhaensliae*	30.74	64.81	1.51
T *Lychnocanoma babylonis*	33.75	78.63	1.49
T *Thyrsocyrtis tetracantha*	35.30	84.78	0.33
B *Calocyclas bandyca*	36.74	90.95	2.28
B *Lophocyrtis jacchia*	37.06	94.10	1.02
B *Cryptocarpium azyx*	37.52	95.28	1.50
B *Calocyclas turris*	38.67	105.89	1.47
B *Lithocyclia aristotelis group*	39.73	108.98	1.50
B *Dorcadospyris anastasis*	39.98	112.38	2.00
B Podocyrtis goetheana	40.16	112.38	2.00
T *Podocyrtis trachodes*	41.23	130.85	1.03
B *Podocyrtis chalara*	41.54	133.47	1.51
B *Cryptocarpium ornatum*	42.10	136.27	1.42
T *Eusyringium lagena*	42.69	140.21	1.54
B *Podocyrtis helenae*	44.14	141.61	3.52
T *Podocyrtis phyxis*	44.44	144.37	0.75
T *Podocyrtis diamesa*	44.44	144.37	0.75
T *Spongatractus balbis*	44.77	147.83	2.71
B *Podocyrtis mitra*	44.77	147.83	2.71
B *Podocyrtis ampla*	44.77	147.83	2.71
Foraminifers			
T *Paragloborotalia opima*	26.9	33.08	5.90
B *Globigerina angulisuturalis*	29.2	44.49	5.52
T *Subbotina angiporoides*	29.8	53.25	3.24
B *Paragloborotalia opima*	30.8	53.25	3.24

Note: T = top, B = bottom, X = abundance crossover, Tc = top common.

Table T36. Results from APCT-3 temperature profiles, Site U1332. (See table notes.)

Core	Temperature (°C) Average at mudline	Temperature (°C) Minimum above mudline	Depth DSF (m)	In situ temperature (°C)	Thermal resistance (m^2K/m)
320-U1332B-					
2H	1.569	1.458	11.6	1.77	14.4
3H	1.540	1.458	19.6	3.60	25.5
5H	1.527	1.453	38.6	Undetermined	46.5
7H	1.536	1.456	57.6	5.97	64.7
9H	1.515	1.458	76.6	7.05	81.3
12H	1.509	1.461	100.6	9.11	111.2
320-U1332C-					
4H	1.510	1.454	36.0	4.35	44.7
9H	1.518	1.450	75.5	7.00	80.3
Average:	1.528	1.456			

Notes: In situ temperatures were determined using the TP-Fit software by Martin Heesemann. Thermal resistance was calculated from thermal conductivity data (see "Physical properties") corrected for in situ conditions (see "Downhole measurements" in the "Methods" chapter).